Investigations into the chromatin and transcriptional regulatory network of skin pigmentation homeostasis

Thesis submitted to Jawaharlal Nehru University

for the degree of

DOCTOR OF PHILOSOPHY

by

SHALINI YADAV

SCHOOL OF LIFE SCIENCES

JAWAHARLAL NEHRU UNIVERSITY

NEW DELHI-110067

2018

SCHOOL OF LIFE SCIENCES

JAWAHARLAL NEHRU UNIVERSITY

NEW DELHI-110067

INDIA

<u>CERTIFICATE</u>

The research work embodied in this thesis entitled **"Investigations into the chromatin and transcriptional regulatory network of skin pigmentation homeostasis"** has been carried out in the School of Life Sciences, Jawaharlal Nehru University, New Delhi, 110067, India. The work is original and has not been submitted so far, in part or in full, for award of any degree or diploma of any University.

Shalini Yadav

(Candidate)

Prof. K. Natarajan

(Supervisor)

Krishnamurthy Natarajan, Ph.D.
Professor
School of Life Sciences
Jawaharlal Nehru University
New Delhi-110067

Prof. S.K.Goswami

(Dean)

Prof Shyamal K. Goswami
Dean
School of Life Sciences
Jawaharlal Nehru University
New Delhi-110067

ACKNOWLEDGMENTS

Dedicated To My Beloved Parents

TABLE OF CONTENTS

ABBREVIATIONS

α-MSH	Melanocyte-stimulating hormone
ACTH	Adrenocorticotropic hormone
bHLH-Zip	Basic helix loop helix leucine zipper
BPS	Bathophenanthroline disulfonate
cAMP	Cyclic adenosine monophosphate
cGMP	Cyclic guanosine monophosphate
CREB	cAMP response element binding protein
DAVID	Database for Annotation, Visualization, and Integrated Discovery
DLR	Dual Luciferase Assay
DPBS	Dulbecco`s Phosphate Buffered Saline
DMSO	Dimethyl sulphoxide
DCT	Dopachrome tautomerase
DE	Differentially Expressed
TEM	Transmission electron microscopy
FAC	Ferric ammonium citrate
GO	Gene Ontology
HQ	Hydroxyquinone
IBMX	3-isobutyl-1-methylxanthine
IFN	Interferon
KA	Kojic Acid
LA	Linoleic Acid
M-Box	Transcription factor recognition motif with the 5'-TCATGTGCT- 3'sequence
MAPK	Mitogen-activated protein kinase
MC1R	Melanocortin 1 receptor
MITF	Microphthalmia-associated transcription factor
NCC	Neural crest cells

OCA	Oculocutaneous albinism
OxPhos	Oxidative Phosphorylation
PAX3	Paired box 3 transcription factor
PCR	Polymerase chain reaction
PKA	Protein kinase A
qRT-PCR	Quantitative Real-Time PCR
RSAT	Regulatory sequence analysis tool
RIN	RNA Integrity Number
SMS	Sequence Manipulation Suite
SCF	Stem cell factor
SOX10	Sry-related HMG box 10 transcription factor
SLC	Solute Carrier
TF	Transcription factor
TFBS	Transcription factor binding site
TRED	Transcriptional Regulatory Element Database
TSS	Transcription start site
TYR	Tyrosinase
TYRP1	Tyrosinase-related protein 1
TRITC	Tetramethyl rhodamine
UVR	Ultraviolet radiation

LIST OF FIGURES

LIST OF TABLES

ABSTRACT

The central theme of this research is to identify novel regulators and signaling pathways involved in melanogenesis. Towards this end, we employed a chemo-genomic approach and meta-analysis to decipher transcriptional regulatory networks involved in melanogenesis.

The skin is the largest organ in the human body and acts as an interface with the environment. Skin executes two critical functions viz., offering protection from harmful UV-rays and by minimizing the transepidermal water loss. Human skin is composed of three layers, epidermis, dermis, and the hypodermis. The epidermis-dermis interface is separated by a single layer of cells, composed of the melanocytes, where melanin is synthesized in a specialized organelle called melanosomes. The melanocytes and the keratinocytes in the epidermis together give rise to functional epidermal melanin units that results in the characteristic human skin color.

Skin pigmentation is a complex process and occurs through an intricate network of pathways involving several signaling and regulatory molecules leading to controlled melanin formation. Melanin is synthesized by three critical enzymes-tyrosinase (TYR), tyrosinase-related protein2/dopachrome tautomerase (TRP2 or DCT), and tyrosinase-related protein1 (TRP-1). Microphthalmia-associated transcription factor (MITF) is a master regulator of pigmentation and binds to the M-box sequence found in the promoters of the melanin biosynthetic genes. Moreover, MITF has also been shown to regulate both melanocyte development and melanoma progression. Genome-wide studies in 501-mel cells and SK-MEL-28 cells have revealed that MITF-regulated genes are involved in pigmentation, cell cycle, migration, and survival. As these transcriptome studies were performed in

constitutively pigmented or weakly pigmented cells, the immediate relevance of such genes to pigmentation could not be clearly established.

Previous studies in our lab using a tunable mouse B16-F10 cellular model of melanogenesis led to a comprehensive identification of regulatory network occurring during melanogenesis. We treated B16 cells for different time periods with two small molecules IBMX and forskolin, known activators of the cAMP-PKA pathway to induce melanogenesis and carried out genome-wide microarray profiling. Hierarchical clustering analysis showed a temporal pattern of expression of ~1620 genes in response to treatment by both forskolin and IBMX. The DAVID pathway analysis yielded several genes involved in melanosome biogenesis, cell cycle, inflammation and small solute transporters.

Among the 1620 DE genes in our array, 29 small solute transporters (SLC) genes showed time-dependent differential expression. The role of one of the SLC, *Slc24a4* has already been studied in context of melanogenesis. Among 29 SLCs, we found *Slc40a1/Fpn1* to be repressed during melanogenesis in our forskolin and IBMX transcriptome data. The *Fpn1* gene encoding the ferroportin is a membrane-bound protein that plays an essential role in maintaining iron homeostasis by functioning as an iron efflux protein. Therefore, in chapter III 'Elucidation of the requirement of iron homeostasis for melanogenesis', we investigated the role of *Slc40a1/Fpn1I,* known mammalian iron exporter, in melanogenesis. Accordingly, in this chapter, the role of iron in melanogenesis was investigated by culturing B16 cells under iron replete and deplete medium. Interestingly, we found an increased melanin accumulation in iron-replete medium, and a reciprocal decrease in iron deplete medium.

Interestingly, iron deprivation also leads to the activation of adaptive cellular response which employs the transcriptional regulatory program to decrease the levels of transcripts encoding Oxphos complexes viz., C1-*Ndufa9*, CII-*Sdha*, CIV-*Uqcrc2*, CIV-*Cox4il,* and CV-*Atp5a1*. Since melanogenesis is an ATP dependent process, we hypothesize that the decrease in OxPhos transcripts could cause a decreased level of ATP thereby leading to the inhibition of melanogenesis during iron deprivation. Further, our data showed that the expression of iron uptake genes *Tfr1* and *Dmt1* and iron storage gene *Fth1* was found to be modulated by the availability of iron. We found a significant increase in the expression of *Dmt1* gene in the iron depletes in comparison to the iron-replete. However, the expression of *Fth1* was upregulated in the iron-replete condition further indicated an increased intracellular iron inside the cell.

Interestingly we found melanosomes dynamics to be regulated by the availability of iron in the medium. A cellular investigation by TEM analysis suggested that iron promotes melanogenesis by accelerating both melanosome biogenesis as well as the melanosome maturation. The expression of essential genes involved in melanosome biogenesis and transport such as *Pmel17*, *Hps3*, and *Rab27a* was found to be up-regulated in the iron-induced hyper-pigmentation. The level of tyrosinase, a rate-limiting enzyme for melanin synthesis, was found to be modulated during iron chelation. We observed a downregulation of both tyrosinase protein and activity when B16 cells were cultured in iron deplete condition. Next, we carried out microarray profiling to identify cellular processes modulated in iron-replete versus deplete medium. The microarray data analysis showed the enrichment of distinct categories of genes in iron-replete and deplete condition.

Collectively, our data showed that iron regulates different attributes of melanogenesis including melanosome biogenesis and maturation, tyrosinase protein expression and activity, expression of iron storage and uptake genes and the expression of genes involved in oxidative phosphorylation. Thus, our results indicate the importance of nutrient signaling in the context of melanogenesis.

Further, we found significant numbers of transcription factors differentially expressed during melanogenesis. MITF is activated by CREB, which in itself is activated by elevated cAMP levels. Although MITF regulated genes have been reported previously, two important challenges remained. First, a direct connection between pigmentation and MITF-mediated regulation could not be established since the cell lines used for the studies were either constitutively pigmented (501-mel cells) or weakly pigmented (SK-MEL-28). Second, it was not clear if genes that were either bound by MITF or differentially expressed upon MITF overexpression indeed was dependent on MITF. Therefore, we decided to carry out transcriptome profiling upon siRNA-mediated silencing of *Mitf* in B16 cells.

Accordingly, in chapter IV 'Identification of MITF-dependent and -independent regulon during melanogenesis,' we proposed to identify what fraction of genes differentially expressed during hyper-pigmentation are regulated by MITF. We identified differentially expressed genes up- and down-regulated during *Mitf* knockdown in B16 cells. The siRNA-mediated downregulation of *Mitf* leads to the enrichment of distinct categories of genes involved in different processes. Next, we performed a meta-analysis of differentially expressed genes obtained from our forskolin and IBMX data and compared with that of si*Mitf* data. The comparison was done using ~260 up-regulated genes and 269 down-regulated genes commonly regulated by both forskolin and IBMX. Further, these data were analyzed to derive a

core set of genes regulated by MITF during pigmentation. We found that a small subset of 43 genes (16.5%) and 58 genes (21.6%) from up- and down-regulated categories, respectively, showed MITF-dependence. However, an additional 217 up-regulated (83.4%) and 211 down-regulated genes (78.3%) showed MITF-independent response. Interestingly, our study also highlights hitherto unexplored MITF independent genes that could have regulatory roles in melanogenesis. In a previous study, Natarajan et al., (2014) have implicated MITF-independent de-pigmentation of B16 cells. We also found a significant fraction of genes differentially expressed during pigmentation was not under MITF control, that further indicates that a large melanogenesis transcriptome could be regulated in a MITF-independent manner.

To identify genes that are directly controlled by MITF, the si*Mitf* data from B16 cells was compared with 2862 MITF-occupied genes derived from the ChIP-seq data from Strub et al. Comparing our si*Mitf* data, we found that ~123 up-regulated genes and ~156 down-regulated genes were found to be bound by MITF. The majority of genes among 156 genes downregulated and occupied by MITF was found to be associated with the terms such as transport (*Slc45a2, Rab5a, Insig1)*, cellular homeostasis (*Slc24a5, Trpm1, Abcb6),* pigmentation (*Edrnb*, *Tyr*, *Mreg*, *Cited1*, *Rab27a*), cholesterol biosynthetic (*Srebf1*, *Sc5d*, *insig1*). However, surprisingly, 123 genes that were up-regulated in the si*Mitf* data and bound by MITF in Strub et al. data, were associated with the GO terms, angiogenesis (*Nr4a1*, *Rnf213*, *Klf4*), nervous system development (*Id1*, *Mapk3*), cell differentiation (*Cdkn1a*, *Gadd45b*). Thus, from this analysis, it can be inferred that MITF could act as a repressor at several promoters.

Although pathways underlying hyperpigmentation have already been identified, the negative feedback regulatory loops that controls the activated

melanogenesis process are not entirely understood. Further, tyrosinase inhibition is still the most studied mechanism of skin depigmentation. In chapter V 'Transcriptional regulatory pathway(s) involved in skin depigmentation,' we examined the consequence of depigmentation/hypopigmentation on the normal functioning of melanocytes since they are destined to form melanin. To achieve that we selected two known hypo-pigmenting compounds, kojic acid (KA), and linoleic acid (LA) to induce hypo-pigmentation in B16 tunable model.

The B16 cells were treated with KA or LA at four different time points. The time point where the pigmentation status was apparent between the treated versus control was taken to study the transcriptomic changes. The effect of both the hypo-pigmenting compounds was examined on the expression of melanogenic genes, tyrosinase protein stability and activity, and melanosome maturation.

We found that the expression of *Kdelr1* and *Arfgap1* are downregulated during KA-mediated hypo-pigmentation. These proteins are involved in protein trafficking from one organelle to other. Interestingly, through TEM analysis we found that melanosome gets arrested very early in the process of maturation in the KA-treated cells as compared to control DMEM.

We found the expression of many enzymes involved in cholesterol biosynthesis to be differentially expressed and enriched in the downregulated categories during LA-mediated hypo-pigmentation. The expression of cholesterol biosynthetic genes such as *Hmgcs1*, *Hmgcr, Mvks*, *Mvd1,* etc. was found to be down-regulated.

Interestingly, in the si*Mitf* data, we found transcript from the downregulated category to be majorly associated with cholesterol biosynthesis pathway. Further,

MITF is known to interact with PBAF chromatin remodeling complex that is comprised of BRG1 and CHD7. BRG1 regulates the dynamics of MITF occupancy to the set of regulatory elements. Moreover, a meta-analysis of our microarray with MITF and BRG1 ChIP Seq data showed that key regulators of cholesterol synthesis were downregulated and bound by both MITF and BRG1 transcriptional regulators. Together, our result suggests an essential role of MITF in regulating cholesterol homeostasis during melanogenesis.

Next, we employed genome-wide transcriptomic studies to identify molecular signatures under different conditions to develop a tool in predicting the nature of the compound/modulator in the context of skin pigmentation. After the microarray data analysis, the differentially expressed genes were compared with each other to derive a core set of genes that are involved in maintaining the skin pigmentation homeostasis in B16 cells. Similarly, the signatures were also generated for hyperpigmentation (Forskolin, IBMX, and FAC), hydration (urea and glycerol), and desquamation (resorcinol and salicylic acid). These signatures were included in developing the tool eSKIN software (A computational platform for skin research) by persistent technologies. eSKIN software provides the comprehensive platform for skin research to understand and interpret skin associated high throughput data. Currently, this software is fully operational and is used to predict the nature of unknown compounds by matching their transcriptomic signatures to the core signatures of known compounds present in the skin predict tool of eSKIN database. These signatures are of great importance in developing the tool that can rapidly pre-screen small molecules insilico. Thus, pre-screening will further reduce the number of in-vitro and animal experiments by early elimination of undesirable molecule.

Together, these studies lead to the identification of novel genes and pathways derived from a combination of genome-wide transcriptomics data and validation experiments. Future studies will dissect the role of these regulators/targets in the context of pigmentation. The complete repertoire of pathways derived from our analysis would also facilitate an understanding of pigmentation disorders such as vitiligo and melasma. These regulators could also give insights into development and progression of melanoma with the potential for the development of therapeutics.

Introduction

I. INTRODUCTION

Skin pigmentation is an essential human phenotypic trait and is affected by several factors (Lin and Fisher, 2007; Slominski et al., 2004). Darwin during his journey through HMS beagle observed that skin color is significant character leading to variation among individual. Interestingly, the skin pigmentation can be considered as the demonstration as well as the evidence of natural selection occurred thousand years ago. The skin pigmentation is affected by the type and intensity of UV rays (Jablonski and Chaplin, 2010). The skin pigmentation is itself a product of evolution where early humans have been evolved in high UV environments in equatorial Africa. From Africa, they migrated to a different region having different climatic conditions resulting in variation of skin pigmentation. Depending upon the type, mass, and distribution of melanin deposited in melanosome the human skin color ranges from very dark (Africans) to yellowish pink (Northern Europeans). It is primarily evolved to provide defense against UV radiation penetrating the skin, mechanical and chemical factors (Biniek et al., 2012; Jablonski and Chaplin, 2010; Natarajan et al., 2014a; Yamaguchi et al., 2007).

I.1. The architecture of skin

The skin executes two critical functions by protecting from various external environmental stress and by regulating trans epidermal water loss from the body. It provides an interface between organism and external environment. The skin is embryologically divided into stratified epidermis, dermis and subcutaneous hypodermis (Fig.I.1) (Cichorek et al., 2013; Slominski et al., 2004; Yamaguchi et al., 2007).

Epidermis

The epidermis forms the outer most layer of the skin which consists of 90% keratinocyte cells. The four-distinct layer of the epidermis is formed by dedifferentiation of keratinocyte cells (Madison, 2003). This demarcation divides epidermis into stratum corneum, stratum granulosum, stratum spinosum, and stratum germinativum (Yousef and Sharma, 2018). Stratum germinativum separates the epidermis from the dermis by the single layer of cells. The basal layer comprises two neural crest-derived cells, the Merkel cells, and the melanocyte. The Merkel cells are responsible for the sense of touch whereas; melanocyte is the specialized cells responsible for the skin pigmentation. Melanocytes are present at the junction of epidermis and dermis, eye, hair matrix, mucous membrane, ear and leptomeninges (the pia mater and arachnoid mater covering the brain and spinal cord).

The melanocytes are in close contact with the surrounding keratinocytes with one melanocyte in contact with around thirty-six keratinocytes via their dendritic processes to form epidermal melanin unit. Several enzymes are involved in synthesizing melanin, which is then deposited together with melanosomal structural proteins to form mature melanosome. Formation of melanin polymer from tyrosine (substrate) requires three crucial enzymes, tyrosinase (TYR), tyrosinase-related protein2/dopachrome tautomerase (TRP2 or DCT), and tyrosinase-related protein1 (TRP-1). The melanin formed in melanosome act as a natural sunscreen to protect against harmful ultraviolet radiation and breakdown of folate.

Dermis

The dermis is composed of collagen fibers, elastic fibers and an interfibrillar gel comprising. Glycosaminoglycans, salts and water. Collagen-rich fibroblast, which is

the primary cells of dermis account for tensile strength of the skin's fabric. The dermis is an enclosed network of blood vessels, nerve, sweat glands, hair follicles and sebaceous glands. The hair follicles are the repository of stem cells like melanocyte stem cell, keratinocyte stem cell, dermal stem cell and epidermal neural crest stem cell. Several glycoproteins, glycosaminoglycans, hyaluronic acid is also present in the dermis. Glycoproteins such as laminins fibronectin are primarily involved in cell adhesion, cell migration, and cell-cell communication. The glycosaminoglycans (GAGs) and proteoglycan (PGs) present in the dermis are chondroitin sulfate, dermatan sulfate, keratin sulfate, heparin sulfate, heparin, versican and perlecan.

Hypodermis

The subcutaneous hypodermis layer is present directly below the dermis. Its primary function is to connect the skin to the underlying fibrous tissue of the bones and muscles. Further, it consists of well-vascularized, loose, areolar connective tissue and adipose tissue. These tissues store fat and provide insulation and cushioning for the integument.

I.2. Development of Melanocyte from Neural Crest Cell

Stem cells like neural crest cell are the specialized cells that have a capacity of self-renewal and form different lineages of cells (Sauka-Spengler and Bronner-Fraser, 2008). Neural crest formation requires both inducer (ectoderm & paraxial mesoderm) and competent cell (neural plate). The neural crest is derived from ectoderm of the vertebrate embryo. Because of the plasticity as they get differentiated into different lineages, they are considered to be the "fourth germ layer."

The neural plate, as well as epidermis, contributes to the formation of the neural crest. NCC is divided into four main regions by their characteristic derivatives and the functions they perform (Knecht and Bronner-Fraser, 2002). Although NCC is pluripotent, cells originated from different anteroposterior regions are different. There are four types of neural crest cells, cranial (cephalic) NCC, trunk NCC, Vagal & Sacral NCC and cardiac NCC. The migration of Trunk NCC after neural tube formation follow two pathways namely the ventral and the dorsiventral pathway. Cells which migrate first after neural tube closure follow ventral pathway at the embryonic stage between the days 8.5-10.5 (Gilbert, 2017).

Several fate mapping experiments show that they form sensory, sympathetic neurons, adrenomedullary cells, and Schwann cells. NCC which fail to initiate the process of neurogenesis acquire glial fate termed as Schwann cell precursor (SCP). SCP differentiates into Schwann cells, melanocytes and fibroblast. The cells that follow dorsoventral pathway at the embryonic stage between 10.5-12.5 migrate with limited cell division under the epidermis and basal layer to acquire melanocytic fate. After reaching their final destination under the epidermis, they start expanding and cover the skin of trunk and limbs. Thus, the cells specified to become melanocytes are both spatially as well as temporally separated by the cells destined to become neurons (Ernfors, 2010).

Development of NCC into different lineages depends upon the balance between these extrinsic and intrinsic signaling (Bhatt et al., 2013). FoxD3 is an vital TF which is critical for neural crest cell migration, regulates lineage switch between neuronal cells and melanocytes. FoxD3down regulates the expression of melanocyte-specific TF MITF (microphthalmia-associated transcription factor). Cells which migrate early express FoxD3 in conjunction with other MITF inducing factors like Sox10, Pax3 &

LEF1. FoxD3 interacts with Pax3 and Sox10 and inhibits their binding to MITF promoter. Hence, it inhibits the process of melanogenesis in the cells which are specified to become neurons or glial cells (Mort et al., 2015; Thomas and Erickson, 2009).

MITF functions as the master regulator which is involved in development as well as the survival of melanocyte. MITF genes have alternate promoter organization which generates nine isomers. Among them, MITF-M is selectively expressed in melanocytes. MITF-M is targeted by several TFs, eg. PAX3 (paired box gene3), CREB (cAMP responsive element binding protein), SRY (sex-determining region Y)-box10 SOX10, LEF1 (lymphoid enhancer –binding factor 1). MITF recognizes CAYRTG consensus sequence located in the promoter region of target genes (TYR, TYRP1, DCT, EDNRB, TBX2, MC1R, BIRC1, etc. (Dupin and Le Douarin, 2003; Goding, 2000; Hou and Pavan, 2008; Levy et al., 2006).

The Sox10 function's as a central transcription regulator of neural crest development. It is expressed in the neural crest at the time of migration, and its expression continues in the differentiated cells (Agarwal et al., 2011; Knecht and Bronner-Fraser, 2002). Various experiments suggest that NCC formed in the absence of Sox10 undergo programmed cell death which is mediated by p53. Both Pax3 and Sox10 interact synergistically and regulate survival as well as differentiation of neural crest cell.

Neuregulins-1 (NRG1) and its receptor ErbB2/ErbB3 are required for SCP survival and migration. NRG1 activates Schwann cell differentiation and inhibits differentiation of melanocytes. Schwann cell precursor (SCP) divides rapidly and competes for membrane-bound NRG1 available only when they are in physical contact

with nerves. Cells that have limited neuregulin signaling undergo apoptosis or acquire melanocyte fate (Ernfors, 2010; Yaar and Park, 2012).

Wnt signaling regulates neural crest induction and differentiation during neural crest development. Neural crest cell fates are subjected to temporal control by Wnt/βcatenin (Hari et al., 2012). When it is activated in premigratory NCC, it promotes the formation of neurons whereas suppresses melanocyte formation. In the nervous system, it leads to the patterning of CNS, regulates neuronal growth and survival. Cells which migrate dorsoventrally form melanocytes by activating Wnt pathway. In melanoblasts, binding of Wnt to its transmembrane receptor Frizzled activates MITF transcription. MITF-M promoter has LEF 1 binding site, which is an activator. During embryonic development, there is a gradient of BMPs which is maintained by BMP inhibitors secreted by paraxial mesoderm (noggin, chordin, & follistatin). BMPs belonging to TGF-β family are suppressors of NCC differentiation into both neurons and melanocytes. It induces ectoderm to become epidermal tissue (Yaar and Park, 2012).

Fibroblast growth factors (FGFs) are membrane-bound factors which are expressed by keratinocytes that surround melanocytes and fibroblasts. These FGFs through cell-cell interaction activate proliferation of melanocytes by binding to tyrosinase kinase FGF-receptor2. It acts as a potent melanocyte mitogen that functions as a cAMP stimulator. FGF1 and FGF2 play essential roles in proliferation, differentiation, axonal guidance and survival of cells of the nervous system. Expression of FGF is also seen in the adult nervous system, suggesting its role in maintenance and survival of adult neurons (Guillemot and Zimmer, 2011).

Melanocytes express p75NTR and TrkA as well as NT3 that is a high-affinity receptor. During UV irradiation, keratinocyte (KC) start secreting NGF, which act as a chemotactic signal for melanocyte by inducing dendrite formation and also increases Bcl2 (anti-apoptotic protein). Hence, coordinated expression of p75^{NTR} and TrkA and their binding to NGF and NT3 cytokines released by KCs increases melanocyte survival after UV irradiation. Similar, function is performed in the nervous system and enhances neuronal survival in CNS as well as in PNS. BDNF plays a vital role in the survival of motor neurons by binding to high-affinity TrkB receptor. In the adult nervous system, they also regulate synaptic plasticity and neuronal survival (Hock et al., 1998).

Many signaling molecules are involved in the migration of melanocytes and neurons to their final destination. Steel factor (also known SCF, kit ligand and CD117) is one of them. Kit ligand expressed by keratinocytes and the c-kit receptor is present on melanocyte. As soon as the receptor is expressed by melanocytes and kit ligand by KCs, they start migrating towards skin and hair follicles. Several disorders are caused due to a mutation in either ligand or receptor. Piebaldism is an autosomal dominant disorder caused by a mutation in kit ligand or c-kit receptor causing depigmented patches present on trunk and forehead. In this disorder, melanocytes fail to migrate to the skin. Endothelins (21aa long proteins) formed by proteolysis of larger precursor molecule characterized by their vasoactive properties. This family of proteins includes ET1, ET2, and ET3. These receptors are present in melanocytes and neuronal cells. During UV irradiation, ET1 synthesized and secreted from keratinocytes, binds to EdrnA on melanocyte and induces photoprotective responses. Signaling molecules activate downstream pathways by binding to their receptor. Two major signaling pathways shared by melanocytes and neurons protein kinase C (PKC) –dependent pathway and p53-dependent pathway. Receptor such as EdrnA, EdrnB, Trk and FGF

when get activated, leads to the formation of secondary messenger diacylglycerol which further activates PKC. PKC phosphorylates serine/threonine residues many downstream targets proteins. Melanocytes express five isoforms of PKC to regulate melanin formation, survival after stress and dendrite formation. PKC β is mainly envolved in regulating the activity of tyrosinase present in melanosome by phosphorylating it. During UV irradiation, Trk and Eden get activated to facilitate melanocyte survival (activation of anti-apoptotic factor Bcl2) and transfer of melanosome from melanocytes to keratinocytes by extending dendrites. This is mainly achieved through mediating cleavage of diacylglycerol and activation of PKC.

Tumor-suppressing protein p53 plays an essential role during cellular stress. It regulates DNA damage repair, cell cycle arrest, and apoptosis. UV irradiation both directly by DNA damage and indirectly through activators like H_2O_2 activates p53. Activated p53 increases the process of melanogenesis by upregulating mRNA and protein of tyrosinase enzyme. p53 also activates transcription of proopiomelanocortin (polypeptide precursor of alpha MSH), an inducer of melanogenesis.

I.3. Epidermal Melanin Units: Melanocyte-Keratinocyte Interactions

The epidermal melanin unit composed of one melanocyte that is surrounded by approximately 35-40 keratinocyte presents at the basal layer of the epidermis (Cichorek et al., 2013). It is a functional unit which produces and distribute melanin-containing melanosome from melanocyte to keratinocyte. The melanin is synthesized in a specialized organelle called melanosome. The melanin-loaded melanosomes are translocated from their site of formation in the perinuclear cytoplasm towards the melanocyte dendrite tips with the help of microtubule- and actin-based motor proteins. They are then transferred into the surrounding keratinocytes where they are dispersed

into the cytoplasm (Fig.I.2). The movement of the melanosomes is bidirectional where the retrograde movement is controlled by dynein and the anterograde movement by kinesin. Dispersion of pigment granules is brought about by kinesin whereas cytoplasmic dynein is responsible for the pigment aggregation (except in fishes where it mediates distribution). At the tip of the dendrites, the melanosomes are captured by the myosin Va in the actin-rich region. Myosin Va enables melanosome to bind to the actin through the linker proteins Rab27A and melanophilin (Mlph) (Hearing, 2011b; Natarajan et al., 2014a).

Two types of melanin are synthesized within melanosomes, the eumelanin which is a dark-brown to black insoluble polymer and pheomelanin which is a light red-yellow sulfur containing the polymer. Tyrosine, a substrate for tyrosinase is formed in the cytoplasm of melanocyte from phenylalanine with the help of enzyme phenylalanine hydroxylase. Tyrosine is then transferred from cytoplasm of melanocyte to melanosome where three essential enzymes reside (Slominski et al., 2004). The enzyme tyrosinase that brings about this conversion is a 60-70 kDa glycoprotein which catalyzes the hydroxylation of the monophenol L-tyrosine to the o-diphenol 3,4 dihydroxyphenylalanine (DOPA) (Fig.I.3). The conversion of tyrosine to DOPA is considered the rate-limiting step in melanin biosynthesis. Next hydroxylation of DOPA leads to the formation of DOPAquinone. The DOPAquinone rapidly cyclizes, decarboxylates and oxidizes to form DHI-melanin. In the presence of DCT, the carboxylic acid group of DOPAchrome is maintained, and DHICA-melanin is formed instead of DHI-melanin the former is more soluble is of lower molecular weight and lighter color. DHI and DHICA form oligomeric structure through covalent bonding, and they are considered as the primary molecular units of melanin. Further, the

secondary structure of melanin is still controversial (Ando et al., 2007; Hearing, 2011a; Park et al., 2009).

The proton level in melanosomes is regulated by the cascades of four ion transporters, vacuolar proteins, ATPases Na^+/H^+ exchangers, SLC24A5 and TPC2. The net result of these transporters is to create low acidity (neutral pH) environment that leads to high tyrosine and less cysteine forming a dark color phenotype. The activity of tyrosinase enzyme is maximum at this pH. Polymorphism of these ion transporters would make melanosome acidic and then results in the suppression of eumelanogenesis (Ancans et al., 2001; Kondo and Hearing, 2011).

Regulation of skin pigmentation homeostasis is critical since prolonged activation of melanogenesis can have disastrous consequence because it is an energy-intensive pro-oxidative process. The mechanism how epidermal cells recovers to the basal state is less understood. The only pathway known is the programmed shedding of corneocyte to get rid of melanin granules.

Recently, the role of cytokine IFN-gamma is identified in regulating the temporal skin pigmentation. The IFN-gamma through stalling the maturation of melanosome ensures the faster recovery of basal pigmentation (Natarajan et al., 2014b).

Many factors play a role in increased pigmentation, an increase in pigmentation over and above the constitutive basal level is referred to as tanning. One of the chief factors to play a role in tanning is exposure to ultraviolet radiation. This leads to an immediate darkening of skin called as immediate tanning response and a delayed darkening of the skin that takes place over a couple of days called the delayed tanning response. These changes are due to the oxidation and polymerization of existing melanin and their redistribution to the surrounding keratinocytes. In the delayed

tanning, the response takes longer time due to the regulation of several pathways taking place inside the melanocyte (Natarajan et al., 2014a).

The exposure of UV rays leads to the increased expression of transcription factor MITF that by binding to the promoter of important melanogenic genes like TYR, TYRP1, DCT, PMEL, etc. controls the process of pigmentation. The UV spectra is broken down into UVA (320-400 nm) UVB (280-320nm) and UVC (100-280nm). The UVC spectrum is absorbed by the ozone layer and is not present in sunlight reaching earth surface. The melanin synthesis inhibits the formation of carcinogenic cyclobutane pyrimidine dimer and pyrimidine photoproducts. Melanin leads to the movement of unpaired electrons between different energy levels and this, in turn, helps in the absorption of UVR. The increased pheomelanin lead to increased risk of melanoma due to its photosensitinsing effect. p53 is said to play a role in the UV induced pigmentation response. In dark-skinned individuals, the UV does not penetrate deep enough to induce a maximal p53 response. However, the response in case of light-skinned individuals is optimum and p53 activation, in turn, leads to the upregulation of the melanogenic enzymes which lead to increased melanosome formation and subsequent transfer to keratinocytes via the melanocyte dendritic processes.

Melanosomes are large organelle (diameter,500nm) and they are visible under the bright-field microscopy (Marks and Seabra, 2001). They are lysosome-related organelles and are comprised of compartments carrying secretory cargoes. They seem to share some protein like acid hydroxylases and lysosomal-associated membrane proteins (LAMP) with lysosomes and are appeared to be derived from endosomes. Melanosomes have considered as an excellent model organelle for the study of organelle biogenesis and motility. The ultrastructural studies have revealed four embryonically distinct stages of melanosome (Fig.I.4). Melanosome shows four

characteristic stages that have incorporation of multiple structural and enzymatic proteins. Stage I are non-pigmented vacuolar structure derived from the endosomal system. Stage II is characterized by the presence of internal striation. These striations are formed by the cleavage structural protein PMEL17/silver/gp100. Critical melanogenic enzymes TYR and TYRP1 are trafficked to stage II melanosome to initiate the process of melanin formation and eventually give rise to stage III melanosome. Stage I and II are also known as premelanosome stages. Melanin deposition on this formed striation starts from the stage III and eventually give rise to mature, fully melanized stage IV melanosomes. There are two possible models for stage I melanosome formation. One of them suggests that stage I melanosomes arise directly from the ER, and the other suggests that it derives from the compartments of the late secretory (post-Golgi) and or endocytic pathways. The structural protein present in melanosomes that is responsible for the fibrillar striations is the Pmel17/ silver/gp100 protein (Raposo and Marks, 2007; Schiaffino, 2010).

The various possible mechanism for melanosome has been suggested on the basis of data derived from early light and electron microscopy studies. In exocytosis first, the melanosomal membrane fuses with the plasma membrane of the melanocyte. This is followed by the release of melanosomes in the intracellular spaces and then phagocytosis by the surrounding keratinocytes. Cytophagocytosis involves the keratinocytes engulfing the entire melanocyte dendritic tip containing the melanosome. The engulfed melanocyte then undergo fusion with the lysosomal membranes and the phagolysosomes then break up to release the pigment granules. In the fusion of plasma membrane and transfer by membrane vesicle, the melanocyte dendrites show the presence of thin filopodia. To transfer melanin containing melanosome these filopodia fuses with the plasma membrane of keratinocyte. In transfer by vesicles, the

melanosome filled vesicles are shed from melanocytes this is followed by phagocytosis and then fusion with the keratinocyte plasma membrane. Protease-activated receptor-2 (PAR-2) plays an important role in the transfer of melanosomes to keratinocytes. This is a seven transmembrane G-protein which induces keratinocyte phagocytosis, in vivo PAR-2 activation results in increased melanin deposition and inhibition leads to disruption of melanosomal processing (Chen et al., 2009; Hearing, 2011b; Marks and Seabra, 2001; Natarajan et al., 2014a).

I.4. Microphthalmia-Associated Transcription Factor (MITF) and signaling pathways involved in melanogenesis

MITF is the master regulator of melanocyte development, differentiation, and survival. It belongs to the basic helix-loop-helix (bHLH) of the transcription factors with TFE3, TFEB, and TFEC. These family of transcription factors binds to the consensus sequence (Goding, 2000; Widlund and Fisher, 2003). CA [T/A] GTC was known as E-box. There are nine isoforms of MITF that have tissue-specific expression. MITF-M is selectively expressed in melanocyte and retinal pigment epithelium cells, whereas other isoforms are shown as express in non-pigmented cells that includes osteoclast and mast cells (Bharti et al., 2008; Shibahara et al., 2001).

The heterozygous mutation in MITF causes Waardenburg Syndrome Type IIA that exhibit congenital white forelock and deafness. Moreover, complete loss of MITF leads to loss of pigmentation due to the absence of melanocyte rather that loss of melanin synthesis (Cortes-Gonzalez et al., 2016).

MITF has a crucial role in the regulation of proliferation, invasive and properties of melanoma cells. In melanomas, MITF act as lineage-specific survival oncogenes and has been seen to be amplified in 5-20% of melanoma (Shain and Bastian, 2016). To

explain the regulation by MIF rheostat model has been proposed. The level of MITF has a paradoxical role where it can have a pro-survival and anti-survival effect. The low level of MITF corresponds to the increased motility, and invasive capacity of melanoma cells and higher levels are associated with increased proliferation capacity. The invasiveness and proliferation are regulated by the expression of DIAPH1, involved in actin polymerization. At the low level of MITF invasiveness is controlled by downregulation of Dia1, p27 ^{Kip1} and reorganization of the actin cytoskeleton (Goding, 2011; Wellbrock and Arozarena, 2015).

The expression of MITF is regulated at both transcriptional and post-transcriptional level. At the transcriptional level, it is controlled by several TF's like paired box gene 3 (PAX3), sex determining region Y-box10 (SOX10), cAMP-responsive element binding protein (CREB), lymphoid enhancer binding factor-1 (LEF1/TCF), one cut domain 2(ONE CUT-2) and MAPK signals. The post-transcriptional level of MITF is regulated by phosphorylation, sumoylation, and ubiquitination. The phosphorylation of MITF is done by MAPK pathway. C-kit phosphorylates MITF at the Ser73 residue by ERK2 and Ser409 by p90 ribosome kinase. MITF phosphorylated at Ser73 recruits coactivators p300 and also targets MITF for ubiquitination and proteolysis (Carreira et al., 2005; Carreira et al., 2006; Goding, 2000; Strub et al., 2011; Wellbrock and Arozarena, 2015; Widlund and Fisher, 2003).

Sumoylation of MITF is mediated by PIAS3 (protein inhibitor of activated STAT3). Both PIAS3 and PKC together represses the transcriptional activation of MITF by interacting directly with MITF thereby inhibiting its DNA-binding activity. Studies through pedigree analysis have shown that mutation of sumoylation site leads to the development of melanoma in the predisposed family members (Levy et al., 2002).

Through high throughput studies, it has been shown that MITF regulates several targets. The methods like DNA microarray on melanocyte and melanoma, ChIP coupled to sequencing. The target of MITF include genes involved in pigmentation (Tyr, Dct, Tyrp1, AIM-1, MART-1, PDE4D3), survival (BCL2, BCL2A1, BIRC7), motility and invasive (c-Met, SLUG), metabolism (PGC-1α), oxidative stress (APEX1/REF1, HIF1α) (Hoek et al., 2008; Strub et al., 2011).

There are several pathways which control pigmentation response. In response to external stimuli, some signals are generated which may trigger the basal melanocyte population with the help of POMC (proopiomelanocortin) and its derivatives. The POMC is produced in the pituitary and is also synthesized in the epidermal keratinocyte. The derivatives of POMC include α- MSH and ACTH, which bind to the Melanocortin 1 receptor (MC1R) this is a family of five related proteins with seven transmembrane domain (GPCR). α- MSH functions mainly through elevating cyclic adenosine monophosphate levels in the cell. Activation of the frizzled receptor by Wnt, in turn, leads to the activation of downstream effector molecules like beta-catenin, Rho GTPase, PKA, PKC. The beta-catenin enters the nucleus and interacts with the LEF1/TCF family of transcription factors; these, in turn, modulate transcription of target genes. KIT and EDNRB signal pathways induce the phosphorylation of MITF in mature melanocytes. MITF acts on its downstream target genes like Bcl2 (anti-apoptotic gene), MET which is involved in survival, p16, p21, CDK2, tbx2 involved in proliferation and TYR, TRP1, SILVR, DCT, MART1, AIM1, MC1R involved in differentiation.

I.5. Chromatin regulation of skin pigmentation

Cellular processes like growth, development, differentiation, DNA repair and replication take place due to strict regulation of genetic material. The tightly compacted

structure of chromatin inhibits access of transcription factors and other machinery to the promoter of specific genes by sequence recognition (Razin et al., 2007; Razin and Ulianov, 2017). So, active transcription occurs when chromatin is relaxed. Cells have distinct sets of the specific mechanism, i.e., histone modification and chromatin remodelers to regulate the chromatin architecture (Cutter and Hayes, 2015; Poirier et al., 2009; Sadakierska-Chudy and Filip, 2015; Ye and Heng, 2017). The nucleosome is the fundamental component of chromatin in the nuclei consisting of four histones H2A, H2B, H3, and H4 that form the octamer center of the nucleosome with 146 nucleotide pairs wrapped around the center 1¾ turns. H1 histone plays a role in linking the nucleosome structures together to condense chromatin (Sadakierska-Chudy and Filip, 2015).

Histones protein undergoes posttranslational modification at amino-terminal tails present at the surface of nucleosome as well as on the core region (Cosgrove 2004). These modifications are methylation, acetylation, phosphorylation, sumoylation, and ubiquitinylation. Enzymes that post-translationally and covalently modify chromatin structure are histone acetyltransferases (HATs), histone deacetylases (HDACs), kinases, methyltransferase and demethylase (Li et al., 2018; Zou and Mallampalli, 2014). Histone modifications affect chromatin compaction through at least two distinct mechanisms(Bannister and Kouzarides, 2011; Bottomley, 2004). First, the change in the structure of histones or their binding to DNA because of altered electrostatic charge. Second, these modifications act as binding sites for protein recognition modules, such as the bromodomains (recognize acetylated lysine) or chromodomains (identify methylated lysine). Histone modifications and recognition modules form "histone code" (Gallagher et al., 2015; Yun et al., 2011).

Histone variants also play an essential role in regulating chromatin compaction by replacing canonical histones. (Histone replacement model) (Kamakaka and Biggins, 2005). The acetylation occurs on the conserved lysine residues of N-terminal tail. H3k4 methylation act as an active gene-specific modification mark that recruits the preinitiation complex on promoters during transcriptional activation in both yeast and mammalian cells. Proteins that contain SET domain methylate's the lysine present in the N-terminal tail of histones. The SET domain-containing SUV39H1 protein methylate's specifically H3K9 and represses transcription through the recruitment of HP1(Das and Tyler, 2013; Henikoff and Smith, 2015). The HDAC10 is known to control the expression of melanogenic promoters like TYRP1, DCT, MITF by forming the ternary complex with Pax3 and KAP1 (Lai et al., 2010).

Cells have evolved set of specialized chromatins remodeling enzymes which by ATP hydrolysis move, destabilize, eject or restructure the nucleosome. There are four different families of chromatin remodeling complexes. SWI/SNF, ISWI (Imitation Switch), CHD (Chromodomain), NuRD (Nucleosome Remodeling and Deacetylases) and INO80 (inositol requiring 80). All of them utilize ATP hydrolysis to alter histone-DNA contacts and share a similar ATPase domain. The SWI/SNF family includes yeast Snf2 and Sth2, Drosophila melanogasterbrahma (BRM) and mammalian BRM and Brahma-related 1 (BRG1). The ATPase subunit of the SWI/SNF family of proteins has a bromodomain which preferentially binds acetylated histones (Tessarz and Kouzarides, 2014; Zhang et al., 2016).

In spite of recent approaches, the epigenetic regulation of pigmentation is still incomplete. Recently, SWI/SNF was shown to be required for activation of a subset of MITF regulated genes (Mehrotra et al., 2014). Using fibroblasts model where MITF is ectopically expressed within an inducible dominant negative version of BRM or

BRG1, activation of tyrosinase, TRP1, and TRP2 are shown to be dependent on afunctional SWI/SNF. It was further demonstrated that SWI/SNF is recruited to and remodels chromatin structure on the TRP1 promoter. Chromatin immunoprecipitation studies illustrate binding of both MITF and BRG1 to the TRP1 and tyrosinase promoters (Marathe et al., 2017; Ondrusova et al., 2013; Vachtenheim et al., 2010).

MITF novel interactome has been identified by performing tandem affinity purification and mass spectroscopy. It has been found that the novel cofactors identified by this technique are involved in regulating transcription, DNA replication and repair and chromatin organization. BRG1 has been shown to control the proliferation of normal melanocyte. MITF has been shown to interact with PBFA chromatin remodelers complex that comprises of BRG1 and CHD7. Both MITF and SOX10 recruit BRG1 to the MITF-associated regulatory complex (MARE) of active enhancers (Fig.I.5) (Laurette et al., 2015).

The ISWI family contains a SANT (SWI3, ADA2, N-CoR and TFIIIB B) domain and the absence of a bromodomain. The SANT domain preferentially binds to nucleosomes containing linker DNA over core nucleosomes (Boyer et al., 2004). The CHD (chromodomain, helicase, DNA binding) family remodelers interact with methylated histone tails. CHD family remodelers contain two tandem chromodomain at their N- terminal region. hCHD1 tandem chromodomains bind H3K4me2 or me3, marks correlated with active chromatin. Some of the CHD members also have a repressive role, namely Mi-2/NuRD (nucleosome remodeling and deacetylase) complex containing histone deacetylases (HDAC1/2) and methyl CpG-binding domain (MBD) proteins (Zhang et al., 1999). Some CHD remodelers function by sliding or emitting nucleosomes resulting in enhanced transcription of genes. Members of the CHD family often contain DNA-binding domains, Plant Homeo Domains (PHD), BRM

and Kismet domains (BRK), and SANT domains. (Micucci et al., 2015) IN080 family of remodelers contains ten subunits having split ATPase domain. They play an essential role in transcriptional activation and DNA repair processes. They are also involved in restructuring the nucleosome by replacing the canonical H2A-H2B dimers with H2A.Z-H2B variants of histone (Bartholomew, 2014; Henikoff et al., 2004).

I.6. Disorders of Pigmentation

Skin color is a complex trait which is controlled by numerous genes. The visible difference in the skin color is due to variation in the size and number of melanosomes but not due to the amount of melanocyte. Disorders of pigmentation can result from the impairment of melanosome transfer from melanocyte to keratinocyte, defect in melanin synthesis, defect in degradation and removal of melanin (Fig.I.6). During embryogenesis abnormalities in the migration of melanocyte from neural crest cells also lead to pigmentation disorders. Also, the pigmentation disorders can also be due to the immunologic or toxic mediated destructions of melanocytes. Table I.2 shows the cloned mice pigmentation genes with corresponding phenotypes. The human orthologs along with their disease condition, if any, are indicated [Modified from (Bennett and Lamoreux, 2003)].

Disorders of pigmentation are classified in hypo- or hyperpigmentation which can occur as a genetic or acquired disease (Rees, 2011).

I.6. 1. Hypopigmentation Disorders

Hypopigmentation is classified by the age of onset of the disorder and involved pathogenesis mechanisms. Hypopigmentation phenotype has been characterized by various patterns, e.g., diffuse, localized, linear and patchy. The diffuse hypopigmentation phenotype

is present at the time of birth or can manifest during childhood. The two diffuse form can occur in the individual where the hair, skin, and eyes are affected whereas in second group skin and hair is affected.

Piebaldism and Waardenburg syndrome is caused due to abnormal migration of melanoblasts during the neural crest migration in the skin. The piebaldism phenotype is characterized by a pigment deficient white forelock on the middle of the forehead, eyebrows, and chin, and on the central portion of the thorax, and abdomen. The margins of hypopigmented areas are surrounded by the patches of hyperpigmentation. Piebaldism is inherited in an autosomal dominant pattern, and Waardenburg syndrome in an autosomal recessive manner. Albinism (incidence of 1:5000–1: 40 000) is a hereditary pigmentation deficiency caused due to a genetic defect in tyrosinase. Albinism patients have poor vision as well as very light hair and skin. Menkes syndrome is an X-chromosome disorder in which the copper metabolism is affected. For the tyrosinase enzymatic activity copper plays an essential role. During copper deficiency, the oxidation of tyrosine to DOPA is diminished and thus lead to hypopigmentation. The gene responsible for Menkes syndrome is copper-transporting ATPase.

Phenylketonuria (incidence of 1:6 000–1:16 000) is an autosomal recessive metabolic disorder which caused due to a deficiency in phenylalanine hydroxylase. This lead to lack of synthesis of tyrosine, a substrate for melanin synthesis.

Abnormal melanosome biogenesis causes Hermansky-Pudlak (HPS) and Chediak-Higashi syndrome (CHS) disease. It is characterized by the defect in the biogenesis of lysosomal organelles including melanosomes. Griscelli syndrome (GS) is caused due to abnormal melanosome transfer to the dendrites. As a result, the

melanosome remains accumulated in the melanocyte. Elejalde syndrome patients are characterized by a silvery hair due to the abnormal melanosome transfer from the melanocytes to the keratinocytes.

Vitiligo (incidence of 1:200) is an autoimmune disorder that is caused due to the destruction of melanocytes.

I.6. 2. Hyperpigmentation Disorder

The increased skin pigmentation can be due to skin adaptation to UV rays like tanning response or unrepaired DNA damage to skin cells (e.g., metastasizing melanoma). Addison disease is caused due to adrenal cortical insufficiency and is characterized by a diffuse brown coloration. In 50% of the patients, it is an autoimmune disorder whereas, in 25–30 % autoantibodies against the adrenal cortex tissue have been detected. Acromegaly and Cushing syndrome is caused by activation of melanogenic genes in melanocyte by the action of MSH. Both are characterized by diffuse hyperpigmentation. The Café-au-lait spots are one of the phenotypes occurs during neurofibromatosis. These spots have normal pigmentation with a sharp border. The brown color spots are formed due to increased melanin accumulation in the melanocytes.

Melasma is a hyper pigmentary patch that occurs predominantly in the women due to hormonal changes. There are two types of melasma, epidermal and dermal types, depending upon the region where melanin is getting deposited. In epidermal type, the melanin is accumulated in the basal and suprabasal whereas in the cutaneous nature it is in the perivascular macrophages of the upper and deep vascular plexus.

I.7. Summary

Skin act as an interface between the organism and the external environment. It consists of embryologically distinct layers called epidermis (derived from ectoderm) and dermis (derived from mesoderm). Melanocyte present at the basal layer of the epidermis has an essential function to play. The epidermal-melanin unit involves interacting melanocyte and keratinocyte, which together forms a functional unit necessary for melanogenesis. The melanin is synthesized inside the lysosome-like organelle called melanosome. Melanin act as a natural sunscreen that protects against harmful UV radiation. In the melanosome reside three crucial melanogenic enzymes, TYR, TYRP1 and DCT. Tyrosinase is a rate-limiting enzyme in the process of melanin synthesis. Disruption of its function leads to several hypopigmentation disorders.

Although studies on pigmentation genes and the mechanism of pigmentation have been going on for the past 100 years the regulation of pigmentation genes in respect to the epigenetic control is still unclear. Recent studies have shown that SWI/SNF complexes are required for activation of a bunch of MITF regulated genes in various cell lines. This interaction is further validated in several autoimmune disorders like SLE and rheumatoid arthritis. The epigenetic basis gives indirect evidence for an epigenetic role in depigmentation disorders like vitiligo which is said to have an autoimmune basis. All this aspect of skin pigmentation together is necessary to understand the cause or origin of several pigmentation disorders and the process of tanning.

Table. I.1. Summary of the cloned mice genes with their chromosome locations. The information on human syndromes was obtained from OMIM. The genes are categorized into melanocyte development, components of melanosomes and their precursors, melanosome construction/protein routing, melanosome transport, eumelanin and pheomelanin and systemic effects. The highlighted genes indicate transcription factors. The legend for the symbols in the syndrome column is given below:

N: none known, BCL: B-cell lymphoma, CHS: Chediak–Higashi syndrome, GS: Griscelli syndrome, OA: ocular albinism, OCA1-4: oculocutaneous albinism types 1–4, PS: piebald syndrome, RH: red hair (included although not a defect), US 1B: Usher syndrome, type 1B, WS1-3: Waardenburg syndrome types 1–3, WSS: Waardenburg–Shah syndrome (Waardenburg syndrome type 4).

Symbol (old symbol)	Name (old name)	Chromosome	Function	Human symbol	Human chromosome	Syndrome
Melanocyte development						
Edn3 (ls)	Endothelin 3 (lethal spotting)	2	Growth and differentiation factor	EDN3	20q13	HD, WSS
Ednrb (s)	Endothelin receptor type B (piebald spotting)	14	Growth factor receptor	EDNRB	13q22	HD, WSS
Kit (W)	Kit oncogene (white spotting)	5	Growth factor receptor	KIT	4q11-q12	PS
Kitl (Sl)	Kit ligand (steel)	10	Growth and differentiation factor	KITLG	12q22	N
Lmx1a (dr)	LIM homeobox transcription factor 1α (dreher)	1	Transcription factor	LMX1A	1q22–23	N
Mitf (mi)	Microphthalmia-associated transcription factor (microphthalmia)	6	Transcription factor	MITF	3p12–14	WS2
Pax3 (Sp)	Paired box gene 3 (splotch)	1	Transcription factor	PAX3	2q35	WS1, WS3
Snai2	Snail homolog 2/Slug	16	Transcription factor	SNAI2	8q11	WS2
Sox10 (Dom)	SRY-box containing gene 10 (dominant megacolon)	15	Transcription factor	SOX10	22q13.1	WSS
Sox18 (rg, Dcc1)	SRY-box containing gene 18 (ragged, dark coat color 1)	2	Transcription factor	SOX18	20q13.33	N
Wnt1	Wingless-related MMTV integration site 1	15	Growth factor/morphogen	WNT1	12q13	N
Wnt3a	Wingless-related MMTV integration site 3A	11	Growth factor/morphogen	WNT3A	1q42	N
Components of melanosomes and their precursors						
Dct (slt)	Dopachrome tautomerase (slt)	14	Melanosomal enzyme	DCT	13q31-q32	N
Gpnmb	Glycoprotein (transmembrane) NMB	6	Apparent melanosomal component	GPNMB	7p15	N
Matp (uw)	Membrane-associated transporter protein (underwhite)	15	Apparent transporter	MATP	5p	OCA4
Rab38 (cht)	RAB38, member RAS oncogene family (chocolate).	7	Targeting of Tyrp1	RAB38	11q14	N
Si (si)	Silver (silver)	10	Melanosome matrix	SILV	12q13-q14	N
Tyr (c)	Tyrosinase (color, albino)	7	Melanosomal enzyme	TYR	11q21	OCA1
Tyrp1 (b)	Tyrosinase-related protein 1 (brown)	4	Melanosomal protein	TYRP1	9p23	OCA3
Melanosome construction/protein routing						
Oa1	Mouse homolog of human ocular albinism 1 (Nettleship-Falls)	X	Melanosome biogenesis and size	OA1	Xp22.3	OA
p	Pink-eyed dilution	7	Glutathione transport in ER. Melanosomal protein processing and routing.	P	15q11-q12	OCA2
Lyst (bg)	Lysosomal trafficking regulator (beige)	13	Organelle biogenesis and size	LYST	1q42	CHS
Melanosome transport						
Mlph (ln)	Melanophilin (leaden)	1	Melanosome transport	MLPH	2q37	N
Myo5a (d)	Myosin Va (dilute)	9	Melanosome transport	MYO5A	15q21	GS
Myo7a (sh-1)	Myosin VIIa (shaker-1)	7	Melanosome transport (pigmented retina)	MYO7A	11q13.5	US 1B
Rab27a (ash)	RAB27A, member RAS oncogene family (ashen)	9	Melanosome transport	RAB27A	15q15-q21	GS
Eumelanin and pheomelanin						
Mc1r (e)	Melanocortin 1 receptor (extension)	8	Eumelanin/pheomelanin switch (among others)	MC1R	16q24.3	RH
Systemic effects						
Bcl2	B-cell leukemia/lymphoma 2	1	Inhibitor of apoptosis	BCL2	18q21.3	BCL

(Modfied from Bennett DC., 2003)

Aims and Objectives

AIMS AND OBJECTIVES

Skin pigmentation is primarily evolved to provide defense against the harmful UV radiation**.** Pigmentation is an outcome of the interplay between melanocytes and keratinocytes. Melanocyte produces melanin which gets sequestered within specialised organelles called melanosomes. The process of pigmentation involves biogenesis, maturation, and transfer of melanosomes to keratinocyte. The melanin formation inside the melanosome requires three critical enzymes, TYR, TYRP1, and DCT. The transcription factor MITF governs the expression of these melanogenic enzymes by binding to the M-box sequence present at the promoter. The skin pigmentation is controlled at multiple step and dysregulation of any of these enzymes or pathways leads to either hypo- or hyper-pigmentation. Further, the genetic alteration affecting the melanocyte regulation often results in visible and yet viable phenotype. This advantage can, therefore, be used to design large-scale molecule-based screens. These studies can be conducted to dissect the new molecular mechanism by which pigmentation homeostasis is regulated. Chemical perturbation followed by genome-wide transcriptomics studies provide an opportunity to elucidate molecular mechanisms by which melanogenesis is regulated. Although pathways underlying hyperpigmentation have been identified, negative feedback regulatory loops that control the activated melanogenesis process are not entirely understood. Therefore, we used chemogenomic profiling to identify novel regulators of melanogenesis.

This project aims to understand the regulatory mechanism underlying skin pigmentation homeostasis. Although high throughput studies have identified the subset of MITF target genes, these studies are conducted in constitutively pigmented or weakly pigmented cell lines. Therefore, a comprehensive picture of the complex pigmentation

homeostasis remains unclear. Keeping in mind this lacuna, we used a small molecule-based tunable model of melanogenesis in B16 cells to address the following questions:

What are the novel genes and regulators involved in melanogenesis? Is there MITF -independent genes that are involved in melanogenesis? Besides regulating the activity or protein stability of tyrosinase, what other regulators or signaling pathways that are implicated in the process of hypo-pigmentation? Since they are destined to form melanin, what are the consequences of hypo-pigmentation on melanocytes?

Materials and Methods

II.1. List of plasmids

Plasmid	Relevant Description	Source
pGL4.23[luc2/minP]	Vector encodes synthetic firefly (Photinus pyralis) luciferase reporter gene *luc2,* Ampicillin resistance	IGIB
pGL4.75[*hRluc*/CMV]	Vector encodes Renilla ((Renilla reniformis) luciferase reporter gene *hRluc,* Ampicillin resistance	IGIB
pmCherry-C1	Mammalian Expression Vector with N-terminal mCherry tag, Kanamycin resistance (bacterial selection), neomycin (mammalian selection)	IGIB
SY1	Tyrosinase (*Tyr*) promoter cloned upstream of luciferase gene (*luc2*) in pGL4.23 vector backbone	This work
SY2	Tyrosinase-related protein 1 (*Tyrp1*) promoter cloned upstream of luciferase gene (*luc2*) in pGL4.23 vector backbone	This work
SY3	Dopachrome tautomerase (*Dct*) promoter cloned upstream of luciferase gene (*luc2*) in pGL4.23 vector backbone	This work
SY4	Microphthalmia-associated transcription factor (*Mitf*) promoter cloned upstream of luciferase gene (*luc2)* in pGL4.23 vector backbone	This work
pM40a1-2	mCherry coding region including an initiation codon (ATG) and lacking in-frame stop codon present at the N-terminal of cloned SLC24A4	This work

II.2. List of oligonucleotides

RT-PCR Primers				
Primer	**Length**	**Sequence**	**Locus**	**Notes**
ONM1	22	5'-CGTAATCCTGGAAACCATGACA-3'	*Tyr*	5' RT primer for *Tyr*
ONM2	26	5'-GTCAAACTCAGACAAAATTCCACATC-3'	*Tyr*	3' RT primer for *Tyr*
ONM3	23	5'-GATCCGTTCTAGAAGCACCAAGA-3'	*Tyrp1*	5' RT primer for *Tyrp1*
ONM4	23	5'-CCTCAGCATAGCGTTGATAGTGA-3'	*Tyrp1*	3' RT primer for *Tyrp1*
ONM5	22	5'-TAATTGTGGAGGCTGCAAGTTC-3'	*Dct*	5' RT primer for *Dct*
ONM6	18	5'-AGGATGGCCGGCTTCTTC-3'	*Dct*	3' RT primer for *Dct*
ONM37	20	5'-CATCATCAGCCTGGAATCAA -3'	*Mitf*	5' RT primer for *Mitf*
ONM38	20	5'-TCAAGTTTCCAGAGACGGGT-3'	*Mitf*	3' RT primer for *Mitf*
ONM99	21	5'-CAACTTTGGCATTGTGGAAGG-3'	*Gapdh*	5' RT primer for *Gapdh*
ONM100	18	5'-AGCCTTGGCAGCACCAGT-3'	*Gapdh*	3' RT primer for *Gapdh*
ONM121	19	5'-TGGACGGAGAGACCAAGCA-3'	*Pmel*	5' RT primer for *Pmel*
ONM122	20	5'-GGAGCTGAAGGGCAAAGATG-3'	*Pmel*	3' RT primer for *Pmel*
ONM209	21	5'-GGTGCCAAGAAGTGGGTTTTC-3'	*Hmgcs1*	5' RT primer for *Hmgcs1*

RT-PCR Primers				
Primer	**Length**	**Sequence**	**Locus**	**Notes**
ONM210	17	5'-GCCAGGCTTGCCCATTG-3'	*Hmgcs1*	3' RT primer for *Hmgcs1*
ONM211	19	5'-CGTGGGCCTTCAGTTGGTT-3'	*Hmgcs1*	5' RT primer for *Hmgcs1*
ONM212	29	5'-GTGTTATTTATACTGGGTTTGGAAATGTT-3'	*Hmgcs1*	3' RT primer for *Hmgcs1*
ONM213	29	5'-GCTAAGTAGTGCTAAATAGTTCTTGACGA-3'	*Hmgcr*	5' RT primer for *Hmgcr*
ONM214	27	5'-CAAAGACTCACAGAGATAAATGCAGTG-3'	*Hmgcr*	3' RT primer for *Hmgcr*
ONM215	23	5'-TTGGTTACTACATCTTCCGAGGG-3'	*Tm7sf2*	5' RT primer for *Tm7sf2*
ONM216	19	5'-CTCAAGACCAGCCACGCTG-3'	*Tm7sf2*	3' RT primer for *Tm7sf2*
ONM217	18	5'-CCGTGCCTGGCAGGAGTA-3'	*Tm7sf2*	5' RT primer for *Tm7sf2*
ONM218	27	5'-GCTTCAGTAGACATAGGGTATGATTCG-3'	*Tm7sf2*	3' RT primer for *Tm7sf2*
ONM219	21	5'-CCATTGAAGAAGGGAGGCTTT-3'	*Dhcr7*	5' RT primer for *Dhcr7*
ONM220	23	5'-CCCTGAATATTCCAGTCCACTGT-3'	*Dhcr7*	3' RT primer for *Dhcr7*
ONM221	25	5'-AGAACATTATTAGGCCACTTTCCAA-3'	*Nsdhl*	5' RT primer for *Nsdhl*
ONM222	23	5'-TCAGAGAACAGAAATGGCTGGAT-3'	*Nsdhl*	3' RT primer for *Nsdhl*
ONM223	23	5'-CCCACACTAAGAAAGGACTGCAA-3'	*Slc40a1*	5' RT primer for *Slc40a1*
ONM224	19	5'-TCGGCCCAAGTCAGTGAAG-3'	*Slc40a1*	3' RT primer for *Slc40a1*

RT-PCR Primers				
Primer	**Length**	**Sequence**	**Locus**	**Notes**
ONM238	22	5'-CGTAGCCTCCATTATTCCGTTT-3'	*Hps3*	5' RT primer for *Hps3*
ONM239	18	5'-GGCCGGCAACAGTGTCTT-3'	*Hps3*	3' RT primer for *Hps3*
ONM240	20	5'-CTGATCATGAAGCGGATGGA-3'	*Rab27a*	5' RT primer for *Rab27a*
ONM241	20	5'-CGTACCACTCCCTCCGGAAT-3'	*Rab27a*	3' RT primer for *Rab27a*
ONM242	23	5'-GAATAATGGGTGTTGGGAAGACA-3'	*Tfrc*	5' RT primer for *Tfrc*
ONM243	24	5'-CCACCATAGTGATGAGCAGGTACA-3'	*Tfrc*	3' RT primer for *Tfrc*
ONM244	22	5'-TGCCACAGCAGGTAGAGATCCT-3'	*Fth117a*	5' RT primer for Fth117a
ONM245	17	5'-GGCGCAGGTTGGTCATG-3'	*Fth117a*	3' RT primer for *Fth*117a
ONM246	19	5'-GGCAGCAGAATTCCTTGCA-3'	*Dmt-1*	5' RT primer for *Dmt-1*
ONM247	21	5'-CACCCCATCCCTGTACAAATG-3'	*Dmt-1*	3' RT primer for *Dmt-1*
ONM248	19	5'-AAGATGGGTGCCCCTGAAG-3'	*Fth*	5' RT primer for *Fth*
ONM249	21	5'-CCAGGGTGTGCTTGTCAAAGA-3'	*Fth*	3' RT primer for *Fth*
ONM274	18	5'-ACGGCGGCATCGTACCTA-3'	*Ndufa9*	5' RT primer for *Ndufa9*
ONM275	21	5'-AGGCTTGGTTTCCTCGATCTC-3'	*Ndufa9*	3' RT primer for *Ndufa9*
ONM276	20	5'-CACTGTGGGCACCATCATTC-3'	*Sdha*	5' RT primer for *Sdha*

		RT-PCR Primers		
Primer	**Length**	**Sequence**	**Locus**	**Notes**
ONM277	24	5'-GAAGGCTCAGCTTGCTCTTATACA-3'	*Sdha*	3' RT primer for *Sdha*
ONM278	27	5'-GCACATCAAAGTCAGGTCTCTTAATAA-3'	*Uqcrc2*	5' RT primer for *Uqcrc2*
ONM279	25	5'-ACACTAGGACAGCTGGGAGTCACTA-3'	*Uqcrc2*	3' RT primer for *Uqcrc2*
ONM280	19	5'-TGCAGACCAAGCGAATGCT-3'	*Cox4i1*	5' RT primer for *Cox4i1*
ONM281	18	5'-GGCGGAGAAGCCCTGAAT-3'	*Cox4i1*	3' RT primer for *Cox4i1*
ONM282	23	5'-TCAGGTGTGTACCAGGATTTGTG-3'	*Atp5a1*	5' RT primer for *Atp5a1*
ONM283	23	5'-GGTGGAAGGAGGGTACTGTCATA-3'	*Atp5a1*	3' RT primer for *Atp5a1*
ONM284	19	5'-CAGGCCTGATCCTGGGATT -3'	*Rarb*	5' RT primer for *Rarb*
ONM285	20	5'-GCCACTTGCCCATACCTTCA-3'	*Rarb*	3' RT primer for *Rarb*
ONM286	25	5'-AAATGGGTACCAAAATGAGAGATCA-3'	*Vdr*	5' RT primer for *Vdr*
ONM287	19	5'-GCAGGCAGCAGGAGGATTC-3'	*Vdr*	3' RT primer for *Vdr*
ONM288	24	5'-GGTGACCATCAGAAGCACTTAACC-3'	*Atoh8*	5' RT primer for *Atoh8*
ONM289	17	5'-TCAGGGCCCAGCACAGA-3'	*Atoh8*	3' RT primer for *Atoh8*

Primers for Gene Cloning					
Primer	**Length**	**Sequence**	**Locus**	**Notes**	
ONM69	30	5'-ATTACTCGAGAGGTGGGAAAGAGTTACAAA-3'	*Tyr*	5' primer for amplifying 1365bp *Tyr* promoter; -1287 to -1263 w.r.t. TSS	
ONM70	38	5'-AGTGCTAGATCTTTTCTCCTTTAGATCATACAAAATCT-3'	*Tyr*	3' primer for amplifying 1365bp *Tyr* promoter; +48 to +77 bp w.r.t. TSS	
ONM71	29	5'-ATTACTCGAGTGACAAAAATGGGAAAGAT -3'	*Tyrp1*	5' primer for amplifying 2078bp*Tyrp1* promoter; -1194 to -1174 w.r.t. TSS	
ONM72	32	5'-AGTGCTAGATCTTCTTCTCGAAGCAAGAGTTC -3'	*Tyrp1*	3' primer for amplifying 2078bp*Tyrp1* promoter; +268 to +288 w.r.t. TSS	
ONM97	33	5'-ATTACTCGAGTGAACATATCATTAAGAGTCCCA-3'	*Dct*	5' primer for amplifying 1567bp Dct promoter; -1099 to -1081 w.r.t. TSS	
ONM98	31	5'- ATGGCGATATCGCCTTCTTAATTGGGAGGCC-3'	*Dct*	3' primer for amplifying 1567bp Dct promoter; +449 to +467 w.r.t. TSS	
ONM75	29	5'-ATTACTCGAGTGACCTTGCAACACCATCT-3'	*Mitf*	5' primer for amplifying 1221bp Mitf promoter; -1083 to -1064 w.r.t. TSS	
ONM76	29	5'-AGTGCTAGATCTGACTCCCTCTTGCCCGC-3'	*Mitf*	3' primer for amplifying 1221bp Mitf promoter; +109 to +126 w.r.t. TSS	
ONM77	20	5'-CTAGCAAAATAGGCTGTCCC-3'	pGL4.23	5' primer for amplifying pGL4.23 sequencing primers	
ONM78	20	5'-GACGATAGTCATGCCCCGCG-3'	pGL4.23	3' primer for amplifying pGL4.23 sequencing primers	

ONM79	20	5'-ATGGCTTTGTGCAGCTGCTC-3'	pGL4.23	3' primer for amplifying pGL4.23 internal to luciferase gene sequencing primers
ONM230	23	5'-TCAGATCTATGACCAAGGCAAGA-3'	*Slc40a1*	5' primer for amplifying SLC40A1 coding sequence
ONM231	28	5'-GCGGTACCTTATACAACAGATGTATTCG-3'	*Slc40a1*	3' primer for amplifying SLC24A4 including mCherry stop codon for fusion protein
ONM234	17	5'- TCCTCCGAGCGGATGTA-3'	mCherryC1	5'primer to sequence mCherry-SLC40A1
ONM235	19	5'- CAGACGTCACTGGTGGTTC-3'	*Slc40a1*	Primer to sequence mCherry-SLC40A1
ONM236	21	5'- TGAATGTGAACAAGAGCCCAC-3'	*Slc40a1*	Primer to sequence mCherry-SLC40A1
ONM237	21	5'- GGTCCTTTGATTTGACGGTGA-3'	*Slc40a1*	3' Primer to sequence mCherry-SLC40A1

II. MATERIALS AND METHODS

II.3. Culture media, cell culture and growth conditions

II.3.1. Preparation of growth media

DMEM (Dulbecco's Modified Eagle Medium, high glucose) and DMEM/F-12 (Dulbecco's Modified Eagle's Medium/Nutrient Mixture F-12 Ham). The DMEM (D5648) and DMEM/F-12 (D8900) media was purchased from Sigma-Aldrich, Fetal bovine serum (FBS, Gibco[TM], 26140-087), DPBS (1X phosphate buffer solution, without calcium and magnesium,Gibco[TM], 14190250), Trypsin (Gibco[TM], 15090046), Versene (Gibco[TM], 15040066), Penstrep (Gibco[TM], 15140122) and Gentamicin (Gibco[TM] ,15710064) were obtained from Life technologies. All the plastic wares were obtained from Orange Scientific and Eppendorf.

The components of each bottle of powdered media were dissolved in 1 liter of autoclaved double distilled water. Tissue grade sodium bicarbonate was added to the media (3.7g for DMEM and 1.2g for DMEM/F-12), and the bottle was gently stirred till the salt dissolved. The media was filtered and 1ml each of gentamicin and pen-strep (penicillin-streptomycin) was added to it. The media was filtered again in the autoclaved 1-liter glass bottle after addition of antibiotics. For DMEM media, pH was adjusted using 1N HCl until it reached pH7-7.5. Media aliquots were made in 50 ml falcon and stored at 4°C for further use.

The fetal bovine serum (FBS) was heated at 56°C for 30 minutes to inactivate the complement system. The B16 cells lines have been shown to grow better in heat-inactivated serum.

II.3.2. Culturing of B16 cells

Maintenance of B16 cells

The B16-F10 mouse melanoma cells were maintained either in DMEM (pigmentation permissive) or DMEM/F12 (pigmentation non-permissive) media supplemented with 10% FBS (heat inactivated) at 5% CO_2 and 37°C in the conventional CO_2 incubator. The cultures were usually maintained in DMEM/F12 media at the density of $0.2x10^4$ cells (named as DMEM/F12 precultured cells) and allowed to remain in culture for six days before harvested and seeded for experiments. On the sixth day, precultured DMEM/F12 cells were seeded at the density depending upon the culture flask or well plate to be used in DMEM media. Table.II.3 Shows the list of cultured flask/plate their growth area (cm^2), working volume (mL) and the of cells (10^6) required for initial seeding to support optimal cell growth of B16 cells.

Harvesting and cell counting

The media supernatant was aspirated, and the cells were washed with 1X DPBS. The cells were treated with 0.1% trypsin and kept in the incubator for 2 minutes, the flasks/plates were tapped gently before adding media supplemented with FBS to quench the trypsinization reaction. The cells were collected in 15ml falcons and centrifuged at 5000 rpm for 5 minutes. The media supernatant was discarded, and the cells were resuspended in fresh media. A single cell suspension of the cells was made, and trypan blue was added to an aliquot of the cells in a ratio of 1:1 to visualize dead cells. The cells were counted using a hemocytometer. The following calculation was used for determining cell count.

Concentration of viable cells (per mL) = $A \times C \times D$

Concentration of nonviable cells (per mL) = $B \times C \times D$

Total number of viable cells = concentration of viable cells $\times$ volume

Where A is the mean number of viable cells counted, B is the mean number of nonviable cells counted, C is the dilution factor (in this case, it is 2), D is the correction factor supplied by the hemocytometer manufacturer (this is the number required to convert 0.1 mm^3 into milliliters; It is usually 10^4) (Freshney, Culture of Animal Cells: A Manual of Basic Technique and Specialized Applications, 6th Edition, 2010).

Cryopreservation and thawing of B16-F10 cells

The cell culture should be 80-90% confluent before the preparation of the frozen stock to ensure the maximum viable cells when reviving from the frozen stock. The cells were grown to 80-90% confluency in T-75 flasks in DMEM/F12 media. The cells were harvested by performing trypsinization. After harvesting, the cell pellet was resuspended in a cryoprotectant medium containing 90% of chilled FBS and 10% DMSO to achieve a concentration of at least 2x10^6 cells per ml. Further, an aliquot of 0.2 ml of cell suspension was made into cryogenic tubes. The cryogenic tubes were then placed in the isopropanol-filled cryo 1°C freezing container and stored at -80°C overnight. The frozen cells were then immediately transferred to the liquid nitrogen vapor phase storage. For thawing the frozen cells, 10 ml of the growth media supplemented with heat-inactivated 10% FBS was taken in a T-75 flask and pre-warmed in the 37°C incubator. The cryovial was removed from liquid nitrogen and kept at 37°C water bath until the suspension was thawed.1ml of pre-warmed media was added to the cryovial and the cell suspension was transferred to the media. The flask was kept in the CO_2 incubator, and the cells were allowed to adhere for two hours before replacing with the fresh cultured media.

II.4. MTT Cell Proliferation Assay

MTT(3-(4,5-Dimethylthiazol-2-yl)-2,5-diphenyltetrazolium bromide)) assay was performed to check for the viability of B16 cells when treated with different compounds. The MTT assay was performed in 96 well format was the different density of cells were seeded for different time points. For 24h and 48h time points of 4000 cells/well were seeded and for 72h time point, 3000 cells/well were seeded. After overnight adherence, the cells were treated with different concentrations of the compounds for a period of 24h, 48h or 72h. The treatments were done in triplicates for two biological replicates per time point. At the appropriate time point, media was aspirated, and in each well, 15 µl of MTT in 100 µl was added and incubated for 4 hours at 37°C in a 5% CO_2 incubator. After incubation of the cells, formazan crystals (presumably directly proportional to the number of viable cells) formed were dissolved in 150 µl of DMSO solvent. The absorbance of the dissolved crystals was taken at 570 nm. The percentage viability was calculated using the OD of untreated cells as a control.

$$\text{Percentage of viability: } 100 \times \frac{\text{Absorbance}_{treated}}{\text{Absorbance}_{control}}$$

Preparation of MTT reagent (5 mg/ml)

50ml PBS buffer was added to a beaker and placed on a magnetic stirrer. 0.25g MTT powder (Sigma M-5655) was added to PBS. The beaker was wrapped in aluminum foil to protect from light. The solution was filtered in the hood, split into aliquots of 4-6 ml, and stored at 4°C.

II.5. Cell cycle analysis by Flow cytometry

The cells were trypsinized and counted, and $1x10^6$ cells were harvested in 1x Ca and Mg free DPBS. The cells were pelleted down at a speed of 600g for 5 minutes. The pellet was resuspended in 70% chilled ethanol and stored at 4°C for at least 24h. The ethanol-fixed cells were pelleted down at 600g for 5 minutes and washed with 1X DPBS. The cells were stained by adding 1ml of PI stain and kept at RT for 15minutes on nutator before proceeding for flow cytometry. The instrument used was BD FACS caliber. All raw data was acquired using cell quest software, and the data analysis was carried out in FloJo software using the Dean-Jett-Fox model for fitting the cell cycle phases.

Reagents required for PI stain

100 ml Ca and Mg-free PBS, 5 mg RNase (should be DNase free),

2.5 mg of Propidium Iodide

30 µl of TX100 or NP40 or Tween20. The solution was wrapped in aluminum foil and stored at 4°C.

II.6. Melanin Estimation using synthetic melanin

For melanin estimation, $1x10^5$ cells were solubilized in 200µl of 1N NaOH and 10% DMSO for 2hrs at 80°C. 1mg/ml stock of synthetic melanin (Cat no. M0418-100MG) was prepared in 1N NaOH and 10% DMSO. The standard curve using synthetic melanin covering the concentration range of 0-20µg/ml was prepared. Sample and standard tubes were then centrifuged at 12,000g for 10min at RT and supernatants were transferred to 96 multi-well plates. The absorbance of the supernatant was

measured at 410nm and melanin content was determined using a standard curve. The values were expressed as μ per $1x10^5$ cells. (The protocol is obtained from PMID: 24317198).

II.7. Detection of ROS using DCFDA

DCFDA (2',7'–dichlorofluorescein diacetate) is non-fluorescent, but in the presence of ROS, when this reagent is oxidized, it becomes green fluorescent. The fresh stock of DCFDA was prepared in DMSO. The cells were counted, and 2 million cells were collected in the 1ml tube to perform the assay. The harvested cells were washed with DPBS to remove traces of medium. The final concentration of 20μM of DCFDA was prepared in regular culture medium with reduced serum (2%). The cells were then loaded with 1ml of DCFDA and incubated for 30 minutes in the dark, in a conventional incubator (37°C, 5% CO_2). After that DCFDA containing medium was discarded and washed twice with DPBS to remove the traces of dye. From this step forward, cells were protected from the light. The cells were resuspended in 1ml DPBS and transferred to respective FACS tubes. The ROS levels were assessed immediately by flow cytometry using the FL1 channel (green fluorescence).

II.8. Imaging of mouse B16 cells

II.8.1. Phase contrast microscopy

The B16 cells were imaged while in culture in either T-75, six well or 96 well plates as per the requirement of the experiment. Nikon Eclipse Ti-S inverted microscope was used, and the images were acquired in phase contrast settings. Software used for acquiring images was NIS-Elements AR.

II.8.2. Fluorescence microscopy

Sample preparation

B16-F10 cells were transfected with the construct containing the fluorophore (mCherry) tagged protein in a 6-well plate. After 48h post-transfection image was acquired using fluorescence microscopy. Before image acquisition media was aspirated and wells were washed with 1ml DPBS to remove the traces of media.

Microscopy and Image Acquisition

Fluorescence microscopy was carried out on Nikon Eclipse Ti-E inverted microscope system with filter sets for TRITC (red) emission. Images were captured using Nikon NIS- Elements Advanced Research, Version 4.00.00. Firstly, the mercury light source was turned ON, to begin with, fluorescence imaging. It was allowed to warm up for around 15 minutes to reach constant illumination. Then the DPBS was aspirated from the six-well plate, and the plate was placed on the stage and secured. Then the white light source was turned on in the microscope. The sample was focused on the lowest power to find the area of interest. Then the white light was turned off, and the dye for imaging was selected to illuminate the sample. TRITC filter was used to illuminate mCherry. Finally, fine adjustments were made, and images were captured. Adjustments to the exposure times were made for different fluorophores. Exposure time was kept constant when comparing features with the same dye on different samples. Images were saved, and background subtraction was done using Nikon NIS- Elements Advanced Research, Version 4.00.00 analysis software.

II.8.3. Confocal microscopy

Sample preparation

B16-F10 cells were transfected with pM40a1-2 construct on a coverslip in each

well of a six well/12 well plate. pmCherry vector alone was taken as control. To prepare the sample for microscopy, the media from the wells was aspirated and discarded. Cells on the coverslips were washed twice with DPBS. Fixation was done by incubating the cells in 100% methanol (chilled at -20°C) for 3 min at RT. After 3min cells were washed with cold DPBS (3x, 5min each). The cells were permeabilized using 0.1% Triton X-100 for 10 min at RT. The cells were washed with cold DPBS (3x, 5min each). The cell was then incubated with 1% BSA, 22.52mg/ml glycine in PBST for 30min at RT to block the non-specific interaction of antibody. After 30 min of blocking cells were incubated overnight in respective primary antibody prepared in 1% BSA at 4°C. Next day, antibody from each well was transferred in a fresh tube that can be used to perform western blotting. The cells were washed with cold DPBS (3x, 5min each). Further, the cells were incubated in secondary antibody (dilution prepared in 1% BSA) for 1hr at RT in dark space. After incubation cells were washed with cold DPBS (3x, 5min each). Counter staining of cells was done by incubating them in Hoechst stain/DAPI at the ratio of 1:2000 for 10 min and then rinsed with DPBS.

Slide preparation

The slides were wiped, and 20µl of 50% glycerol was dropped in the middle of the slide. The stained coverslips were inverted using forceps so that the side having the cells should rest on glycerol. Carefully, the coverslips were rested on the slide to avoid any air bubbles. The coverslip sides were sealed with transparent nail paint.

Microscopy and Image Acquisition

Confocal microscopy was carried out on Nikon Eclipse Ti-E inverted microscope system with filter sets for mCherry and DAPI emission. Images were captured using software AndoriQ, Version 2.7. Firstly, the light source was turned

ON, to begin with, fluorescence imaging. The slide was placed on the stage and secured. In the TRITC filter, the sample was focused on the lowest power to find the area of interest. TRITC filter was used to illuminate mCherry. DAPI filter was used to illuminate the stained nucleus. Finally, fine adjustments were made, and images were captured. Adjustments to the exposure times were made for different fluorophores. Exposure time was kept constant when comparing features with the same dye on different samples. Images were saved, scales were added, and background subtraction was done using Nikon NIS- Elements Advanced Research, Version 4.00.00, analysis software.

II.9. Transmission electron microscopy

Cells were fixed overnight at 4ºC in fixative containing 2.5% glutaraldehyde and 4% paraformaldehyde for 24 hours. Cells were then washed with 0.1M sodium cacodylate buffer to remove excess fixative and cells were embedded in 2% agar blocks before proceeding further. Samples were then post-fixed in 2% osmium tetroxide for 1 hour. The sample was dehydrated in a graded series of ethanol (30%, 50%, 70%, and 100%) and infiltrated in upon resin and polymerized at 60°C for 72 hours. Ultrathin sections (70 nm – 90nm) were cut on an Ultramicrotome, placed on copper grids and stained with 5% uranyl acetate and 0.2% lead citrate. Sections were examined on a transmission electron microscope (Tecnai twin 20, FEI).

II.10. Plasmid DNA isolation

Minipreparation of Plasmid DNA

Plasmid DNA isolation was done by the alkaline lysis method as described (Sambrook and Russel, 2001). Bacterial cells were inoculated in 1.5 ml of LB liquid

media with the required antibiotic. The cultures were incubated in an orbital shaker at 37°C for 16 hours with shaking at 200 rpm. The cultures were harvested at 6000 rpm for 2 minutes in 2ml microfuge tubes and the supernatant decanted. The 100µl of ice-cold solution I was added to the tubes and the cells resuspended by vortexing vigorously. The tubes were incubated on ice for 5 minutes. 200µl of solution II at room temperature was added to the tubes, and the contents mixed gently by inverting the tubes a few times. The samples were kept on ice further for 5 minutes. 150µl of ice-cold solution II was added, and the contents of the tube were mixed by inverting a few times. The samples were further incubated on ice for 5 minutes and then centrifuged at 13,000 rpm at room temperature for 10 minutes to remove cell debris. The clear supernatant was collected in a fresh 1.5ml tube to which an equal volume of isopropanol was added and the mixture incubated for 30 minutes at 37°C.

The precipitated plasmid DNA was pelleted at 13,000 rpm for 10 minutes at room temperature and the supernatant decanted. The pellet was washed with 70% ethanol and re-centrifuged at 13,000 rpm for 5 minutes at room temperature. The ethanol was aspirated out carefully, and the pellet was air-dried at 37°C. The plasmid DNA was re-suspended in 25 µl of 1x TE, pH 8.0, containing 20µg/ml of RNase A and the tubes were incubated for an hour at 37°C.

Preparation of media

Luria-broth (LB) media: 0.5% Yeast extract, 1% Tryptone, 1% NaCl

The components were dissolved in the water with constant stirring and mild heating. Water volume was adjusted after adjusting the pH:7 with 10N NaOH. Media was autoclaved and stored at RT. An appropriate antibiotic was added just before use.

For the preparation of LB plates, 1.5% agar was added after adjusting the pH and before autoclaving. Media was allowed to cool to 60°C, and an appropriate antibiotic was added. Mixed carefully on the stirrer and poured on plates.

Reagents for plasmid isolation (Miniprep)

Solution I: 25mM Tris-Cl, pH 8.0; 10mM EDTA, pH 8.0; 50mM Glucose.

Solution II: 0.2N NaOH, 1% SDS.

Solution II: 3M Potassium Acetate, 11.5% Glacial Acetic Acid.

Midi-preparation of Plasmid DNA

For isolation of plasmid DNA in larger amounts, a single colony from a streak out of the desired bacterial strain was inoculated in 5-10 ml of LB media with ampicillin at a final concentration of 75µg/ml. The cultures were incubated in an orbital shaker at 37°C for 16 hours with shaking at 200 rpm. Cells were harvested at 6000 rpm for 2 minutes multiple 2ml microfuges and the supernatant decanted. The pellet was washed and re-suspended in 1.25 ml STE buffer and the cells collected by centrifugation at 6000 rpm for 2 minutes at RT. The samples were then proceeded with as for miniprep DNA isolation and the extracted plasmid resuspended in a total volume of 20µl per tube. Samples from different tubes were pooled together after RNase digestion.

To obtain purified DNA preparations, plasmid DNA was extracted using a phenol-chloroform-isoamyl alcohol mix (ratio 25:24:1), which was added in equal volume to the plasmid DNA solution. The mix was vortexed vigorously and then centrifuged at 13,000 rpm for 3 minutes at room temperature to separate the aqueous and organic phases. The upper aqueous phase was collected to fresh tubes, which was

then extracted with an equal volume of chloroform-isoamyl alcohol mix (ratio 24:1). The tubes were vortexed and centrifuged at 13,000 rpm for 3 minutes at room temperature and the aqueous phase collected to fresh microfuge tubes.

The plasmid DNA was precipitated by adding 1/10th the volume of 3M sodium acetate, pH 5.3 and two volumes of 100% ethanol. The plasmid was precipitated at -80°C for half an hour and then centrifuged at 13,000 rpm at 4°C for 15 minutes. The pellet was washed with 70% ethanol and re-centrifuged at 13,000 rpm for 3 min, the supernatant aspirated and the pellet air-dried. The pure plasmid DNA was resuspended in a small volume of water or 1X TE as required.

<u>Reagents for plasmid DNA isolation (Midi-prep)</u>

STE buffer: 10mM Tris-Cl, pH 8.0; 1mM EDTA, pH 8.0; 100mM NaCl.

Solution I: 25mM Tris-Cl, pH 8.0; 10mM EDTA, pH 8.0; 50mM Glucose.

Solution II: 0.2N NaOH, 1% SDS.

Solution III: 3M Potassium Acetate, 11.5% Glacial Acetic Acid.

II.11. Preparation of Bacterial Competent Cells and Bacterial Transformation

Electrocompetent *E. coli* DH10B cells were prepared as described (Sambrook and Russel, 2001). Briefly, a single colony of DH10B bacterial cells from a freshly revived stock was inoculated in 25ml of LB medium and incubated in an orbital shaker at 37°C with shaking at 220 rpm for 16 hrs. The cell density of the pre-culture was determined by measuring the OD600 of a 1:10 diluted culture and seeding of 500ml pre-warmed secondary culture in LB media was done with a starting OD/ml of 0.05. The culture was incubated at 37°C with shaking at 220 rpm. The cells were grown to a density of 0.5 OD/ml and the cells chilled in an ice water bath for 15 minutes with

intermittent swirling. The cultures were harvested in sterile centrifuge bottles at 8000rpm for 10 minutes at 4°C. The cell pellet was washed three times with sterile, chilled 10% glycerol (Qualigens). The washes were done sequentially with equal, half and 1/25th the secondary culture volume. Cells were resuspended in 800μl sterile, chilled 10% glycerol (USB) and the cell density adjusted to 100 OD/ml of glycerol or ~2-3 x 10^{10} cells/ml. Aliquots of the cells were made and frozen at 80°C.

Electroporation of Bacterial cells

An aliquot of electrocompetent cells was thawed on ice and 20μl of it mixed with the DNA to be transformed (plasmid or ligation mix). The cells-DNA mix was incubated on ice for 1 minute and then pipetted into a chilled 1mm cuvette. As a positive transformation control, a known amount of a closed circular plasmid DNA such as pLitmus28 or pUC19 was also used. The components of SOC medium were prepared just before electroporation. The cells were transformed with the electroporator (Gene PulserXcell^{TM} electroporation system, Bio-Rad) set to 1800V, 25μF, 200Ω. The electroporated cells were resuspended in 1ml SOC and transferred to a 15ml tube, incubated in an orbital shaker at 37°C for 1hr at 200 rpm. The cells were pellet down and resuspended in 200μl of a/c DDW. The plating was performed using the appropriate volume (100μl of 200μl) of transformed cells on LB plates with the appropriate antibiotic, and the plates were incubated at 37°C for 14-16 hrs. The transformation efficiency was calculated as:

Transformation efficiency: Cfu/pg DNA used x 10^6 x Dilution factor.

Reagents for electroporation:

SOB medium: 2% tryptone, 0.5% yeast extract, 0.05% NaCl, 25mM KCl. Adjusted to pH7.0 with NaOH.

SOC medium: SOB with 20mM each of $MgCl_2$, $MgSO_4$, and Glucose.

II.12. Transfection of mouse B16 cells

Transfection of siRNA using Dhermafect

For siRNA transfections, Dhermafect (Invitrogen) was used as the transfection reagent. B16 cells were seeded at a density of 32000 cells/ well in six-well plates and allowed to adhere for 24 hours before transfection. Suspension A (containing 100nM of smart pool siRNA) was prepared in a volume of 100µl OptiMem and was gently mixed by inversion and kept at RT for 5 minutes. Suspension B (containing 6µl of Dhermafectin 100µl of OptiMem) was also mixed by inversion and kept at RT for 5 minutes. Suspension B was added to A and mixed by inversion. The tube was allowed to stand at RT for 45 minutes for complex formation. Post incubation 800µl of OptiMem was added to the tube. The cells were prepared for transfection during the incubation period. The media was aspirated out of the wells and stored in 2ml microfuge tubes and kept in the CO_2 incubator. The cells were washed once with 1X DPBS and once with 500µl OptiMem. The transfection mix (1ml) was added to the cells dropwise. The transfection was carried out for 6 hours after which the cells were washed twice with DPBS, and the original media of the cells was replaced. Compound treatments, whenever required, were carried out after replacing the media.

Transfection of Plasmid using Cellfectin

For plasmid transfections, cellfectin (Invitrogen) was used as the transfection reagent. B16 cells were seeded at a density of 32000 cells/ well in six-well plates and allowed to adhere for 24 hours before transfection. Suspension A (containing1 µg of the construct) was prepared in a volume of 100µlOptiMem and was gently mixed by inversion and kept at RT for 5 minutes. Suspension B (containing 6µl of cellfectin in 100µl of OptiMem) was also mixed by inversion and kept at RT for 5 minutes.

Suspension B was added to A and mixed by inversion. The tube was allowed to stand at RT for 45 minutes for complex formation. Post incubation 800µl of OptiMem was added to the tube. The cells were prepared for transfection during the incubation period. The media was aspirated out of the wells and stored in 2ml microfuge tubes and kept in the CO_2 incubator. The cells were washed once with 1X DPBS and once with 500µl OptiMem. The transfection mix (1ml) was added to the cells dropwise. The transfection was carried out for 6 hours after which the cells were washed twice with DPBS, and the original media of the cells was replaced. Compound treatments, whenever required, were carried out after replacing the media.

II.13. Isolation of genomic DNA from rat tissues

Genomic DNA was isolated from the eight different tissues of rat by the method of Hewish & Burgoyne, 1973 with some modifications as described by Chaturvedi & Kanungo, 1985. 1g of tissue was finely minced on ice and homogenized in 20ml ice-cold Solution I (0.34M Sucrose, 15mM Tris-Cl pH 7.4, 15mM NaCl, 60mM KCl, 15mM β-mercaptoethanol, 0.15mM Spermine, 0.5mM Spermidine, 0.2mM PMSF, 2mM EDTA, 0.5mM EGTA and 0.5% TritonX-100) in a glass homogenizer fitted with a Teflon pestle driven by a motor at 3,000 rpm by10 strokes up and down on ice. The homogenate was filtered through four-layered pre-chilled cheese-cloth soaked with the buffer and centrifuged at 6000xg for 20 minutes 4°C. The supernatant was decanted out, the nuclear pellet was resuspended (by Pasteur pipette) and washed with 20 ml Solution I three times and then resuspended in ice-cold Solution II (0.34M Sucrose, 15mM Tris-Cl pH 7.4, 15mM NaCl, 60mM KCl, 15mM β-mercaptoethanol, 0.15mM Spermine, 0.5mM Spermidine, 0.2mM PMSF, 0.2mM EDTA and 0.1% Triton-100) and kept on ice. The nuclei were lysed by adding first 5M NaCl, mixed and then 10% SDS, remixed up to the final concentrations of 1M NaCl

and 1% SDS respectively followed by gentle swirling/rolling of the mixture for 30 minutes at room temperature (RT). The 5M NaCl and 10% SDS should be previously kept at room temperature. An equal vol. of TNE-buffer-saturated phenol (pH 8.0) was added, and the mixture was extracted by gentle-shaking/rolling for overnight and centrifuged at 18,000g for 15 minutes at 4°C. The aqueous-phase was carefully collected, extracted with an equal vol. of chloroform and recovered by centrifugation.

The genomic DNA was precipitated from the aqueous-phase with 2.5 vol. of ice-cold ethanol (Merck-grade) after first adding $1/10^{th}$ vol. of 3M sodium-acetate (pH 5.2). The high molecular weight genomic DNA precipitates out at this point, which was spooled out from the mixture by a spiral glass rod or the mass of DNA precipitate can be picked by a sterile forceps and put into a Microfuge tube and then washed with 80% ethanol. The DNA-pellet was briefly air-dried to remove the water content (not too much dried) and dissolved in 10mM Tris-Cl, pH 7.5 with ten mMNaCl and the concentration of the DNA was measured by absorbance at A260 and A280 nm in a spectrophotometer. One A260nm unit was taken as 50µg/ml of double-stranded DNA. The A260/280 nm ration should be around 1.8. A wavelength scan of 220 to 300 nm was also obtained to ensure the expected curve and purity of DNA. Genomic DNA was also checked by slow electrophoresis in 0.6% agarose-TAE gel in the presence of ethidium bromide to ensure its high molecular mass (>30 kb) and presence of no smear. The concentration of genomic DNA was adjusted to the concentration of 200ng/µl and stored at 4°C (not frozen).

II.14. Isolation of genomic DNA from B16 mouse melanoma cells

Two million B16 cells were harvested from a confluent T-75 flask. The cells were washed with 500µl of DPBS and centrifuged at 500g for 5 minutes at 4°C. The

cell pellet was resuspended in 1ml of native lysis buffer and incubated for 10 minutes on ice. An equal volume of PCI was added to the sample, and the tube was centrifuged for 15 minutes at 13000rpm. The aqueous layer was collected, and an equal volume of chloroform and isoamyl alcohol was added. Centrifugation was carried out at 13000rpm for 15 minutes. The aqueous layer was taken, and half its volume of 7.5M ammonium acetate was added along with twice the volume of 100% ethanol. Strings of DNA were removed with the help of Pasteur pipette and washed with 70% ethanol. The pipette tip containing DNA was air dried and dissolved in 100µl of 1X TE O/N. The high molecular weight genomic DNA band was checked on 0.8% agarose gel.

<u>Reagent for lysis buffer</u>: 10mM TrisCl pH: 8, 25mM EDTA pH: 8, 100mM NaCl, 0.5% SDS and 100µg Proteinase K.

II.15. Construction of luciferase reporter vectors for mouse gene promoters

Promoters for the pigmentation genes *Tyr, Tyrp1, Mitf* and *Dct* were cloned upstream of the luciferase gene in the pGL4.23 luciferase reporter vector. The *Tyr, Tyrp1* and *Mitf* promoters were amplified from B16 genomic DNA using the primer pairs ONM69-ONM70 (*Tyr*), ONM71-ONM72 (*Tyrp1*) and ONM75-ONM76 (*Mitf*). The forward primer for all incorporated the XhoI restriction site and the reverse primer incorporated the BglII restriction site. The size of *Tyr, Tyrp1* and *Mitf* promoters amplified were 1365bp, 2078bp and 1221bp respectively. The PCR products were checked on an agarose gel to confirm the presence of correctly sized inserts, which were then gel purified and digested sequentially by XhoI and BglII. For vector preparation, pGL4.23 was digested sequentially with XhoI and BglII and dephosphorylated using Antarctic Phosphatase (NEB). Ligation was carried out at 16°C overnight in a cooling water bath. Vector alone was used as a ligation control. The ligation reactions were

transformed into DH10B. Positive clones were screened to pop out *Tyr*, *Tyrp1* and *Mitf* inserts. Positive clones were sequenced and the constructs transfected into B16 cells.

The Dct promoter was amplified from genomic DNA isolated from mouse liver. The primer pairs used for amplification were ONM97-ONM98, and the size of the amplicon was 1667bp. The restriction sites incorporated into the forward and reverse primers were XhoI and EcoRV respectively.

II.16. Dual-Luciferase Reporter assay

The DLR assays were performed to measure the activity of the promoters of interest. The transfections were carried out as discussed previously. The assay was carried out using the DLR kit (Promega) according to manufacturers' protocol. Briefly, at appropriate time points, the cells were washed with DPBS and 100µl of 1X passive lysis buffer provided in the DLR assay kit was added to each well and kept on the rocker at RT for 15 minutes. The lysed cells were harvested, and the clear supernatant was taken after spinning the tubes at 13000 rpm for 15 minutes at 4°C.

The DLR Assay was performed by adding 50µl of Luciferase assay reagent II (LARII) in 10µl of lysate and reading was taken using GloMax® 20/20 luminometer. After the first measurement, 50µl of Stop &Glo reagent was added & reading was taken. The ratio of Firefly vs. Renilla gave the relative promoter activity regarding the ratio of RLUs.

II.17. Construction of C-terminal mCherry tagged SLC40A1

The gene for transporter protein SLC40A1 was cloned into the pmCherry-N1 vector to generate a C-terminal mCherry tagged protein. The primers used were ONM230-ONM231 having BglII and Acc651 sites respectively. The gene was

amplified using cDNA derived from B16 cells, and the amplicon had a size of ~1.7kb. The insert and vector were processed, and the clone was constructed as described above.

II.18. In-silico localization prediction

The cDNA sequence of Slc40a1 was assessed for their potential to localize in different subcellular compartments, using PSORT II localization prediction program (http://psort.hgc.jp/form2.html).

II.19. Western Blotting and Immunodetection

The cell lysate was prepared using the native lysis buffer as described above. The protein estimation was carried out using the Pierce BCA Protein Assay Kit according to manufacturer's protocol. 10% SDS-PAGE gel of 1.5mm thickness was used for immunodetection. About 15µg of whole cell extract was mixed with 5X SDS-PAGE dye to a final concentration of 1x in a total volume of 30µl and boiled for 5minutes in a boiling water bath. Samples were loaded onto the SDS-PAGE gel and run at 80 V in running buffer. The gel was allowed to run until the dye front reached the stacking-resolving junction, and the voltage was increased to 100 V. The run was stopped when the dye front reached the sealing portion of the gel, following which a transfer of the proteins was setup onto a PVDF or a nitrocellulose membrane. The transfer was carried out in transfer buffer for 3 hours at 30V.

After transfer, the gel was checked for transfer efficiency by staining with 0.25% (w/v) Coomassie brilliant blue R250 in 20% methanol and 10% acetic acid and destained. The membrane was checked for total protein levels, as well as for transfer efficiency by staining with 0.1% Ponceau S. The membrane was first washed with 1% acetic acid to remove excess Ponceau S stain, scanned and a record kept. Further

washing was performed with 1x PBST and kept overnight at 4°C in freshly prepared 5% blocking solution. The membrane was washed with 5% blocking solution for an hour at RT after the overnight incubation following which it was incubated with primary antibody diluted in 5% blocking for 1hr at RT on a nutator.

The membrane was washed with 25ml of 1x PBST three times giving 10min washes at each step and then incubated with secondary antibody diluted 20,000-fold in 5% blocking solution for 1hr at RT. The membrane was washed with 25ml of 1x PBST three times giving 10min washes at each step. The bound antibody was detected with ECL-Plus western blot detection reagent and the chemiluminescent signal captured by exposure to a Kodak X-Omat XAR2 X-Ray film. The film was developed in a dark room and multiple exposures are taken for each blot. The films were scanned and images saved.

Reagents for western blot

Resolving gel: 10% Acrylamide-Bis acrylamide mix (29:1 from a 30% w/v stock), 0.39M Tris-Cl, pH 8.8, 0.1% (w/v) Ammonium persulfate, 0.04% (v/v) TEMED.

Stacking gel: 5% Acrylamide-Bis acrylamide mix (29:1 from a 30% w/v stock), 0.127M Tris-Cl, pH 6.8, 0.1% (w/v) Ammonium persulfate, 0.1% (v/v) TEMED.

Running buffer: 1x Tris glycine (25mM Trizma® base, 192mM glycine) and 0.1% SDS (w/v).

Transfer buffer: 1x Tris-glycine (25mM Trizma® base, 192mM glycine), 20% methanol

Ponceau S: 0.1% Ponceau S in 1% Glacial acetic acid

1x PBST: 1x PBS with 0.1% Tween-20

Blocking solution: 5% skim milk

II.20. In-gel DOPA assay to study tyrosinase activity

In brief, after treatment of the cells with different compounds, the cells were harvested by trypsinization. The cell lysate was prepared by adding 50µl of native lysis buffer in each tube and 15 minutes incubation was done on the ice. Samples were centrifuged at 13000rpm for 10 minutes at 4°C, and the supernatant was transferred to the fresh tube. The protein estimation was carried out using the Pierce BCA Protein Assay Kit according to manufacturers' protocol. 10% SDS-PAGE gel of 1.0mm thickness was used to perform DOPA assay. 15µg of the protein lysate with 6x DNA loading dye to a final concentration of 1x in a total volume of 15µl was run on native (non-denaturing) polyacrylamide gel. Samples were loaded onto the SDS-PAGE gel and run at 80 V in running buffer. The gel was allowed to run until the dye front reached the stacking-resolving junction and the voltage was increased to 100V. The gel was washed with 0.1M phosphate buffer (pH 6.0) for half an hour and with 0.1M phosphate buffer (pH 6.8) for 5 minutes. The gel was then incubated with 10mM of DOPA in phosphate buffer (pH 6.8) at 37°C, in the dark for around 1hr. The enzymatic activity was observed based on the chromogenic band at ~60kDa on the gel. The gel was scanned, and a record kept.

<u>Reagents for native lysis buffer</u>

0.05M Tris pH 8, 0.5% Sodium deoxycholate, 1% NP-40, 1X Protease inhibitor cocktail, 0.15M NaCl the volume was made up by adding autoclaved double distilled water.

<u>Recipe for Phosphate Buffer</u>

13.2 ml of 1M K_2HPO_4 and 86.8 ml of 1M KH_2PO_4 was added to 1L of distilled water to make a 0.1M phosphate buffer of pH 6.0. For making a 0.1M phosphate buffer of pH 6.8, 49.7ml of K_2HPO_4 and 50.3 ml of KH_2PO_4 was added to 1L of distilled water.

II.21. RNA isolation of mouse B16 cells

RNA was isolated using TRI reagent as per the manufacturers' protocol. Briefly, 1ml of trizol was added/well in a six-well plate and incubated for 5 min. The cells were harvested and stored at -80°C. Before isolation the samples were allowed to thaw at RT and 1/5th volume of chloroform was added and mixed well. Samples were centrifuged at 13000 rpm for 10 minutes at 4°C. The aqueous phase was collected, and an equal volume of isopropanol was added to it. The samples were mixed by inversion and allowed to stand at RT for 10 minutes. The RNA pellet was collected by centrifugation at 13000 rpm and was washed with 70% ethanol before air drying and resuspending in 100µl of RNase free water. The RNA was purified using RNeasy kit according to manufacturers' protocol. Briefly, 350µl of buffer RLT was added to each sample followed by 250µl of 100% ethanol. The sample was then transferred onto the purification column. Flow through was discarded after a brief spin and the column was washed with 500µl buffer RPE twice. The column was given an empty spin before eluting the RNA using warm RNase free water. The RNA was collected in a fresh tube and quantitated using nanodrop absorbance at 260nm.

II.22. cDNA synthesis and Real-time PCR

500ng of RNA was treated with DNase (Invitrogen). 0.25µl of DNase was added to the RNA sample for 15 minutes using a final concentration of 0.25U of DNase I, Amp grade (1U/µl, Invitrogen). The tubes were kept at room temperature. The reaction was heat inactivated by adding 0.5 µl of 25mM EDTA stock and kept at 65°C for 20 minutes. The RNA was reverse transcribed to cDNA using either the Superscript III kit (Invitrogen) or High Capacity cDNA Reverse Transcription kit (ABI) according to manufacturers' protocol. The PCR program for synthesis using superscript III kit was 25°C for 10 minutes followed by 50°C extension for 1hour. The PCR program for

cDNA synthesis using ABI kit was 25°C for 10 minutes, followed by 37°C for 2 hours. The reaction mixture was heat inactivated at 85°C for 5 minutes. The cDNA samples were stored at -20°C. To study expression levels of target genes real-time primers were designed using either the Primer Express (ABI) tool or the online Primer depot tool (NCI, NIH).

Quantitative analysis of the PCR products was performed using SYBR Green chemistry in an ABI 7500 or ABI 7500 Fast real-time PCR system according to the manufacturer's cycling conditions. Primers were designed for all amplicons having an efficiency E = 1.9±0.06. The DNA template was diluted in 0.1X TE such that the C_T values generated for each sample were in the range of optimum amplification by the primers used, in the exponential phase of the PCR reaction. The concentration of the forward and reverse primers in the reaction was kept at 0.5µM. A dissociation curve analysis was carried out for each reaction run after 40 cycles. All reactions were setup in duplicate or triplicate using independently-made dilutions of each template sample. An endogenous control reaction was setup with each PCR run, along with a no-template control. The endogenous control gene used for normalization was the housekeeping gene Gapdh.

The CT values obtained from each reaction were used for calculation of the relative difference in gene expression using the $2^{-\Delta\Delta CT}$ method for relative quantification. Mean CT values were calculated for the duplicates or triplicates. Outliers were excluded from the analysis. The target gene ΔCT value was calculated by subtracting the endogenous gene CT value from the target gene CT. The ΔΔCT was calculated by subtracting the experimental ΔCT from the calibrator ΔCT. The fold change was calculated as the $2^{-\Delta\Delta CT}$ value.

II.23. Microarray Data and Statistical Analysis

Isolated RNA samples were sent for hybridization using Genotypic technologies, Bangalore for hybridization using Agilent platform. For Agilent platform Mouse 8x60K (AMADID: 65570) array was used. Details of hybridization for each platform are described in chapter III and IV. Agilent data analysis was carried out using the GeneSpring software. Microarray data analysis was carried out using a statistical approach like ANOVA analysis to identify differentially expressed genes. Using the online database for annotation, visualization, and integrated discovery (DAVID, https://david.ncifcrf.gov/), we identified biological themes by acquiring Gene Ontology (GO) in the category of biological process (BP) p-value less than 0.05.

II.24. Computational tools used

UCSC genome browser, TRED database, and NCBI were used to retrieve sequence information for genes of interest. Online tool TRANSFAC from the BIOBASE database was used to analyze the transcription factor binding sites in promoters. RSAT tool was used to map binding site on promoters. Online tool VENNY and BioVenn were used to identify overlaps between different datasets. IDT oligoanalyzer and Primer Express 3.0 was used to design primers. Reverse complementation and translate tool of Sequence manipulation suite (SMS) were used for sequence analysis. NEB cutter tool was used to generate vector maps and identify RE cut sites.

Results and Discussion

Chapter III

Elucidation of the requirement of Iron homeostasis for melanogenesis

III. ELUCIDATION OF THE REQUIREMENT OF IRON HOMEOSTASIS FOR MELANOGENESIS

III.1. Introduction

The pigmentation in melanocyte is modulated by several physiological factors released form keratinocyte such as α-MSH, TNF-α, bFGF, etc. The physiological modulators can either activate or repress pigmentation depending upon the secretory factors released by the keratinocytes. (Miyamura et al., 2007; Yamaguchi et al., 2007). The pigmentation phenotype is also altered by small molecules and have thus found their way to cosmetics and dermatology.

III.1.2. Background

III.1.2.1 *Small solute transporters differentially expressed during small molecule induced melanogenesis*

Previous studies performed in our lab has identified comprehensive regulatory network occurring during melanogenesis. We have developed a tunable model of melanogenesis using small molecules to carry out the genome-wide studies. The mouse B16-F10 melanoma cells exposed to two small molecules, IBMX and forskolin, known activators of the cAMP-PKA pathway for the different duration to induce melanogenesis (kirty, 2015). Treatment with forskolin and IBMX led to increased tyrosinase protein levels and enzyme activity, hyper-dendricity, transcriptional upregulation of melanin biosynthetic pathway genes and melanin accumulation. Electron microscopic imaging showed that the two small molecules enhanced the maturation of melanosomes. The genome-wide microarray profiling was carried out to uncover several novel genes and pathways differentially expressed upon induction of the melanogenesis programme.

Microarray data analysis showed that forskolin and IBMX commonly regulate a large number of genes. Hierarchical clustering analysis showed a temporal pattern of expression of ~1620 genes. DAVID pathway analysis yielded several genes involved in melanosome biogenesis, cell cycle, inflammation and small solute transporters enriched during melanogenesis.

Among 1620 DE genes we found 29 small solute receptors (SLCs) to be differentially expressed during compound induced hyper-pigmentation (kirty, 2015). The list of SLC genes with their names extracted from Mouse genome informatics (MGI, http://www.informatics.jax.org/) is provided in Table. III.1. Among the 29 SLC genes, *Slc18a1*, *Slc22a4*, *Slc24a4*, *Slc19a2*, *Slc25a25*, *Slc35a2*, *Slc31a2* and *Slc35f5* were up-regulated at 48h and 72h. Additionally, *Slc13a3*, *Slc40a1*, *Slc35f1*, *Slc29a1*, *Slco31* and *Slc2a4* were down-regulated from 48h to 72h. It was also previously reported that forskolin treatment led to the upregulation of *Slc24a4*, *Slc24a5*, and *Slc45a2* and down-regulation of *Slc6a6* and *Slc9a3r1* (Cheli et al., 2009).

In humans, the genes SLC45A2 and SLC24A5 have been shown to be linked to skin color variation as identified in genome-wide association studies (Liu et al., 2015). SLC45A2 is a Membrane-Associated Transporter Protein (MATP) that is reported to help in maintaining an optimal melanosomal pH for maximal tyrosinase activity (Bin et al., 2015). Besides, the cAMP levels also seem to regulate the expression of the membrane transporters that belong to the SLC family. A previous report showed that SLC24A5 is involved in the maintenance of melanosomal proton level (Kondo and Hearing, 2011) to maintain optimal pH for sustenance of tyrosinase activity.

Previous studies from our lab particularly examined the role of *Slc24a4* that showed high expression levels across all time points and treatments. Although the role

of *Slc24a4* has been linked to eye and hair pigmentation (Han et al., 2008), its purpose and mechanism in regulating skin pigmentation were unclear. Functional validation of *Slc24a4* was done using siRNA and effect on melanogenesis. Real-time qPCR analysis showed that *Slc24a4* mRNA levels were reduced by ~75% when normalized with respect to the mock control. Interestingly, the expression of all the important melanogenic genes *Tyr, Tyrp1, Dct,* and *Mitf* was found to be down-regulated during *Slc24a4* knockdown (kirty, 2015), suggesting an important role for *Slc24a4* role in regulating or promoting melanogenesis.

In this work, the 29 differentially expressed SLC genes were analyzed further to explore their role in melanogenesis. Interestingly, we found that *Slc40a1/Fpn1* was consistently and progressively downregulated across time points. The *Fpn1* gene encoding the ferroportin is a membrane-bound protein that plays an essential role in maintaining iron homeostasis by functioning as an iron efflux protein (Abboud and Haile, 2000; Nemeth et al., 2004). Consistent with such a critical role, *Fpn1* knock-out is embryonically lethal (Donovan et al., 2005).

The human ferroportin is composed of 571 amino acids having multiple transmembrane (TM) segments (Bonaccorsi di Patti et al., 2014). Initially, the topology of ferroportin was predicted to have nine or twelve transmembrane regions with the N-terminal region positioned intracellularly, and the C-terminal region positioned either intracellularly or extracellularly depending on the number of transmembrane segments (Bonaccorsi di Patti et al., 2014). A recent report suggested that both the N- and C-terminal extremes of ferroportin are intracellular (Bonaccorsi di Patti et al., 2014), indicating that ferroportin contains an even number of transmembrane segments. Fig.III.1 shows the relevant structural features of ferroportin, and the large intracellular loop between TM6 and TM7 contains residues that are required for the internalization

and degradation of ferroportin, and an extracellular loop between TM7 and TM8 having the binding site of hepcidin (Bonaccorsi di Patti et al., 2014).

The hepatic hormone hepcidin is encoded by the HAMP gene and is a master regulator of iron metabolism (Rishi et al., 2015). Upon binding of hepcidin, ferroportin is internalized and degraded, thus limiting iron export leading to reduced iron availability in serum (Nemeth et al., 2004).

Cellular iron homeostasis is regulated by coordinated expression of transferrin receptor and ferritin. These two proteins mediate iron uptake and storage. Transferrin (*Tfr1*), Divalent metal transporter 1 (*Dmt1*), ferritin (*Fth*) and ferroportin (*Fpn1*) are regulated post-transcriptionally. This process involves two cytoplasmic iron regulatory proteins IRP1 and IRP2 (Anderson et al., 2012). Upon iron deprivation, IRPs stabilizes the expression of *Tfr1* and *Dmt1* by binding to 3'UTR and inhibit the translation of *Fth1* and *Fpn1* by binding to the iron-responsive elements (IRES) within the 5'UTR (Silva and Faustino, 2015). Previous studies have provided a link between mitochondria and iron homeostasis. Iron deprivation led to down-regulation of the transcription of nuclear-encoded mitochondrial gene expression in brown preadipocytes (Rensvold et al., 2016). Moreover, iron deprivation also led to a reduction the expression levels of at least one of the transcripts encoding subunits of the five oxidative phosphorylation (OxPhos) complexes (Rensvold et al., 2016), suggesting that iron deprivation signals to the mitochondria to regulate energy production.

The role of iron in the context of melanogenesis comes from one study where the retinal pigment epithelial cells were grown in iron-replete condition and effect on the melanogenesis programme was studied (Wolkow et al., 2014). The melanogenic genes such as *TYR*, *TYRP1*, Hermansky-Pudlak Syndrome 3 (*HPS3*), *PMEL*, *DCT,* and

MITF were upregulated. Iron treatment led to enhancement of pigmentation and melanosome numbers in the retinal epithelial cells. Furthermore, transcription factors such as PAX3, LEF1, SOX9, SOX10, and OTX2 that are known to regulate MITF transcription, were also found to be up-regulated by iron (Wolkow et al., 2014). However, the role of ferroportin in the regulation of iron homeostasis in melanocyte is still unknown. The purpose of other solute transporters in the context of melanogenesis is unclear, and it would be interesting to decipher their role in the context of melanogenesis.

III.2. Results and Discussion

As *Slc40a1/Fpn1* gene is down-regulated during melanogenesis, we wished to decipher the role of iron in melanogenesis. Towards this end, we next describe our experiments that led to uncovering the essential requirement of iron during melanogenesis.

III.2.1. Role for *Slc40a1* in Melanogenesis

As *Slc40a1*/*Fpn1* expression was downregulated in a time-dependent manner during melanogenesis, we next validated this data by qRT-PCR. Total RNA was extracted from B16 cells after 48h of forskolin and IBMX treatment. Consistent with the microarray data, *Fpn1* expression (normalized with respect to *Gapdh*) was found to be downregulated at 48h during compound induced hyper-pigmentation (Fig.III.2A).

Next, we performed siRNA-mediated silencing of *Slc40a1* using smart pool siRNA to decipher its role during melanogenesis. The effect of *Slc40a1* knockdown was studied on the expression of melanogenic genes by qRT-PCR. We found ~80% reduction in the expression of *Fpn1*, but the expression of *Tyr*, *Tyrp1*, *Dct,* and *Mitf*

genes was unchanged (Fig.III.2B). Upon *Slc40a1* knockdown, the cellular morphology and melanin level were also studied in B16 cells. Interestingly, increased melanin accumulation was seen in *Slc40a1* knockdown cells in comparison to si*Mitf* and mock-transfected cells at 48h, indicating that *FPN1* is required for melanogenesis (Fig.III.2C-D).

III.2.2. Subcellular localization of SLC40A1/FPN in B16 cells

Next, we wished to examine the sub-cellular localization of *Fpn1*. To predict localization in silico, the protein sequence of *Fpn1* was retrieved from UCSC genome browser. Next, the protein sequence was taken as an input to examine its potential to localize in different subcellular compartments using PSORT II localization prediction program. (http://psort.hgc.jp/form2.html). The FPN1 protein was predicted to be localized in the plasma membrane (69.6 % probability), endoplasmic reticulum (26.1% probability) and mitochondrial (4.3% probability) suggesting a putative localization in plasma membrane and/or endoplasmic reticulum.

To study the localization of ferroportin in B16 cells, the coding sequence of FPN1 was cloned downstream of a mCherry reporter in mCherryC1 vector (www.addgene.org). The coding sequence was amplified from cDNA obtained from the RNA of B16 cells using primer pairs ONM230-ONM231 (Fig.III.3). To facilitated cloning, a BglII site was added in the forward primer, and Acc651 site was added in the reverse primer. The size of the amplified insert was ~1.7kb. The mCherryC1 vector was digested sequentially with BglII and Acc651, dephosphorylated using Antarctic phosphatase (NEB), and ligated at 16°C overnight in a cooling water bath. After overnight incubation, the ligation mixture was transformed into *E. coli* DH10B bacterial strain. About 15 colonies were screened by Acc651 digestion, and the positive clones

were further screened by second digestion with BglII to release the ~1.7kb *Fpn1* insert. The positive clones were sequenced, and the correct clone pM40a1-2 was chosen for transfection.

For transfection, B16 cells were seeded at a density of 32000 cells/well in a six-well plate. After overnight incubation for adherence of cells, ~1µg of the plasmid constructs, pM40a1-2 was transfected using Cellfectin reagent, and mock was taken as control. After 6h post-transfection, the cells were washed twice with DPBS, and the original media was returned to the cultures. The transfected cells were harvested at 24h post-transfection by adding native lysis buffer directly to the plate, and protein estimation was done using the BCA kit. About 30µg of total protein from each sample was used for western blot analysis. The blot was probed with anti-mCherry primary antibody (Rabbit polyclonal, 1:1000 dilution). In pM40a1-2 transfected cells, we obtained a band of the expected size of ~89kDa band in addition to two possible breakdown products of 72kDa and 55kDa (Fig.III.4A). In the case of the control (vector only) transfected sample, a 28kDa band corresponding to the size of mCherry alone was obtained (data not shown), and in mock-transfected cells, no bands were observed (Fig. III.4A). These results showed that Fpn1 was being expressed in B16 cells as an mCherry fusion.

The construct pM40a1-2 was used for cellular localization of FPN1 by fluorescence microscopy. The B16-F10 cells were grown on cover slips in a 6-well plate and transfected with pM40a1-2. After 24h post-transfection, media was aspirated, and the wells were washed with 1ml DPBS to remove any trace amounts of media. Fluorescence microscopy was carried out on Nikon Eclipse Ti-E inverted microscope system with filter sets for TRITC (red) emission, and Nikon NIS- Elements Advanced

Research software. Thus, the fluorescence microscopy showed that FPN1-mCherry was expressed in vivo at 24h of post-transfection (Fig.III.4B).

Next, to detect intracellular localization of FPN1-mCherry in B16 cells, we carried out confocal microscopy. B16-F10 cells were grown on a coverslip and transfected with pM40a1-2. After 24h post-transfection, confocal microscopy was carried out to detect mCherry fluorescence, and also counterstaining by Hoechst stain to visualize nuclei. Confocal microscopy was carried out on Nikon Eclipse Ti-E inverted microscope system with filter sets for TRITC and DAPI emission, and images captured at 60x using Andor iQ version software. The confocal microscopy revealed punctate staining of SLC40A1 protein predominantly found on the plasma membrane (Fig.III.5A). Fig.III.5B shows the fluorescence quantification for mock and FPN1 transfected samples. The mock samples were taken as a control to ruled out the possibly of autofluorescence in B16 cells. We found high fluorescence intensity from the FPN1 cells as compared to that of mock samples. Our observation indicates the plasma membrane localization of FPN1 protein in B16-F10 cells consistent with FPN1 localization on plasma membrane of Kupffer cells, and splenic macrophages cells reported previously (D'Anna et al., 2009; Delaby et al., 2005).

III.2.3. Modulation of melanogenesis by iron homeostasis in B16 cells

As ferroportin expression was downregulated upon melanogenesis, we next wanted to assess the role of iron during melanogenesis. We cultured B16 cells in ferric ammonium citrate (FAC) or in presence of bathophenanthroline disulfonate (BPS), a chelator of iron. We carried out pilot experiments to determine the optimal concentration of both compounds by performing MTT assay for cell viability. The B16 cells were treated with different concentration of FAC and BPS for 24h and 72h and

cell viability assessed by MTT assay. The MTT data showed that up to 500µM FAC and 200µM BPS cell viability was between 70-80% (Fig. III.6A-B), and accordingly, we chose these concentrations to carry out further studies on cell morphology and phenotype.

To determine cellular morphology, 32000 cells/well were seeded in DMEM media in a 6-well plate and kept in a CO_2 incubator for adherence overnight (Fig.III.7A). After the cells adhered to the plate, compound treatment was done and at 48h of treatment cell imaging was performed using phase-contrast/bright field microscopy. FAC treatment lead to a very high melanin level and increased dendrite formation compared to cells in control DMEM medium or that in BPS medium (Fig.III.7B-C). Next, the cellular melanin accumulation was visualized. The B16 cells were treated with these two compounds for three different time points, 24h, 48h, and 72h. After respective time points, cells were trypsinized, harvested and the cell number was counted using Neubauer hemocytometer. About $1x10^6$ cells were pelleted in a microcentrifuge tube, and melanin content was visualized and photographed. The pellet color of FAC-treated cells was significantly darker than the DMEM control (Fig.III.7B). Moreover, iron depletion by BPS caused a marked decrease in pellet color, which could be reversed by supplementation of iron in the culture medium (Fig.III.7D).

We also found that cell proliferation was directly influenced by iron levels in the culture medium as assessed by cell counts. Whereas the cell number was 3.7 $x10^6$/ml and 1.21 $x10^6$/ml in BPS medium and 6.72 $x10^6$/ml and 7.7 $x10^6$/ml in FAC-containing culture compared to $5.1x10^6$/ml and 5.6 $x10^6$/ml in DMEM alone at 48h and 72h respectively (Fig.III.7E). Moreover, the rate of melanin accumulation also

was greatly promoted by iron levels. While the media and cell pellet color were visibly brown/dark brown by 72h in DMEM medium, the FAC-treated cells were visibly dark from 24h and reached the darkest at 48h (Fig.III.7A). Cells treated with BPS remained depigmented even up to 72h. The media color also mirrored the cell pellet color in the three media tested (Fig.III.8A). Next, we quantified the melanin levels in cells harvested after 48h of compound treatment where the pellet color difference between different conditions was significant. For melanin estimation, $1x10^5$cells were collected and melanin estimated as described in Materials and Methods using a standard plot constructed for synthetic melanin (Fig.III.8B). We found that melanin content in FAC-treated cells was ~3-fold higher compared to that in control DMEM medium (Fig.III.8C). In BPS-treated samples, however, the melanin level was ~4-fold lower compared to that in DMEM samples (Fig.III.8C). Hence, we found increased melanization in the presence and decreased melanization in the absence of iron that further indicates that iron homeostasis is important for melanogenesis.

III.2.4. Cellular investigations (TEM) and expression analysis (real-time qPCR) to decipher the role of iron homeostasis on melanosome formation and maturation

To understand the melanogenesis regulation by iron, we conducted ultrastructural studies of B16 cells cultured under iron replete and deplete conditions. Cells were seeded at a density of $0.25x10^6$ per T-75 flask in DMEM/ F12 media and incubated for 24h in a CO_2 incubator at 37°C. Cells were treated with FAC, BPS or control DMEM media and harvested at 48h time point. As shown in Fig.III.7B, at 48h of FAC treatment the melanin accumulation was significantly higher than the BPS and control DMEM media. Cells were fixed with 2.5% glutaraldehyde and embedded in 2% agar blocks before being processed and placed on copper grids and stained

(Section.II.9). The grids containing the sections were scanned, and three cells per sample were imaged using the FEI Tecnai^{TM} Twin-20 transmission electron microscope. The cells were imaged at various magnifications of 550x, 1700x, 2500x, and 3500x. As discussed in section I.3, melanocytes contain four stages of melanosomes on the basis of resident protein and melanin accumulation. To carefully establish the conditions for identifying various organelles and melanosome stages, we visualized cells at different magnifications and melanosomes were marked. Fig.III.9A shows the ultrastructure of a melanocyte at 550x magnification in a B16 cell grown in DMEM medium. The various organelles like the nucleus, the nucleolus, mitochondria and vesicular bodies are labeled in Fig.III.9A. The different stages of melanosome can be distinguished from mitochondria at1700x magnification (Fig.III.9B). Next, we further magnified the images and identified the various melanosome stages from I to IV on the basis of increased melanin accumulation. From these images, we created a montage representing each stage of melanosome maturation as indicated in Fig.III.9C. Stage I melanosomes are non-pigmented vacuolar structure derived from the endosomal system, and the presence of internal striations characterizes stage II. The melanogenic enzymes TYR and TYRP1 are trafficked to stage II melanosome to initiate the process of melanin formation and eventually give rise to stage III melanosome. Stage I and II are also known as premelanosome stages. Melanin deposition on this formed striation starts from the stage III and eventually give rise to mature, fully melanized stage IV melanosomes. Stage III and the mature IV melanosomes are indicated with more melanin granules, with stage IV being the most densely packaged dark structure.

Using this as a reference, all melanosome stages were identified in 1700x images. Fig.III.10A shows the representative EM images for DMEM, FAC and BPS at

1700X magnification at 48h time point. Melanosomes were counted from three B16 cells per sample and a total of 102, 151, 37 melanosomes in stages III and IV were identified respectively in DMEM, FAC and BPS samples, and melanosome number for each condition was plotted. The total number of stage III and IV melanosomes in FAC-treated sample was higher (p-value of <0.001) compared to DMEM and BPS Fig.III.10B. Thus, cellular investigation suggested that replete iron leads to increased stage III and IV melanosome whereas depletion of iron caused melanosome arrest very early in the process of maturation (Fig.III.10A-B).

Next, we checked the expression of genes known to be required for melanosome biogenesis (Marks and Seabra, 2001). The *Hps3* gene, encoding a premelanosome component, *Pmel17* (a melanosome component), *Rab27a*, a melanosome mobility component was studied at 24h and 48h of FAC and BPS treatment. For the expression analysis, the $2^{-\Delta\Delta CT}$ analysis was done using cells grown in DMEM media as reference. Interestingly, we found these genes to be upregulated ≥2-fold at 48h of iron-induced hyper-pigmentation. (Fig.III.10C). This result further strengthened the observation of increased melanin accumulation at 48h of FAC treatment with respect to BPS and the control DMEM sample. Together, we conclude that iron promotes melanogenesis by accelerating both melanosome biogenesis as well as the maturation underscoring the crucial role of iron in regulating intracellular membrane dynamics during melanogenesis.

III.2.5. Examining the effect of iron replete and deplete on mRNA and protein expression of melanogenic genes

To understand how iron status controls melanogenesis, we next probed the expression of melanogenesis genes and the cognate proteins. Single-stranded cDNA

was prepared using oligo(dT) as a primer, and real-time qPCR analysis was done to assess the expression of the melanogenic genes *Tyr*, *Tyrp1*, *Dct,* and *Mitf.* The qRT-PCR data is summarized below. *Tyr* expression was not significantly altered in FAC or BPS media at 24h to 72h, although *Tyr* mRNA was upregulated at 72h in BPS medium (Fig.III.11A-B). The *Tyrp1* mRNA expression is not highly regulated in FAC or BPS media at 24h-72h, although *Tyrp1* expression was elevated at 48h in FAC, and at 72h in BPS containing medium. No change in *Dct* expression was observed in both the condition at all the three-time points. The *Mitf* mRNA expression was elevated at 24h and 48h after FAC or BPS addition, but its expression was down-regulated at 72h in both media (Fig.III.11A-B). These data showed that of the three melanogenic gene mRNAs, only the *Tyrp1* mRNA level was substantially upregulated in FAC medium. Furthermore, *Mitf* mRNA is upregulated in both FAC and BPS containing media during early periods of melanogenesis.

We next studied tyrosinase protein level in FAC or BPS containing media since TYR protein is known to be controlled at post-transcriptional level (Bae-Harboe and Park, 2012; Newton et al., 2007). B16 cells were treated with 500µMof FAC, or 250µM of BPS for three time periods, trypsinized, harvested and lysate prepared. For Western blot analysis, 20µg whole cell lysate proteins were run on 10% SDS-PAGE, blotted to PVDF membrane and blot was probed with murine α-Tyrosinase antibody (1:10,000; a kind gift from Vincent Hearing NCI, NIH) and MITF antibody (59kDa,1:2000). As a loading control, the blot was probed with a murine HRP-conjugated anti-β-actin antibody (1:100000 dilution). The western blot data showed that TYR protein level was highly downregulated in BPS media (Fig.III.11C). In FAC

medium, TYR expression was highly elevated even at 24h in comparison to that in DMEM medium (Fig.III.12A), but no significant difference of TYR protein level was found at 48h and 72h with reference to that in DMEM control. The MITF protein level was down-regulated at 72h in both FAC and BPS media (Fig.III.11C), consistent with the down regulation at mRNA level (Fig.III.11A-B). In summary, the expression analyses suggested that depigmentation upon iron depletion is mediated by reduction in TYR protein expression. Moreover, accelerated pigmentation observed in FAC medium is also coincident with elevated TYR protein expression.

III.2.6. Expression analysis of iron uptake and storage genes

Next, we investigated the regulation of known iron homeostasis genes in BPS- and FAC-mediated modulation of pigmentation in B16 cells. It is well established that the cellular iron homeostasis is regulated by a coordinated expression of transferrin receptor and ferritin, and their expression although predominantly controlled at post-transcriptional level, also are regulated at the transcriptional level (Huang et al., 2014; Torti and Torti, 2002). Our qRT-PCR data showed that the expression of ferritin (*Fth1*) gene was upregulated in FAC medium at 24h and 48h, and reciprocally, *Fth1* mRNA was down-regulated in BPS medium (Fig. III.12). The expression of both *Tfr1* and *Dmt1* was up-regulated at 48h of FAC treatment. In BPS medium, however, *Tfr1* and *Dmt1* mRNA was elevated at 24h but down-regulated by 48h (Fig. III.12). The expression of *Fpn1* was highly up-regulated in FAC medium and down-regulated in BPS medium (Fig. III.12). These data are consistent with the fact that upregulation of ferritin (*Fth1*) is required for iron storage and upregulation of ferroprotein (*Slc40a1*) for iron export (Fig.III.12).

III.2.7. Effect of iron deprivation on the transcript encoding oxidative phosphorylation (OxPhos) complexes

Iron is an essential cofactor that is required for various cellular processes such as oxidative phosphorylation, DNA maintenance, and gene expression. Further, iron deprivation in Brown preadipocytes has been shown to regulate the gene expression of complexes involved in oxidative phosphorylation (OxPhos) (Rensvold et al., 2016). Since melanogenesis is itself an ATP-driven process. Therefore, we wished to study the expression of these OxPhos genes during iron deplete and replete medium. The expression of genes involved in OxPhos such as C1-*Ndufa9*, CII-*Sdha*, CIII-*Uqcrc2*, and CIV-*Cox4i*, and CV-*Atp5a* was studied at 24h and 48h of FAC and BPS treatment. Interestingly, we found a significant decrease in the expression of C1-*Ndufa9*, CII-*Sdha*, CIII-*Uqcrc2*, and CIV-*Cox4i*, OxPhos transcripts at 48h of BPS induced iron deprivation (Fig.III.13). This result further indicates that during BPS induced iron deprivation adaptive cellular response is activated by employing the transcriptional regulatory program to decrease the transcript encoding Oxphos complexes.

III.2.8. Genome-wide transcriptomic changes during iron replete and deplete condition

To identify global transcriptomic response to iron levels, we carried out microarray analysis. B16 cells were seeded at a density of $2x10^4$ cells/T-75flasks in Ham's DMEM/F-12 medium and cells grown for five days (named as F12 precultured cells). In the DMEM/F12 medium, melanogenesis is inhibited, and B16 cells remain depigmented. These cells were seeded at a starting cell density of $0.25x10^6$ cells/T-75 in DMEM media. After overnight adherence, 500µM FAC or 250µM BPS were added

to the culture medium and grown at 37°C with 5% CO_2. Cells were harvested at 24h and 48h post-treatment along with cells grown in DMEM media (control). At the respective time points, medium was aspirated, Trizol reagent added and cells were harvested. Total RNA was isolated using Qiagen's RNeasy mini kit (Cat#74106) from two biological replicates after compound treatment. The RNA integrity was analyzed by gel electrophoresis and concentration estimated by UV spectrometry.

The integrity of total RNA samples was analyzed by Agilent Bioanalyzer and found to be acceptable with RIN number 9.0 or more. A representative set of BioAnalyzer images are shown in Fig.III.14. A-C. Total RNA was processed for microarray hybridizations using the Agilent two-color platform as follows. The RNA samples were labeled with Cy5 and Cy3 fluorophore dyes using Agilent's Quick-Amp labeling Kit (p/n:5190-0442), and in all cases, the specific activity (pmole dye/µg cRNA) of the labeled samples were ≥ 10.0. The Cy5/Cy3-labelled samples were hybridized to Agilent mouse microarray slides GXP_8X60k (AMADID:65570) by Genotypic Technology Pvt. Ltd. using the Agilent in Situ Hybridization Kit using the two-color platform. The hybridized arrays were scanned using Agilent Feature Extraction software, and images were manually verified to be devoid of uneven hybridization, streaks, blobs and other artifacts. Hybridization across the slide was assessed to be good based on the number of features that were significantly above background. As the microarray contained multiple (n≥2) oligonucleotides spots (also called features) for each gene/ORF, the replicate spots were averaged and data normalized, using the LOWESS method, using the Agilent GeneSpring GX 12.5 software. This procedure resulted in the data as the normalized $\log_2$ ratio for each gene.

III.2.9. Identification of differentially expressed genes in iron-replete and deplete condition

As mentioned above, two-color hybridization was carried out that involves treatment and control labeled with Cy5 or Cy3 to obtain a Cy5/Cy3 ratio. The entire hybridization planned had eight arrays for two compounds at two-time points, 24h and 48h, with two biological replicates. The experimental design is shown in the table III.2.

The complete normalized data was used to perform the analysis. These 55698 probes total lists were used as an input for file GeneSpring. The total of 34834 genes was obtained after combining the probes in GeneSpring software, and this list was further used to do the analysis. Technology files were created, and 2-Dhierarchical clustering generated a heat map for these 34834 genes (Fig.III.15A). The 2-fold cutoff was applied to obtain the significant list of genes in both iron deplete and replete condition. Fig.III.15A shows the microarray data analysis done to identify novel regulators in iron-replete and deplete condition.

Using the online database for annotation, visualization, and integrated discovery (DAVID), we identified biological themes by acquiring Gene Ontology (GO) in the category of biological process (BP) both in iron-replete and deplete conditions. The transcript upregulated and downregulated at 24h and 48h time points were found to be associated with distinct categories.

At 24h of FAC treatment, 71 upregulated transcripts were associated with ontology terms, such as ion transport, central nervous system, and cellular homeostasis. Moreover, 58 transcripts upregulated at 48h were associated with cellular homeostasis, G-protein coupled receptor signaling pathway and response to stress.

Further, 367 transcripts downregulated at 24h of FAC treatment was found to be involved in the processes such as regulation of biosynthetic process, mitotic cell cycle process, and regulation of nucleocytoplasmic transport. However, 62 genes downregulated at 48h of FAC treatment was found to be associated with cellular component organization, regulation of endocytosis and cell motility. We found *Slc11a1* (*Nramp1*) to be downregulated at 49h of iron-replete condition. The protein encoded by this genes is a multipass proton-coupled divalent metal ion transporters. SLC11A1 is a transporter for divalent ions such as iron and manganese (Anderson et al., 2012). The expression of *Slc11a1* has been shown to be regulated by the availability of iron in the medium (Hedges et al., 2013). Next, it would be interesting to study the role of *Slc11a1* in context of melanogenesis.

At 24h of BPS treatment, 80 upregulated transcripts was involved in G-protein coupled receptor signaling pathway, response to endogenous stimulus and positive regulation of metabolic process whereas 51 genes upregulated at 48h were involved in establishment of localization, developmental process involved in reproduction and nitrogen compound metabolic process.

~93 genes downregulated at 24h of BPS treatment were involved in canonical Wnt signaling pathway, regulation of epithelial cell proliferation and positive regulation of cell proliferation. Importantly, we found *Wnt10b* to be downregulated during iron deplete condition. Wnt10b by activating canonical Wnt signaling pathways regulates differentiation and pigmentation of melanocyte in mouse hair follicle (Ye et al., 2013). Moreover, the role of Wnt signaling in the proliferation and differentiation of human epidermal melanocyte have been reported in some studies (Yamaguchi et al., 2005; Yamaguchi et al., 2004). Therefore, it would be interesting to study the role and

mechanism of iron-regulated activation of the Wnt signaling pathway during melanogenesis.

Further 100 genes downregulated at 48h of BPS treatment were involved in protein complex biogenesis, negative regulation of cell communication and negative regulation of macromolecule biosynthetic process. Thus, from the genome-wide transcriptomic analysis, we found distinct categories of genes to be involved in different processes regulated by the presence and absence of iron in B16 cells.

Among 29 SLCs genes, we found *Slc18a1* up-regulated >2-fold at 48h and 72h time points during compound induced melanogenesis. The protein encoded by this gene is a vesicular amine transporter 1, whose function in pigmentation is not known but was also found in melanosomes by a proteomic approach (Chi et al., 2006), and its expression was markedly stimulated by both forskolin and IBMX.

Nevertheless, the data presented above indicate that cAMP may significantly influence ionic equilibrium in melanocytes and melanosomes. The role of other solute carrier transporter in context of pigmentation is unknown and need to be investigated. The localization of these solute carriers to the melanocyte as well as the mechanisms by which this modulates melanosomal pH remains to be elucidated.

III.3. Summary

The process of melanogenesis in cultured B16 cells has been shown to be substantially modulated by different regulatory molecules. Among 1620 genes, we found 29 SLCs genes to be differentially expressed during hyper-pigmentation. This class of transporters includes passive transporters, symporters, and antiporters. They are primarily localized in the cellular and organelle membranes. The metals are required

to be actively transported by the metal ion transporters to the destined intracellular compartments to maintain the proper functioning of the cell. Among 29 SLC genes, *Slc40a1,* a mammalian iron exporter was found to be at the top in the list of down-regulated SLC genes. The expression of *Slc40a1* was found to be downregulated across all the time points. Interestingly, we observed increased melanin accumulation in the mouse B16 cells where the *Slc40a1* was knocked down. Taken together, this observation suggests the crucial role of *Slc40a1* gene during melanogenesis.

The SLC40A1 protein was found to be predominantly localized on the plasma membrane of mouse B16 cells. It would be interesting to observe the localization of SLC40A1 in the compound induced hyper-pigmentation.

Taking this observation into account, the relationship between iron and melanogenesis was examined. Interestingly, melanogenesis was found to be modulated by the availability of iron in the medium. We found significantly increased melanin accumulation in iron-replete condition. We also observed the expression of *Slc40a1* to be differentially modulated by the presence and absence of iron.

The expression of *Slc40a1* was 6-fold up-regulated at 24h, and 48h of iron-replete in comparison to iron deplete condition. We also found the expression of the iron storage gene *Fth1* to be increased in iron-replete condition. These observations further indicate that to minimize the iron-induced redox stress inside the cell, iron induces the expression of both *Fth1* and *Slc40a1*. Our result points to the maintenance of a homeostatic balance between the iron storage and export. Therefore, to maintain the minimum pool of iron required for cell survival during iron deprivation, the expression of both iron storage and exporter genes are downregulated.

Melanosome is an excellent model system to study organelle biogenesis and motility. Although, significant advances have been made to explore the mechanism behind the melanosome biogenesis still many essential features of this process remain obscure. The cellular investigation through TEM suggests that iron promote melanogenesis by accelerating both the process of melanosome biogenesis as well as the melanosome maturation. The expression of essential genes involved in melanosome biogenesis like *Pmel17, Hps3,* and *Rab27a* was found to be upregulated in the iron-induced hyper-pigmentation. The regulation of melanosome biogenesis by nutrient like iron further provide new avenues to study organelle biogenesis.

Interestingly, we found mitochondrial genes involved in oxidative phosphorylation to be significantly downregulated during iron deprivation. Following iron deprivation, the adaptive cellular response is activated, that employs the transcriptional regulatory program to decrease the transcript encoding Oxphos complexes like C1-*Ndufa9*, CII-*Sdha*, CIII-*Uqcrc2*, CIV-*Cox4il,* and CV-*Atp5a1.* Hence, the link between downregulation of gene involved in mt OxPhos and melanogenesis needs to be explored. We do find some studies where it has been shown that the mitochondria physically contact the melanosome through the fibrillar bridges formed by mitofusin 2 (Daniele et al., 2014; Wu and Hammer, 2014). The inhibition of ATP synthesis has also been shown to reduce both the contact between the organelle and melanosome formation. Melanogenesis is an ATP dependent process, and the decrease in the OxPhos transcripts might cause a decreased level of ATP, that further leads to the inhibition of melanogenesis during iron deprivation. Therefore, we hypothesize that the reduction in the OxPhos transcript causes a reduced level of ATP and that might further lead to inhibition of melanogenesis during iron deprivation. This link between mitochondria and melanogenesis regulation is an exciting lead that will

be addressed in follow up studies. These can potentially lead to novel insights into nutrient signaling during melanogenesis.

Collectively, we demonstrate that deprivation of iron induces the transcriptional repression of genes involved in melanosome biogenesis (*Pmel17, Hps3,* and *Rab27a)*, iron storage (*Fth1*), iron export (*Slc40a1*), and nuclear-encoded mitochondrial OxPhos transcripts (C1-*Ndufa9*, C1-*Ndufs3*, CII-*Sdha*, CIII-*Uqcrc2*, CIV-*Cox4il,* and CV-*Atp5a1)*. Further, these studies add a new dimension to the regulation of melanogenesis by iron. Future studies would be directed to understand the role of iron homeostasis in the context of melanogenesis.

Chapter IV

Identification of Mitf-dependent and –independent regulon during melanogenesis

IV. IDENTIFICATION OF MITF-DEPENDENT AND -INDEPENDENT REGULON DURING MELANOGENSIS

IV.1.1. Introduction

Transcription factors belonging to a diverse family of proteins that initiate and regulate the transcription of genes. The specificity to control a broad set of genes under different conditions comes from the DNA binding domains of the TF that binds to a specific sequence of the DNA. The evolution of TFs has further led to changes in their activity and specificity which is a significant source of evolutionary adaptation and phenotypic diversity (Bustamante et al., 2005). They have been classified by their DNA binding domains, and ~80% of the TF repertoire belongs to the C2H2 zinc-finger, homeodomain and HLH family of TFs in humans (Vaquerizas et al., 2009).

MITF gene, Myc-related family of transcription factor, is known as the master regulator of pigmentation (Levy and Fisher, 2011; Steingrimsson et al., 2004). MITF plays a vital role in survival, differentiation, migration, and proliferation of normal melanocytes as well as melanoma progression. MITF genes have other promoter organization which generates nine isomers among them MITF-M selectively expressed in melanocytes (Levy et al., 2006).

MITF recognizes CAYRTG consensus sequence located in the promoter region of target genes such as TYR, TYRP1, DCT, EDNRB, TBX2, MC1R, etc.) (Aoki and Moro, 2002; Fang et al., 2002; Levy et al., 2006; Zhang et al., 2012). The transcription factor such as SOX10 binding plays an essential role in TYR and DCT activation in addition to MITF, and PAX3 is known to repress DCT (Harris et al., 2013; Kubic et al., 2008).

MITF-M is positively regulated by several transcription factors including PAX3, CREB, SOX10, LEF1 (Goding, 2000; Steingrimsson et al., 2004). Co-transfection assays with MITF promoter constructs and SOX10 or/and PAX3 cDNA in human HeLa cell lines have been carried out, and it has been suggested that PAX3 acts synergistically with SOX10 activate the transcription of MITF (Bondurand et al., 2000). Transfection and deletion mutagenesis studies along with gel shift assays in human embryonic kidney cell line 293T and human fibroblast line NIH3T3 have shown that DCT promoter is activated by SOX10 (Jiao et al., 2004). Another regulator, SOX9, induces transcription of MITF, TYR, and DCT in adult and neonatal human melanocytes (Passeron et al., 2007). However, transcription factors like BHLHE40, ATF4, BRN2/POU3F2, and GLI2 repress the expression of MITF (Cheli et al., 2012; Falletta et al., 2017; Goodall et al., 2008).

MITF not only regulate genes involved in pigmentation, but it is also crucial for cell survival and cell cycle control. The potential of MITF to regulates several genes has been summarized using "rheostat model" which describes three critical scenarios of MITF function which depends upon the level of MITF activity in melanoma cells. The high level of MITF promotes differentiation, low-level invasion and absence of MITF lead to senescence or cell death (Carreira et al., 2006; Hoek and Goding, 2010). The expression and level of MITF target genes depend upon the TFs that bind to regulatory elements as MITF or separate elements associated with the same gene. This regulation is further strengthened by the study where forced ectopic expression of MITF in non- melanocyte cell types results in the absence of full melanocyte differentiation program (de la Serna et al., 2006; Vachtenheim et al., 2001; Yang et al., 2014).

Through high throughput studies, several novel MITF targets have been identified. The comparison of genes expressed in MITF transfected SK-MEL-28 with

that of untransfected-MEL-28 cells lead to the identification of 2-fold up-regulated 6936 differentially expressed genes. Of 6936 genes 84 genes showed high correlation with MITF expression. (Hoek et al., 2008).

Studies using chromatin immunoprecipitation coupled to high throughput sequencing (ChIP-seq) and RNA sequencing analyses in 501 Mel cells have shown that MITF regulates genes ranging from pigmentation to cell cycle, DNA replication, and repair (Strub et al., 2011).

Together, these studies have identified pigmentation-related genes in melanoma cell lines. A significant limitation of these studies is that expression profiles were obtained in constitutively pigmented or de-pigmented cells and therefore many genes unconnected with pigmentation could be identified.

IV.1.2. Background

IV.1.2.1 Novel Regulators of Skin Pigmentation Identified by Genome-Wide Transcriptome Analysis

As discussed in Chapter III.1.2.1 we developed a tunable model of melanogenesis using small molecules to carry out the genome-wide studies. The mouse B16 cells were exposed to two small molecules, IBMX and forskolin, known activators of the cAMP-PKA pathway for the different duration to induce melanogenesis (kirty, 2015). Microarray data analysis showed that forskolin and IBMX commonly regulate a large number of genes. Hierarchical clustering analysis showed a temporal pattern of expression of ~1620 genes. DAVID pathway analysis yielded several genes involved in melanosome biogenesis, cell cycle, inflammation and small solute transporters enriched during melanogenesis.

To characterize the gene expression patterns, we constructed a 2-D hierarchical clustered map using the Gene Spring software (Fig.IV.1A). We have identified twelve clusters of DE genes by their gene expression pattern. The group of genes that sustained-induction (cluster I1, I4), late-induction (cluster I2, I3, I5 and I7) and early-induction (cluster I6). In the down-regulated cluster of genes, we found several genes that sustained-repression (cluster R1, R2), late-repression (cluster R3) and early-repression (cluster R4, R5).

Using the online database for annotation, visualization, and integrated discovery (DAVID), we identified biological themes by acquiring Gene Ontology (GO) in the category of biological process (BP) and KEGG pathways to identify enriched functional description of the gene groups. The early-induction cluster (cluster I6), contained genes involved in the glycoprotein metabolic processes, sustained-induction cluster (cluster I1, I4) involved in transport and establishment of localization and late-induction cluster (cluster I2, I3, I5 and I7) in carbon metabolism, ribosome biogenesis, cell motility and TNF-chemokine mediated signaling pathways. The early-repression cluster (cluster R4, R5) included anatomical structure development, sustained-repression group (cluster R1, R2) included genes involved in the cell cycle, and late-repression cluster (cluster R3) included genes involved in cellular metabolic processes. To identify significantly enriched biological processes that mapped to the list of 1620 genes, we selected up-regulated ($\log_2 \geq 0.585$) or down-regulated ($\log_2 \leq -0.585$) genes that showed differential expression in at least one of the four-time points in both forskolin and IBMX. We obtained 513 DE genes up-regulated during forskolin induction and 301 genes up-regulated during IBMX induction. 260 DE genes commonly induced by both the compounds (Fig.IV.1B). We found 23 genes involved in apoptosis, 14 genes in the negative regulation of cell proliferation and 13 genes in the process of inflammation

(Fig.IV.1C). However, 502 DE genes were found to be down-regulated during forskolin treatment whereas 328 DE genes were down-regulated during IBMX treatment. We found 269 DE genes to be down-regulated in both the compounds (Fig.IV.1C). The down-regulated genes mapped to the GO terms representing cell cycle, mitotic nuclear and cell division. On combining the genes involved in the various cell cycles related processes a total of 38 unique genes were identified. 38 genes involved in the mitotic cell cycle were down-regulated; consistent with the idea that transcriptional regulation mediates cAMP-stimulated G1-phase cell-cycle arrest (Zambon et al., 2005). To conclude we have seen different sets of genes getting expressed at different time points. Therefore, this different cluster of genes at each time points was considered as a signature at that time points and they been seen to be associated with the various biological process.

IV.2. Results and Discussion

As discussed above we employed a tunable cellular model of pigmentation to uncover core regulators of pigmentation. The time course genome-wide transcriptomic analysis was carried out by inducing the mouse B16 cells with two known hyper-pigmenting compounds, forskolin, and IBMX.

The primary goal of this study is to identify what fraction of genes differentially expressed during hyper-pigmentation are regulated by the master regulator, MITF. In part of this chapter first we identified differentially expressed genes up- and down-regulated during *Mitf* silencing in mouse B16 cells. Next, we performed a meta-analysis of DE genes obtained from different conditions and sources to obtain MITF-regulated genes in mouse B16 cells. Figure IV.2. shows the pipeline followed during meta-analysis to identify MITF-regulated genes. Intriguingly, this meta-analysis leads to the

identification of MITF-dependent and -independent regulation of a subset of genes involved in different biological processes. Furthermore, the comparison of the dataset obtained from various cell lines has also lead to the identification of a core set of genes involved in pigmentation.

IV.2.1. Cloning of luciferase reporter construct of melanogenic genes to predict the nature of small molecules

The promoter of melanogenic genes like *Tyr*, *Tyrp1*, *Dct*, and *Mitf* was constructed to rapidly pre-screen the nature of compounds Insilco. For this, the promoter of these genes was cloned upstream of the luciferase gene in the pGL4.23 vector. The expression of the luciferase gene is directly correlated with the activity of cloned promoters. The *Tyr*, *Tyrp1* and *Mitf* promoters were amplified from B16 genomic DNA using the primer pairs ONM69-ONM70 (*Tyr*), ONM71-ONM72 (*Tyrp1*) and ONM75-ONM76 (*Mitf*). The forward primer for all incorporated the XhoI restriction site and the reverse primer incorporated the BglII restriction site. The size of *Tyr*, *Tyrp1* and *Mitf* promoters amplified were 1365bp, 2078bp and 1221bp respectively. The *Dct* promoter amplified from genomic DNA isolated from mouse liver. The primer pairs used for amplification were ONM97-ONM98, and the size of the amplicon was 1667bp. The restriction sites incorporated into the forward and reverse primers were XhoI and EcoRV respectively. First, to check the functionality of these cloned constructs the small molecules like forskolin was used to study the activity of promoters. Forskolin is known to activate melanogenesis by increasing the level of the secondary messenger, cAMP. cAMP by phosphorylating CREB activates the expression of MITF, a master regulator of melanogenesis. MITF by binding to the promoter of melanogenic genes activate their expression and hence melanin formation (Fig.IV.3A).

The effect of forskolin studied on the promoter of *Tyr*, *Tyrp1*, *Dct*, and *Mitf*. DLR assays were carried out to evaluate the promoter activity of these melanogenic genes in the presence of forskolin-treated B16 cells. For the transfections, 32000 cells were seeded in six-well plates and allowed to adhere for 24h. The transfection of B16 cells was carried out for six hours and after post-transfection forskolin treatment was done for 48h. After 48h of treatment, the cells were lysed using passive lysis buffer, and the luminescence was measured using the luminometer Glomax. The luminescence plotted as the ratio of luciferase and Renilla Relative Luminescence Units (RLUs). All three melanin biosynthetic genes, *Tyr*, *Tyrp1* and *Dct*, showed an increase in promoter activity after forskolin treatment (Fig.IV.3B).

Further, the ~1.6kb construct of *Dct* along with the 2.1-, 1.8-kb promoter fusions were shown to be repressed in the presence of IFN-γ (Natarajan et al., 2014). Natarajan et al. have demonstrated that IFN-γ mediates hypo-pigmentation in B16 cells in the MITF-independent manner by down-regulating *Dct* by activating IRF-1.

We also performed the time course study to examine the effect of forskolin induction on the promoter activity of tyrosinase, the rate-limiting enzyme in melanin synthesis. Dual luciferase assay was performed as mentioned above for seven different time points, 0h, 2h, 6h, 12h, 24h, 48h, and 72h. From the Fig.IV.3C it can infer that forskolin treatment significantly activates the promoter of tyrosinase at later time points (48h and 72h) in comparison to control DMEM and DMSO (Vehicle). The activity of tyrosinase promoter was also increased in control, DMEM, and DMSO since they are known to induce melanogenesis (Fig.IV.3C).

IV.2.2. Small interfering RNA (siRNA)-mediated *Mitf* knockdown in B16 mouse melanoma cells

Mitf was silenced in B16 mouse melanoma cells using 100nM of smart pool siRNA against *Mitf*. For, siRNA transfections Dhermafect (Invitrogen) transfection reagent was used. The transfection was performed by seeding of 32000 cells/ well in six-well plates and allowed to adhere for 24 hours before transfection (Section II.12). After 48h of the post-transfection, the effect of *Mitf* silencing was observed on the pigmentation status of mouse B16 cells. The total melanin accounts both the intracellular as well as secreted melanin. We studied the impact of *Mitf* silencing on both the intracellular melanin accumulation and change in the media color (secreted melanin). *Mitf* knockdown in B16 cells leads to decreased melanin accumulation and no change in the media color as compared to mock at 48h (Fig.IV.4A-B). The effect of *Mitf* silencing was also studied on the protein level of tyrosinase by performing western analysis (Section II.19). MITF is known to transcriptionally activate the expression of tyrosinase by binding to the M-box sequence (CATGTG) present in the promoter of this gene. After silencing *Mitf*, the cells were induced with IBMX or DMSO as a control for 48h. Though the tyrosinase protein level was slightly higher in IBMX induced samples than DMSO, overall, we found decreased protein level in *Mitf* silenced samples as compared to their scrambled control siRNA (Fig.IV.4C).

The In-gel DOPA assay was performed to check the tyrosinase activity (Section II.20). The assay was carried out with the lysates from the cells transfected with 100nM si*Mitf* for 48h in DMEM media. We found decreased tyrosinase activity in the *Mitf* silenced cells. (Fig.IV.4D).

After observing the effect of *Mitf* silencing on B16 cells, we employed the same condition to perform microarray to identify differentially expressed genes on *Mitf* silencing. After 48h post-transfection cells were harvested by adding Trizol reagent. The RNA isolation was performed using the RNeasy kit and quantitation was done using a Nanodrop spectrophotometer. The integrity of RNA was also checked by running 500ng of RNA in 0.8% agarose gel (Fig.IV.5A). The purified RNA was sent to Genotypic Technology Pvt. for Agilent single color hybridization. For, normalization mock samples were used instead of scrambled siRNA because we have observed the change in the media of the sample where scrambled siRNA was used. This further suggests that scrambled siRNA may be targeting the gene directly or indirectly involved in pigmentation. RNA isolation of mock and si*Mitf* B16 cells was done in biological duplicates followed by Agilent one color hybridization.

IV.2.3. Transcriptomic profiling upon MITF-knockdown in B16 cells

Single color microarray hybridization using Agilent platform

As discussed above, the purity of isolated RNA was checked using the Nanodrop spectrophotometer and gel electrophoresis. The integrity of isolated RNA was also analyzed on the Bioanalyzer (Agilent; 2100 expert). The quality of RNA was determined by 260/280 ratio (Nanodrop estimation), rRNA 28S/18S ratios (electrophoresis) and RNA integrity number (RIN) (Bioanalyzer). All the samples had RIN number optimum (9-10) for hybridization, the bioanalyzer images are shown (Fig.IV.5B-E). The samples, Mock1, Mock2, siMi1 and siMi2 at 48h were labeled using the Agilent Quick-Amp labeling Kit (p/n5190-0442). The table.IV.1 shows the hybridization plan.

The 500ng of RNA was used to reverse transcribed to ds cDNA 40°C using oligo dT primer that is tagged to a T7 polymerase promoter. The cRNA generation where generated using double-stranded cDNA.

To generated cRNA, in vitro transcription was employed and the dye Cy3 CTP (Agilent) incorporated during this step. Both the cDNA synthesis and in vitro transcription were carried out at 40°C. Cy3-Labeled cRNA was cleaned up using Qiagen RNeasy Mini kit columns (Qiagen, Cat No: 74106). To assess the quality of yield and specific activity Nanodrop ND-1000 was used. Labeled cRNA sample was fragmented at 60ºC and hybridized on to Agilent Mouse Gene expression Microarray 8x60K (AMADID: 65570) arrays. The labeled RNA was fragmented and hybridized using Gene Expression Hybridization kit of (Agilent Technologies, In situ Hybridization kit, Part Number 5190-0404). The process of hybridization was carried out in Agilent's Sure hyb Chambers at 65º C for 16 hours. The hybridized slides were washed using Agilent Gene Expression wash buffers (Agilent Technologies, Part Number 5188-5327). The scanning was done using the Agilent Microarray Scanner (Agilent Technologies, Part Number G2600D). The data was extracted from the images using Agilent Feature Extraction software Version 11.5. Agilent GeneSpring GX software was used to analyze extracted data. The 75th percentile shift method was used to normalize the data in GeneSpring GX. The fold change values obtained by comparing treated samples wrt control. The differential pattern of expression identified among the samples. The filter of regulated fold ≥ 0.8 (logbase2) and down-regulated ≤ 0.8 (logbase2) was applied to identify differentially expressed genes. The volcano plot algorithm was used to apply statistical student T-test p-value among the replicates. The genes differentially expressed were clustered using hierarchical clustering based

on Pearson coefficient correlation algorithm. Genes were classified based on functional category and pathways by performing DAVID analysis (http://david.abcc.ncifcrf.gov/).

IV.2.4. Identification of differentially expressed genes upon MITF-knockdown

The expression fold values were obtained in log base2. The total probe list of 34836 was obtained, and the cut off fold ≥ 0.6 or ≤ 0.6 was applied to filter up- and down-regulated genes. A total of 1430 gene were found to be up-regulated, and 1048 genes were down-regulated upon *Mitf* silencing. Using the online database, DAVID, we identified biological themes by acquiring Gene Ontology (GO) in the category of biological process (BP) p-value less than 0.05.

We found genes involved in steroid biosynthesis, melanogenesis, cholesterol biosynthesis glutathione metabolism, nitrogen metabolism, etc. to be enriched in the downregulated category (Fig.IV.6A). These genes included *Tyr*, *Kit*, *Ednrb*, etc. Interestingly, the role of transcription factor MITF regulating steroid biosynthesis is still unknown, but we do find the link between melanogenesis and cholesterol synthesis in some studies. In contrast, up-regulated cluster, we found genes involved in chemokine signaling pathway, cytosolic DNA-sensing pathway cytokine-cytokine receptor interaction, and other processes involved in immune responses to be enriched (Fig.IV.6B).

The real-time qPCR validation of the genes involved in distinct categories was done after 48h of post-silencing. We found genes involved in chemokine signalings like *Ccl1*, *Cxcl1*, and *Cxcl3* to be >2 fold up-regulated whereas, the genes involved in melanogenesis like *Tyr* and *Ednrb* and steroid biosynthesis like *Hmgcr*, *Dhcr7* and *Tm7sf2* were downregulated upon *Mitf* silencing (Fig.IV.6C). The up- and down-regulated genes indicate distinct functional categories enriched upon *Mitf* silencing.

IV.2.5. MITF regulation in Forskolin-and IBMX - induced Transcriptome

IV.2.5.1. Identification of MITF-dependent regulon

Next, we were interested in identifying the regulation of the 1620 DE genes identified during compound induced hyper-pigmentation during MITF knockdown. Interestingly, a number of these DE genes showed a MITF independent response as can be observed by comparing the si*Mitf* treated samples with the forskolin/IBMX treated samples. These analyses suggested that a significant fraction of the DE genes is seemingly not under direct MITF control, thereby raising the possibility that a large melanogenesis transcriptome could be regulated in a MITF-independent manner (Fig.IV.7).

From the list of 260 genes up-regulated during hyperpigmentation induced by forskolin and IBMX, 43 (16.5%) genes were down-regulated when *Mitf* was silenced whereas, from the list of 269 genes down-regulated during hyper-pigmentation, 58 (21.6%) genes were up when *Mitf* was silenced. The 3D heat cluster map of these 101 genes was constructed using gene spring software (Fig.IV.8A-B).

Among 101 common genes, 43 transcripts up-regulated in Forsk /IBMX and down-regulated in si*Mitf*. They were found to be primarily associated with ontology terms such as protein maturation (*Ero1l*, *Chac1*, etc.), metal ion homeostasis (*Lgals3*, *Slc24a4*, etc.), and cellular response to stress (*Bnip3*, *Dh2*, etc.).

Both *Ero1l* (Endoplasmic Reticulum Oxidoreductase 1 Alpha) and *Chac1* (ChaC Glutathione Specific Gamma-Glutamyl cyclotransferase 1) regulate the ER stress and mediates the pro-apoptotic effects and hence regulate the proper protein folding and maturation (Chen et al., 2016; Mungrue et al., 2009).

Lgals3 (Galectin 3), encodes a member of the galectin family of carbohydrate binding proteins that bind with a high affinity to β-galactoside sugars. It plays an essential role in numerous cellular processes like apoptosis, immunity and cell adhesion. In melanoma cells, *Lgals3* have been shown to regulates expression of several genes such as NFAT1 and autotaxin that contribute to melanoma growth and metastasis (Braeuer et al., 2012). Genome-wide association study has identified *Slc24a4*, candidate gene that might play an important role in regulating melanogenesis (Sturm, 2009). The previous research from our lab has shown that silencing of *Slc24a4* leads to downregulation of the expression of important melanogenic genes such as *Tyr*, *Tyrp1*, *Dct*, and *Mitf* (kirty, 2015). *Bnip3* (BCL2/adenovirus E1B 19kDa interacting protein 3) is a known HIF (Hypoxia-Inducible Factors) target gene which is a master regulator of cellular metabolism. The expression of HIF-1α was found to be up-regulated when melanogenesis was induced in melanoma cells (Slominski et al., 2014). Further, the expression *Bnip3* is shown to directly correlated with that of HIF-1α expression (Bellot et al., 2009). Therefore, it would be interesting to study the role of *Bnip3* in context of pigmentation.

Dh2 (Dehydrogenase/Reductase 2) encodes a member of the short-chain dehydrogenases/reductases (SDR) family. This enzyme metabolizes many different compounds, such as steroid hormones, prostaglandins, retinoids, lipids and xenobiotics.

However, 58 transcripts downregulated in forsk/IBMX and up-regulated in si*Mitf* were involved in the regulation of signaling pathways like cell surface receptor signaling (*Atoh8*, *Lgr6*, etc.) mitotic cell cycle (*Fgf8*, *Kif20b*, etc.) and apoptotic signaling (*Vdr*, *Bmf*, etc.).

The *Vdr* gene encodes the nuclear hormone receptor for vitamin D3. Interestingly mice lacking VDR have shown to have defective epidermal differentiation

(Bikle et al., 2006). The transcription factor ATOH8 (atonal homolog 8) is known to regulate bind the E-box element present at the promoter of the target gene along with other b-HLH TFs. Their role in the context of melanogenesis is unknown until now.

IV.2.5.2. Identification of MITF-independent regulon

Interestingly we found a significant fraction of genes to show a MITF-independent response in forskolin and IBMX induced hyper-pigmentation. Based on forskolin and IBMX transcriptomic data, 217 genes up-regulated (83.4%) and 211 genes (78.3%) down-regulated, showed MITF independent response.

The upregulated transcripts were primarily associated with the ontology terms such as cellular response to apoptosis and stress, intracellular signal transduction, response to a steroid hormone, cellular response to growth factor stimulus, and regulation of cell proliferation. The downregulated clusters were found to be involved in cell cycle regulation, DNA metabolic process, DNA recombination during the double-strand break, and cytoskeleton organization.

The distinct categories of genes that showed MITF-independent response were involved in processes such as changes in the cell morphology, cell cycle regulation and activation of signaling pathways involved in DNA damage response, GF stimulus, etc.

The analysis indicates that MITF regulates only a fraction of the DE genes that are induced by pigmenting compounds. Also, some MITF associated DE genes have previously not been characterized in the context of pigmentation. This raises interesting possibilities of exploring potential novel MITF dependent and independent genes that might be involved in melanogenesis.

IV.2.6. Transcription factors differentially expressed during melanogenesis

We were then interested in identifying the various TFs that might be differentially regulated by compound treatment. We used the cisBP database to extract the list of known TFs using only the direct and the inferred evidence type. These were then identified in the MGI, and a total of 1553 TFs were obtained. From the list of 101genes differentially expressed we found 3 TFs, *Rarb*, *Vdr* and *Atoh8* to show a different pattern of expression depending upon the pigmentation status of the B16 cells (Fig.IV.8C).

In the microarray data, *Vdr* and *Atoh8* were found to be 2-fold down-regulated at the later time points in both forskolin and IBMX conditions whereas their expression was >2fold up-regulated when *Mitf* was silenced. On the other hand, expression of *Rarb* was 2-fold up-regulated in both forskolin and IBMX samples at 24h and 48h of time points whereas it was 2-fold down-regulated during *Mitf* silencing. The expression of these TFs was further validated by performing real-time PCR at 48h time points (Fig.IV.9A).

We analyzed the 1.5kb mouse promoter and 5'UTR sequences for *Rarb*, *Vdr*, and *Atoh8*. The known TF motifs E-box (CAYRTG), M-box CATGTG, PAX3 (GTGTGA), LEF-1 (TTAGGG) and SOX10 (A/TA/TCAAT/AG) used as query patterns in RSAT. Interestingly, in the *Rarb* gene, we found the M-box site at position-260 to -255 in the promoter whereas, the PAX3 and LEF1 in the 5'UTR at the position +410 to +415 and +236 to +241 respectively.

Vdr showed the presence of three PAX3 binding sites at the positions -662 to -657 and -758 to -753 and -1018 to -1013, two LEF1 binding sites at +17 to +22 and -1399 to -1394 and two M-box at -1206 to -1201 and -1213 to -1208 (Fig.IV.9B).

Atoh8 showed the presence of two E-box at the positions -230 to -225 and -1251 to -1246. Thus, the regulation of these differentially expressed genes could be via any of this melanogenesis regulating TFs.

Rarb encodes retinoic acid receptor beta that binds to retinoic acid and activates cellular signaling pathways involved in cell growth and proliferation. *Rarb* is tumor suppressor genes that mediate growth inhibition via all-trans retinoic acid (ATRA). In 70% of malignant melanoma, there is aberrant methylation and loss of *Rarb*, and also they are resistance to the antiproliferative effect of ATRA (Sarkar et al., 2015). In 501 Mel cells, *Rarb* is shown to be occupied by POU3F2 along with *Mitf-M*, *Tyr* and *Tyrp1*(Kobi et al., 2010). Interestingly, from the RSAT analysis, we have seen *Mitf* M-box, PAX3 and LEF1 binding site at the promoter of *Rarb* gene. Further, the role of *Rarb* in context of melanogenesis is still unexplored, and it would be interesting to study its function in the normal melanocyte.

The *Vdr* gene encodes the nuclear hormone receptor for vitamin D3. The target of this nuclear hormone receptor is primarily involved in metabolic pathways occurring during an immune response and in cancer (Pike and Meyer, 2012). The skin is the source of Vitamin D for the body and is capable of responding to metabolites of Vit D, 1,25-dihydroxy vitamin D_3 (1,25(OH)$_2$D) through VDR (Bikle and Pillai, 1993). Interestingly mice lacking VDR have shown to have defective epidermal differentiation (Bikle et al., 2006). However, the role of *Vdr* gene in the context of melanogenesis is not clear yet and would be interesting to study how beside regulating the genome integrity in skin epidermis it also controls melanogenesis.

The transcription factor ATOH8 (atonal homolog 8) is known to regulate bind the E-box element present at the promoter of the target gene along with other b-HLH

TFs. Further, it regulates cell proliferation and differentiation in endothelial cells through NOS3 (Fang et al., 2014). The role of *Atoh8* during melanogenesis is still unclear, but from our study we found it to be downregulated during melanogenesis. The expression of *Atoh8* was up-regulated when *Mitf* was silenced making the possibility of it acting as a negative regulator of melanogenesis.

From the list of 1430 genes up-regulated and 1048 genes down-regulated during *Mitf* silencing, as discussed earlier, we found 88 TFs to be 1.5-fold up-regulated and 46 TFs 1.5-fold down-regulated when *Mitf* was silenced. We found four common genes (*Barx2*, *Id3*, *Klf4*, and *Id1*) between 88 Tfs and 260 up-regulated cluster and two common elements (*Vdr* and *Atoh8*) between 88TFs and 269 down-regulated categories of genes. Further, we found two elements common (*Egr1* and *Rarb*) between 46 down-regulated TFs and 260 up-regulated cluster. Together it would be interesting to study the role of these transcription factors and their regulation in context of pigmentation.

IV.2.7. Role of MITF in regulating melanogenesis through iron homeostasis via IL6-Hamp-FPN1 axis

As discussed in Chapter III 29 SLCs were found to be differentially expressed during small molecule induced pigmentation. Next, we were interested to study the regulation of these small solute transporters by MITF. Among 29 SLC genes differentially expressed during forskolin and IBMX induced hyper-pigmentation, we found 3Slc genes (*Slc40a1*, *Slc25a27*, and *Slc35f1*) to be up- and 3Slc genes (*Slc2a4*, *Slc37a1*, and *Slc24a4*) to downregulated during *Mitf* silencing. Interestingly, we found *Slc40a1* which was down-regulated during melanogenesis, to be ~7- fold up-regulated when *Mitf* was silenced (Fig.III.10B). This raises the exciting possibilities that *Mitf* can activate melanogenesis by regulating iron homeostasis in the melanocyte.

Iron homeostasis is known to be regulated by IL6-Hamp-FPN1 axis in hepatic cells (Gardenghi et al., 2014; Wrighting and Andrews, 2006) ,but its role in melanocytic cells is unknown. Interestingly we found the expression of *Il6* gene to be >10 up-regulated at 72hrs of forskolin and IBMX treatment (kirty, 2015). Further, *Il6* promoter analysis was carried out to examine the transcription factor binding site, we found MITF binding site (M-box, CATGTG) at position -468 and -463 (data not shown). The differential expression of *Slc40a1* raises the interesting possibility that *Mitf* can activate melanogenesis by regulating iron homeostasis via IL6-SLC40A1 axis in the melanocyte. The mechanism by which *Mitf* is regulating iron homeostasis remains to be elucidated.

IV.2.8. Meta-analysis using high throughput data to identify novel regulators involved in melanogenesis

To identify *Mitf* target genes, we looked for overlap between 1430 and 1048 genes and the *Mitf* target genes identified previously (Hoek et al., 2008; Strub et al., 2011). Comparison of 118 genes induced by MITF overexpression in SK-MEL-28 cells by Hoek et al., 2008 was done with DE genes obtained from si*Mitf* silencing. We found 22 genes to be direct MITF target when the comparison was done between genes that were up-regulated in MITF-expressing cells with the gene downregulated in B16 cells following *Mitf* silencing (Fig.IV.11A). The majority of genes (p-value <0.05) among them were found to be involved in pigmentation (*Edrnb*, *Tyr*, *Mreg*, *Cited1*, *Rab27a*), melanocyte differentiation (*Edrnb*, *Mreg*, *Cited1*, *Rab27a*), melanin biosynthetic process (*Slc45A2*, *Tyr*, *Cited1*) cGMP-mediated signaling (*Slc45A2*, *Edrnb*, *Mreg*) melanosome transport (*Mreg* and *Rab27a*) regulation of pH (*Edrnb* and *Car14*) (Fig.IV.11B).

Further to identify the genes that are directly regulated by MITF, the si*Mitf* data from mouse B16 cells was compared with 2862 MITF-occupied sites derived from the ChIP-seq Strub et al.2011 123 genes from up- and 156 from the down-regulated list was found to be occupied by MITF (Fig.IV.12). The majority of genes downregulated were associated with GO terms such as transport (*Slc45a2*, *Rab5a*, *Insig1*), cellular homeostasis (*Slc24a5*, *Trpm1*, *Abcb6*), pigmentation (*Edrnb*, *Tyr*, *Mreg*, *Cited1*, *Rab27a*), cholesterol biosynthetic (*Srebf1*, *Sc5d*, *Insig1*). The genes upregulated were associated with the regulation of apoptosis (*Serpine1*, *Ddit3*) angiogenesis (*Nr4a1*, *Rnf213*, *Klf4*), nervous system development (*Id1*, *Mapk3*), cell differentiation (*Cdkn1a*, *Gadd45b*). Although MITF has been shown to activate several of its targets, from this analysis, it can be inferred that it might act as a repressor at some promoters.

The comparison was also done taking Strub et al., 2011 (ChIP seq: 5578), and Hoek et al., 2008 (6937 genes) datasets to identify genes directly up-regulated by MITF expression. The total common 1593 genes were then used to compare the list from the down-regulated gene list. 111 genes from down-regulated were common between 1593 genes obtained from Strub and Hoek data set. Next, DAVID analysis was done to identify the category of biological process regulated by these genes (Fig.IV.13A). The 111 genes downregulated and occupied by MITF were involved in cellular processes like pigmentation, ion homeostasis, melanosome localization and hypoxia (Fig.IV.13B).

The enrichment of distinct GO terms indicates that transcripts downregulated on *Mitf* suppression are primarily involved in regulating melanogenesis. During

melanogenesis, the role of ion homeostasis in maintaining the melanosomes pH is an essential factor in determining the activity of tyrosinase. The proton levels in melanosomes are regulated through several transporters. The net result of the maximal activity of these transporters leads to low pH and high tyrosinase activity.

It has already been established that suppression of *Mitf* in melanoma cells activates senescence programme (Giuliano et al., 2010). Depending on the level of its expression, MITF can have pro- or anti-proliferative effects. The inflammatory response also arises when cellular senescence programme is activated because of stress. The senescence is not limited to an arrest in the cell proliferation. In fact, senescent cells are metabolically active, and they are characterized by the release of senescence-associated secretory phenotype (SASP). The SASP basically includes interleukins and inflammatory cytokines (Coppe et al., 2010; Coppe et al., 2008).

To examine the total number of SASP associated with inflammatory response, SASP markers were collated from the literature mining. We compiled 46 SASPs, which included signaling factors such as interleukins, chemokines, and growth factors (Coppe et al., 2010; Coppe et al., 2008; Laurette et al., 2015). Interestingly, we found 6 SASP to be 2-fold up-regulated when *Mitf* was silenced which included, *Ccl2*, *Serpine1*, *Fgf1*, *Cyr61*, *Cxcl1*, and *Cxcl5*. Among these SASP signatures, *Ccl2* and *CxCl1* were also up-regulated during forskolin and IBMX induced hyper-pigmentation. Importantly, the previous study done in our lab through beta-galactosidase activity has ruled out the possibility of senescence occurring during forskolin and IBMX induced hyper-pigmentation. Further, it has been already shown through senescence-associated heterochromatic foci and β-galactosidase activity that siRNA-mediated silencing of MITF induces senescence in melanoma lines (Strub et al., 2011).

The comparison of the dataset with the available MITF targets indicates that besides acting as an activator for a subset of genes involved in several processes, it can also act as an inhibitor of some target.

IV.2.9. BRG1 regulates gene expression of several genes involved in distinct metabolic and cellular processes

MITF is known to interact with PBAF chromatin remodeling complex that is comprised of BRG1 and CHD7. BRG1 has been shown to be essential for the normal melanocyte development and melanoma proliferation. MITF and SOX10 recruit BRG1 to MITF-associated regulatory elements present at the active enhancers. BRG1 regulates the dynamics of MITF occupancy to the set of regulatory elements (Laurette et al., 2015).

To examine the genes commonly regulated by BRG1 and MITF in B16 cells the differentially expressed genes during BRG1 (501Mel cells) and MITF (B16 melanoma cells) silencing were compared. The RNA seq followed by shBRG1 in 501Mel cells led to the identification of >4000 genes downregulated and >5400 genes upregulated during BRG1 silencing (Laurette et al., 2015).

Upon MITF and BRG1 silencing, ~213 DE genes were found to be down-regulated. These down-regulated genes were enriched in ontology terms associated with transport, cholesterol biosynthesis, and cell differentiation. From these 213 genes, 137 genes were bound shown to be repressed on shBRG1 and bound by BRG1. The genes encoding factors involved in melanin synthesis, *Tyr*, and *Ednrb*, *Rab27a*, melanosome motility, *Slc24a5*, a membrane-associated transporter protein involved in

melanin synthesis were found to be downregulated on both MITF and BRG1 silencing. Further, the transcriptional activator of lipid homeostasis, *Srebf1* (Sterol Regulatory Element Binding Transcription Factor 1) And its target gene *Ldlr* (LDL receptor), *Hmgcr* (HMG-CoA Reductase), the rate-limiting enzyme in cholesterol biosynthesis, was found to be downregulated. The *Rarb* TF which was up-regulated in both forskolin and down-regulated during *Mitf* silencing was found in the list of a gene commonly repressed upon *Mitf* and BRG1 knockdown and bound by BRG1. The gene *Insig1* (Insulin-Induced Gene 1), regulates the cholesterol homeostasis in the endoplasmic reticulum was also found to be commonly repressed by MITF and BRG1 (Fig.IV.14A-C).

Further, 107 genes were commonly upregulated on MITF and BRG1 silencing and were associated with the terms like cellular organization, chemokine signaling, nutrient signaling and metal ion homeostasis (Fig.IV.14C). From the 107 genes, 48 genes were shown to be bound by upregulated on shBRG1 and bound by BRG1. They were involved in p53 signaling (*Gadd45a*, *Gadd45b*, and *Serpine1*), TGF-beta signaling (*Id1*, *Smad6*, and *Id3*), Hippo signaling (*Id1*, *Smad6*, and *fgf1*) (Fig.IV.14B).

Although MITF is known to regulate many genes involved in diverse biological processes, little is known about their regulation in a chromatin context. Here, through the meta-analysis, we identified different novel targets of both MITF and BRG1 that might have a significant role in regulating pigmentation. Next, it would be exciting to study the requirement for specific chromatin remodeling complexes during melanocyte-specific gene expression and melanocyte differentiation.

IV.3. Summary

MITF is known as a master regulator for both melanocyte development and melanoma progression. Previous studies have shown that MITF regulates a broad variety of genes, that range from pigment production to cell cycle regulation during DNA repair and replication. It is also interesting to note that loss of MITF leads to defective DNA replication and repair and ultimately leading to senescence.

Through small interfering RNA (siRNA) mediated MITF knockdown in B16 cells we identified an extensive set of genes that are involved in pathways previously not known to be implicated in pigment production. We have also used existing transcriptomic datasets to identify genes that might be novel targets of MITF. The comparison of our dataset with high throughput RNA seq and ChIP data have also identified a subset of genes that are negatively regulated by MITF. Earlier studies have primarily emphasized the role of MITF as an activator. However, through meta-analysis, we found several genes to be occupied and negatively regulated by MITF in B16 cells. Further studies are required to decipher the role of MITF as a negative regulator in the context of melanogenesis that can further the understanding of melanocyte biology.

The siRNA mediated downregulation of MITF in our study lead to the enrichment of distinct categories of genes involved in different processes. The transcript downregulated during MITF silencing were implicated in steroid biosynthesis, melanogenesis, cholesterol biosynthesis, glutathione metabolism and nitrogen metabolism. Further, the downregulation of MITF leads to increased chemokine signaling pathway, cytosolic DNA-sensing pathway, cytokine-cytokine receptor interaction, and other processes involved in immune responses.

Further, we have also studied the MITF regulation of genes differentially expressed during compound induced hyper-pigmentation. From the 529 core set of genes differentially regulated by both forskolin and IBMX, we found only 101 genes to show MITF-dependency. However, we found a large number of genes which showed MITF independent regulation. Among 101 genes showing MITF dependency, 43 transcripts were found to be up-regulated in Forsk /IBMX and down-regulated in si*Mitf*. They were found to be primarily associated with ontology terms such as protein maturation, metal ion homeostasis, and cellular response to stress. Of these, 58 transcripts downregulated in Forsk/IBMX and up-regulated in si*Mitf* were found to be involved in the regulation of signaling pathways like cell surface receptor signaling, mitotic cell cycle, and apoptotic signaling.

Interestingly, we found he role of iron homeostasis important for melanogenesis. The expression of iron exporter, *Slc40a1* was found to be up-regulated 7-fold when *Mitf* was silenced in B16 cells. Further, from the meta-analysis, we found *Slc40a1* to be upregulated and occupied by MITF also indicates that MITF can act as a repressor for *Slc40a1* gene regulation. We discovered that *Mitf* is regulating the expression of *Slc40a1* and thus intracellular iron depending on the pigmentation status of the B16 cells.

MITF is known to be phosphorylated by cAMP. In our study, we have used IBMX as one of the compounds to induce hyperpigmentation. IBMX is a phosphodiesterase inhibitor and thereby leads to increased accumulation of cAMP. Earlier studies have shown that induction of cAMP signaling causes MITF to regulate the phosphodiesterase, PDE4D3 directly. This further creates a negative homeostatic

control of the cAMP pathway that also controls the expression of *Mitf* during melanogenesis (Khaled et al., 2010). The level of tyrosinase, a rate-limiting enzyme for melanin synthesis, was found to be modulated during iron depletion. Iron deprivation through chelation caused downregulation of both tyrosinase protein and activity in B16 cells.

Importantly, we found the expression of *Mitf* to be downregulated in both iron replete and deplete condition. This further indicates that iron is directly or indirectly regulating the expression of *Mitf*, that in turn controls *Slc40a1* during melanogenesis. Accordingly, it is entirely possible that during iron-mediated regulation of melanogenesis the negative homeostatic regulation comes into play to regulate the expression of both *Mitf* and *Slc40a1*.

Previous studies by Natarajan et al., have shown that IFN-γ mediates hypo-pigmentation in B16 cells in a MITF-independent manner by down-regulating DCT through activation of IRF-1. This observation further strengthens the MITF independent regulation of genes required to maintain the genome integrity and homeostasis necessary for normal functioning of the melanocyte, particularly in the context of the depigmentation response.

Several small solute transporters were found to be differentially regulated during MITF knockdown. The only known iron exporter in mammalian cells, SLC40A1 was found to be down-regulated during compound induced hyper-pigmentation whereas it was up-regulated during hypo-pigmentation induced by MITF silencing. Together these observation/results allow us to extensively study the role of iron homeostasis during melanogenesis (covered in the next chapter).

Interestingly, our study also highlights hitherto unexplored MITF independent genes that might have regulatory roles in the process of melanogenesis. We found a significant fraction of genes differentially expressed during pigmentation not under MITF control. Thus, raising the possibility that a large melanogenesis transcriptome could be regulated in MITF-independent manner.

Chapter V

Transcriptional regulatory pathway(s) involved in skin depigmentation

V. TRANSCRIPTIONAL REGULATO RY PATHWAY(S) INVOLVED IN SKIN DEPIGMENTATION

V.1.Introduction

Melanin plays an essential role in protecting skin from harmful UV radiation. Melanin formation is catalyzed by three crucial melanogenic enzymes TYR, TYRP1, and DCT. The tyrosinase (EC 1.14.18.1) is the critical rate-limiting enzyme in the process of melanin formation (D'Mello et al., 2016). The tyrosinase, membrane-bound copper containing glycoprotein is subsequently processed in the ER and Golgi and trafficked to melanosomes (Watabe et al., 2004). The variation of skin color occurs at the level of epidermal melanin unit and depends upon the number, size, and dispersion of melanosomes to the surrounding keratinocytes. In the skin and hair, the visible phenotype is formed by transferring the melanin-containing melanosome to surrounding keratinocyte (Cichorek et al., 2013). The level of tyrosinase protein inside the cell is regulated by the balance of its synthesis and degradation. The effect on the stability and activity of tyrosinase has a dramatic impact on the process of pigmentation. The accumulation of abnormal melanin as pigmented patches occurs in specific parts of the skin in many pigmentation disorders such as melasma, freckles, ephelides, senile lentigines. The irregular hyperpigmentation is caused by excess melanin production and also abnormal distribution in the skin (Yamaguchi and Hearing, 2014).

Many approaches are available to treat hyper-pigmentary disorders either by inhibiting tyrosinase catalytic activity by competitive or non-competitive inhibitors or by disrupting tyrosinase maturation and stability (Ando et al., 2007). To modulate pigmentation, tyrosinase transcription and its post-transcriptional stability are

manipulated as potential avenues. The tyrosinase enzyme is usually targeted to develop therapies to cure hyper-pigmentary disorders such as melasma, and age spots.

V.1.2. Approaches to inhibit melanin synthesis via tyrosinase modulation

Many melanogenic inhibitors are known to control melanogenesis via modulating tyrosinase at different levels. Some targets control melanin synthesis via regulating the transcription (5-bromodeoxyuridine, TPA, TNF-α, etc.), maturation by asparagine-linked oligosaccharide processing (glucosamine/tunicamycin, glutathione, etc.), catalytic activity (phenylthiourea, kojic acid, arbutin, etc.), degradation (TGF-β1, TNF-α, Linoleic acid). These inhibitors are generally used to treat hyper-pigmentary disorders. In the process of melanin formation three enzymes are involved, TYR, TYRP1, and DCT. Several inhibitors target tyrosinase directly because it regulates the amount of melanin produced whereas others modify the type of melanin to be synthesized (Ando et al., 2007).

In addition to multiple approaches mentioned above the melanin synthesis is also regulated by a variety of other factors. Extracellular and intramelanosomal pH of melanocyte also governs the process of melanin synthesis (Yamaguchi et al., 2007). The intramelanosomal pH of melanocyte actively regulates the stability/trafficking of tyrosinase and hence the constitutive skin colors (Kageyama et al., 2004). The addition and depletion of glucose and galactose also regulate the melanin synthesis (Wang and Androlewicz, 2000). The cholesterol homeostasis also plays a crucial role in trafficking and glycosylation of tyrosinase as cholesterol starvation inhibits tyrosinase maturation (Hall et al., 2004).

Although tyrosinase inhibition is still the most studied mechanism of skin depigmentation, newer pathways are being identified. It would be exciting to

understand the complex homeostasis mechanism taking place in depigmentation or hypopigmentation. It is also unclear the consequence of depigmentation/hypo-pigmentation on melanocyte physiology since they are destined to form melanin. These studies will further help us to understand the dynamic processes like skin tanning and wound healing where many complexes interacting pathways contribute to maintenance of genome integrity in epidermal cells and in pigmentation disorders like vitiligo.

V.2. Results and Discussion

In this chapter, we propose to understand the regulatory mechanism underlying skin pigmentation homeostasis. Although several studies have delineated the pathways involved in hyperpigmentation, mechanisms that dampen or that maintain skin pigmentation homeostasis is not entirely understood. In this work, two small molecules kojic acid and linoleic acid were used to determine melanocyte response to these depigmenting agents by genome-wide transcriptome identification of genes that respond to these molecules. Further, we also identified gene signatures generated from different pigmenting/depigmenting molecules that could be used as an effective tool for screening small molecules.

V.2.1. B16 cell-based model to study depigmentation/ hypopigmentation

Media-dependent perturbation of melanogenesis

The melanocyte and pigment cell melanoma is often used to study the melanogenesis programme in vitro. Among them, B16-F10 mouse melanoma cells are generally used to investigate the melanogenic effect of various compounds. They are spontaneous melanoma derived from C57BL/6 mice that are a mixture of spindle-shaped and epithelial-like cells. A variety of media has been used to culture B16-F10

cells which includes MEM, RPMI1640 and DMEM. These cells have been found to show variable pigmentation under different media conditions. Routinely, B16 cells are cultured in two media viz., Dulbecco's Modified Eagle's medium (DMEM, D5648) and Dulbecco's Modified Eagle's medium (DMEM)/Hams Nutrient mixture F12 (DMEM/F12, D8900). The B16 cells were seeded at the density of 0.25×10^6 cells/T-75 flask in these two media and cultured for 48h. Upon completion, cell morphology and pellet color were recorded (Fig.V.1A-B). We observed that cells cultured in DMEM/F12 media were bipolar and unable to pigment, whereas, in DMEM media, cells were hyper-dendritic and accumulated melanin at 48h (Fig.V.1A). Since tyrosinase is the rate-limiting enzyme of melanogenesis, we carried out western blot analysis and DOPA assay to study the effect of DMEM/F12 and DMEM media on the tyrosinase protein and activity.

In brief, B16 cells cultured in DMEM/F12 and DMEM media were trypsinized, harvested and lysed. For Western blot, whole cell lysate was prepared (Section.II.19), and 20µg total proteins from the extracts were run on the 10% SDS-PAGE, blotted to PVDF membrane and blot was probed with a murine α-Tyrosinase antibody (1: 10,000; anti-PEP7, a gift from Vincent Hearing NCI, NIH). As a loading control, the blot was probed with a murine HRP-conjugated anti-beta-actin antibody (1lakh dilution). Interestingly we found a complete absence of tyrosinase protein in DMEM/F12 cultured cells (Fig.V.1C). Hence, DMEM/F12 provides a non-permissible condition for B16 cells to pigment by downregulating tyrosinase protein level.

For the further experiments, B16 cells were first seeded at a density of 2×10^4 cells/T-75 flasks in Ham's DMEM/F-12 medium and cells were grown for five days (named as F12 precultured cells) and were then seeded at a starting cell density of

0.25×10^6 cells/T-75 flask in DMEM medium. After overnight adherence, test compounds were added to the culture media and grown at 37°C, 5% CO_2.

Next, to understand the differential effects of the two media on pigmentation, we compared the composition of the two media as provided by the vendor. The DMEM/F12 medium is composed of 47 components, and, DMEM medium is composed of 31 components. Of these, 25 constituents are exclusively present in the DMEM/F12 and nine only in the DMEM medium (Fig.V.1D). A careful comparison of these components leads to the identification of one known hypo-pigmenting compound, linoleic acid (LA) in DMEM/F12 medium.

V.2.2. Small molecule-induced hypopigmentation in B16-F10 cells

Previous reports indicated that kojic acid (Lima et al., 2014) and LA (Ando et al., 1999; Ando et al., 1998) treatment led to hypopigmentation. Kojic acid is a known inhibitor of tyrosinase activity and works by chelating copper and by suppressing the tautomerization of dopachrome to DHICA (Draelos, 2007; Picardo and Carrera, 2007). Linoleic acid has been shown to cause ubiquitin-proteasome pathway-mediated degradation of tyrosinase (Ando et al., 2004). Therefore, we treated B16 cells with these two molecules to identify specific pathways, if any, leading to depigmentation.

V.2.3. Dose optimization of hypopigmenting compounds

Based on the previously published literature, a range of concentrations was finalized, and cell viability was tested using the MTT assay at different time points. Table V.1. shows the different concentrations of these compounds used to test viability by MTT assay. We found that for a viability of 80-90%, the optimal linoleic acid concentration was 75µM and kojic acid 2.5mM.

V.2.4 Examining the effect of small molecules on B16 cells

Next, after optimizing KA and LA concentrations, their effects were examined on cell morphology, and melanin accumulation. The B16 cells were treated with these two compounds for three different time points, 24h, 48h, and 72h. After respective time points, cells were trypsinized, harvested and the cell number counted using a Neubauer hemocytometer. About 1×10^6 cells were pelleted in a microcentrifuge tube, and melanin content was visualized and recorded. Further, for kojic acid, the pellet color difference was significant at 72h of treatment as compared to DMEM (control) (Fig.V.2A). Linoleic acid treatment led to a substantial decrease in the pellet color at 48h and 72h in comparison to vehicle control (ethanol) (Fig.V.2B). However, no major difference in cellular morphology was observed in KA- and LA-treated cells (Fig.V.2A-B).

V.2.5 Studying the effect of KA and LA on tyrosinase protein and activity

The effect of the two hypopigmenting compounds was studied on the tyrosinase protein and activity. Western blot analysis was done to check the inhibitory effect of KA and LA on the tyrosinase protein level. At 48h of KA treatment where the differences in the pellet color were apparent, there was no change in the tyrosinase protein level between treated and untreated samples (Fig.V.3A). Further, in-gel DOPA assay showed that kojic acid inhibits tyrosinase activity in a time and concentration-dependent manner (Fig.V.3B). The tyrosinase activity and protein level were also studied after treating the cells with linoleic acid. There was no change in the level of tyrosinase protein and activity in linoleic acid and ethanol (control) treated cells, but interestingly we found a difference in the pellet color at 48h and 72h of treatment (Fig.V.3C-D). Further, it would be interesting to study the cause behind the linoleic acid-mediated hypopigmentation.

The inhibitory effect of kojic acid and linoleic acid on melanogenesis was also confirmed by first inducing melanogenesis for 24h with forskolin, and then replacement of forskolin with the hypo-pigmenting compounds KA and LA for 48h. This treatment regimen also suppressed melanogenesis in KA and LA-treated samples (Fig.V.4). Interestingly, the pigmentation continued to progress in the vehicle control samples suggesting that the activation signal provided by forskolin was sufficient for 24h. In any case, these results indicated that KA and LA could inhibit melanogenesis even after the forskolin-induced melanogenesis program was initiated.

Next, we analyzed the expression of genes encoding the melanogenic enzymes *Tyr*, *Tyrp1*, *Dct* and the transcription factor *Mitf* by qRT-PCR in KA and LA-treated RNA samples. For this 0.25×10^6 B16 cells were seeded in duplicate T-75 flasks. After overnight adherence, KA (2.5mM) and LA (75µM) treatment were done along with DMEM and ethanol control samples. Cells were harvested by adding 3ml Trizol in each T-75 flask after 24h, 48h, and 72h of treatment, and total RNA was isolated. The data showed that only *Tyr* mRNA expression was down regulated at 72h of KA treatment, whereas other melanogenic mRNA levels were unchanged (Fig.V.5A). The western blot data indicated that the TYR protein level was unchanged at 72h of KA treatment suggesting that TYR protein is stable for quite a long time despite a down-regulation of *Tyr* mRNA level. During LA-mediated hypopigmentation the expression of all the melanogenic genes were found to be downregulated at 48h and 72h in comparison to 24h time point (Fig.V.5B).

V.2.6. Genome-wide transcriptome analysis during small molecule induced hypo-pigmentation

To identify differentially expressed genes during hypo-pigmentation, we carried out microarray analysis. B16 cells were treated with KA and LA for 48h, total RNA

isolated, and Bioanalyzer carried out. The analysis showed that the RNA integrity was checked by Agilent Bioanalyzer and found to be acceptable for all RNA samples with RIN number >9.0. A representative ethidium bromide stained gel, and BioAnalyzer image is shown in Fig.V.6. The RNA samples were processed, labeled and hybridized to microarray slides.

The complete normalized data was analyzed and genes with the $\log_2$ ratio of ≥0.585 (up-regulated) and ≤0.585 (down-regulated genes) in both biological replicates were short-listed for further analysis. This analysis yielded 34 up-regulated genes and 39 down-regulated genes in KA treatment, and 449 upregulated genes and 426 down-regulated genes upon LA treatment. These differentially expressed genes were were classified based on functional category and pathways using the biological analysis tool DAVID (http://david.abcc.ncifcrf.gov/) and PubMed literature mining.

V.2.7. Analysis of differentially expressed genes during small induced hypo-pigmentation

V.2.7.A. *Kojic acid:* The 34 up-regulated transcripts were primarily associated with ontology terms such as regulation of cell cycle, G-protein coupled receptor signaling pathway, response to chemical and regulation of transport. This further indicated that KA treatment led to alteration of cell cycle in B16 cells during hypo-pigmentation. In upregulated categories there are genes like *Nf1* which is already shown to inhibit the process of melanogenesis. Neurofibromin (Nf1) is a Ras-GAP that acts downstream of the receptor tyrosine kinases that is also shared by granulocyte and monocyte colony-stimulating factor such as IL3 and IL5. Melanogenesis is shown to be increased in the *Nf1* mutant mice in a nerve injury experiment (Choi et al., 2017; Rizvi et al., 2002). *ATP8a1*, P-type ATPase that transports the ions across the membrane by utilizing ATP

was found to be upregulated. There are several subfamilies of P-type ATPases. ATP8a1 is a member of the third subfamily of P-type ATPases which transport amphipaths like phosphatidylserine (Dong et al., 2016; Mouro et al., 1999). One subfamily catalyzes transport of heavy metal ions, and another subfamily transports non-heavy metal ions such as ATP7A. The role of ATP7A, a known copper transporter is known to control melanogenesis by regulating tyrosinase activity (Matsui et al., 2015). However, the role of ATP8a1 is unknown during melanogenesis.

The 39 down-regulated genes were associated with the ontology terms cell membrane, regulation of transport, phosphoprotein and disulfide bond. In the down-regulated cluster, we found genes that are mainly involved in sorting of proteins like *Kdelr1*, which is an endoplasmic reticulum protein retention receptor required for retention of proteins resident to ER through vesicular recycling. ARFGAP1, which interacts with KDELR1, was also found to be downregulated in these samples (Luo et al., 2016; Nepal et al., 2018). ARFGAP1 functions as GTPase-activating protein (GAP) for the ADP ribosylation factor 1 (ARF1) and promotes hydrolysis of the (Donaldson et al., 2005). Metadherin (Mtbh) involved in aberrant proliferation, survival and increased migration of tumor cells was found to be downregulated. Expression of Mtbh was shown to be significantly higher in melanoma, breast, esophageal, gastric, hepatocellular, endometrial and prostate cancers (Huang and Li, 2014; Liu et al., 2018). Mtbh promotes tumor progression by modulating multiple signaling pathways, such as NF-κB, PI3K/Akt, and Wnt/β-catenin pathways (Emdad et al., 2006; Hu et al., 2009; Li et al., 2017).

The decrease in melanin accumulation can be due to a defect in melanosome biogenesis. Interestingly, we found genes such as *Kdelr1* and *Arfgap1* that are involved in protein trafficking to be down-regulated during KA mediated hypo-pigmentation.

Further during melanogenesis, TYR, TYRP1, and DCT is trafficked from ER to Golgi to stage II of melanosome to initiate the process of melanin formation. Therefore, we decided to do ultrastructural studies with transmission electron microscopy (TEM) at 72h were a significant difference in the pellet color was found. Melanosome indexes were calculated by taking the ratio of a number of each type of melanosome and total no. of melanosome counted in each cell (Fig.V.7A). There was a drastic decrease in the number of darkly pigmented stage III, and IV melanosomes in kojic acid treated cells in comparison to DMEM (Fig.V.7B). These cells instead accumulated electron-lucent lysosome-related organelles that are characteristic of early stage I and II melanosomes. Cellular investigations through phase contrast and transmission electron microscopy revealed that on kojic acid treatment there was no significant change in cell morphology, but interestingly we found that melanosomes get arrested early in the process of maturation. This observation suggests that there can be a dysregulated post-translational modification of tyrosinase enzyme or protein trafficking to the early melanosome. These findings would need to be experimentally validated in the future.

V.2.7.B. *Linoleic acid***:** The pathways like the MAPK signaling pathway, the Notch signaling pathway, non-small cell lung cancer, angiogenesis, Dorso-ventral axis formation and pathways in cancer were found to be up-regulated during linoleic acid treatment (Fig.V.8A). The genes down-regulated during LA-mediated hypo-pigmentation were found to be primarily involved in steroid biosynthesis, cholesterol biosynthesis, terpenoid backbone biosynthesis and biosynthesis of unsaturated fatty acids were found to be downregulated (Fig.V.8B).

Fig.V.9A-B shows the cholesterol biosynthetic pathway and the expression ratio of genes encoding the enzymes in each of the steps derived from the microarray data. The schematic diagram shows the regulation of lipid synthesis in non-hepatic

cells. The sterol regulatory element binding protein (SREBPs) transcription factor is membrane-bound and when cleaved enters the nucleus to activate genes involved in synthesis and uptake of cholesterol and fatty acid. They bind to the SRE in the promoter region of HMGCoAR gene. SREBPs are escorted by SCAP (SRREP cleavage-activating protein) from ER to Golgi. Moreover, Insig1 is involved in regulating cholesterol biosynthesis by binding to SCAP, and as a result, SCAP/SREBP complex stay longer in the ER and thus SCAPs are prohibited from carrying the activated SREB to Golgi (Fig.V.10A-B).

Using String database, the functional protein association network of the cholesterol biosynthetic genes was obtained (Fig.V.11A). Some of the genes involved in cholesterol biosynthesis were selected like *Hmgcs1*, *Hmgcr* (rate-limiting enzyme), *Tm7sf2, Dhcr7* and *Nsdhl* and real-time qPCR validation was done. We found all the selected genes to be 1.5-fold down-regulated during LA-induced hypopigmentation (Fig.V.11B). The comparison between microarray and real-time qPCR derived fold change showed good correlation (R^2 =0.79). Next, the expression analysis of melanogenic genes such as *Tyr*, *Tyrp1*, *Dct,* and *Mitf* was also studied. Interestingly we found *Tyr*, *Dct,* and *Mitf* to be downregulated at 48h of linoleic acid treatment whereas, expression of *Tyrp1* gene was unchanged (Fig.V.11C). Although we found decreased mRNA of *Tyr,* we observed stable tyrosinase protein across the time points.

Thus, LA treatment led to the decreased expression of genes involved cholesterol biosynthesis and melanogenesis. However, it needs to be determined if down-regulation of cholesterol is functionally linked to the hypo-pigmentation.

Next, we investigated the effect of LA treatment on melanosome formation and maturation. Interestingly, we found a decreased number of melanosomes in LA-treated

samples in comparison to vehicle control (Fig.V.12). We also observed electron lucent structures reminiscent of lipid droplet-like structure in LA-treated samples. The nature of these structures needs to be further investigated (Fig.V.12).

V.2.8. MITF regulates the expression of cholesterol biosynthetic genes during melanogenesis

In the Chapter IV.2.4, we have observed that *Mitf* knockdown in B16 cells leads to the enrichment of distinct categories of genes. The cholesterol biosynthetic genes were found to be downregulated upon *Mitf* silencing (ChapterIV, Section IV.2.4, Fig.IV.6). The real-time expression analysis was done to validate the expression of *Hmgcr*, *Tm7sf2*, *Dhcr7,* and *Nsdhl* in si*Mitf* microarray data. We found 1.5-fold downregulation of this gene in the si*Mitf* induced hypo-pigmentation (Fig.V.13).

Further, through meta-analysis, we have found these genes to be downregulated and occupied by MITF (Chapter IV, Section, IV.2.8, Fig.IV.12). Interestingly, we also found two transcription factors, *Srebf1,* and *Srebf2*, and receptor *Ldlr* to be occupied by both MITF and BRG1 (Chapter IV, Section, IV.2.9, FigIV.14). These genes were also found to be downregulated when BRG1 was silenced.

Next, it would be interesting to examine the role of cholesterol homeostasis in context of melanogenesis. Thus, together this observation and meta-analysis further adds a new dimension to the study of melanogenesis wherein MITF might have a significant role in regulating cholesterol biosynthesis.

V.2.9. Skin centric analysis of microarray data using eSKIN software

Next, the skin centric analysis of microarray data was done using eSKIN software, a computational platform for skin research developed by the collaborative

effort of IGIB, JNU, NCL, and NII. The eSKIN software provides a comprehensive platform for skin research to understand and interpret skin-associated high throughput expression data. The genes differentially expressed during KA and LA mediated hypo-pigmentation was used to obtain the physiological manifestation of the data related to skin. The differentially expressed genes were overlaid in eSKIN software to know the nature of the compound and the pathway enriched.

The 123 differentially expressed genes during KA-mediated hypo-pigmentation at 48h time point was matched with the data available in eSKIN (Fig.V.14A-B), and skin-associated pathway enrichment analysis was done. The cytoskeletal modification was enriched in KA-induced hypopigmentation (Fig.V.14C). The nature of the compound was also predicted using the skin predict tool in eSKIN. Interestingly, we found a strong correlation (correlation coefficient 1.0) between KA data and the gene signatures already present in eSKIN for hypo-pigmentation derived from primary melanocyte (Fig.V.14D). Similarly, we overlaid the LA data in eSKIN software and a total of 977 genes matched with the data available in eSKIN, and the skin-associated pathway enrichment analysis was done (Fig.V.15A-B). We found 5 out of 35 skin-associated pathways to be enriched during LA-induced hypopigmentation which included lipid synthesis, inflammation, immune response, wound healing and chemokine signaling Fig.V.15C). Further a strong correlation between LA data with the signatures already present in eSKIN for hypo-pigmentation (Fig.V.15D). Thus, we identified core set of genes involved in hypo-pigmentation. Further, it would be interesting to study their role in context of melanogenesis. Taking these signatures, large number of compounds can be pre-screen and the nature can be predicted without exploiting the animal model.

V.2.10. Identification of hyper- and hypo-pigmentary signatures in B16 cells

Analysis of microarray data derived from different conditions was done to identify the core set of genes required to regulate melanogenesis. To carry out this analysis, the complete normalized data was filtered using GeneSpring Software to identify significant genes ($p < 0.05$) in both the biological replicates at each time points. Next, the threshold fold change of 1.5-fold was applied to the unique gene list and sorted in decreasing order to identify top and bottom 10% genes. Since we have time course data and at each time points different set of genes are expressed. Therefore, we have used different clusters of genes DE at different time points as a signature for specific compounds at that time point. These signatures derived from similar nature of compounds were compared to identify core sets of genes that might have a role in activating or repressing pigmentation.

Based on literature mining, we identified four chemical compounds that have been reported to cause either hydration or desquamation response in cell culture and skin. To induce hydration, we chose urea and glycerol. To induce desquamation salicylic acid and resorcinol were chosen.

The genes differentially expressed during forskolin, IBMX and FAC induced hyper-pigmentation was compared. First, the genes differentially expressed in the particular compound was identified. These differentially expressed genes are then analyzed together to get the core set of genes either up-regulated and downregulated during compound induced hyper-pigmentation. Similarly, to determine the hypo-pigmentary signatures, the differentially expressed genes from the kojic acid, linoleic acid, and BPS was compared.

The 260 up- and 269 downregulated genes commonly regulated by forskolin and IBMX was compared with 262 up- and 322 downregulated genes during FAC (+Fe) induced hyper-pigmentation. We found four genes upregulated to be commonly upregulated whereas, 18 genes, be commonly downregulated by these compounds (Table.V.2).

Similarly, a gene differentially expressed during compound induced hypo-pigmentation was compared. The differentially expressed genes during BPA (-Fe), KA and LA, was analyzed to retrieve a core set of genes. The 48h microarray data were compared where the hypo-pigmenting effect of these compounds was maximum. We found five genes to be commonly upregulated and four genes to be widely downregulated by these compounds (Table.V.3).

Next, we examined the common signatures derived from hydration (Urea and Glycerol) and desquamation (Resorcinol and Salicylic acid). These compounds are keratolytic compounds and what effect they have on melanocyte is unknown. Therefore, we tried to explore the effect of these compounds on melanocyte and signatures were identified. The optimal concentration of these compounds were determined by MTT assay and effect was studied on B16 cells. Table.V.4 represents the concentrations used and the ones that have been finalized are highlighted in bold. We found the percentage viability of finalized concentration having cell viability between 70-80% 30h after treatment (data not shown). The genome-wide transcriptomic studies were performed at 10h and 30h of compound treatment. We found 44 differentially expressed genes to be commonly regulated during hydration whereas, 62 differentially expressed genes were commonly regulated during desquamation. These signatures will be further be used to build a comprehensive platform for skin biology research to understand and interpret the associated skin

pathways. Further, it will also provide an in silico platform for skin-specific data analysis in eSKIN software.

V.3. Summary

In this chapter, we examined the consequence of depigmentation/ hypopigmentation on the normal functioning of melanocytes. To induce depigmentation in B16 mouse melanoma cells, we selected two known hypo-pigmenting compounds, kojic acid (KA), and linoleic acid (LA). The mouse B16 cells were grown in pigmentation permissive DMEM media and treated with kojic acid and linoleic acid at four different time points. The time point where the hypopigmentation status was apparent between the treated versus control samples was taken to study the transcriptomic changes. The effect of both the hypo-pigmenting compounds was examined on the expression of melanogenic genes, tyrosinase protein stability and activity, and melanosome maturation. In an attempt to find critical players underlying the compound dependent hypo-pigmentation, we analyzed the melanosome architecture using transmission electron microscopy. The analysis of TEM data suggested that KA and LA treatment significantly inhibited melanosome maturation in B16 cells.

In the process of melanogenesis, intracellular membrane dynamics is critical. Through microarray data analysis we identified several regulators that might have a role in sorting the proteins from one organelle to other. Downregulation of these regulators, as seen in kojic acid treated samples leads to alteration of trafficking pathways that further leads to dysregulation of cargo delivery. We hypothesize that changes in posttranslational modification of tyrosinase enzyme and alteration of melanogenic protein trafficking to the early melanosome could be one of the mechanisms by which hypopigmentation is induced.

Interestingly, we found the expression of many enzymes involved in cholesterol biosynthesis differentially expressed and enriched in the downregulated categories during LA-mediated hypo-pigmentation. The expression of cholesterol biosynthetic genes such as *Hmgcs1*, *Hmgcr, Mvks*, *Mvd1,* etc. were found to be down-regulated. Some previous studies indicate the role of cholesterol in the regulation of melanogenesis in human epidermal melanocyte and melanoma cells. Experiments done both in situ and invitro suggest that melanocyte are able to synthesize and transport cholesterol. The expression of both *Hmgcr* and *Ldlr* have been detected in melanocyte. Melanogenesis have been shown to be enhanced by cholesterol signaling via *Ldlr* (Schallreuter et al., 2009). These reports further strengthen the validity of hits obtained in our microarray data and gene ontology studies.

Interestingly, we found the cholesterol biosynthesis pathway to be enriched in the downregulated category of si*Mitf* data as well. Further, by comparing our dataset with other published datasets, *Hmgcr*, the rate-limiting enzyme in the process of cholesterol synthesis was found to be downregulated and occupied by MITF and BRG1. We also found the expression of the transcription factor, *Srebf1,* and receptor, *Ldlr* to be downregulated on *Mitf* silencing. Together, our result suggests an essential role of MITF in regulating cholesterol homeostasis during melanogenesis.

Finally, we employed genome-wide transcriptomic studies to identify molecular signatures under different conditions to develop a tool in predicting the nature of the compounds/modulators in the context of skin pigmentation. After the microarray data analysis, the differentially expressed genes were compared with each other to derive a core set of genes that are involved in maintaining the skin pigmentation homeostasis in mouse B16 cells. Similarly, the signatures were also generated for hyperpigmentation (Forskolin, IBMX, and FAC), hydration (urea and glycerol), and desquamation

(resorcinol and salicylic acid). These signatures were included in developing the tool e-skin by persistent technologies. Currently, this software is fully operational and is used to predict the nature of unknown compounds by matching their transcriptomic signatures to the core signatures of known compounds present in the e-skin database.

Conclusions and Future Perspectives

CONCLUSIONS AND FUTURE PERSPECTIVES

MITF is a known master regulator that controls both the process of melanogenesis in melanocyte and melanoma progression. Despite the subset of MITF target genes identified by various studies, the complete network of signaling pathways in the context of melanogenesis remains uncharacterized. In this study, we have analyzed a combination of genome-wide transcriptomic data including a compound based tunable pigmentation model and siRNA mediated knockdown of MITF, to arrive at a set of novel MITF dependent regulators of melanogenesis.

Interestingly, our study also highlights hitherto unexplored MITF independent genes that might have regulatory roles in the process of melanogenesis. We found a significant fraction of genes differentially expressed during pigmentation not under MITF control. Thus, raising the possibility that a significant part of the pigmentation induced transcriptome could be regulated in a MITF-independent manner.

Although MITF has been shown to activate several of its targets, from the meta-analysis, it can be inferred that it might act as a repressor at some promoters. Thus, our studies have identified several novel regulators of skin pigmentation. The subset of the gene has been shown to be regulated in a MITF-independent manner.

Through, the genome-wide transcriptomic analysis we have identified 29 SLCs genes to be differentially expressed during compound induced hyper-pigmentation. Among these, *Slc40a1/Fpn1* was found to be downregulated across the time point when the pigmentation is induced in the B16 cells. Interestingly, the expression of *Fpn1* was found to be up-regulated in si*Mitf* data, indicating the possibility that iron is required for the process of melanogenesis.

Interestingly, iron replete and deplete conditions have been shown to modulate pigmentation in B16 cells. The pigmentation is a multi-step process that is controlled at several levels by different regulators. Interestingly, iron has been shown to regulate melanogenesis at several levels. It governs function ranging from controlling melanosome biogenesis and maturation, tyrosinase protein and activity, to the expression of its exporter, *Fpn1*, and the expression of essential genes involved in oxidative phosphorylation to generate ATP.

Further, the melanosomes dynamics play a significant role during melanogenesis. Interestingly, we have observed increased melanosome biogenesis and maturation in iron-replete condition Altogether; our work indicates the critical role of iron in regulating the melanosome dynamics during melanogenesis.

We observed iron homeostasis to be important in regulating melanogenesis. Our result indicates that the role of MITF in regulating the expression of *Fpn1* is essential in determining the pool of iron present inside the cell. During hyper-pigmentation, MITF activates the expression of its target genes including melanogenic enzymes, *Tyr*, *Tyrp1*, and *Dct* whereas it down-regulates the expression of *Fpn1*. This observation indicates that during hyper-pigmentation iron pool inside the cell is higher and that in turn activates melanogenesis. This observation is further strengthened by the fact that in *Mitf* silenced cells we found increased *Fpn1* expression. The possible hypothesis for this is that melanocytes are destined to form melanin, siRNA mediated knockdown of *Mitf* causes the downregulation of its target genes and hence decreased melanin accumulation. Therefore, the expression of *Fpn1* is increased as an adaptive cellular response to hypopigmentation caused by *Mitf* silencing. Further, the differential expression of *Fpn1* raises the exciting possibilities that *Mitf* can activate melanogenesis by regulating iron homeostasis. The mechanism by which *Mitf* is regulating iron homeostasis remains to be elucidated.

Next, we tried to dissect the complete transcriptional regulatory networks of skin hypo-pigmentation/depigmentation. After treating the B16 cells with known hypo-pigmentation agents, kojic acid, and linoleic acid, the whole genomic trancriptomic analysis was carried out. We found a large number of genes differentially expressed on compound induced hypo-pigmentation. We have observed that melanosome gets arrested very early in the KA-mediated hypo-pigmentation. Further, genes involved in protein trafficking from one organelle to other was also found to be downregulated. We found many genes involved in cholesterol biosynthesis to be down-regulated during LA-mediated hypo-pigmentation. The rate-limiting enzyme, *Hmgcr*, was found to be down-regulated in the si*Mitf* data also. Thus, this observation suggests the role of MITF in regulating cholesterol homeostasis during melanogenesis.

Further through microarray data, we obtained a core set of genes regulated during hyperpigmentation and hypopigmentation. The genes were considered as the signatures of that particular phenotype. Additionally, the compound-specific signatures were also identified since different compound can elicit a different response by inducing different sets of genes. At various time points, different clusters of genes can be expressed. Therefore these genes were considered as the signature of that time points. These signatures can be used as a screening tool in predicting the nature of the unknown compounds without exploiting the model organism.

Altogether we found the large subset of genes differentially expressed during small molecule induced melanogenesis have been shown to have MITF-independent regulation. Further, MITF acting as a repressor for many targets adds another dimension to the study of melanocyte biology. Melanosomes are an excellent model organelle to study the organelle biogenesis and motility. Although the important advances have been made to understand the melanosome biogenesis, many essential features are obscure. Altogether, our work adds a link between nutrient availability

and organelle biogenesis and hence to melanogenesis. The activation of adaptive cellular response by regulating the transcript abundance of oxidative phosphorylation complex further suggest the link between mitochondria and melanogenesis. This study has potential clinical importance because we do find some evidence of iron overload and hyperpigmentation in the patient suffering from Hemochromatosis type 4. Further to treat hyper-pigmentation disorders like melasma, combination or specially formulated creams with hydroquinone is generally prescribed. However, prolonged use of this phenolic compound leads to permanent discoloration of skin commonly known as Hydroquinone-induced ochronosis. We have also examined the effect of hydroquinone on B16 cells (data not shown) and found that is has a cytotoxicity effect on melanocyte which is irreversible. Therefore, we propose deferrization as a reversible supportive therapy by using siderophore like desferrioxamine to treat hyperpigmented disorders like melasma.

Next, the signatures identified by microarray analysis in different condition can generate the skin centric regulators. Since we have time course data, and at each time different sets of genes are expressed. Therefore, we have used a different cluster of genes at each time points as a signature for the specific compound at that time point. These signatures can be employed as a screening tool to predict the nature of unknown compound/molecule and also help us in identifying new targets that have therapeutic value in the context of -hyper or -hypopigmentation disorders.

Thus studies gleaned from the microarray data not only increase our understanding of the normal melanocyte biology but also have clinical relevance in the treatment of pigmentation disorders. Further, our studies shed light on the potential regulators that might be involved in development and progression of melanoma. Future studies using human cell lines will validate the roles of these genes in the context of melanoma.

References

REFERENCES

Abboud, S., and Haile, D.J. (2000). A novel mammalian iron-regulated protein involved in intracellular iron metabolism. J Biol Chem *275*, 19906-19912.

Agarwal, P., Verzi, M.P., Nguyen, T., Hu, J., Ehlers, M.L., McCulley, D.J., Xu, S.M., Dodou, E., Anderson, J.P., Wei, M.L.*, et al.* (2011). The MADS box transcription factor MEF2C regulates melanocyte development and is a direct transcriptional target and partner of SOX10. Development *138*, 2555-2565.

Ancans, J., Tobin, D.J., Hoogduijn, M.J., Smit, N.P., Wakamatsu, K., and Thody, A.J. (2001). Melanosomal pH controls rate of melanogenesis, eumelanin/phaeomelanin ratio and melanosome maturation in melanocytes and melanoma cells. Experimental cell research *268*, 26-35.

Anderson, C.P., Shen, M., Eisenstein, R.S., and Leibold, E.A. (2012). Mammalian iron metabolism and its control by iron regulatory proteins. Biochimica et biophysica acta *1823*, 1468-1483.

Ando, H., Kondoh, H., Ichihashi, M., and Hearing, V.J. (2007). Approaches to identify inhibitors of melanin biosynthesis via the quality control of tyrosinase. J Invest Dermatol *127*, 751-761.

Ando, H., Watabe, H., Valencia, J.C., Yasumoto, K., Furumura, M., Funasaka, Y., Oka, M., Ichihashi, M., and Hearing, V.J. (2004). Fatty acids regulate pigmentation via proteasomal degradation of tyrosinase: a new aspect of ubiquitin-proteasome function. J Biol Chem *279*, 15427-15433.

Andrews, N.C. (2004). Anemia of inflammation: the cytokine-hepcidin link. The Journal of clinical investigation *113*, 1251-1253.

Aoki, H., and Moro, O. (2002). Involvement of microphthalmia-associated transcription factor (MITF) in expression of human melanocortin-1 receptor (MC1R). Life sciences *71*, 2171-2179.

Bannister, A.J., and Kouzarides, T. (2011). Regulation of chromatin by histone modifications. Cell Res *21*, 381-395.

Bartholomew, B. (2014). Regulating the chromatin landscape: structural and mechanistic perspectives. Annual review of biochemistry *83*, 671-696.

Bellot, G., Garcia-Medina, R., Gounon, P., Chiche, J., Roux, D., Pouyssegur, J., and Mazure, N.M. (2009). Hypoxia-induced autophagy is mediated through hypoxia-inducible factor induction of BNIP3 and BNIP3L via their BH3 domains. Molecular and cellular biology *29*, 2570-2581.

Bennett, D.C., and Lamoreux, M.L. (2003). The color loci of mice--a genetic century. Pigment cell research / sponsored by the European Society for Pigment Cell Research and the International Pigment Cell Society *16*, 333-344.

Bharti, K., Liu, W., Csermely, T., Bertuzzi, S., and Arnheiter, H. (2008). Alternative promoter use in eye development: the complex role and regulation of the transcription factor MITF. Development *135*, 1169-1178.

Bhatt, S., Diaz, R., and Trainor, P.A. (2013). Signals and switches in Mammalian neural crest cell differentiation. Cold Spring Harbor perspectives in biology *5*.

Bikle, D.D., Elalieh, H., Chang, S., Xie, Z., and Sundberg, J.P. (2006). Development and progression of alopecia in the vitamin D receptor null mouse. Journal of cellular physiology *207*, 340-353.

Bikle, D.D., and Pillai, S. (1993). Vitamin D, calcium, and epidermal differentiation. Endocrine reviews *14*, 3-19.

Bin, B.H., Bhin, J., Yang, S.H., Shin, M., Nam, Y.J., Choi, D.H., Shin, D.W., Lee, A.Y., Hwang, D., Cho, E.G*., et al.* (2015). Membrane-Associated Transporter Protein (MATP) Regulates Melanosomal pH and Influences Tyrosinase Activity. PloS one *10*, e0129273.

Biniek, K., Levi, K., and Dauskardt, R.H. (2012). Solar UV radiation reduces the barrier function of human skin. Proc Natl Acad Sci U S A *109*, 17111-17116.

Bonaccorsi di Patti, M.C., Polticelli, F., Cece, G., Cutone, A., Felici, F., Persichini, T., and Musci, G. (2014). A structural model of human ferroportin and of its iron binding site. The FEBS journal *281*, 2851-2860.

Bondurand, N., Pingault, V., Goerich, D.E., Lemort, N., Sock, E., Le Caignec, C., Wegner, M., and Goossens, M. (2000). Interaction among SOX10, PAX3 and MITF, three genes altered in Waardenburg syndrome. Hum Mol Genet *9*, 1907-1917.

Bottomley, M.J. (2004). Structures of protein domains that create or recognize histone modifications. EMBO reports *5*, 464-469.

Boyer, L.A., Latek, R.R., and Peterson, C.L. (2004). The SANT domain: a unique histone-tail-binding module? Nature reviews. Molecular cell biology *5*, 158-163.

Braeuer, R.R., Zigler, M., Kamiya, T., Dobroff, A.S., Huang, L., Choi, W., McConkey, D.J., Shoshan, E., Mobley, A.K., Song, R*., et al.* (2012). Galectin-3 contributes to melanoma growth and metastasis via regulation of NFAT1 and autotaxin. Cancer research *72*, 5757-5766.

Bustamante, C.D., Fledel-Alon, A., Williamson, S., Nielsen, R., Hubisz, M.T., Glanowski, S., Tanenbaum, D.M., White, T.J., Sninsky, J.J., Hernandez, R.D*., et al.*

(2005). Natural selection on protein-coding genes in the human genome. Nature *437*, 1153-1157.

Carreira, S., Goodall, J., Aksan, I., La Rocca, S.A., Galibert, M.D., Denat, L., Larue, L., and Goding, C.R. (2005). Mitf cooperates with Rb1 and activates p21Cip1 expression to regulate cell cycle progression. Nature *433*, 764-769.

Carreira, S., Goodall, J., Denat, L., Rodriguez, M., Nuciforo, P., Hoek, K.S., Testori, A., Larue, L., and Goding, C.R. (2006). Mitf regulation of Dia1 controls melanoma proliferation and invasiveness. Genes Dev *20*, 3426-3439.

Cheli, Y., Giuliano, S., Fenouille, N., Allegra, M., Hofman, V., Hofman, P., Bahadoran, P., Lacour, J.P., Tartare-Deckert, S., Bertolotto, C*., et al.* (2012). Hypoxia and MITF control metastatic behaviour in mouse and human melanoma cells. Oncogene *31*, 2461-2470.

Cheli, Y., Luciani, F., Khaled, M., Beuret, L., Bille, K., Gounon, P., Ortonne, J.P., Bertolotto, C., and Ballotti, R. (2009). {alpha}MSH and Cyclic AMP elevating agents control melanosome pH through a protein kinase A-independent mechanism. J Biol Chem *284*, 18699-18706.

Chen, K.G., Leapman, R.D., Zhang, G., Lai, B., Valencia, J.C., Cardarelli, C.O., Vieira, W.D., Hearing, V.J., and Gottesman, M.M. (2009). Influence of melanosome dynamics on melanoma drug sensitivity. Journal of the National Cancer Institute *101*, 1259-1271.

Chen, X., Duan, L.H., Luo, P.C., Hu, G., Yu, X., Liu, J., Lu, H., and Liu, B. (2016). FBXO6-Mediated Ubiquitination and Degradation of Ero1L Inhibits Endoplasmic Reticulum Stress-Induced Apoptosis. Cellular physiology and biochemistry : international journal of experimental cellular physiology, biochemistry, and pharmacology *39*, 2501-2508.

Chi, A., Valencia, J.C., Hu, Z.Z., Watabe, H., Yamaguchi, H., Mangini, N.J., Huang, H., Canfield, V.A., Cheng, K.C., Yang, F*., et al.* (2006). Proteomic and bioinformatic characterization of the biogenesis and function of melanosomes. J Proteome Res *5*, 3135-3144.

Choi, K., Komurov, K., Fletcher, J.S., Jousma, E., Cancelas, J.A., Wu, J., and Ratner, N. (2017). An inflammatory gene signature distinguishes neurofibroma Schwann cells and macrophages from cells in the normal peripheral nervous system. Scientific reports *7*, 43315.

Cichorek, M., Wachulska, M., Stasiewicz, A., and Tyminska, A. (2013). Skin melanocytes: biology and development. Postepy dermatologii i alergologii *30*, 30-41.

Coppe, J.P., Desprez, P.Y., Krtolica, A., and Campisi, J. (2010). The senescence-associated secretory phenotype: the dark side of tumor suppression. Annual review of pathology *5*, 99-118.

Coppe, J.P., Patil, C.K., Rodier, F., Sun, Y., Munoz, D.P., Goldstein, J., Nelson, P.S., Desprez, P.Y., and Campisi, J. (2008). Senescence-associated secretory phenotypes reveal cell-nonautonomous functions of oncogenic RAS and the p53 tumor suppressor. PLoS biology *6*, 2853-2868.

Cortes-Gonzalez, V., Zenteno, J.C., Guzman-Sanchez, M., Giordano-Herrera, V., Guadarrama-Vallejo, D., Ruiz-Quintero, N., and Villanueva-Mendoza, C. (2016). Tietz/Waardenburg type 2A syndrome associated with posterior microphthalmos in two unrelated patients with novel MITF gene mutations. American journal of medical genetics. Part A *170*, 3294-3297.

Cutter, A.R., and Hayes, J.J. (2015). A brief review of nucleosome structure. FEBS letters *589*, 2914-2922.

D'Mello, S.A., Finlay, G.J., Baguley, B.C., and Askarian-Amiri, M.E. (2016). Signaling Pathways in Melanogenesis. International journal of molecular sciences *17*.

Daniele, T., Hurbain, I., Vago, R., Casari, G., Raposo, G., Tacchetti, C., and Schiaffino, M.V. (2014). Mitochondria and melanosomes establish physical contacts modulated by Mfn2 and involved in organelle biogenesis. Current biology : CB *24*, 393-403.

Das, C., and Tyler, J.K. (2013). Histone exchange and histone modifications during transcription and aging. Biochimica et biophysica acta *1819*, 332-342.

De Domenico, I., Ward, D.M., Langelier, C., Vaughn, M.B., Nemeth, E., Sundquist, W.I., Ganz, T., Musci, G., and Kaplan, J. (2007). The molecular mechanism of hepcidin-mediated ferroportin down-regulation. Molecular biology of the cell *18*, 2569-2578.

de la Serna, I.L., Ohkawa, Y., Higashi, C., Dutta, C., Osias, J., Kommajosyula, N., Tachibana, T., and Imbalzano, A.N. (2006). The microphthalmia-associated transcription factor requires SWI/SNF enzymes to activate melanocyte-specific genes. J Biol Chem *281*, 20233-20241.

Donovan, A., Lima, C.A., Pinkus, J.L., Pinkus, G.S., Zon, L.I., Robine, S., and Andrews, N.C. (2005). The iron exporter ferroportin/Slc40a1 is essential for iron homeostasis. Cell metabolism *1*, 191-200.

Dupin, E., and Le Douarin, N.M. (2003). Development of melanocyte precursors from the vertebrate neural crest. Oncogene *22*, 3016-3023.

Ernfors, P. (2010). Cellular origin and developmental mechanisms during the formation of skin melanocytes. Experimental cell research *316*, 1397-1407.

Falletta, P., Sanchez-Del-Campo, L., Chauhan, J., Effern, M., Kenyon, A., Kershaw, C.J., Siddaway, R., Lisle, R., Freter, R., Daniels, M.J*., et al.* (2017). Translation reprogramming is an evolutionarily conserved driver of phenotypic plasticity and therapeutic resistance in melanoma. Genes Dev *31*, 18-33.

Fang, D., Tsuji, Y., and Setaluri, V. (2002). Selective down-regulation of tyrosinase family gene TYRP1 by inhibition of the activity of melanocyte transcription factor, MITF. Nucleic acids research *30*, 3096-3106.

Fang, F., Wasserman, S.M., Torres-Vazquez, J., Weinstein, B., Cao, F., Li, Z., Wilson, K.D., Yue, W., Wu, J.C., Xie, X*., et al.* (2014). The role of Hath6, a newly identified shear-stress-responsive transcription factor, in endothelial cell differentiation and function. Journal of cell science *127*, 1428-1440.

Gallagher, S.J., Tiffen, J.C., and Hersey, P. (2015). Histone Modifications, Modifiers and Readers in Melanoma Resistance to Targeted and Immune Therapy. Cancers *7*, 1959-1982.

Gilbert, S.F. (2017). Developmental biology, the stem cell of biological disciplines. PLoS biology *15*, e2003691.

Giuliano, S., Cheli, Y., Ohanna, M., Bonet, C., Beuret, L., Bille, K., Loubat, A., Hofman, V., Hofman, P., Ponzio, G*., et al.* (2010). Microphthalmia-associated transcription factor controls the DNA damage response and a lineage-specific senescence program in melanomas. Cancer research *70*, 3813-3822.

Goding, C.R. (2000). Mitf from neural crest to melanoma: signal transduction and transcription in the melanocyte lineage. Genes Dev *14*, 1712-1728.

Goding, C.R. (2011). Commentary. A picture of Mitf in melanoma immortality. Oncogene *30*, 2304-2306.

Goodall, J., Carreira, S., Denat, L., Kobi, D., Davidson, I., Nuciforo, P., Sturm, R.A., Larue, L., and Goding, C.R. (2008). Brn-2 represses microphthalmia-associated transcription factor expression and marks a distinct subpopulation of microphthalmia-associated transcription factor-negative melanoma cells. Cancer research *68*, 7788-7794.

Guillemot, F., and Zimmer, C. (2011). From cradle to grave: the multiple roles of fibroblast growth factors in neural development. Neuron *71*, 574-588.

Hall, A.M., Krishnamoorthy, L., and Orlow, S.J. (2004). 25-hydroxycholesterol acts in the Golgi compartment to induce degradation of tyrosinase. Pigment cell research / sponsored by the European Society for Pigment Cell Research and the International Pigment Cell Society *17*, 396-406.

Han, J., Kraft, P., Nan, H., Guo, Q., Chen, C., Qureshi, A., Hankinson, S.E., Hu, F.B., Duffy, D.L., Zhao, Z.Z*., et al.* (2008). A genome-wide association study identifies novel alleles associated with hair color and skin pigmentation. PLoS genetics *4*, e1000074.

References

Hari, L., Miescher, I., Shakhova, O., Suter, U., Chin, L., Taketo, M., Richardson, W.D., Kessaris, N., and Sommer, L. (2012). Temporal control of neural crest lineage generation by Wnt/beta-catenin signaling. Development *139*, 2107-2117.

Harris, M.L., Buac, K., Shakhova, O., Hakami, R.M., Wegner, M., Sommer, L., and Pavan, W.J. (2013). A dual role for SOX10 in the maintenance of the postnatal melanocyte lineage and the differentiation of melanocyte stem cell progenitors. PLoS genetics *9*, e1003644.

Hearing, V.J. (2011). Milestones in melanocytes/melanogenesis. J Invest Dermatol *131*, E1.

Henikoff, S., McKittrick, E., and Ahmad, K. (2004). Epigenetics, histone H3 variants, and the inheritance of chromatin states. Cold Spring Harbor symposia on quantitative biology *69*, 235-243.

Henikoff, S., and Smith, M.M. (2015). Histone variants and epigenetics. Cold Spring Harbor perspectives in biology *7*, a019364.

Hock, C., Heese, K., Muller-Spahn, F., Hulette, C., Rosenberg, C., and Otten, U. (1998). Decreased trkA neurotrophin receptor expression in the parietal cortex of patients with Alzheimer's disease. Neuroscience letters *241*, 151-154.

Hoek, K.S., and Goding, C.R. (2010). Cancer stem cells versus phenotype-switching in melanoma. Pigment cell & melanoma research *23*, 746-759.

Hoek, K.S., Schlegel, N.C., Eichhoff, O.M., Widmer, D.S., Praetorius, C., Einarsson, S.O., Valgeirsdottir, S., Bergsteinsdottir, K., Schepsky, A., Dummer, R*., et al.* (2008). Novel MITF targets identified using a two-step DNA microarray strategy. Pigment cell & melanoma research *21*, 665-676.

Hou, L., and Pavan, W.J. (2008). Transcriptional and signaling regulation in neural crest stem cell-derived melanocyte development: do all roads lead to Mitf? Cell Res *18*, 1163-1176.

Jablonski, N.G., and Chaplin, G. (2010). Colloquium paper: human skin pigmentation as an adaptation to UV radiation. Proc Natl Acad Sci U S A *107 Suppl 2*, 8962-8968.

Jiao, Z., Mollaaghababa, R., Pavan, W.J., Antonellis, A., Green, E.D., and Hornyak, T.J. (2004). Direct interaction of Sox10 with the promoter of murine Dopachrome Tautomerase (Dct) and synergistic activation of Dct expression with Mitf. Pigment cell research / sponsored by the European Society for Pigment Cell Research and the International Pigment Cell Society *17*, 352-362.

Kageyama, A., Oka, M., Okada, T., Nakamura, S., Ueyama, T., Saito, N., Hearing, V.J., Ichihashi, M., and Nishigori, C. (2004). Down-regulation of melanogenesis by phospholipase D2 through ubiquitin proteasome-mediated degradation of tyrosinase. J Biol Chem *279*, 27774-27780.

Kamakaka, R.T., and Biggins, S. (2005). Histone variants: deviants? Genes Dev *19*, 295-310.

Khaled, M., Levy, C., and Fisher, D.E. (2010). Control of melanocyte differentiation by a MITF-PDE4D3 homeostatic circuit. Genes Dev *24*, 2276-2281.

kirty, k. (2015). Dissecting Transcriptional Regulatory Networks involved in Melanogenesis. In School of life Sciences (Jawaharlal Nehru University), p. 116.

Knecht, A.K., and Bronner-Fraser, M. (2002). Induction of the neural crest: a multigene process. Nature reviews. Genetics *3*, 453-461.

Kobi, D., Steunou, A.L., Dembele, D., Legras, S., Larue, L., Nieto, L., and Davidson, I. (2010). Genome-wide analysis of POU3F2/BRN2 promoter occupancy in human melanoma cells reveals Kitl as a novel regulated target gene. Pigment cell & melanoma research *23*, 404-418.

Kondo, T., and Hearing, V.J. (2011). Update on the regulation of mammalian melanocyte function and skin pigmentation. Expert review of dermatology *6*, 97-108.

Kubic, J.D., Young, K.P., Plummer, R.S., Ludvik, A.E., and Lang, D. (2008). Pigmentation PAX-ways: the role of Pax3 in melanogenesis, melanocyte stem cell maintenance, and disease. Pigment cell & melanoma research *21*, 627-645.

Laurette, P., Strub, T., Koludrovic, D., Keime, C., Le Gras, S., Seberg, H., Van Otterloo, E., Imrichova, H., Siddaway, R., Aerts, S*., et al.* (2015). Transcription factor MITF and remodeller BRG1 define chromatin organisation at regulatory elements in melanoma cells. eLife *4*.

Levy, C., and Fisher, D.E. (2011). Dual roles of lineage restricted transcription factors: the case of MITF in melanocytes. Transcription *2*, 19-22.

Levy, C., Khaled, M., and Fisher, D.E. (2006). MITF: master regulator of melanocyte development and melanoma oncogene. Trends in molecular medicine *12*, 406-414.

Levy, C., Nechushtan, H., and Razin, E. (2002). A new role for the STAT3 inhibitor, PIAS3: a repressor of microphthalmia transcription factor. J Biol Chem *277*, 1962-1966.

Li, X., Egervari, G., Wang, Y., Berger, S.L., and Lu, Z. (2018). Regulation of chromatin and gene expression by metabolic enzymes and metabolites. Nature reviews. Molecular cell biology.

Liu, F., Visser, M., Duffy, D.L., Hysi, P.G., Jacobs, L.C., Lao, O., Zhong, K., Walsh, S., Chaitanya, L., Wollstein, A*., et al.* (2015). Genetics of skin color variation in Europeans: genome-wide association studies with functional follow-up. Human genetics *134*, 823-835.

Madison, K.C. (2003). Barrier function of the skin: "la raison d'etre" of the epidermis. J Invest Dermatol *121*, 231-241.

Marathe, H.G., Watkins-Chow, D.E., Weider, M., Hoffmann, A., Mehta, G., Trivedi, A., Aras, S., Basuroy, T., Mehrotra, A., Bennett, D.C*., et al.* (2017). BRG1 interacts with SOX10 to establish the melanocyte lineage and to promote differentiation. Nucleic acids research *45*, 6442-6458.

Marks, M.S., and Seabra, M.C. (2001). The melanosome: membrane dynamics in black and white. Nature reviews. Molecular cell biology *2*, 738-748.

Mehrotra, A., Mehta, G., Aras, S., Trivedi, A., and de la Serna, I.L. (2014). SWI/SNF chromatin remodeling enzymes in melanocyte differentiation and melanoma. Critical reviews in eukaryotic gene expression *24*, 151-161.

Micucci, J.A., Sperry, E.D., and Martin, D.M. (2015). Chromodomain helicase DNA-binding proteins in stem cells and human developmental diseases. Stem cells and development *24*, 917-926.

Miyamura, Y., Coelho, S.G., Wolber, R., Miller, S.A., Wakamatsu, K., Zmudzka, B.Z., Ito, S., Smuda, C., Passeron, T., Choi, W*., et al.* (2007). Regulation of human skin pigmentation and responses to ultraviolet radiation. Pigment cell research / sponsored by the European Society for Pigment Cell Research and the International Pigment Cell Society *20*, 2-13.

Mort, R.L., Jackson, I.J., and Patton, E.E. (2015). The melanocyte lineage in development and disease. Development *142*, 1387.

Mouro, I., Halleck, M.S., Schlegel, R.A., Mattei, M.G., Williamson, P., Zachowski, A., Devaux, P., Cartron, J.P., and Colin, Y. (1999). Cloning, expression, and chromosomal mapping of a human ATPase II gene, member of the third subfamily of P-type ATPases and orthologous to the presumed bovine and murine aminophospholipid translocase. Biochemical and biophysical research communications *257*, 333-339.

Mungrue, I.N., Pagnon, J., Kohannim, O., Gargalovic, P.S., and Lusis, A.J. (2009). CHAC1/MGC4504 is a novel proapoptotic component of the unfolded protein response, downstream of the ATF4-ATF3-CHOP cascade. Journal of immunology *182*, 466-476.

Natarajan, V.T., Ganju, P., Ramkumar, A., Grover, R., and Gokhale, R.S. (2014a). Multifaceted pathways protect human skin from UV radiation. Nature chemical biology *10*, 542-551.

Natarajan, V.T., Ganju, P., Singh, A., Vijayan, V., Kirty, K., Yadav, S., Puntambekar, S., Bajaj, S., Dani, P.P., Kar, H.K*., et al.* (2014b). IFN-gamma signaling maintains skin pigmentation homeostasis through regulation of melanosome maturation. Proc Natl Acad Sci U S A *111*, 2301-2306.

Nemeth, E., Rivera, S., Gabayan, V., Keller, C., Taudorf, S., Pedersen, B.K., and Ganz, T. (2004). IL-6 mediates hypoferremia of inflammation by inducing the synthesis of the iron regulatory hormone hepcidin. The Journal of clinical investigation *113*, 1271-1276.

Newton, R.A., Cook, A.L., Roberts, D.W., Leonard, J.H., and Sturm, R.A. (2007). Post-transcriptional regulation of melanin biosynthetic enzymes by cAMP and resveratrol in human melanocytes. J Invest Dermatol *127*, 2216-2227.

Ondrusova, L., Vachtenheim, J., Reda, J., Zakova, P., and Benkova, K. (2013). MITF-independent pro-survival role of BRG1-containing SWI/SNF complex in melanoma cells. PloS one *8*, e54110.

Park, H.Y., Kosmadaki, M., Yaar, M., and Gilchrest, B.A. (2009). Cellular mechanisms regulating human melanogenesis. Cellular and molecular life sciences : CMLS *66*, 1493-1506.

Pike, J.W., and Meyer, M.B. (2012). The vitamin D receptor: new paradigms for the regulation of gene expression by 1,25-dihydroxyvitamin D3. Rheumatic diseases clinics of North America *38*, 13-27.

Poirier, M.G., Oh, E., Tims, H.S., and Widom, J. (2009). Dynamics and function of compact nucleosome arrays. Nature structural & molecular biology *16*, 938-944.

Raposo, G., and Marks, M.S. (2007). Melanosomes--dark organelles enlighten endosomal membrane transport. Nature reviews. Molecular cell biology *8*, 786-797.

Razin, S.V., Iarovaia, O.V., Sjakste, N., Sjakste, T., Bagdoniene, L., Rynditch, A.V., Eivazova, E.R., Lipinski, M., and Vassetzky, Y.S. (2007). Chromatin domains and regulation of transcription. Journal of molecular biology *369*, 597-607.

Razin, S.V., and Ulianov, S.V. (2017). Gene functioning and storage within a folded genome. Cellular & molecular biology letters *22*, 18.

Rees, J.L. (2011). The genetics of human pigmentary disorders. J Invest Dermatol *131*, E12-13.

Rensvold, J.W., Krautkramer, K.A., Dowell, J.A., Denu, J.M., and Pagliarini, D.J. (2016). Iron Deprivation Induces Transcriptional Regulation of Mitochondrial Biogenesis. J Biol Chem *291*, 20827-20837.

Rizvi, T.A., Huang, Y., Sidani, A., Atit, R., Largaespada, D.A., Boissy, R.E., and Ratner, N. (2002). A novel cytokine pathway suppresses glial cell melanogenesis after injury to adult nerve. The Journal of neuroscience : the official journal of the Society for Neuroscience *22*, 9831-9840.

Sadakierska-Chudy, A., and Filip, M. (2015). A comprehensive view of the epigenetic landscape. Part II: Histone post-translational modification, nucleosome level, and chromatin regulation by ncRNAs. Neurotoxicity research *27*, 172-197.

Sarkar, D., Leung, E.Y., Baguley, B.C., Finlay, G.J., and Askarian-Amiri, M.E. (2015). Epigenetic regulation in human melanoma: past and future. Epigenetics *10*, 103-121.

Sauka-Spengler, T., and Bronner-Fraser, M. (2008). A gene regulatory network orchestrates neural crest formation. Nature reviews. Molecular cell biology *9*, 557-568.

Schallreuter, K.U., Hasse, S., Rokos, H., Chavan, B., Shalbaf, M., Spencer, J.D., and Wood, J.M. (2009). Cholesterol regulates melanogenesis in human epidermal melanocytes and melanoma cells. Experimental dermatology *18*, 680-688.

Schiaffino, M.V. (2010). Signaling pathways in melanosome biogenesis and pathology. The international journal of biochemistry & cell biology *42*, 1094-1104.

Shain, A.H., and Bastian, B.C. (2016). From melanocytes to melanomas. Nature reviews. Cancer *16*, 345-358.

Shibahara, S., Takeda, K., Yasumoto, K., Udono, T., Watanabe, K., Saito, H., and Takahashi, K. (2001). Microphthalmia-associated transcription factor (MITF): multiplicity in structure, function, and regulation. The journal of investigative dermatology. Symposium proceedings *6*, 99-104.

Silva, B., and Faustino, P. (2015). An overview of molecular basis of iron metabolism regulation and the associated pathologies. Biochimica et biophysica acta *1852*, 1347-1359.

Slominski, A., Kim, T.K., Brozyna, A.A., Janjetovic, Z., Brooks, D.L., Schwab, L.P., Skobowiat, C., Jozwicki, W., and Seagroves, T.N. (2014). The role of melanogenesis in regulation of melanoma behavior: melanogenesis leads to stimulation of HIF-1alpha expression and HIF-dependent attendant pathways. Archives of biochemistry and biophysics *563*, 79-93.

Slominski, A., Tobin, D.J., Shibahara, S., and Wortsman, J. (2004). Melanin pigmentation in mammalian skin and its hormonal regulation. Physiological reviews *84*, 1155-1228.

Steingrimsson, E., Copeland, N.G., and Jenkins, N.A. (2004). Melanocytes and the microphthalmia transcription factor network. Annu Rev Genet *38*, 365-411.

Strub, T., Giuliano, S., Ye, T., Bonet, C., Keime, C., Kobi, D., Le Gras, S., Cormont, M., Ballotti, R., Bertolotto, C*., et al.* (2011). Essential role of microphthalmia transcription factor for DNA replication, mitosis and genomic stability in melanoma. Oncogene *30*, 2319-2332.

Sturm, R.A. (2009). Molecular genetics of human pigmentation diversity. Hum Mol Genet *18*, R9-17.

Tessarz, P., and Kouzarides, T. (2014). Histone core modifications regulating nucleosome structure and dynamics. Nature reviews. Molecular cell biology *15*, 703-708.

Thomas, A.J., and Erickson, C.A. (2009). FOXD3 regulates the lineage switch between neural crest-derived glial cells and pigment cells by repressing MITF through a non-canonical mechanism. Development *136*, 1849-1858.

Vachtenheim, J., Novotna, H., and Ghanem, G. (2001). Transcriptional repression of the microphthalmia gene in melanoma cells correlates with the unresponsiveness of target genes to ectopic microphthalmia-associated transcription factor. J Invest Dermatol *117*, 1505-1511.

Vachtenheim, J., Ondrusova, L., and Borovansky, J. (2010). SWI/SNF chromatin remodeling complex is critical for the expression of microphthalmia-associated transcription factor in melanoma cells. Biochemical and biophysical research communications *392*, 454-459.

Vaquerizas, J.M., Kummerfeld, S.K., Teichmann, S.A., and Luscombe, N.M. (2009). A census of human transcription factors: function, expression and evolution. Nature reviews. Genetics *10*, 252-263.

Wakamatsu, K., Nagao, A., Watanabe, M., Nakao, K., and Ito, S. (2017). Pheomelanogenesis is promoted at a weakly acidic pH. Pigment cell & melanoma research *30*, 372-377.

Wang, Y., and Androlewicz, M.J. (2000). Oligosaccharide trimming plays a role in the endoplasmic reticulum-associated degradation of tyrosinase. Biochemical and biophysical research communications *271*, 22-27.

Wellbrock, C., and Arozarena, I. (2015). Microphthalmia-associated transcription factor in melanoma development and MAP-kinase pathway targeted therapy. Pigment cell & melanoma research *28*, 390-406.

Widlund, H.R., and Fisher, D.E. (2003). Microphthalamia-associated transcription factor: a critical regulator of pigment cell development and survival. Oncogene *22*, 3035-3041.

Wolkow, N., Li, Y., Maminishkis, A., Song, Y., Alekseev, O., Iacovelli, J., Song, D., Lee, J.C., and Dunaief, J.L. (2014). Iron upregulates melanogenesis in cultured retinal pigment epithelial cells. Experimental eye research *128*, 92-101.

Wrighting, D.M., and Andrews, N.C. (2006). Interleukin-6 induces hepcidin expression through STAT3. Blood *108*, 3204-3209.

Yaar, M., and Park, H.Y. (2012). Melanocytes: a window into the nervous system. J Invest Dermatol *132*, 835-845.

Yamaguchi, Y., and Hearing, V.J. (2014). Melanocytes and their diseases. Cold Spring Harbor perspectives in medicine *4*.

Yang, R., Zheng, Y., Li, L., Liu, S., Burrows, M., Wei, Z., Nace, A., Herlyn, M., Cui, R., Guo, W.*, et al.* (2014). Direct conversion of mouse and human fibroblasts to functional melanocytes by defined factors. Nature communications *5*, 5807.

Ye, C.J., and Heng, H.H. (2017). High Resolution Fiber-Fluorescence In Situ Hybridization. Methods in molecular biology *1541*, 151-166.

Yousef, H., and Sharma, S. (2018). Anatomy, Skin (Integument), Epidermis. In StatPearls (Treasure Island (FL)).

Yun, M., Wu, J., Workman, J.L., and Li, B. (2011). Readers of histone modifications. Cell Res *21*, 564-578.

Zambon, A.C., Zhang, L., Minovitsky, S., Kanter, J.R., Prabhakar, S., Salomonis, N., Vranizan, K., Dubchak, I., Conklin, B.R., and Insel, P.A. (2005). Gene expression patterns define key transcriptional events in cell-cycle regulation by cAMP and protein kinase A. Proc Natl Acad Sci U S A *102*, 8561-8566.

Zhang, H., Luo, H., Chen, H., Mei, L., He, C., Jiang, L., Li, J.D., and Feng, Y. (2012). Functional analysis of MITF gene mutations associated with Waardenburg syndrome type 2. FEBS letters *586*, 4126-4131.

Zhang, P., Torres, K., Liu, X., Liu, C.G., and Pollock, R.E. (2016). An Overview of Chromatin-Regulating Proteins in Cells. Current protein & peptide science *17*, 401-410.

Zhang, Y., Ng, H.H., Erdjument-Bromage, H., Tempst, P., Bird, A., and Reinberg, D. (1999). Analysis of the NuRD subunits reveals a histone deacetylase core complex and a connection with DNA methylation. Genes Dev *13*, 1924-1935.

Zou, C., and Mallampalli, R.K. (2014). Regulation of histone modifying enzymes by the ubiquitin-proteasome system. Biochimica et biophysica acta *1843*, 694-702.

Appendix

Common buffers and reagents

Reagents	Components	Stock	Amount	Preparation
Ampicillin		25mg/ml	20ml	Weigh out 500mg in a 50ml falcon tube. Add 20 ml of autoclaved water and dissolve by putting on a nutator. Filters sterilize using a 0.22μm membrane. Make aliquots of 0.5ml and store at -20°C.
Kanamycin		10mg/ml	20ml	Weigh out 200mg in a 50ml falcon tube. Add 20ml of autoclaved water and dissolve by putting on a nutator. Filters sterilize using a 0.22μm membrane. Make aliquots of 0.5ml and store at -20°C.
EDTA, tri sodium, pH8.0		0.5M	60 ml; 10.75g tri-sodium EDTA	Dissolve in 30 ml water; stir vigorously. Adjust the pH by NaOH. Makeup the volume. Autoclave and store at 4°C
TAE, pH 8		20X	100ml	Dissolve the components with mild heating or magnetic stirrer and makeup the volume. Autoclave and store at 4°C
	TRIZMA Base		9.68 g	
	Glacial Acetic Acid		2.28 ml	
	EDTA	0.5M	4.0 ml	
EDTA,di sodium, pH8.0		0.5M	60 ml, 11.17g di-sodium EDTA	Dissolve in 40 ml water, stir vigorously. Adjust the pH by adding ~3ml of 10N NaOH. Check pH after every 1 ml of 10N NaOH addition. Stir vigorously. EDTA will go into solution at pH 8. When the solution becomes clear, make up the volume. Autoclave and store at 4°C

TE pH: 8.0		1X	50 ml	No need to autoclave when using sterile components
	TrisHCl, pH:8	1M	0.5 ml	
	EDTA, pH:8	0.5M	0.1 ml	
Ribonuclease A		10mg/ml	1 ml	Weigh 10mg and dissolve in 850μl of 10mM sodium acetate (pH 5.2). Heat to 100°Cfor 15 minutes to inactivate any contaminating DNase. Allow it to cool slowly to RT. Adjust the pH to 7.6 to 8.0 using 1MTrisHCl pH8.0. make up the volume to 1 ml with 10mM sodium acetate (pH 5.2). Dispense into aliquots and store at -20°C.
SDS-PAGE Protein Loading buffer			2 ml	Add 240 mg of SDS to a 2.0 ml vial with pre-warmed 0.6 ml USB glycerol; add 375 μl of Tris-HCl buffer into it. Vortex vigorously and keep in water-bath set at 55°C; repeat process. Add remaining glycerol; mix well and makeup the volume to 2 ml. Add BPB and mix on a nutator.
	TrisHCl, pH 8.0	2 M	0.375 ml	
	Glycerol	100%	1.2 ml	
	BPB			
	SDS		240 mg	
DNA loading Buffer		6X	25ml	Weigh the components and suspend in autoclave MQ water. Add sucrose first and dissolve it completely. Add BPB at last. Nutate for sufficient
	Sucrose	40%	10g	
	BPB	0.25%	62.5mg	
	1M Tris-HCl pH:8.0	10mM	250μl	
	0.5M EDTA pH: 8.0	10mM	500μl	
SDS		10%	60ml;6g SDS Powder	Dissolve gradually in 30ml and make up the volume.Do not autoclave.Filter.Store at RT.

DMEM (Dulbecco's Modified Eagle Medium, high glucose)			1L	Dissolve the component of the bottle in 1 liter of autoclaved double distilled water. Add 3.7g sodium bicarbonate to the media and stir. Filter the media and add 1ml each of gentamycin and pen-strep. Filter the media again after addition of antibiotics. Adjust the pH of the media to pH:7 using 1N HCl. Make aliquots of media and store at 4°C.
	Sodium bicarbonate		3.7g	
	Gentamycin	10mg/ml	1ml	
	Penicillin streptomycin	10,000units/ml 10,000 µg/ml	1ml	
DMEM/F-12 (Dulbecco's Modified Eagle's Medium/Nutrient Mixture F-12 Ham)			1L	Dissolve the component of the bottle in 1 liter of autoclaved double distilled water. Add 1.2g sodium bicarbonate to the media and stir. Filter the media and add 1ml each of gentamycin and pen-strep. Filter the media again after addition of antibiotics. Make aliquots of media and store at 4°C.
	Sodium bicarbonate		1.2g	
	Gentamycin	10mg/ml	1ml	
	Penicillin streptomycin	10,000units/ml 10,000 µg/ml	1ml	
L-DOPA (3,4dihydroxy phenylalanine)		10mM	25ml	Add 49.2 mg of DOPA in 25ml of phosphate buffer pH 6.8. Mwt of DOPA is 197.19
	DOPA		49.2mg	
	Phosphate buffer (pH 6.8)		Volume make up	
Trypsin		2.5%	50ml	Add 2ml of 2.5% trypsin in 48ml of versene and store at 4°C
	Versene		Volume Make up	
Hydroxyurea	0.5M	10ml		Dissolve 380.25mg in water and filter sterilize

			100ml	100 ml Ca and Mg free PBS,5 mg RNase (should be DNase free),2.5 mg of Propidium Iodide, 30 µl of TX100 or NP40 or Tween 20. The solution was wrapped in aluminum foil and stored at 4°C.
Propidium iodide stain	RNase	10mg/ml	500µl	
	Propidium Iodide	5mg/ml	2.5mg	
	TX100 or NP40 or Tween20	10%	30µl	
	DPBS	1X	Volume make up	
MTT [3-(4, 5-Dimethylthiazol-2-yl)-2, 5-diphenyltetrazolium bromide]		5mg/ml	50ml	Add 0.25 g MTT powder (Sigma M-5655) to 50ml PBS buffer and stir. Wrap the beaker with aluminum foil to protect from light. Filter the solution in the hood, split into aliquots of 4-6 ml, and store at 4 °C.
	MTT		0.25g	
	DPBS	1X	Volume make up	
Trypan blue		0.4%	10ml	Dissolve 0.04g of trypan blue powder in 10ml of DPBS. Filter sterilize.
X-gal (5-bromo-4-chloro-3-indolyl-β-galactopyranoside)		50mg/ml		50mg/ml X-gal in DMSO (final: 1mg/ml).Store at -20°C

Table.II.3 Shows the list of cultured flask/plate their growth area (cm^2), working volume (mL) and a number of cells (10^6) required for initial seeding to support optimal cell growth of B16 melanoma cells.

Flasks with filter Lid	Growth area(cm^2)	Working volume (mL)	No. of cells (10^6)
T-25	26.90	5.0	0.096
T-75	77.90	10.0	0.25
T-175	179.50	20.0	0.57
Plates			
6-well	9.40	2.0	0.032
12-well	3.80	1.0	0.012

Table.III.1. 29 SLC genes differentially expressed during compound induced hyper-pigmentation

SLC genes	Name
Slc35a2	solute carrier family 35 (UDP-galactose transporter), member A2
Slc37a4	solute carrier family 37 (glucose-6-phosphate transporter), member 4
Slc31a2	solute carrier family 31, member 2
Slc35f5	solute carrier family 35, member F5
Slc4a2	solute carrier family 4 (anion exchanger), member 2
Slc19a2	solute carrier family 19 (thiamine transporter), member 2
Slc24a4	solute carrier family 24 (sodium/potassium/calcium exchanger), member 4
Slc22a14	solute carrier family 22 (organic cation transporter), member 14
Slc18a1	solute carrier family 18 (vesicular monoamine), member 1
Slco3a1	solute carrier organic anion transporter family, member 3a1
Slc2a4	solute carrier family 2 (facilitated glucose transporter), member 4
Slc40a1	solute carrier family 40 (iron-regulated transporter), member 1
Slc13a3	solute carrier family 13 (sodium-dependent dicarboxylate transporter), member 3
Slc2a8	solute carrier family 2, (facilitated glucose transporter), member 8
Slc2a5	solute carrier family 2 (facilitated glucose transporter), member 5
Slc22a15	solute carrier family 22 (organic anion/cation transporter), member 15
Slc4a3	solute carrier family 4 (anion exchanger), member 3
Slc44a2	solute carrier family 44, member 2
Slc9a1	solute carrier family 9 (sodium/hydrogen exchanger), member 1
Slc35f1	solute carrier family 35, member F1

Slc29a1	solute carrier family 29 (nucleoside transporters), member 1
Slc25a27	solute carrier family 25, member 27
Slc9c1	solute carrier family 9, subfamily C (Na+-transporting carboxylic acid decarboxylase), member 1
Slc4a9	solute carrier family 4, sodium bicarbonate cotransporter, member 9
Slc25a25	solute carrier family 25 (mitochondrial carrier, phosphate carrier), member 25
Slc37a1	solute carrier family 37 (glycerol-3-phosphate transporter), member 2
Slc37a1	solute carrier family 37 (glycerol-3-phosphate transporter), member 1
Slc1a5	solute carrier family 1 (neutral amino acid transporter), member 5
Slc43a1	solute carrier family 43, member 1
Slc38a11	solute carrier family 38, member 11

Table III.2. Hybridization plan for microarray done under iron-replete and deplete condition

Sl. No.	Cy3	Cy5	Comments
1	24DM1	24BPS1	
2	24BPS2	24DM2	Dye swap biological replicate
3	24DM1	24FAC1	
4	24FAC2	24DM2	Dye swap biological replicate
5	48DM1	48BPS1	
6	48BPS2	48DM2	Dye swap biological replicate
7	48DM1	48FAC1	
8	48FAC2	48DM2	Dye swap biological replicate

Note: Prefix 24 and 48 represent the hour of treatment. DM represents DMEM media.

Table IV.1. Single color hybridization plan for si*Mitf* microarray

Slide ID	Sample Name	Analysis Plan
256557010004_1_1	Mock1	Control
256557010004_1_2	Mock2	
256557010004_1_3	SiMi1	Treatment 1
256557010004_1_4	SiMi2	

TableV.1. The concentration of KA and LA used to perform MTT assay

Compound	Concentration
Linoleic acid	15µM, 25µM,50µM,75µM
Kojic acid	2.5mM, 5mM, 10mM

Table.V.2. List of Hyper-pigmenting signatures

DN_Hyper-pigmenting signatures	Description
B130021B11Rik	RIKEN cDNA B130021B11 gene
Mndal	Myeloid nuclear differentiation antigen
Shisa2	Shisa family member 2
B130024G19Rik	Riken cDNA b130024g19
Aspm	Abnormal spindle microtubule assembly
Dock10	Dedicator of cytokinesis 10
Dock11	Dedicator of cytokinesis 10
Gm5141	Predicted gene 5141
Kif20b	kinesin family member 20B
Mis18bp1	MIS18 binding protein 1
Mki67	Antigen identified by monoclonal antibody Ki 67
Phip	Pleckstrin homology domain interacting protein
Phtf2	Putative homeodomain transcription factor2
Sgol2	Shugoshin 2A
Casc5	Kinetochore scaffold 1
Ddhd1	DDHD domain containing 1
Mastl	Microtubule associated serine/threonine kinase
Shcbp1	Shc SH2-domain binding protein 1

UP_Hyper-pigmenting signatures	Description
Ccrl2	Chemokine (C-C motif) receptor-like 2
Colec11	Collectin sub-family member 11
Gm4470	Predicted gene 4470
Rnase10	Ribonuclease,RNase A family, 10 (non-active)

Table.V.3. List of Hypo-pigmenting signatures

UP_Hypo-pigmenting signatures	Description
Atp8a1	ATPase, aminophospholipid transporter (APLT), class I, type 8A, member 1
Psme3	Proteosome activator subunit PA28 gamma ki
Darc	atypical chemokine receptor 1 (Duffy blood group)
Sp6	Trans acting transcription factor 6
Fam219aos	Family with sequence similarity 219, member A

DN_Hypo-pigmenting signatures	Description
Otor	OStoraplin
AK139043	No associated gene
Jpx	Jpx transcript, Xist activator (non-protein coding)
AK142557	No associated gene

Table.V.4. The doses optimized for compounds involved in hydration and desquamation

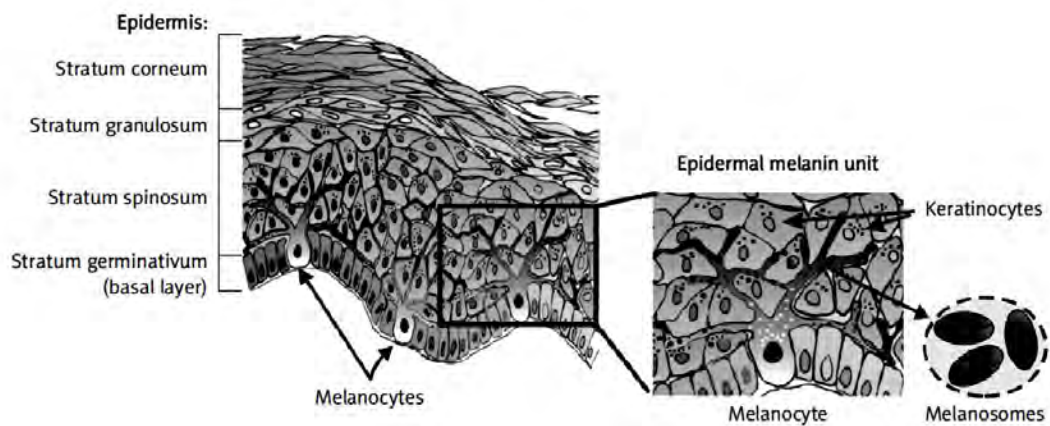| Compound	Stock Concentration	Working Concentrations
Urea	48% in Autoclaved MQ	0.6%,0.8% &**1%**
Glycerol	100% neat (dilutions in respective media)	**2%**, 4% &6%
Salicylic Acid	0.19 % in medium	0.04%,0.08% &**0.1%**
Resorcinol	58 % in Autoclaved MQ	0.01%,**0.02%**&0.06%

Fig. I.1. The architecture of the skin. The schematic diagram depicts the various layers of skin, stratified epidermis, dermis and subcutaneous hypodermis. The four-distinct layer of the epidermis is formed by dedifferentiation of keratinocyte cells. This demarcation divides epidermis into stratum germinativum, stratum spinosum, stratum granulosum and stratum corneum. Melanocytes are present at the basal layer of the epidermis, The epidermal melanin unit composed of one melanocyte that is surrounded by approximately 35-40 keratinocyte presents at the basal layer of the epidermis. It is a functional unit which produces and distribute melanin-containing melanosome from melanocyte to keratinocyte. (Image is obtained from Cichorek & Wachulska.,2013)
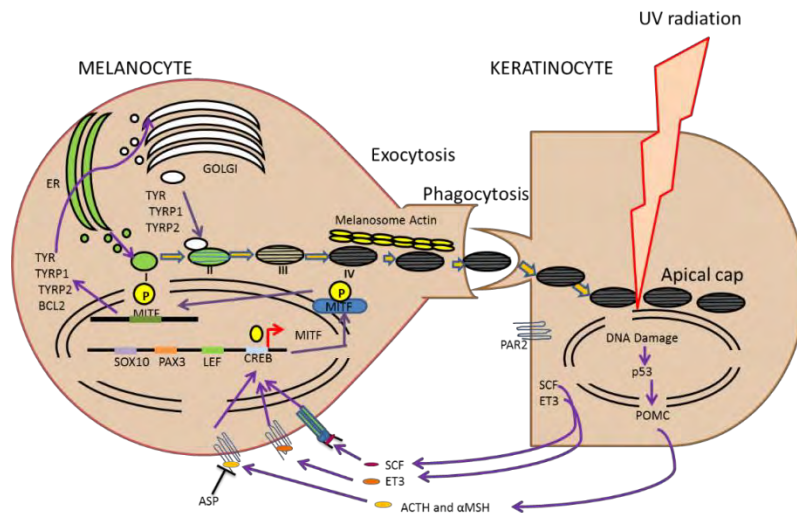
Fig. I.2. Epidermal Melanin Units: Melanocyte-Keratinocyte Interactions

Schematic representation of the pathways involved in the process of melanogenesis.

UV induction of POMC/MSH in keratinocyte is directly controlled by p53. α-MSH released from keratinocyte binds to the MC1R receptor present on melanocyte. This activates the cascade of cAMP-signaling that eventually lead to up-regulation of transcription factor MITF by phosphorylated CREB. MITF regulates the expression of melanin biosynthetic genes like *Tyr*, *Tyrp1*, and *Dct* (kirty, 2015).
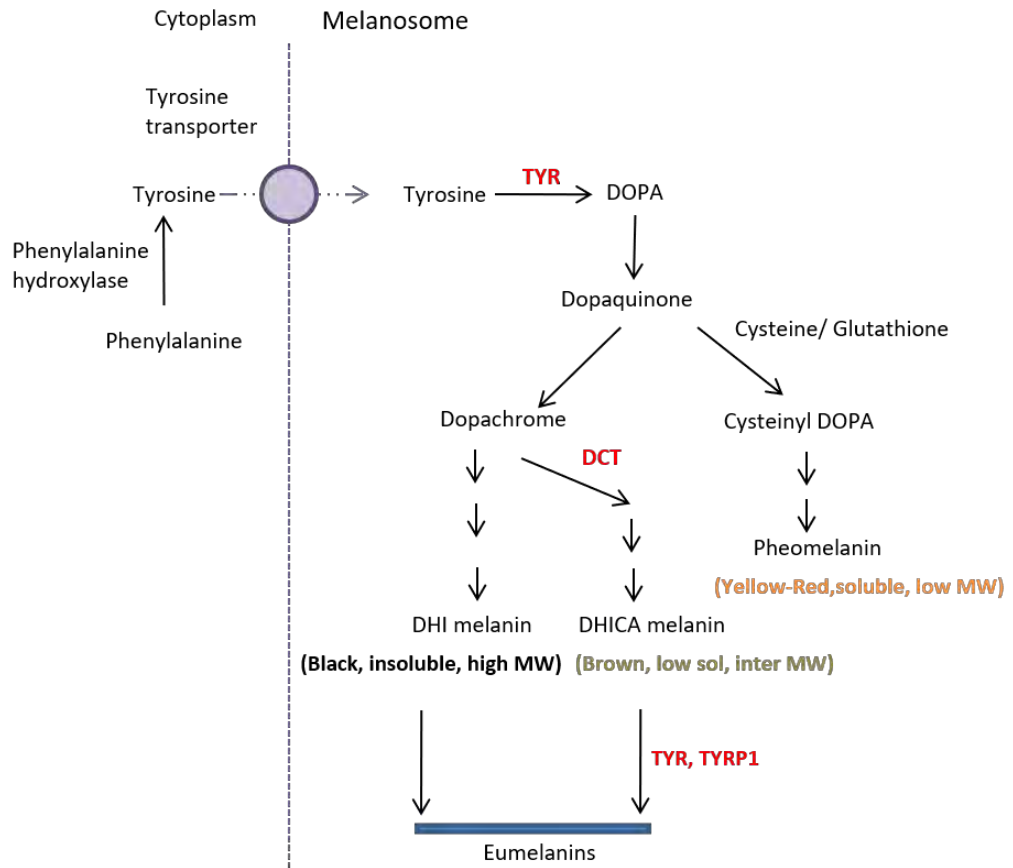
Fig. I.3. Melanin biosynthetic pathway. The schematic representation shows the formation of eumelanin and pheomelanin from tyrosine. Tyrosinase (TYR) catalyzes the conversion of tyrosine to DOPA. Dopachrome tautomerase (DCT) tautomerizes dopachrome to indole derivative DHICA melanin which is a low brown solubility intermolecular weight polymer. Together with DHI which is black and a high molecular weight polymer, it forms the eumelanin. The lightly colored yellow-red soluble, low molecular weight polymer called pheomelanin is derived from the Cysteinyl DOPA. Modified from Morris and Rogers (Journal of nutrition) and Hearing (Milestones Cutaneous Biology).
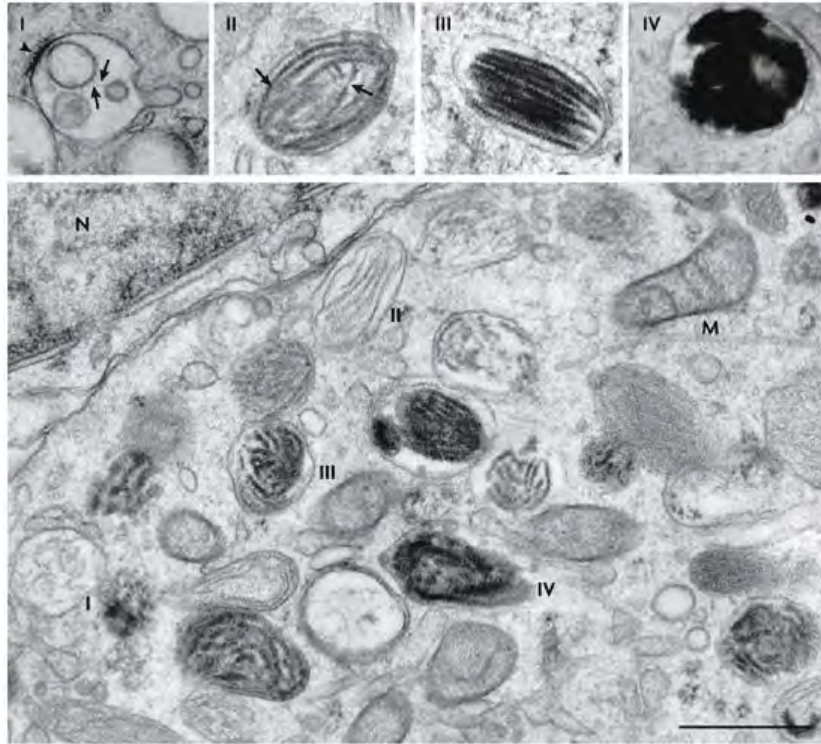
Fig. I.4. Electron microscopy revealed four stages of melanosome maturation. The ultrastructural studies have revealed four embryonically distinct stages of melanosome. Melanosome shows four characteristic stages that have incorporation of multiple structural and enzymatic proteins. The four stages of melanosome development are shown in the upper panels in heavily pigmented MNT-1 cells. The dense bilayered coat (arrowhead) and intraluminal vesicles (arrow) of stage I melanosomes, the proteinaceous fibrils (arrow) of stage II, and the melanin deposition (black) in stages III and IV. The main panel shows a typical field of MNT-1 cytoplasm near the nucleus, which contains all four stages of melanosomes. M, mitochondria; N, nucleus. Scale bar represents 0.5µm. (Raposo & Michael S. Marks., 2007)
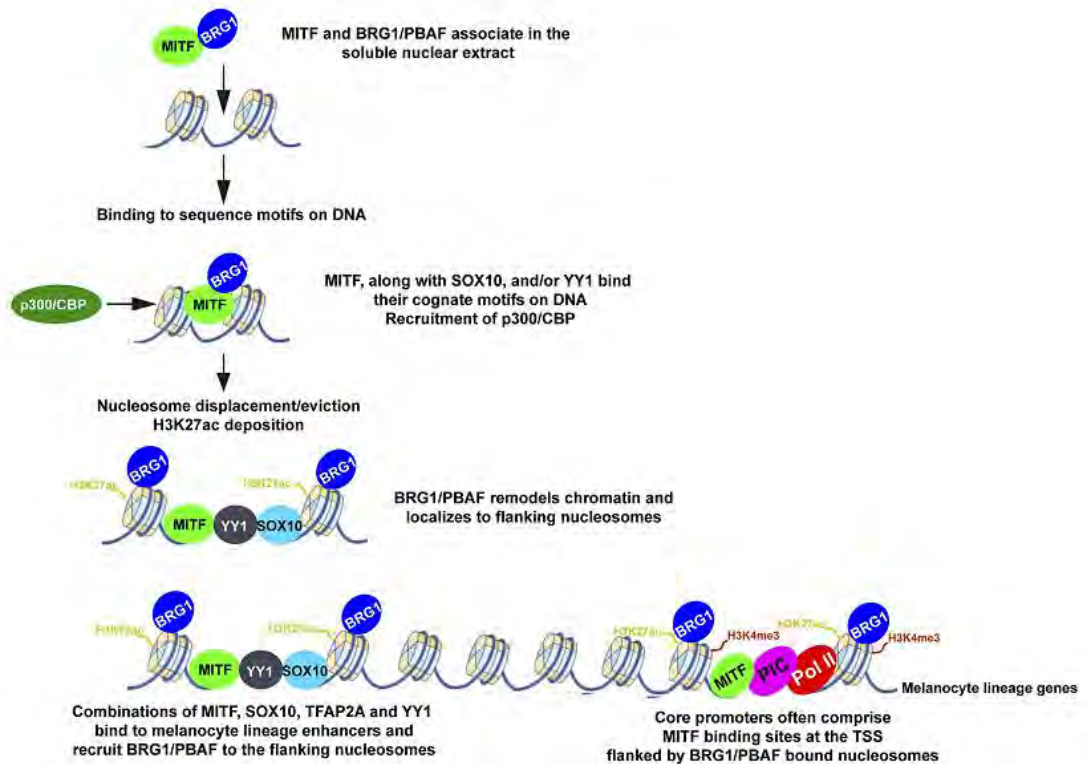
Fig. I.5. BRG1 controls dynamics of MITF binding. MITF-BRG1 interplay plays an essential role in transcription regulation in melanoma. The tandem affinity purification and mass spectroscopy were used to define a comprehensive MITF interactome identifying novel cofactors involved in transcription, DNA replication and repair, and chromatin organization. MITF interacts with a PBAF chromatin remodeling complex comprising BRG1 and CHD7. BRG1 is essential in both in-vitro and in-vivo to control the proliferation of normal melanocyte. MITF and SOX10 recruit BRG1 to the MITF-associated regulatory elements (MAREs) at active enhancers. The specific chromatin organization of the regulatory elements are defined by the combinations of MITF, SOX10, TFAP2A, and YY1 bind between two BRG1-occupied nucleosomes. (Image is obtained from Laurette P. et al.,2015)

Fig. I.6. Disorders of Pigmentation. Skin color is a complex trait which is controlled by numerous genes. The skin pigmentation homeostasis is essential to control the normal functioning of the melanocyte. Impairment of this homeostasis balance can lead to either hypo- or hyperpigmentation which can occur as a genetic or acquired disease. Hypopigmentation Disorders can result from migration abnormalities of melanocytes from the neural crest to the skin during embryogenesis, e.g., Piebaldism and Waardenburg Syndrome. The abnormal skin pigmentation may be due to impairment of melanosome transfer to the surrounding keratinocytes e.g. Chediak-Higashi Syndrome (CH) and Hermansky-Pudlak Syndrome (HPS), an alteration in melanin synthesis, eg. Oculocutaneous Albinism or due to melanocyte loss e.g. Vitiligo. Hyperpigmentation Disorders can result from either increased melanin, e.g., Cushing Syndrome and Melasma or due to increasing melanocyte as occurs in melanoma.

Disorders of Pigmentation

Hypopigmentation

Melanoblast proliferation and migration

Piebaldism

Waardenburg Syndrome

Melanin Synthesis

Oculocutaneous Albinism

Melanosome Synthesis and transfer

Chediak-Higashi Syndrome (CH)

Hermansky-Pudlak Syndrome (HPS)

Melanocyte Loss

Vitiligo

Hyperpigmentation

Increased Melanin

Acromegaly and Cushing syndrome

Melasma
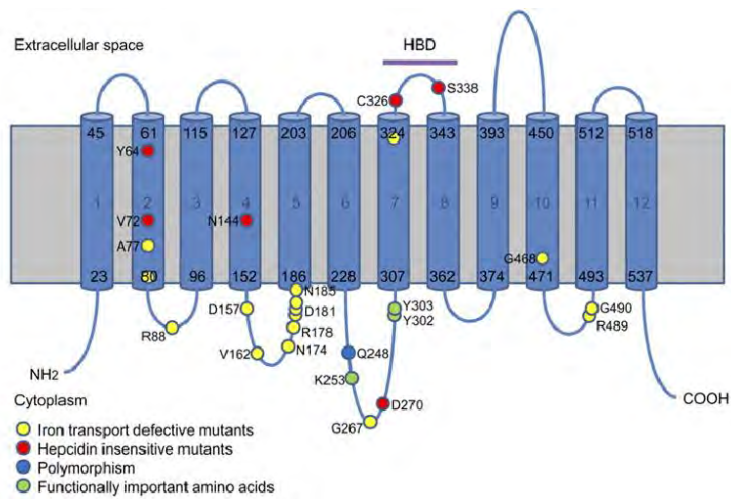


Increased Melanocytes

Melanoma

Fig.III.1. Structure of ferroportin. The ferroportin protein is composed of 571 amino acids having multiple transmembrane (TM) segments. The topology of ferroportin contains intracellular N- and C-terminal extremes which forms even number of transmembrane segments. The intracellular loop between TM6 and TM7 includes the major residues that are required for the internalization and degradation of ferroportin and an extracellular loop between TM7 and TM8 having the binding site of hepcidin. (Wallace et al., 2010)

Fig.III.2. The siRNA-mediated knockdown of *Slc40a1* gene leads to increased melanin accumulation in B16 cells. (A) Real-time qPCR validation of *Slc40a1* expression at 48h of forskolin and IBMX treatment. The normalization of expression values was done wrt endogeneous control *Gapdh.* Delta Ct values indicate significant downregulation of *Slc40a1* expression was observed (p-value <0.05) in forskolin and IBMX treated samples as compared to DMSO at 48h. **(B)** B16 cells were transfected with 100nM of *Slc40a1* siRNA for 48h in DMEM media. RNA isolation and cDNA preparation was carried out for cells harvested 48h post-transfection. qRT PCR analysis was done to examine the expression levels of melanogenic genes after silencing *Slc40a1*. We found 80% reduction in the expression of *Slc40a1*, whereas, expression of genes like *Tyr*, *Tyrp1*, *Dct* and *Mitf* was found to be unchanged. **(C)** B16 cells were transfected with 100nM of *Slc40a1*, *Mitf* and *Slc24a4* siRNA and control (Mock and DMEM) in DMEM media for 48h. After 48h post-transfection the bright field images of B16 cells were captured using Nikon Ti-S at the magnification of 10x. The scale bar indicates 100µm. **(D)** To record the cell pellet after siRNA transfection, media was aspirated, cells were trypsinized and harvested. After hemocytometer counting ~1.0x10^6 cells were taken to record the cell pellet color.

A.

B.
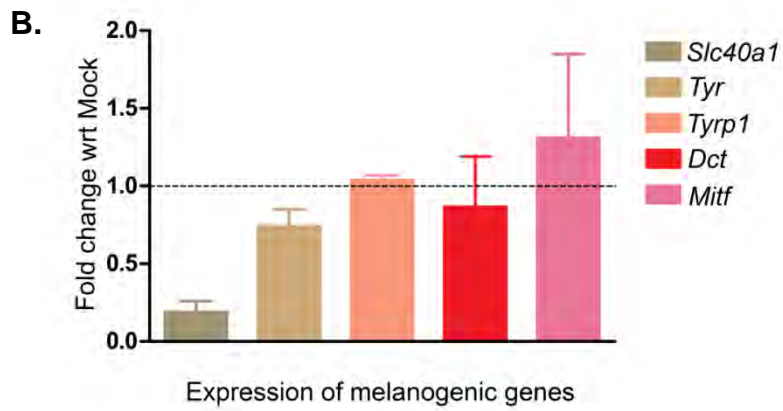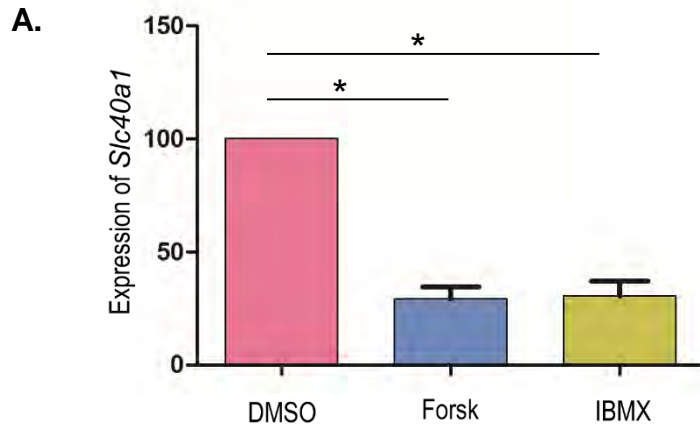
C.
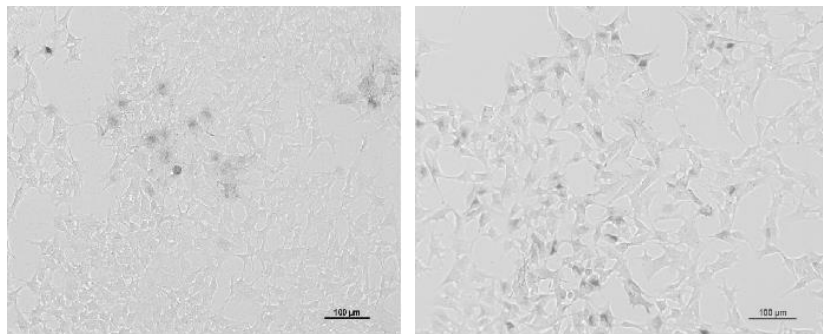
Mock   si*Slc40a1*

D.

DMEM Mock si*Slc40a1* si*Mitf* si*Slc24a4*
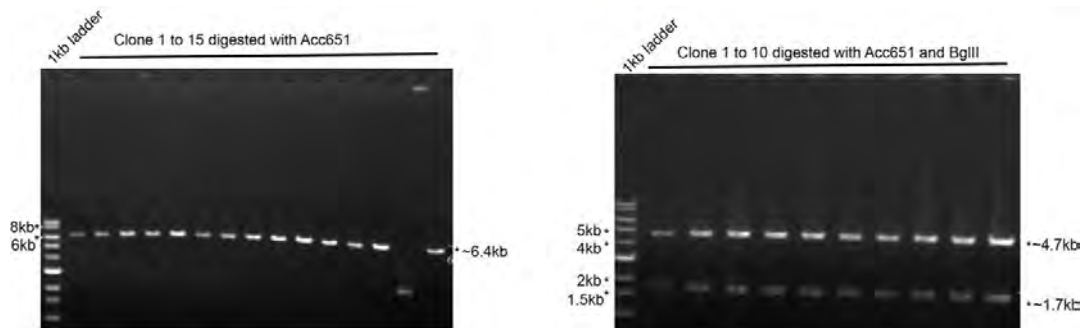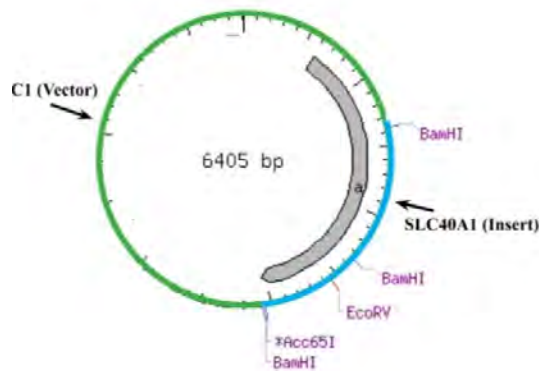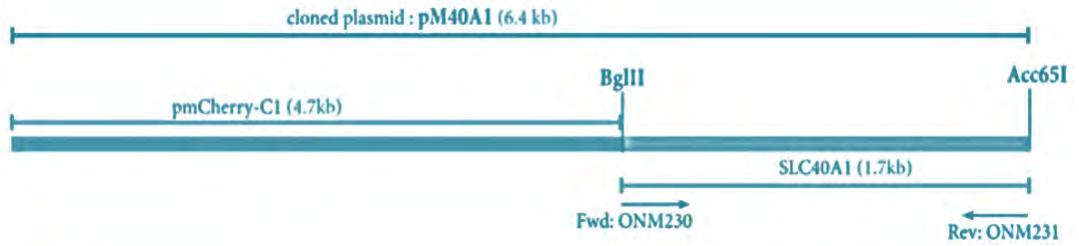
Fig.III.3. The strategy to construct mCherry tagged SLC40A1/FPN1 protein. The protein sequence of SLC40A1 was retrieved from UCSC genome browser (uc007awu.1). The coding region was cloned into the pmCherry-C1 vector to generate a C- terminal mCherry tagged protein. The primers used were ONM230-ONM231 having BglII and Acc651 sites respectively. The gene was amplified using cDNA derived from the RNA of B16 cells, and the amplicon had a size of ~6.4 bp.

Fig.III.4. Western analysis and Fluorescence Microscopy confirmed the expression of mCh-SLC40A1 protein. (A) For transfection, B16 cells were seeded at a density of 32000 cells/ well in six-well plates. After O/N adherence 1µg of pM40a1-2 construct was transfected using cellfectin reagent and mock was taken as control. After 6h post-transfection the cells were washed twice with DPBS, and the original media of the cells was replaced. The transfected cells were harvested at 24h post-transfection by adding native lysis buffer directly to the plate. The protein estimation was done using BCA kit, and ~30µg of total protein was used to perform the western analysis. The blot was probed with an anti-mCherry primary antibody (Rabbit polyclonal, 1:1000 dilution). The band of size 89KDa was observed for pM40a1-2. **(B)** B16-F10 cells grown on slides were transfected with tagged SLC40A1/FPN1 in a 6-well plate and mock was taken as control. After 24h post-transfection image was acquired using fluorescence microscopy. Before image acquisition media was aspirated and wells were washed with 1ml DPBS to remove the traces of media. Fluorescence microscopy was carried out on Nikon Eclipse Ti-E inverted microscope system with filter sets for TRITC (red) emission at the magnification of 20x. The scale bar indicates 100µm. Images were captured using Nikon NIS- Elements Advanced Research, Version 4.00.00.

A.

M   Mock   mCh-SLC40A1

95
72   * 9KDa
55
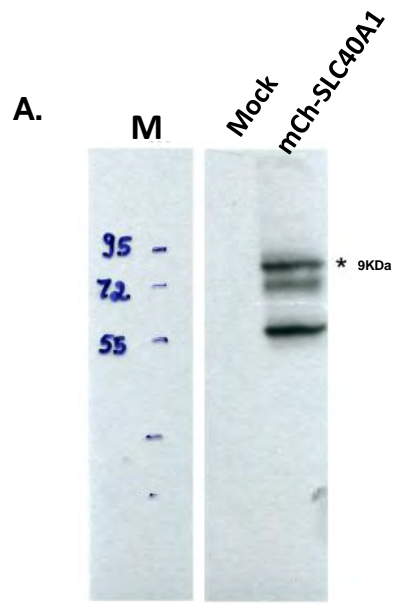
B.

MOCK
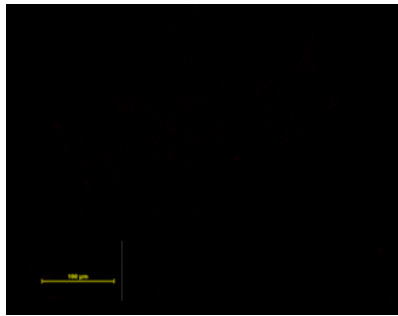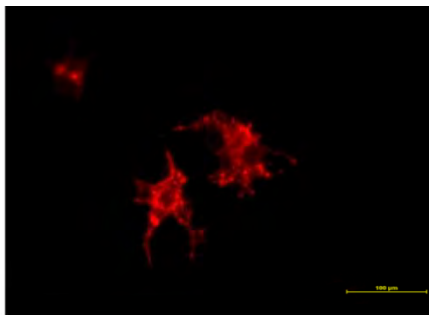
mCh-SLC40A1   mCh-SLC40A1
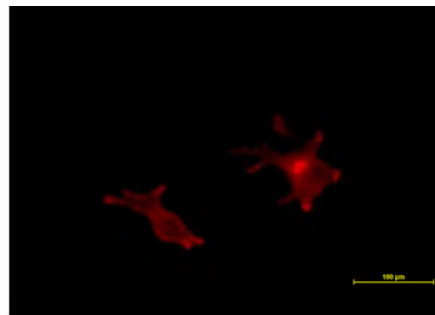
A.
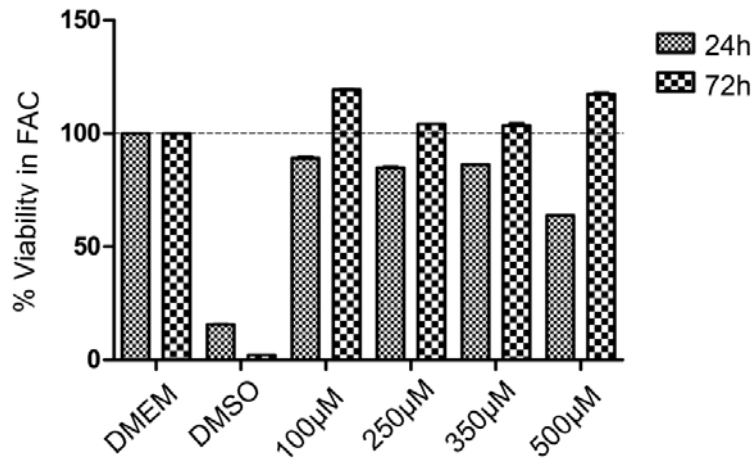
B.
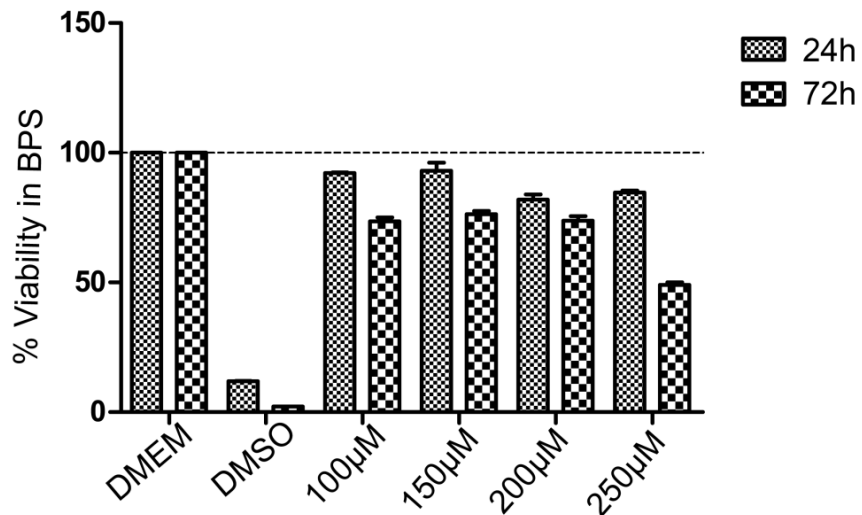
Fig. III.6. The optimal concentration of FAC and BPS was determined by MTT assay. Bar graph showing the viability of B16 cells grown in iron replete and deplete media. B16 cells were seeded at a density of 4000 cells/well for 24h and 3000 cells/well for 72h in 96-well plates in DMEM medium (Section.II.4). After overnight adherence, FAC (+Fe) and BPS (-Fe) treatment was done, DMEM as positive control and DMSO as negative control and cultures were incubated at 24h and 48h cells harvested and MTT assay done, and viability for each treatment was calculated with reference to the viability in DMEM medium (Section II.4). The optimal concentration for FAC was 500µM and for BPS was 200µM were the cell viability was between 70-80 %.

Fig.III.7.   Iron addition leads to increased melanin accumulation and cell proliferation whereas chelation of iron leads to decreased pigmentation and cell number. (A) Experimental set up to study the effect of iron at three different time points (24h, 48h, and 72h). Actively growing B16 cells were seeded in DMEM medium and 24h later, the cultures were treated with 500µM FAC (+Fe) or 200µM BPS (-Fe) and DMEM as a control. **(B)** About ~1.0×10^6 cells were harvested at 24h, 48h and 72h time point and pellet colour were recorded. **(C)** At 48h where the pellet color differences were significant between the control and treated samples the phase contrast images of B16 cells were captured using Nikon Ti-S at the magnification of 40x. The scale bar indicates 50µm. **(D)** Iron depletion through chelation caused a reversible change in the pigmentation status of B16 cells. **(E)** B16 cells were seeded at the density of in 0.25×10^6 per T-75 cultured flask. After overnight adherence, compound treatment was done and cells were harvested at three time points. The cells were stained with trypan blue in the 1:1 ratio and counted using the Neubauer hemocytometer. The cell count shows the proliferation of B16 cells in the presence of iron at 48h and 72h time points as compared to –Fe condition.

A.

B.

24h	48h	72h
DMEM FAC BPS	DMEM FAC BPS	DMEM FAC BPS

C.

DMEM   FAC   BPS

D.

E.

A.

DMEM   FAC   BPS

Melanin secreted in the cultured media at 48hrs
of compound treatment

B.

$y = 0.0077x$
$R^2 = 0.9962$

Absorbance at 410nm

Concentration of synthetic melanin (µg/ml)

C.

Melanin Content at 410nm
(µg/1×10^5)

F12   DMEM   FAC   BPS
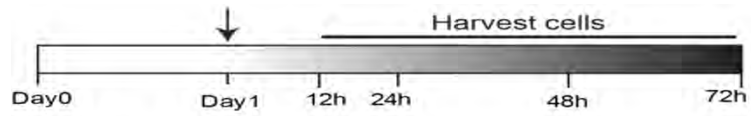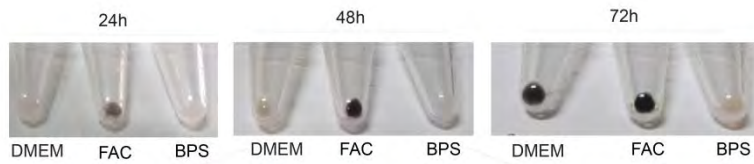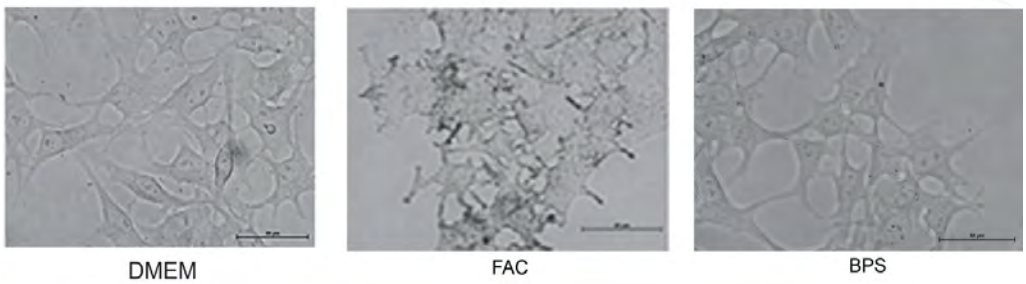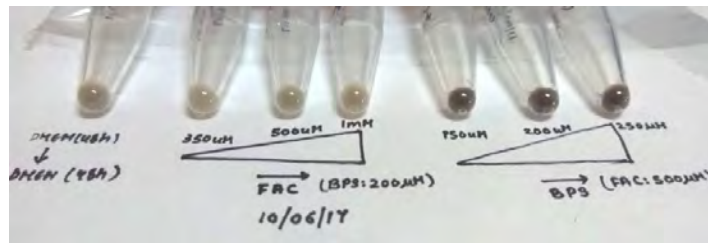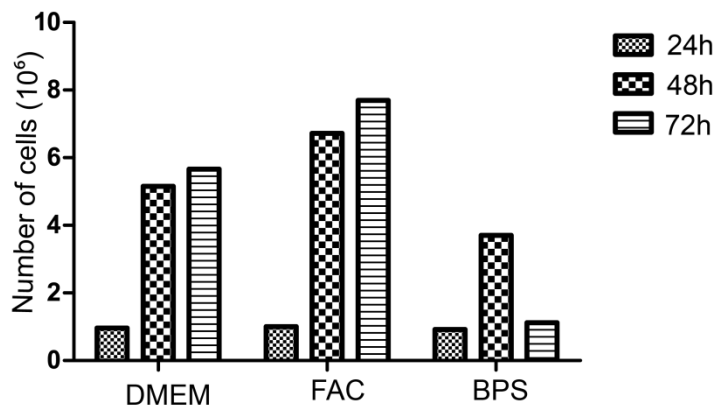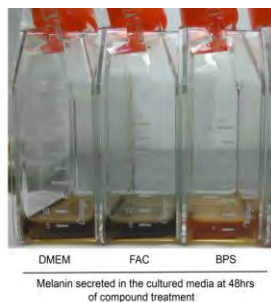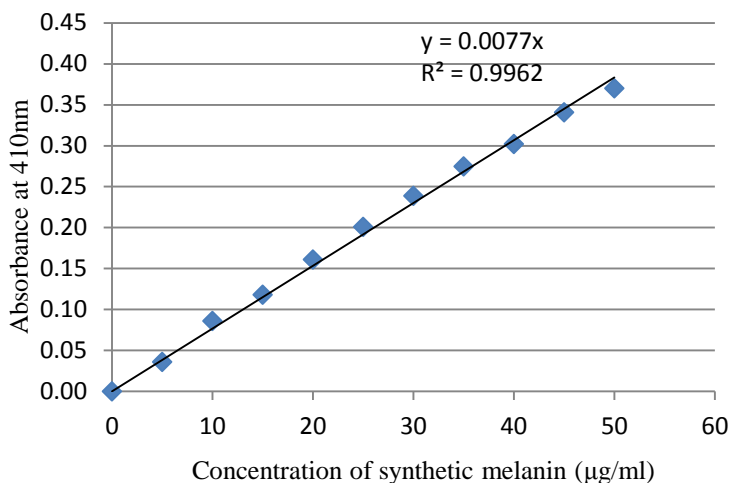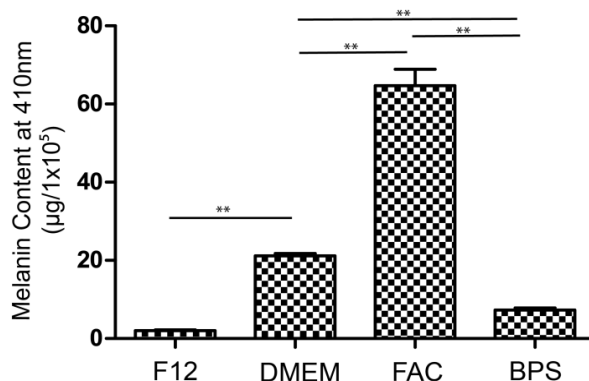
Fig.III.8. The addition of Iron leads to increase of both extracellular and intracellular melanin content in B16 cells. (A) The change in the media color, (considered as secreted melanin), was observed after 48h of FAC (+Fe) treatment as compared to DMEM and BPS (-Fe) condition. **(B-C)** The intracellular melanin estimation was done in which 1×10^5 cells were solubilized in 200µl of 1N NaOH and 10% DMSO for 2h at 80°C. 1mg/ml stock of synthetic melanin was prepared in 1N NaOH and 10% DMSO (Section II.6). The absorbance of the supernatant was measured at 410nm and melanin content was determined using standard curve. The values were expressed as µg per 1×10^5 cells. The significant increase in intracellular melanin was found in +Fe condition as compared to -Fe and controls ($p < 0.01$). Data are displayed as mean ± S.E. of biological duplicate measurements (*, $p < 0.05$; **, $p < 0.01$;***, p<0.001 Student's *t*-test). . (The protocol is obtained from PMID: 24317198).

C.

| I | II | III | IV |
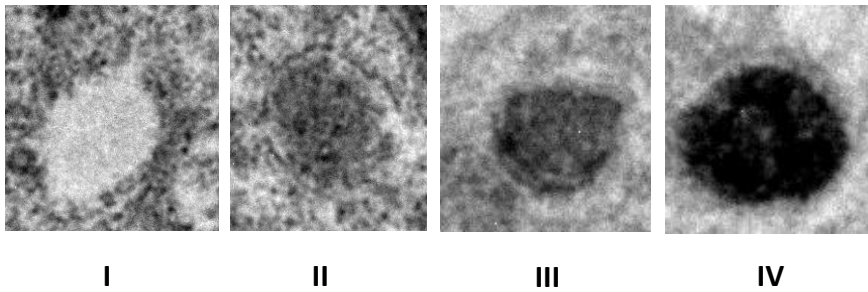
Fig. III.9. Cellular investigations of B16 cells through Transmission Electron Microscopy (TEM). EM images are showing ultrastructure of a B16 cell cultured in DMEM media. The cells were fixed with glutaraldehyde and embedded in agar and imaged with the FEI Tecnai™ Twin-20 transmission electron microscope (Section.II.9). **(A)** The nuclear membrane nucleus, nucleolus, mitochondria and cell membrane are indicated. Each cell is imaged at a magnification of 550x. Scale bar represents 2 µm. **(B)** 1700x magnification of the same cell represented in **A.** Scale bar represents 0.5 µm. **(C)** The various maturation stages of melanosome are shown. Stage I from BPS, stage II from DMEM and stages III and IV, from FAC-treated cells. The melanosomes are characterized on the basis of the amount of melanin accumulation.

A.
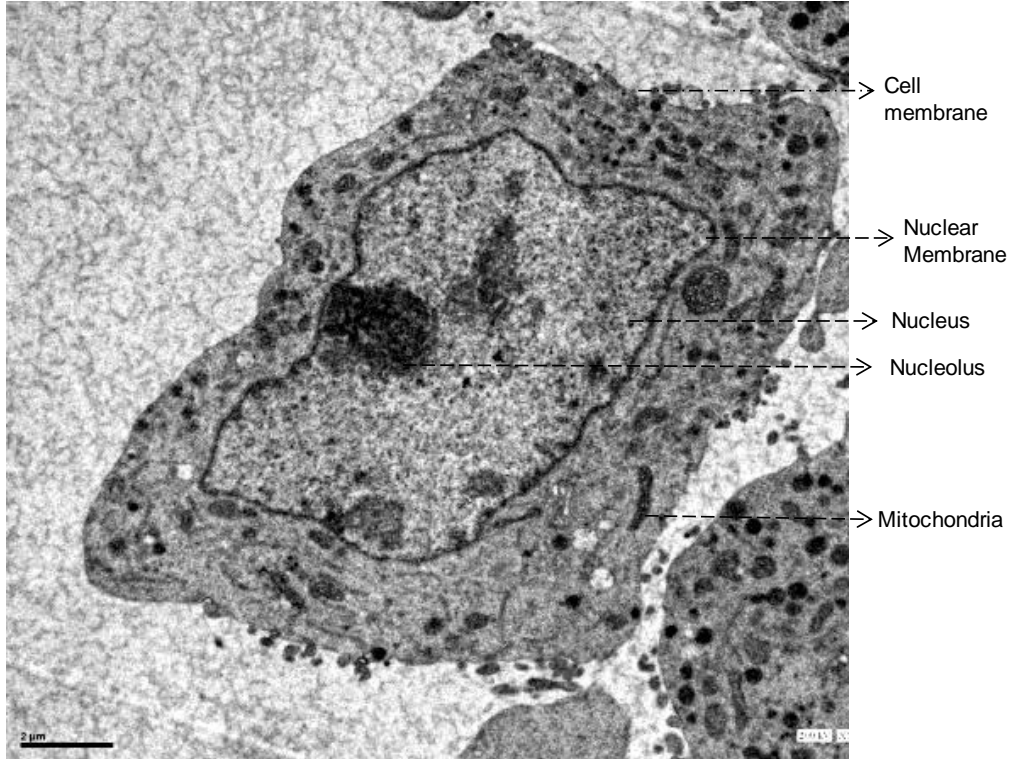
B.
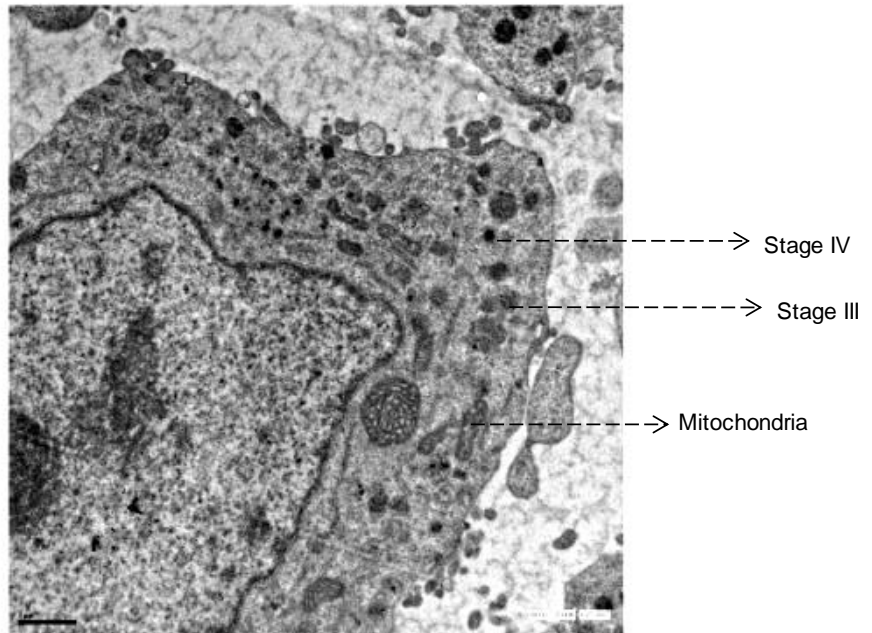
Fig.III.11. The expression analysis of melanogenic genes in iron replete and deplete condition. The time course analysis of melanogenic genes transcript abundance in B16 melanoma cells following forskolin and IBMX treatment as assessed by real-time qPCR. Total RNA from the samples was used for cDNA synthesis. DNase-I treated cDNA was used for real-time qPCR using SYBR Green chemistry (ABI). Relative expression values were calculated as per $2^{-\Delta\Delta CT}$ method. The bar graph plotted shows the expression values in fold change normalized with respect to DMEM versus the various melanogenic genes at 24h, 48h, and 72h time points. **(A)-(B)** Shows expression levels of *Tyr, Tyrp1, Dct* and *Mitf* transcript levels in B16 cells treated with 500µM of FAC (+Fe) and 200µM BPS (-Fe). **(C)** For Western blot, whole cell lysates were prepared (Section II.19), and ~20µg of total protein from the extracts were run on 10% SDS-PAGE, blotted to PVDF. The blot was probed with a murine α-Tyrosinase antibody (70KDa, 1:10,000; anti-PEP7, a gift from Vincent Hearing NCI, NIH) and MITF antibody (59KDa, 1:2000) As a loading control, the blot was also probed with a murine anti-β-actin antibody (42KDa, 1:50,000).

A.
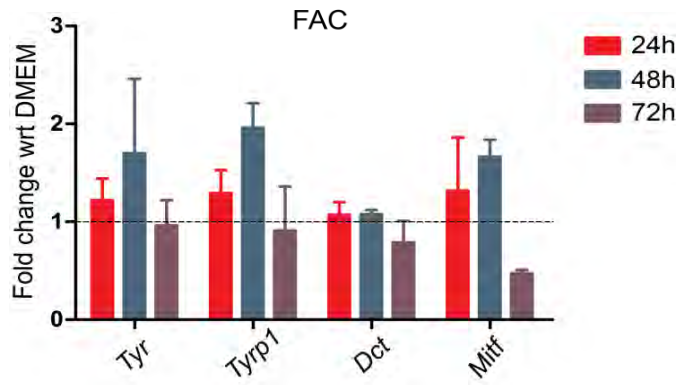
B.
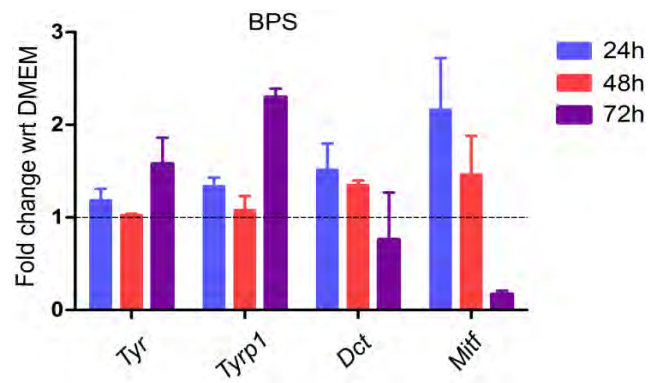
C.
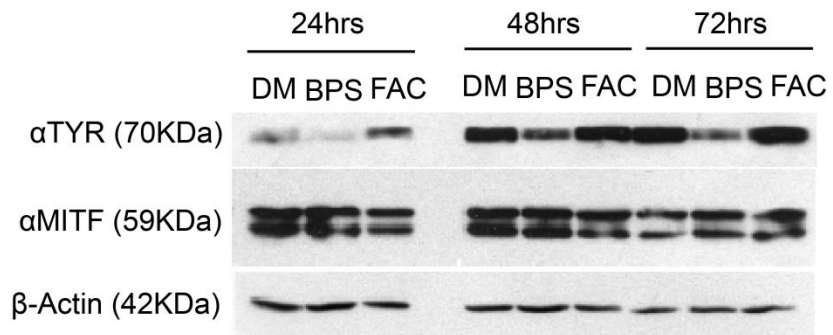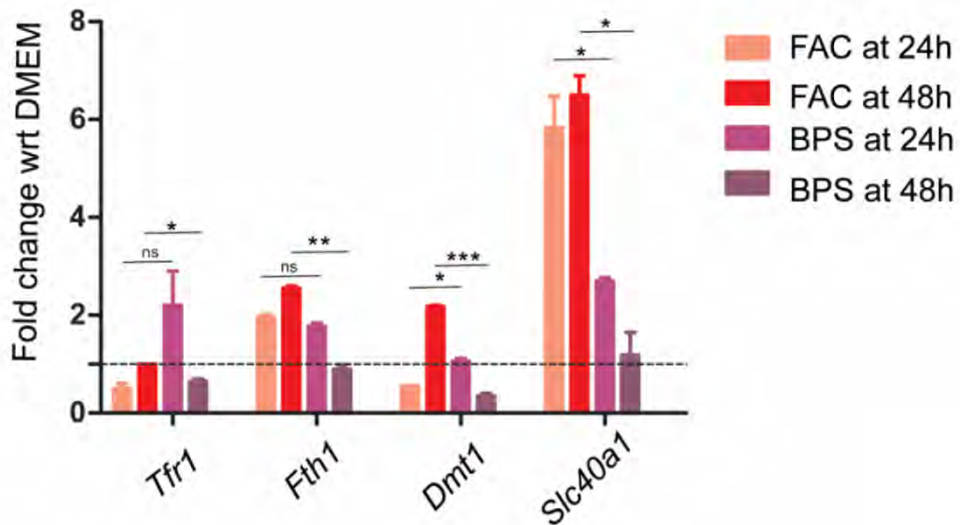
Fig. III.12. The expression analysis of genes involved in iron transport and storage in B16 cells. Total RNA from the samples was used for cDNA synthesis. DNase-I treated cDNA was used for real-time qPCR using SYBR Green chemistry (ABI). Primer pairs for the indicated genes were used in PCR in ABI 7500 FAST instrument. CT values were determined. Relative expression values were calculated as per $2^{-\Delta\Delta CT}$ method. The bar graph plotted shows the expression values in fold change normalized with respect to DMEM. The bar graph shows the expression levels of *Tfr1*, *Fth1*, *Dmt1* and *Slc40a1* in +Fe and –Fe condition at 24h and 48h time points. Data are displayed as mean ± S.E. of biological duplicate measurements (*, $p < 0.05$; **, $p < 0.01$;***, p<0.001 Student's *t*-test).
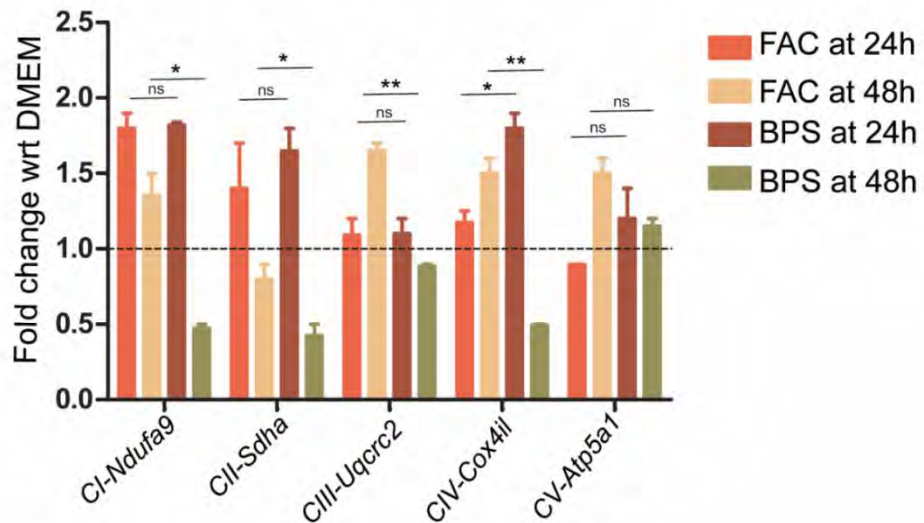
Fig. III.13. Iron deprivation decreases transcription of nuclear encoded mitochondrial OxPhos genes in B16 cells. The analysis of oxidative phosphorylation (OxPhos) complex transcript abundance in B16 mouse melanoma following FAC (+Fe) and BPS (-Fe) treatment as assessed by real-time qPCR at 24h and 48h time points. The bar graph plotted shows the expression values in fold change normalized with respect to DMEM. The expression of C1-*Ndufa9*, CIII-*Uqcrc2, and* CIII-*Cox4il* was significantly downregulated at 48h of iron deprivation. Data are displayed as mean ± S.E. of biological duplicate measurements (*, $p < 0.05$; **, $p < 0.01$; Student's *t*-test).

A. 24_DM_1 [SO_5336]

Overall Results for sample 1 :   **24_DM_1**

RNA Area:	410.9
RNA Concentration:	209 ng/µl
rRNA Ratio [28s / 18s]:	1.7
RNA Integrity Number (RIN):	10 (B.02.08)
Result Flagging Color:	
Result Flagging Label:	RIN:10

Fragment table for sample 1 :   **24_DM_1**

Name	Start Time [s]	End Time [s]	Area	% of total Area
18S	42.05	44.40	119.9	29.2
28S	47.86	51.55	207.2	50.4

B. 24_FAC_1 [SO_5336]

Overall Results for sample 5 :   **24_FAC_1**

RNA Area:	422.4
RNA Concentration:	215 ng/µl
rRNA Ratio [28s / 18s]:	2.0
RNA Integrity Number (RIN):	10 (B.02.08)
Result Flagging Color:	
Result Flagging Label:	RIN:10

Fragment table for sample 5 :   **24_FAC_1**

Name	Start Time [s]	End Time [s]	Area	% of total Area
18S	42.15	44.47	109.1	25.8
28S	48.03	51.28	214.6	50.8

C. 24_BPS_1 [SO_5336]

Overall Results for sample 3 :   **24_BPS_1**

RNA Area:	440.9
RNA Concentration:	225 ng/µl
rRNA Ratio [28s / 18s]:	1.6
RNA Integrity Number (RIN):	10 (B.02.08)
Result Flagging Color:	
Result Flagging Label:	RIN:10

Fragment table for sample 3 :   **24_BPS_1**

Name	Start Time [s]	End Time [s]	Area	% of total Area
18S	42.06	44.37	124.0	28.1
28S	48.16	51.28	194.9	44.2

Fig. III.14. Quality check of RNA samples using bioanalyzer. Total RNA from the samples was run on a bioanalyzer chip (Agilent 2100) and gives a profile of the integrity of RNA. RIN number is calculated using an algorithm that quantifies the RNA degradation. The optimum RIN number is 10. Representative samples are shown in the figure for **(A)** DMEM **(B)** FAC and **(C)** BPS at 24h time point show all the RIN numbers having the value of 10. The sharp 18s and 28s peaks further show intact RNA preparation. The gel representation of the chip on the right panel shows intact low molecular weight bands.

A.

24hB1 24hB2 24hF1 24hF2 48hB1 48hB2 48hF1 48hF2

B.

Agilent two-color Microarray Hybridization

↓

Normalized Data (log$_2$ ratio; Treatment/Control)

↓

Significance analysis to Identify DE genes

↓

Use Significant DE gene for David Analysis
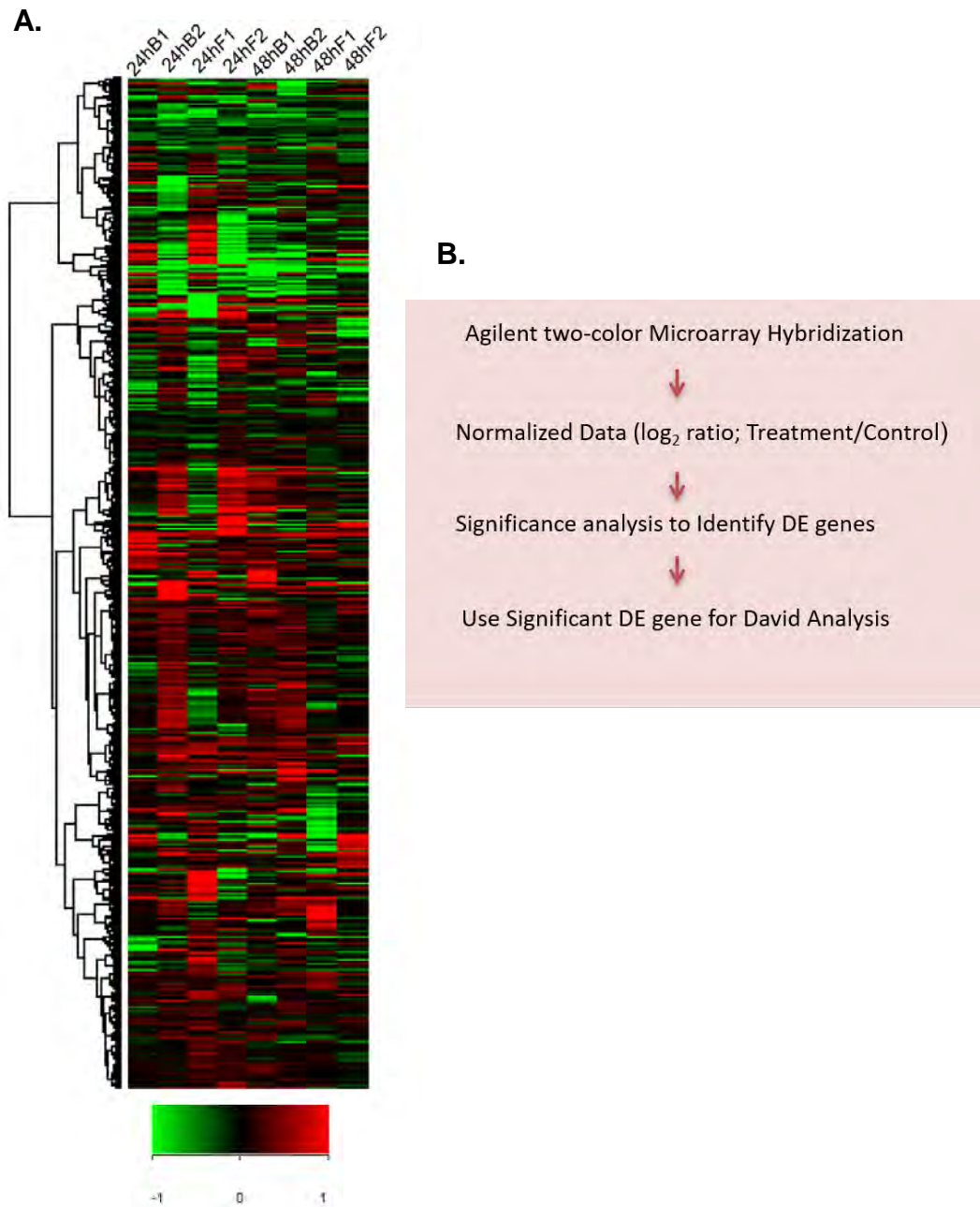
Fig. III.15. Heat map representation of 34834probes used for iron replete and deplete. (A) Summary heat map output of the 34834 genes used to map the genome-wide transcriptomic changes during iron addition and chelation. The output was obtained from the Agilent software gene spring GX12.5. 2-D hierarchical clustering was done on the basis of entities. The entity list is represented vertically. The rows represent the expression value of each gene across eight different samples. Red and green color represents up and down-regulated genes respectively. The color range is set at log2ratio cut off between +1.0 and -1.0. **(B)** Shows the microarray data analysis pipeline to identify differentially expressed genes in iron replete and deplete condition.

B.
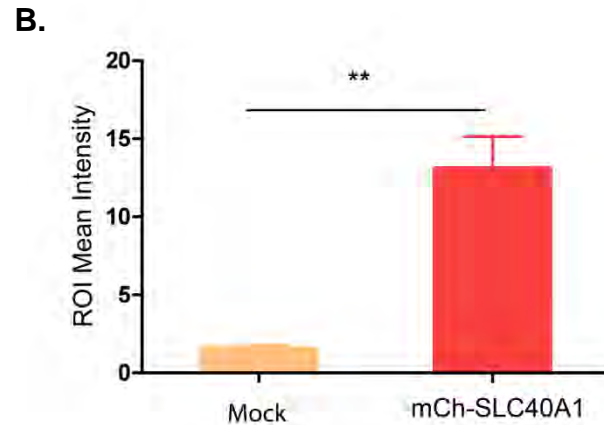
Fig.III.5. **SLC40A1/FPN1 protein predominantly localized on the plasma membrane. (A)** B16 cells grown on coverslip were transfected with mCherry fused SLC40A1/FPN1 (pM40a1-2) or mock as a control. After 24h of post-transfection confocal microscopy was done to detect the fluorescence as discussed in section II.8.3. Counter staining of cells were done by incubating them in Hoechst stain at the ratio of 1:2000. The image from three cells transfected with mCherry fused SLC40A1/FPN has been shown. Confocal microscopy was carried out on Nikon Eclipse Ti-E inverted microscope system with filter sets for TRITC and DAPI emission at the magnification of 60x. The scale bar indicates 10μm. **(B)** The images where quantified and ROI mean intensity for mock and mCh-SLC40a1 was plotted. Images were captured using software AndoriQ, Version. The background subtraction and merged image was done using Nikon NIS- Elements Advanced Research, Version 4.00.00, analysis software.

A.
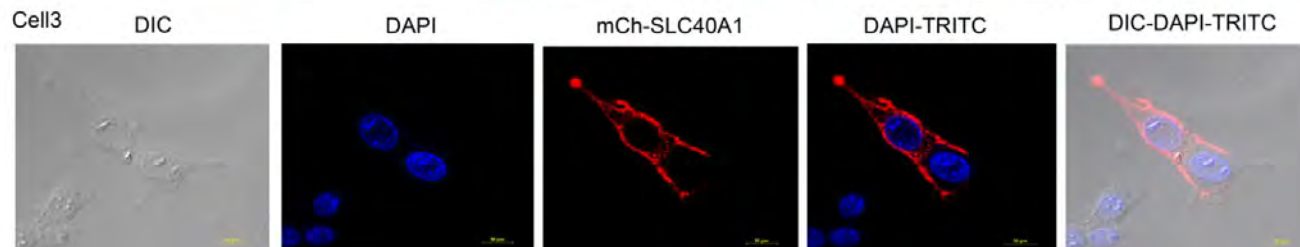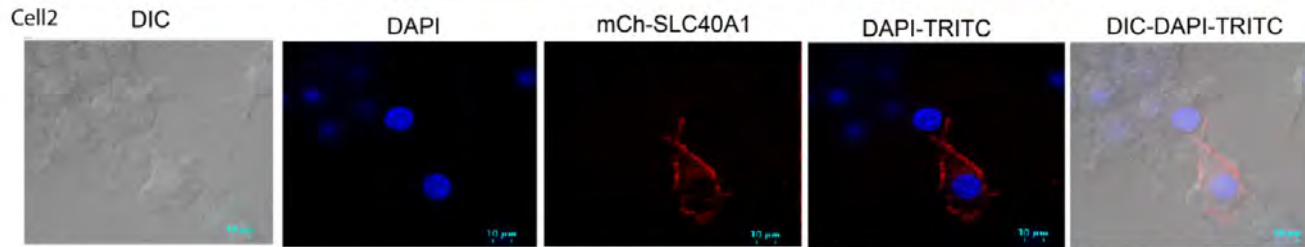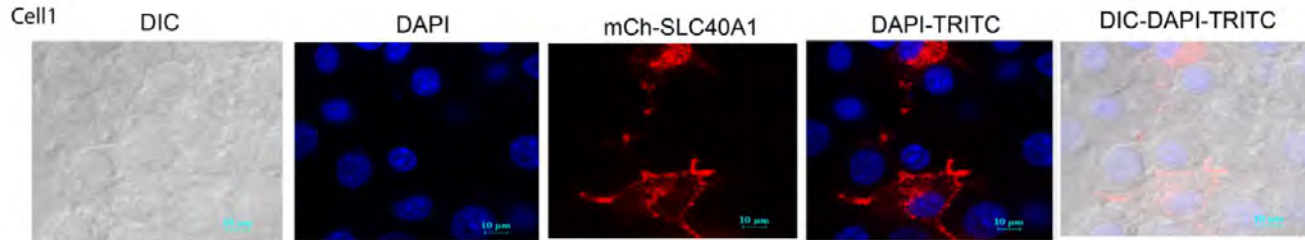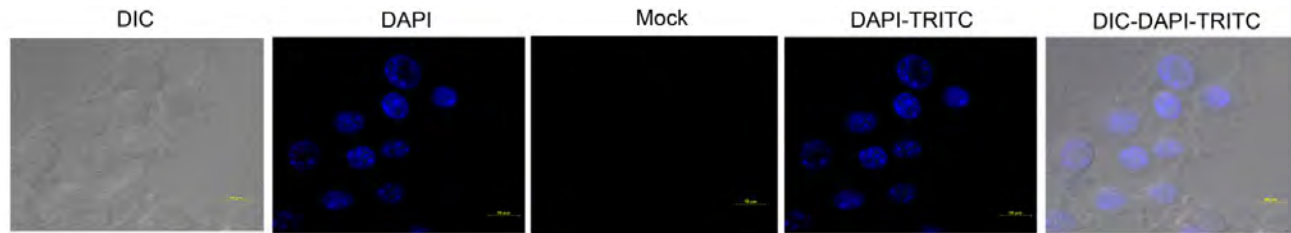
Fig. III.10. Iron accelerates melanosome formation and maturation. (A) The mature stage of melanosomes (III and IV) was increased in the +Fe condition at 48h of treatment. B16 cells were cultured in with +Fe and –Fe conditions or in control DMEM 48h, cells harvested, fixed and embedded. Ultrathin sections were cut, stained and imaged in a transmission electron microscope at a magnification of 1700x (Section II.8.4). The scale bar indicates 1.0µm. **(B)** The bar graph shows the distribution an of a number of stage III and stages IV melanosomes in different conditions. Melanosomes from three representative B16 cells for each sample were categorized into stages I-IV based on melanin content, counted and total mature stage of melanosome III and IV was plotted. The total mature stage of melanosome III and IV were significantly increased in +Fe condition as compared to –Fe condition ($p<0.01$). **(C)** Expression analysis of different components involved in melanosome organogenesis. Premelanosome component, *Hps3*, Melanosome component, *Pmel17* and melanosome motility, *Rab27a*. The bar graph plotted shows the expression values in fold change normalized with respect to DMEM. The expression of these was found to be upregulated in iron-induced hyperpigmentation. Data are displayed as mean ± S.E. of biological duplicate measurements (*, $p < 0.05$; **, $p < 0.01$; Student's *t*-test).

A.

DMEM   FAC   BPS
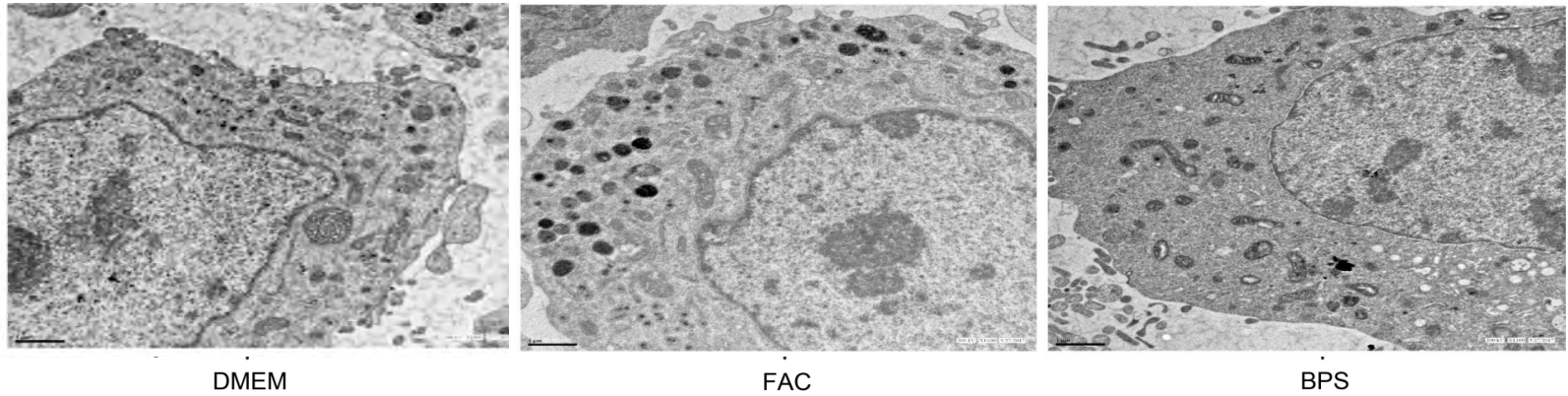
B.
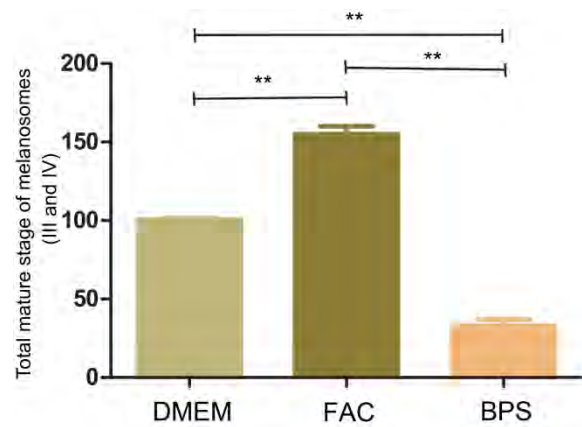
C.
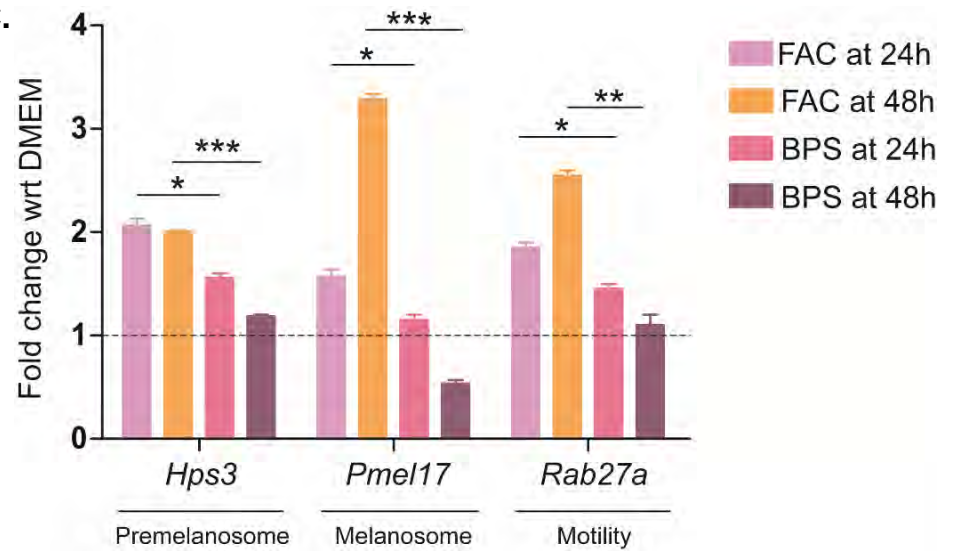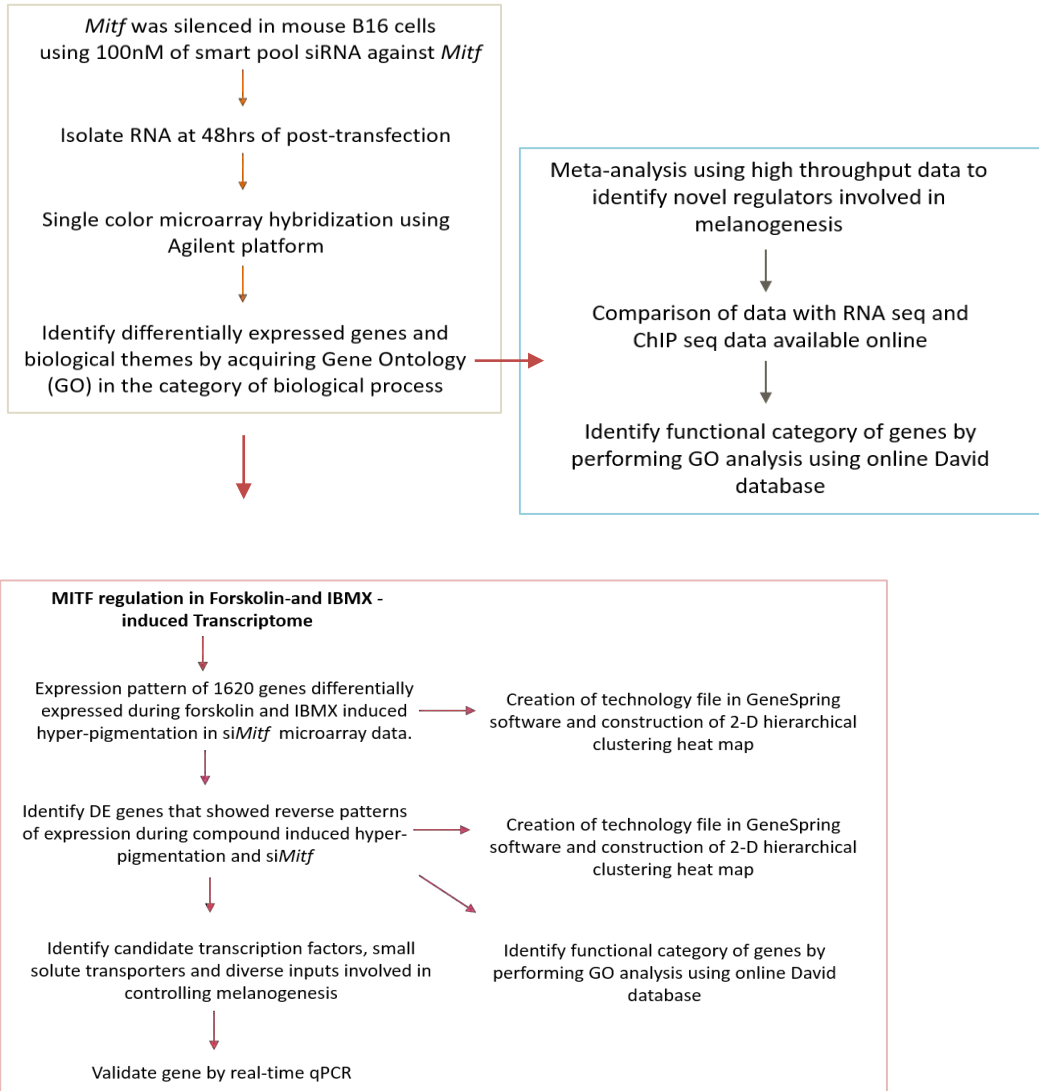
Fig.IV.2. Overview of analysis workflow for microarray transcriptional profiling

A.

B.

C.
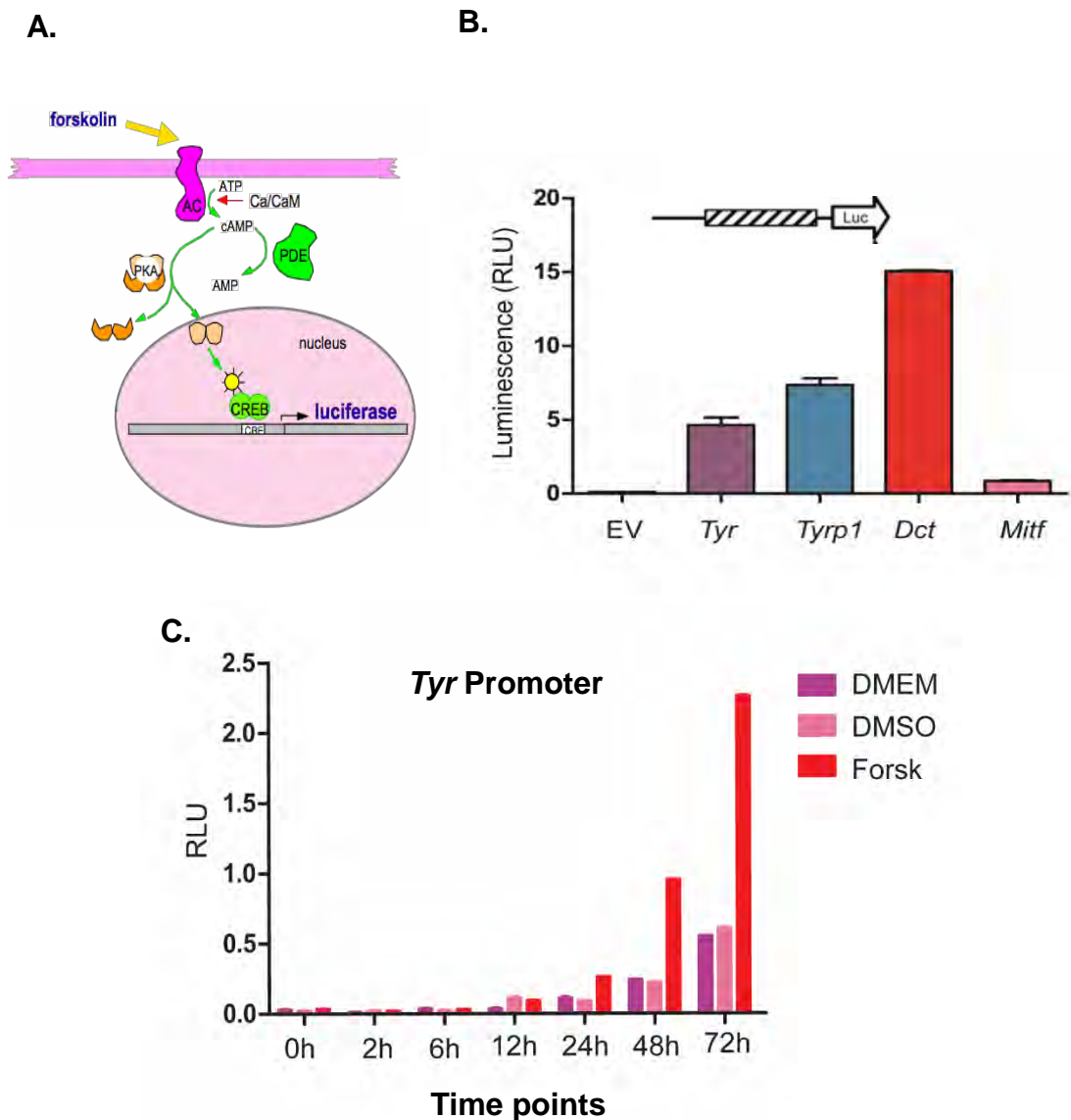
Fig.IV.3. Forskolin induces melanogenic gene promoters. **(A)** Forskolin is known to activate melanogenesis by increasing the level of the secondary messenger, cAMP. cAMP by phosphorylating CREB activates the expression of MITF, a master regulator of melanogenesis. MITF by binding to the promoter of melanogenic genes activate their expression and hence melanin formation. The expression of luciferase gene is directly correlated with the activity of cloned promoters. **(B)** Dual luciferase reporter assay showing forskolin mediated induction promoter activity of all the melanogenic gene promoters at 48h. Transient transfection of pGL4.23 (EV), pGL4.23-Tyr-*luc2,* pGL4.23-Tyrp1-*luc2,* pGL4.23-Dct-*luc2* and pGL4.23-Mitf-*luc2 was done* into B16 cells where, 1:50 ratio of Firefly and Renilla luciferase construct was taken. The luminescence (RLU) was calculated by taking the ration of Firefly Vs Renilla luciferase at 48h. **(C)** Time course luciferase assay done to study the activity of tyrosinase promoter (pGL4.23-Tyr-*luc2)* on forskolin induction at seven different time points. DMEM and DMSO: control

Fig.IV.4. siRNA mediated silencing of *Mitf* lead to decrease in tyrosinase protein and activity. (A) The change in the media color, (considered as secreted melanin), was observed after 48h of post-transfection in Mock, DMEM media and untransfected samples. However, the media color was unchanged in the samples were *Mitf* was silenced. **(B)** To record the cell pellet after siRNA transfection, media was aspirated, cells were trypsinized and harvested. After hemocytometer counting ~1.0×10^6 cells were taken to record the cell pellet color. **(C)** For Western blot, whole cell lysates were prepared (Section II.19), and ~20µg of total protein from the extracts were run on 10% SDS-PAGE, blotted to PVDF and the blot was probed with murine α-Tyrosinase antibody (70KDa, 1:10,000; anti-PEP7, gift from Vincent Hearing NCI, NIH). As loading control, the blot was also probed with murine anti-β-actin antibody (42KDa, 1:50,000). **(D)** Cell lysates containing ~20µg total proteins, without SDS and β-ME were run without heating on a 10% SDS-PAGE for in-gel DOPA assay. For DOPA assay, the gel was incubated with 10mM of DOPA. The intensity of the chromogenic band is indicative of the tyrosinase activity (kirty,2015).

A.

Mock　　Untransfected　　Scrambled siRNA　　*Mitf* siRNA

B.

DMEM　Mock　si*Slc40a1*　si*Mitf*　si*Slc24a4*

C.

IBMX　DMSO

si*Mitf*　Sc-control　si*Mitf*　Sc-control

96KD
72KD
á-TYR (60KDa)

55KD
36KD
β-Actin (42KDa)

D.

Mock　siMitf　siEsrra　siDmrta2　Marker

48h
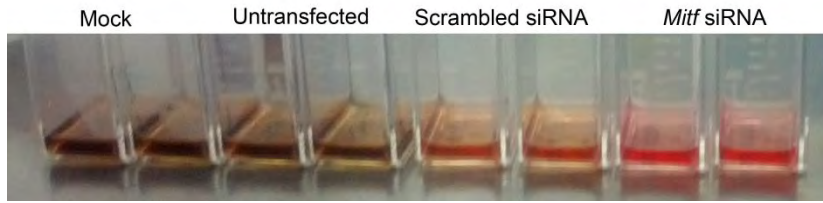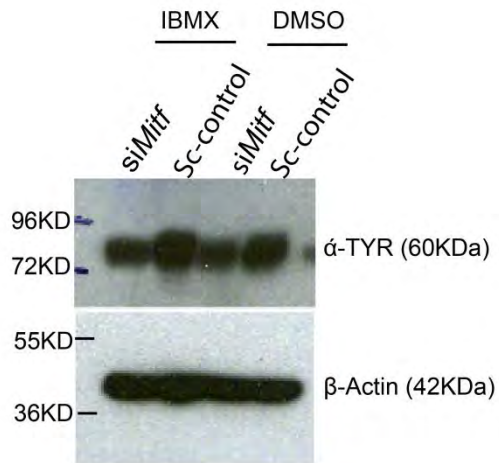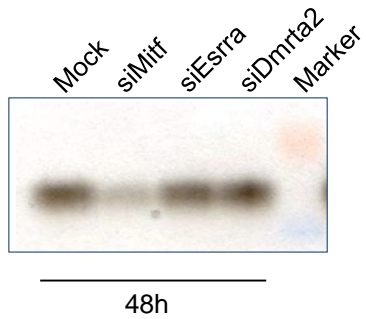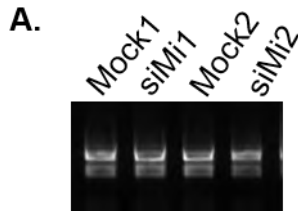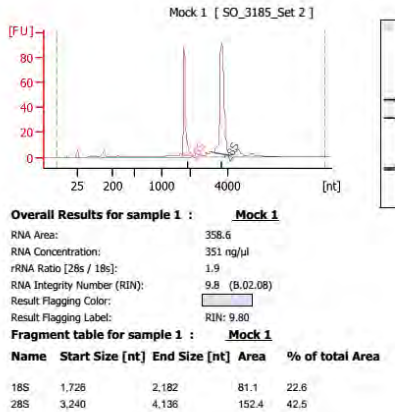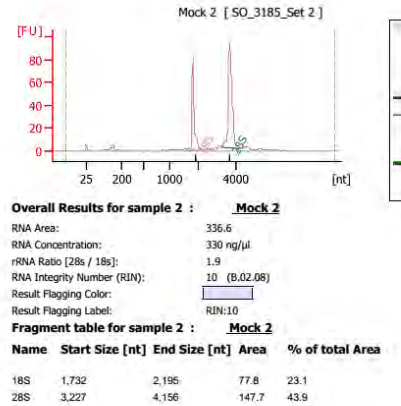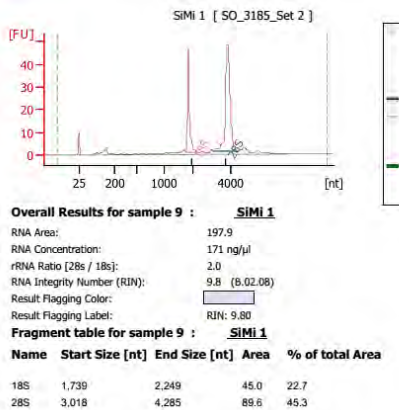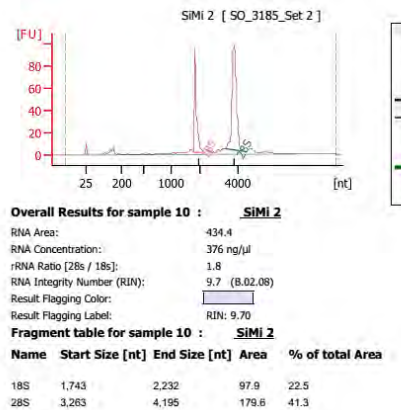
Fig.IV.5. Quality check of RNA samples using bioanalyzer. (A) The integrity of RNA was checked on 0.8% agarose gel. Total RNA from the samples was run on a bioanalyzer chip (Agilent 2100) and gives a profile of the integrity of RNA. RIN number is calculated using an algorithm that quantifies the RNA degradation. The optimum RIN number is~ 9. Representative samples shown in the figure for **(B-C)** Mock1 and Mock2 **(D-E)** siMi1 and siMi2 at 48h time point show the RIN numbers >9. The sharp 18s and 28s peaks further show intact RNA preparation. The gel representation of the chip on the right panel shows intact low molecular weight bands.

A. Gene Ontology 1048 Down-regulated genes

- Melanogenesis
- Steroid biosynthesis
- Glutathione metabolism
- Arginine and proline metabolism
- Cholesterol biosynthesis
- Terpenoid backbone biosynthesis
- Nitrogen metabolism
- Pentose phosphate pathway
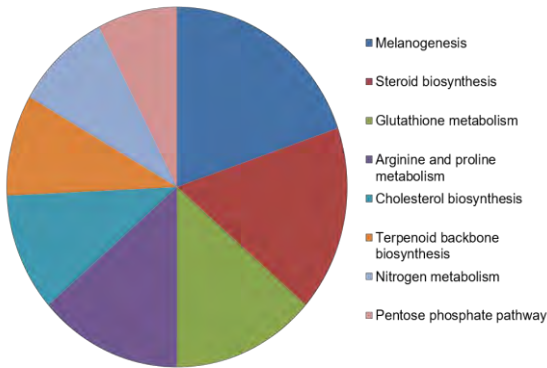
B. Gene Ontology 1430 Up-regulated genes

- Chemokine signaling pathway
- Endocytosis
- Cytokine-cytokine receptor interaction
- Axon guidance
- Focal adhesion
- Antigen processing and presentation
- Cell adhesion molecules (CAMs)
- Graft-versus-host disease
- Viral myocarditis
- Cytosolic DNA-sensing pathway
- Allograft rejection
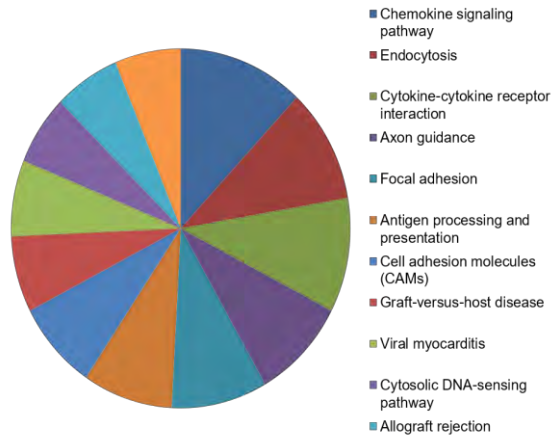
C.
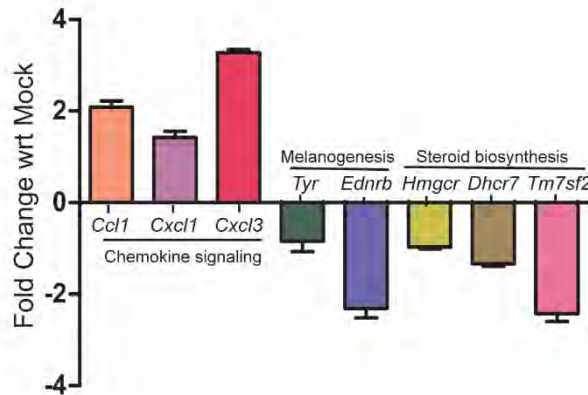
Fig.IV.6. Distinct functional categories of transcripts were enriched during siRNA mediated silencing of *Mitf*. (A-B) A total of 1430 gene were found to be up-regulated, and 1048 genes were down-regulated upon *Mitf* silencing. David analysis done to identify the biological themes these DE genes are associated with the p-value less than 0.05. Downregulated transcripts were primarily associated with ontology terms such as steroid biosynthesis, melanogenesis, cholesterol biosynthesis glutathione metabolism, nitrogen metabolism. In contrast, up-regulated transcripts were associated with chemokine signaling pathway, cytokine-cytokine receptor interaction, cytosolic DNA-sensing pathway and other processes involved in immune. **(C)** The expression of genes upregulated and downregulated was assessed by real-time qPCR at 48h upon *Mitf* silencing. The genes involved in chemokine signaling like *Ccl1*, *Cxcl1,* and *Cxcl3* to be up-regulated whereas, the genes involved in melanogenesis like *Tyr* and *Ednrb* and steroid biosynthesis like *Hmgcr*, *Dhcr7* and *Tm7sf2* were downregulated when *Mitf* was silenced.
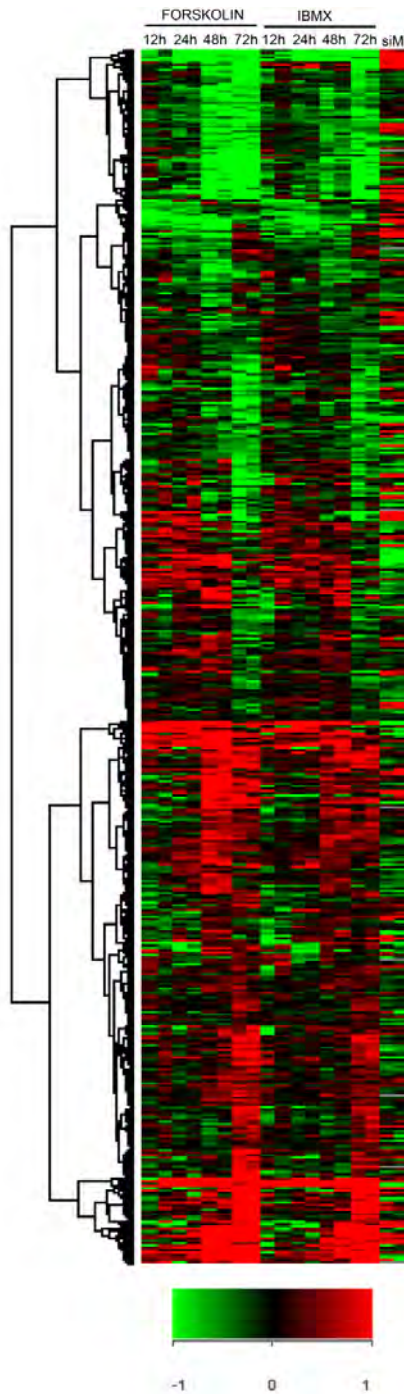
Fig. IV.7. Meta-analysis to examine the regulation of Forskolin and IBMX induced DE genes by MITF. The heat map shows two-dimensional hierarchical clustering of 1620 differentially expressed pigmentation genes (p-value<0.01) and their expression in si*Mitf* data. The colour scale ranges from $\log_2$ +1.0 to -1.0. To characterize the gene expression patterns, we constructed a 2-D hierarchical clustered map using the Gene Spring software. Interestingly, meta-analysis suggested that a large fraction of the DE genes seems to MITF-independent.

Fig. IV.8. Differential regulation of genes in compound induced hyper-pigmentation and si*Mitf* induced hypo-pigmentation. (A) Venn diagram shows the overlap between Forskolin /IBMX and siMitf. From the list of 260 genes up-regulated during hyperpigmentation induced by forskolin and IBMX, 43 genes were down-regulated when *Mitf* was silenced whereas, form the list of 269 genes down-regulated during hyper-pigmentation, 58 genes were up when *Mitf* was silenced. **(B)** The heat map shows two-dimensional hierarchical clustering of the 101 differentially expressed genes (p-value<0.01) common between Forskolin /IBMX and si*Mitf*. The colour scale ranges from $\log_2$ +1.0 to -1.0.The 2-D hierarchical clustered map was constructed using the Gene Spring software. **(C)** The cisBP database was used to extract the list of known TFs using only the direct and the inferred evidence type. These were then identified in the MGI, and a total of 1553 TFs were obtained. Bio Venn shows that from the list of 101genes differentially expressed 3 TFs, *Rarb*, *Vdr* and *Atoh8* shows a different pattern of expression depending upon the pigmentation status of the B16 cells.

A.
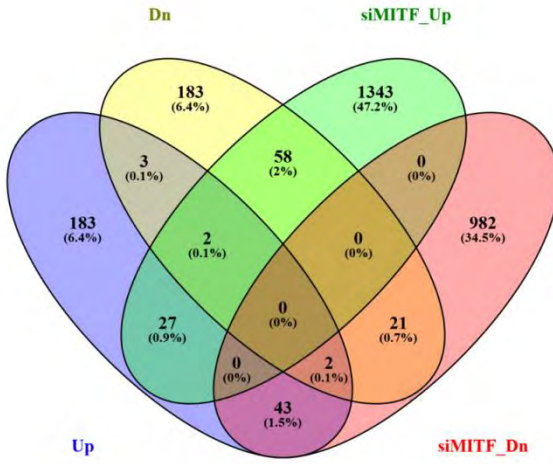
B.
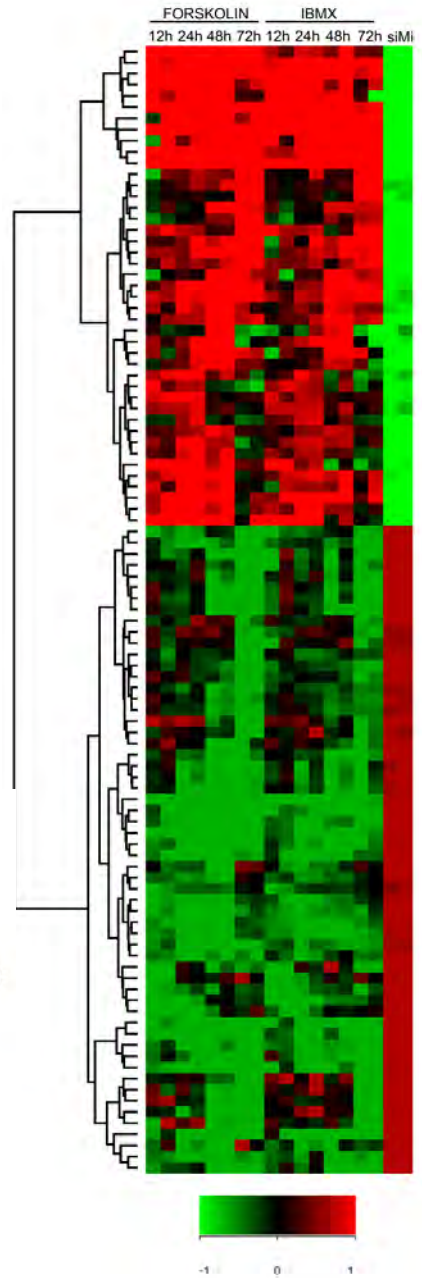
C.
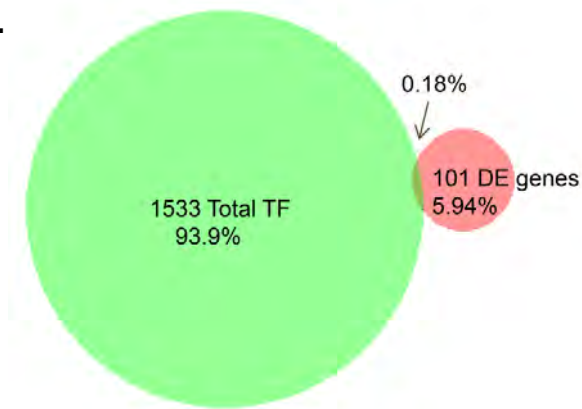
A.
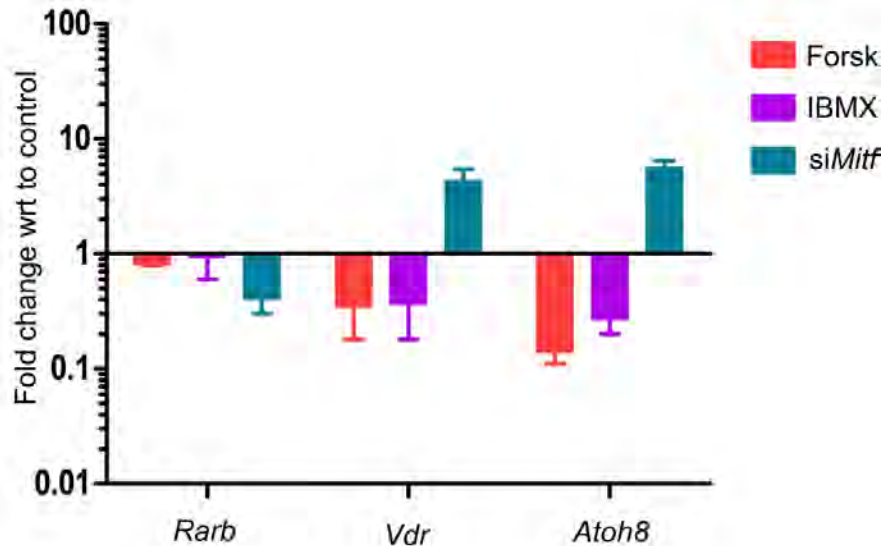
B.
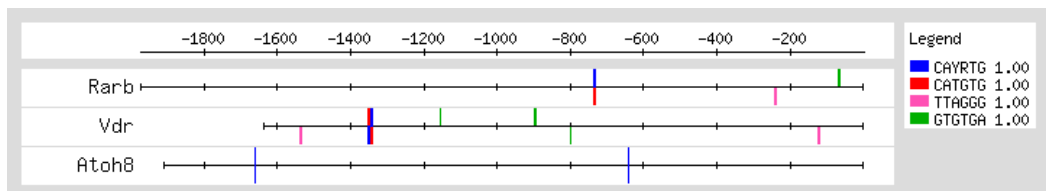
Fig. IV.9. Three transcription factors showed different regulation depending upon the pigmentation status of the B16 cells. **(A)** The analysis of *Rarb*, *Vdr* and *Atoh8* transcript abundance in B16 cells following Forskolin/IBMX and siMitf as assessed by real-time qPCR at 48h time points. The bar graph plotted shows the expression values in fold change normalized with respect to DMSO for Forskolin/IBMX and Mock for siMitf. *Vdr* and *Atoh8* were found to be 2-fold down-regulated in both forskolin and IBMX whereas their expression was >2fold up-regulated when Mitf was silenced. On the other hand, expression of *Rarb* was 2-fold up-regulated in both forskolin and IBMX whereas it was 2-fold down-regulated when Mitf was silenced. **(B)** The 1.5kb promoter and 5'UTR for each transcription factor was retrieved from UCSC genome browser and used to identify the four TFs binding sites using online RSAT tool. Represent the output from RSAT. The blue bars represent the E-Box (CAYRTG), the red box represent the MITF M-box (CATGTG), the pink box represents the LEF1 binding site (TTAGGG) and the green box represent the PAX 3 binding site (GTGTGA).

A.

B.

Expression of melanogenic genes
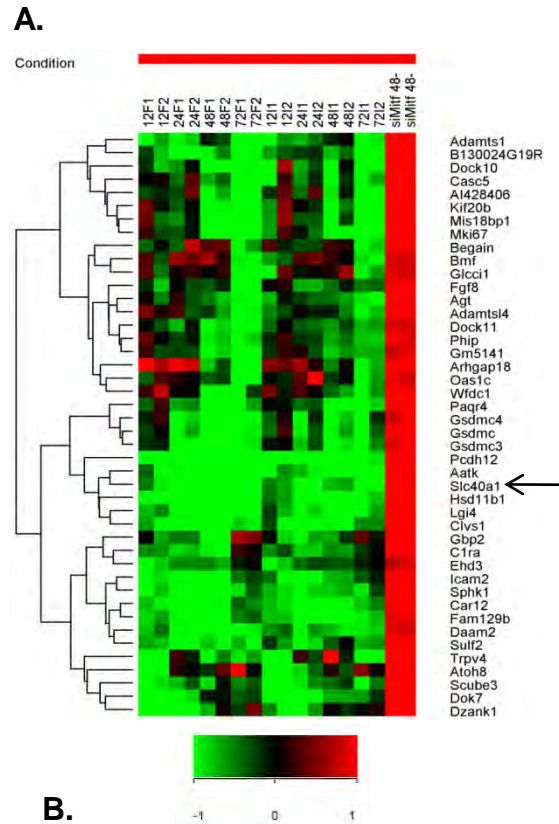
Fig.IV.10. Meta-analysis indicates the role of MITF is regulating iron homeostasis during melanogenesis. (A) B16 cells were transfection with 100nM of *Mitf* siRNA in DMEM media. After 48h of post-transfection RNA isolation was done and the samples were hybridized to Agilent mouse microarray slides. (Section.II.22). The heat map shows the expression of *Slc40a1* down-regulated during hyper-pigmentation to be up-regulated when *Mitf* was silenced. **(B)** The analysis of melanogenic genes and *Slc40a1* transcript abundance in B16 mouse melanoma following *Mitf* silencing was assessed by real-time qPCR at 48h. The bar graph plotted shows the expression values in fold change normalized with respect to mock. The expression of *Tyr* was found to be significantly downregulated whereas, that of *Slc40a1* to be ~7-fold upregulated at 48h during *Mitf* silencing. Data are displayed as mean ± S.E. of biological duplicate measurements (*, $p < 0.05$)

Fig.IV.11. Meta-analysis to identify genes that are regulated by MITF.

The overlap of DE genes from si*Mitf* data with MITF overexpression Hoek et al., 2008 microarray data. (**A)** Venn diagram representing the overlap between 118 (yellow circle) DE genes and 1048 (Blue circle) DE genes from Hoek et al.,2008 and siMitf microarray data. 22 genes were found to be direct Mitf target when the comparison was done between genes undergoing significant upregulation on transfection of SK-MEL-28 with a MITF expressing vector and gene downregulated in B16 cells following *Mitf* silencing. **(B)** Gene ontology of the 22 transcripts was performed using DAVID (http://david.abcc.ncifcrf.gov/). The percentage, *p*-value, and ontology, or pathway terms for each class are indicated**.** The majority of genes (p-value <0.0001 and <0.05) among them were found to be involved in pigmentation (*Edrnb*, *Tyr*, *Mreg*, *Cited1*, *Rab27a*), melanocyte differentiation (*Edrnb*, *Mreg*, *Cited1*, *Rab27a*), melanin biosynthetic process (*Slc45A2*, *Tyr*, *Cited1*) cGMP-mediated signaling (*Slc45A2*, *Edrnb*, *Mreg*) melanosome transport (*Mreg* and *Rab27a*) and regulation of pH (*Edrnb* and *Car14)*.

A.

Genes from Hoek's database

DE genes up in si*Mitf*

89
(3.5%)

7
(0.3%)

1423
(55.4%)

0
(0%)

22
(0.9%)

0
(0%)

1026
(40%)

DE genes down in si*Mitf*

B.

**Gene Ontology
22 Down-regulated genes**

p-value

Category	p-value
Pigmentation	<0.0001
Melanocyte differentiation	<0.0001
Response to lipopolysaccharide	<0.05
Developmental pigmentation	<0.0001
Melanin biosynthetic process	<0.0001
Response to cAMP	<0.05
Tumor necrosis factor	<0.05
Regulation of pH	<0.05
Vasodilation	<0.05
Melanosome transport	<0.05
Macrophage chemotaxis	<0.05
Anagen	<0.05
cGMP-mediated signaling	<0.05

0   5   10   15   20   25

A.

Strub_Hoek data
1482

111

siMitf_down
937

B.

**Gene Ontology
111 Down-regulated genes**

Category	Value
Transport	~17
Negative regulation of apoptotic process	~8
Transmembrane transport	~7
Ion transport	~6
Endocytosis	~4.5
Pigmentation	~4.5
Ossification	~3.5
Negative regulation of inflammation	~3.5
Cell redox homeostasis	~3.5

(axis: 0.0 5.0 10.0 15.0 20.0)

Fig.IV.13. David analysis of 111 genes downregulated upon Mitf silencing and found to be occupied by MITF. (A) Venn diagram representing the overlap between Strub et al.2011 (ChIP seq: 5578), and Hoek et al.2008, (6937 genes) and si*Mitf* (1048 down) datasets to identify genes directly up-regulated by MITF expression. The total common 1593 genes were then used to compare the list of genes down-regulated during si*Mitf*. **(B)** Gene ontology of the 111 transcripts downregulated was performed using DAVID (http://david.abcc.ncifcrf.gov/). The percentage, *P*-value, and ontology, or pathway terms for each class are indicated. The majority of genes (p-value <0.001) among them downregulated on *Mitf* silencing were found to be involved in transport (*Hps3*, *Rab27a*, *Slc24a5*, *Abcb6*, *Tpnc1*, *Trpm1*), endocytosis (*Sort1*, *Tom1*), pigmentation (*Edrnb*, *Tyr*, *Mlph*).

Gene Ontology
137 Down-regulated genes

C.

- Metabolic pathways
- Lysosome
- Insulin resistance
- Pathways in cancer
- Rap1 signaling pathway
- Progesterone-mediated oocyte maturation

Fig.IV.14. BRG1 regulates the dynamics of MITF occupancy to the set of regulatory elements.(A-C) Venn diagram shows the genes commonly regulated by both BRG1 and MITF. From the 213 DE genes commonly downregulated on *Mitf* and BRG1 silencing. 137 were predicted to be bound by BRG1. These genes were associated with the GO terms such as metabolic pathways, lysosome, Rap1 signaling, etc. (p<0.05). **(B)** Venn diagram shows the gene upregulated in *Mitf* and BRG1 silencing and genes that are bound by BRG1. (Laurette et al.,2015)

A.

213 DE down on siMitf and shBRG1   **BRG1 bound, down**

76
(3.8%)

137
(6.9%)

1762
(89.2%)

B.

107 DE up on siMitf and shBRG1   **BRG1 bound, Up**

59
(5.7%)

48
(4.7%)

923
(89.6%)
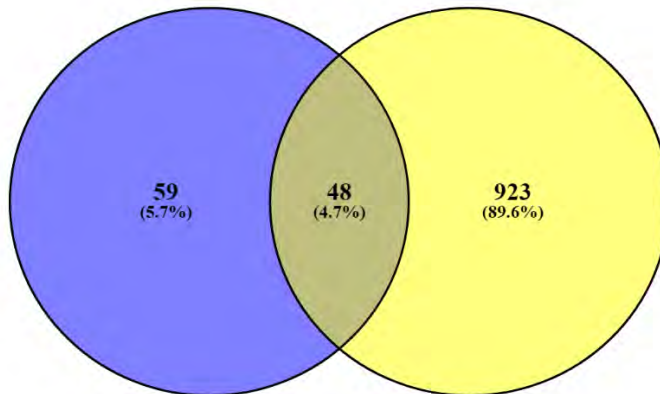
Fig.IV.1. Genome-wide Transcriptome Analysis to Identify Genes Involved in Melanogenesis. Experimental set up for time-course microarray analysis. Actively growing B16 cells were seeded in DMEM medium and 24h later, the cultures were treated with 20μM Fsk, 60μM IBMX or DMSO as a control. About ~1.5-2.0x10^6 cells were harvested at 12h, 24h, 48h and 72h time points in Trizol reagent and total RNA isolated. **(A)** Microarray analysis of global mRNA levels upon Fsk and IBMX treatments at the indicated time points. The heat map shows two-dimensional hierarchical clustering of 1620 differentially expressed genes obtained from two-way ANOVA analysis of normalized microarray data. The Red and Green colors represent Up-regulated (clusters I1-I7) and down-regulated (clusters R1-R5) genes respectively. The color scale ranges from log$_2$ +1.0 to -1.0. **(B)** Genes commonly upregulated (log$_2$ ratio ≥0.585) or down-regulated (≤ -0.585) in both forskolin- and IBMX-treated cells in at least one-time point were identified using BioVenn software. **(C)** The genes differentially expressed upon Fsk, and IBMX treatments were subjected to DAVID analysis to identify biological processes enriched in a statistically significant manner (p-value <0.01).

A.

I1 (87 genes)

I2 (164 genes)

I3 (221 genes)

I4 (16 genes)

I5 (40genes)

R1 (212 genes)

R2 (98genes)

I6 (61genes)

R3 (351 genes)

R4 (50genes)

R5 (94genes)

I7 (226genes)

FORSKOLIN   IBMX
12h 24h 48h 72h   12h 24h 48h 72h

B.

Fsk Up   Fsk Dn
51%   54%

253   233

260   269

41   59

IBMX Up   IBMX Dn
86%   82%

C.

Cell cycle
Mitotic nuclear division
Cell division
Cellular response to DNA damage stimulus
Positive regulation of apoptotic process
Negative regulation of apoptotic process
negative regulation of transcription from RNA
regulation of cell proliferation
apoptotic process
positive regulation of gene expression
Positive regulation of cell proliferation
inflammatory response

0.0   2.0   4.0   6.0   8.0   10.0   12.0   14.0   16.0

Percentage of
Total Up-regulated or Down-regulated genes

I=Induced

R=Repressed

Fig.IV.12. MITF might act as a repressor at the promoters of some genes. Venn diagram representing the overlap between MITF-occupied genes from Strub et al., 2011 (ChIP seq: 2862), and si*Mitf* (1430 up and 1048 down) datasets to identify genes whose expression are regulated by MITF. 123 from up- and 156 genes from down-regulated category were intersected with Strub et al., 2011 MITF-occupied genes. Gene ontology of these transcripts was performed using DAVID (http://david.abcc.ncifcrf.gov/). The percentage, *p*-value, and ontology, or pathway terms for each class are indicated**.** The majority of genes downregulated (p-value <0.0001 and <0.05) were found to be involved in transport (*Slc45a2, Rab5a,Insig1)*, cellular homeostasis (*Slc24a5, Trpm1,Abcb6),* pigmentation (*Edrnb*, *Tyr*, *Mreg*, *Cited1*, *Rab27a*), cholesterol biosynthetic (*Srebf1*, *Sc5d*, *insig1*). The genes upregulated were associated with regulation of apoptosis (*Serpine1*, *Ddit3*) angiogenesis (*Nr4a1*, *Rnf213*, *Klf4*), nervous system development (*Id1*, *Mapk3*), cell differentiation (*Cdkn1a*, *Gadd45b).*

MITF occupied genes
2583

123

156

siMitf_up
1307

siMitf_down
892

- Regulation of apoptotic process
- Angiogenesis
- Nervous system development
- Regulation of DNA binding
- Regulation of cell differentiation

- Establishment of localization
- Cellular homeostasis
- Pigmentation
- Intracellular transport
- Cholesterol biosynthetic process
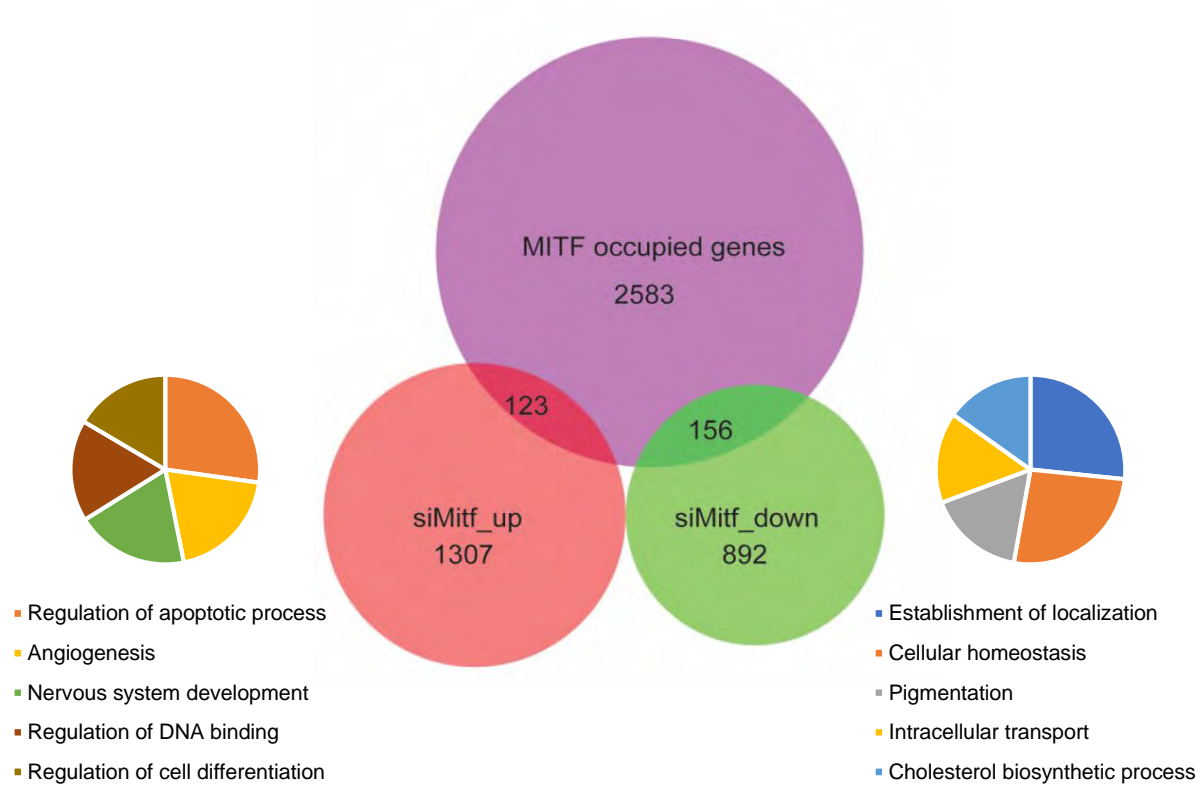
Fig.V.1. Media dependent perturbation of pigmentation in B16 cells. (A) The B16 cells were cultured in DMEM/F12 and DMEM media for 48h. The phase contrast images of B16 cells were captured using Nikon Ti-S at the magnification of 10x. The cells showed variable phenotype when grown in two media conditions. The DMEM/F12 cultured cells were bipolar whereas, DMEM cultured cells were hyper dendritic in nature. **(B)** After 48h of post culturing cells were trypsinized and harvested. After hemocytometer counting, ~1.0×10^6 cells were taken to record the cell pellet color. **(C)** The effect of two media conditions was observed on tyrosinase protein level. For Western blot, whole cell lysates were prepared as before, and ~20µg of total protein from the extracts were run on 10% SDS-PAGE, blotted to PVDF and the blot was probed with murine α-Tyrosinase antibody (70KDa, 1:10,000; anti-PEP7, gift from Vincent Hearing NCI, NIH). As loading control, the blot was also probed with murine anti-β-actin antibody (42KDa, 1:50,000). **(D)** The pigmentation status of B16 cells were shown to be effected by the composition of media. There were 25 elements that were exclusively present in DMEM/F12 and 9 elements present only in DMEM media. The known hypo-pigmenting compound, linoleic acid was one of the constituents of in DMEM/F12 media.

A.
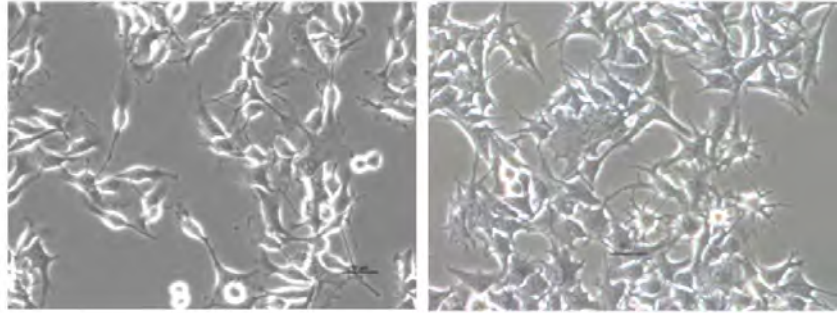
DMEM/F12   DMEM

B.

48h

DMEM/F12   DMEM

C.

	DMEM				F12	LA			
	12h	24h	48h	72h	48h	12h	24h	48h	72h

α-TYR (70kD)

β-Actin (42kD)

D.

DMEM/F12   DMEM

25
(44.6%)

22
(39.3%)

9
(16.1%)
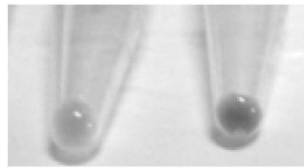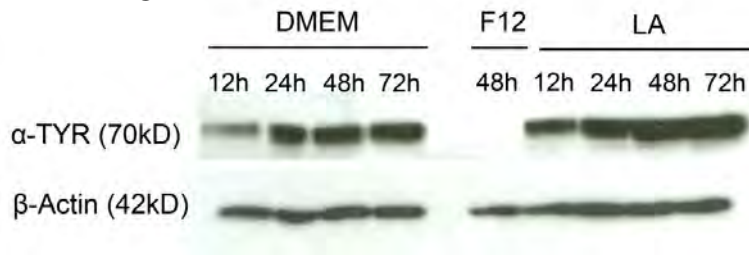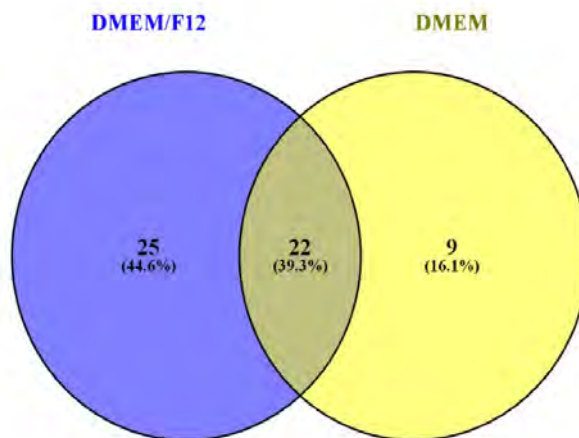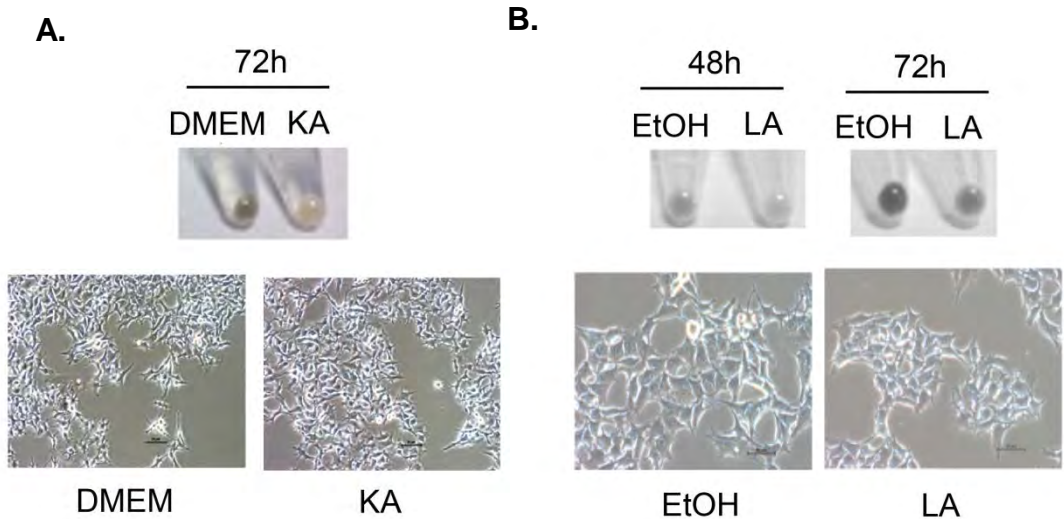
Fig.V.2. kojic acid (KA) and linoleic acid (LA) mediated hypopigmentation in B16 cells. (**A-B**) B16 cells were grown in DMEM medium, and after 24h of adherence, the cultures were treated with 2.5mM kojic acid and 75µM linoleic acid. For kojic acid, DMEM and linoleic acid, ethanol were taken as control. The pellet colour and morphology of B16 cells were recorded at different time points. The change in pellet colour wrt to control was significant at 72h for kojic acid and 48h for linoleic acid. The time points were pellet color differences was significant between the control and treated samples the phase contrast images of B16 cells were captured using Nikon Ti-S at the magnification of 40x. The scale bar indicates 50µm.

A.

B.

C.

D.
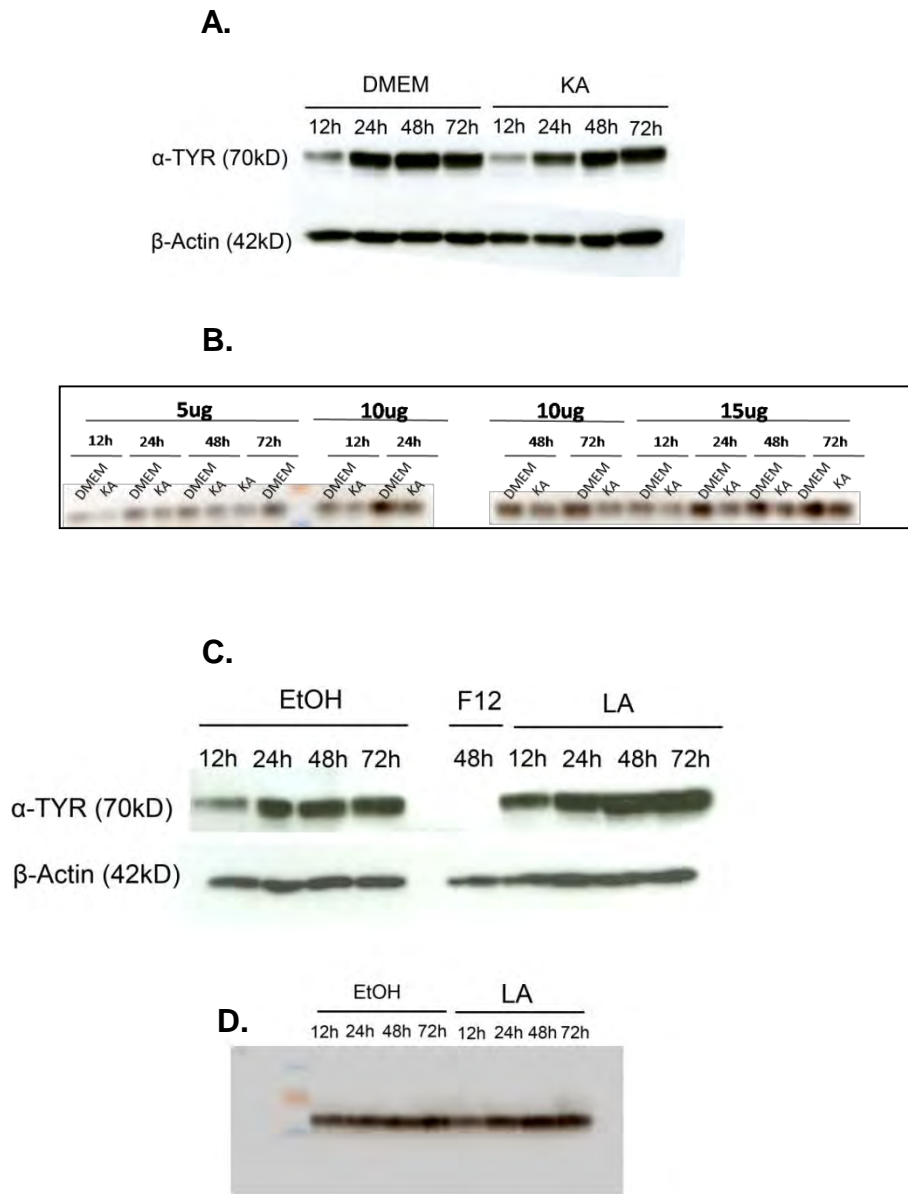
Fig.V.3. Effect of the hypo-pigmenting compound on tyrosinase protein and activity. (**A-B**) To study the effect of kojic acid (**C-D**) linoleic acid on the tyrosinase protein and activity western blotting and in-gel DOPA assay was performed. For Western blot, whole cell lysates were prepared as before, and ~20µg of total protein from the extracts were run on 10% SDS-PAGE, blotted to PVDF, and the blot was probed with a murine α-Tyrosinase antibody (70KDa, 1:10,000; anti-PEP7, a gift from Vincent Hearing NCI, NIH). As for loading control, the blot was also probed with a murine anti-β-actin antibody (42KDa, 1:50,000).For DOPA assay cell lysates was prepared, without SDS and b-ME were run without heating on a 10% SDS-PAGE for in-gel DOPA assay. For DOPA assay, the gel was incubated with 10mM of DOPA. The intensity of the chromogenic band is indicative of the tyrosinase activity.

24h Forsk treatment and 48hrs tretament with other componds

48h

Forsk F12 DMEM EtOH KA LA (25µm) LA (75µm) HQ
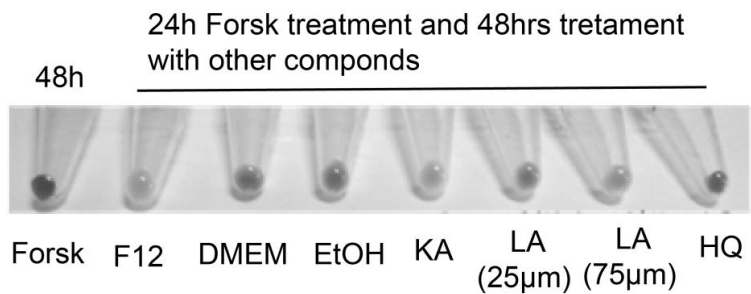
Fig.V.4. KA and LA were able to repress the forskolin induced hyper-pigmentation. The B16 cells were cultured in DMEM media for 24h. After 24h of overnight adherence forskolin (20 µM), known hyper-pigmenting compound, was added in the culture media and incubated for 24h. After 24h of forskolin induction, cells were washed and in the fresh DMEM media compounds treatment was done for 48h. The cells were trypsinized and harvested after 48h of compound treatment. After hemocytometer counting ~1.0×10^6 cells were taken to record the cell pellet color. Forskolin: 20µM, KA: 2.5mM, LA (25µM and 75µM).

A.

B.
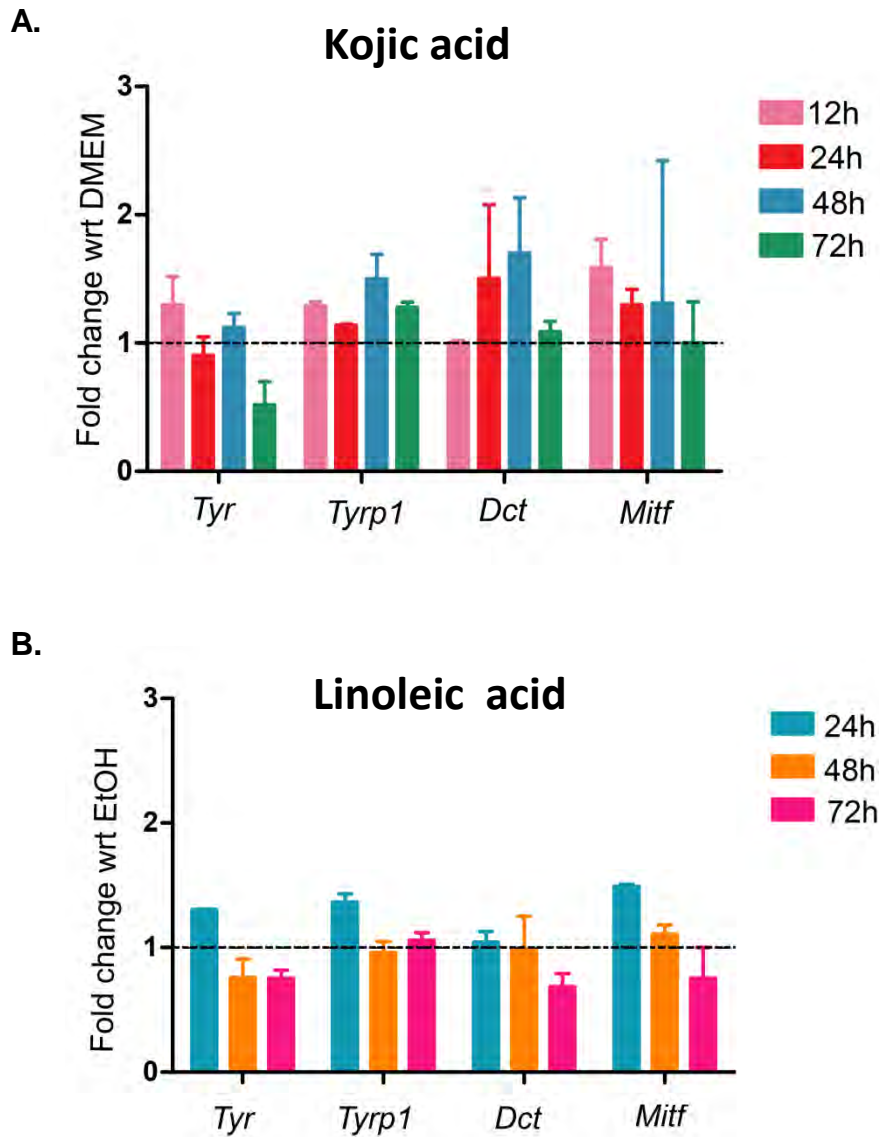
Fig.V.5. The effect of hypo pigmenting compounds on the expression of melanogenic genes. The time course analysis of melanogenic genes transcript abundance in B16 melanoma cells following KA and LA treatment as assessed by real-time qPCR. The bar graph plotted shows the expression values in fold change normalized concerning DMEM for KA and EtOH for LA versus the various melanogenic genes at different time points. **(A)-(B)** shows expression levels of *Tyr, Tyrp1, Dct* and *Mitf* transcript levels in B16 cells treated with 2.5mM of KA and 75µM LA.

A.

B.

48hCK1 [SO_3185]

Overall Results for sample 9 : 48hCK1

RNA Area:	139.5
RNA Concentration:	248 ng/μl
rRNA Ratio [28s / 18s]:	1.6
RNA Integrity Number (RIN):	9.8 (B.02.08)
Result Flagging Color:	
Result Flagging Label:	RIN: 9.80

Fragment table for sample 9 : 48hCK1

Name	Start Time [s]	End Time [s]	Area	% of total Area
18S	41.02	43.08	32.6	23.3
28S	46.23	49.42	51.1	36.6

C.

D.

48h EtOH 1 [SO_3185_Set 2]

Overall Results for sample 11 : 48h EtOH 1

RNA Area:	376.8
RNA Concentration:	326 ng/μl
rRNA Ratio [28s / 18s]:	1.9
RNA Integrity Number (RIN):	10 (B.02.08)
Result Flagging Color:	
Result Flagging Label:	RIN:10

Fragment table for sample 11 : 48h EtOH 1

Name	Start Size [nt]	End Size [nt]	Area	% of total Area
18S	1,739	2,200	87.6	23.3
28S	3,209	4,175	169.6	45.0

Fig. V.6. Quality check of RNA samples using electrophoresis and Bioanalyzer.
(A-B) The integrity of RNA isolated from B16 cells was check on 0.8% agarose gel by performing electrophoresis. The RNA isolation was done in duplicates. **(B-D)** Total RNA from the samples was run on a bioanalyzer chip (Agilent 2100) and gives a profile of the integrity of RNA. RIN number is calculated using an algorithm that quantifies the RNA degradation. The optimum RIN number is 10. Representative samples are shown in the figure for DMEM (CK1) and EtOH (EtOH1) at 48h time point show all the RIN numbers having the value of 10. The sharp 18s and 28s peaks further show intact RNA preparation. The gel representation of the chip on the right panel shows intact low molecular weight bands.

A.

449 Up-regulated genes
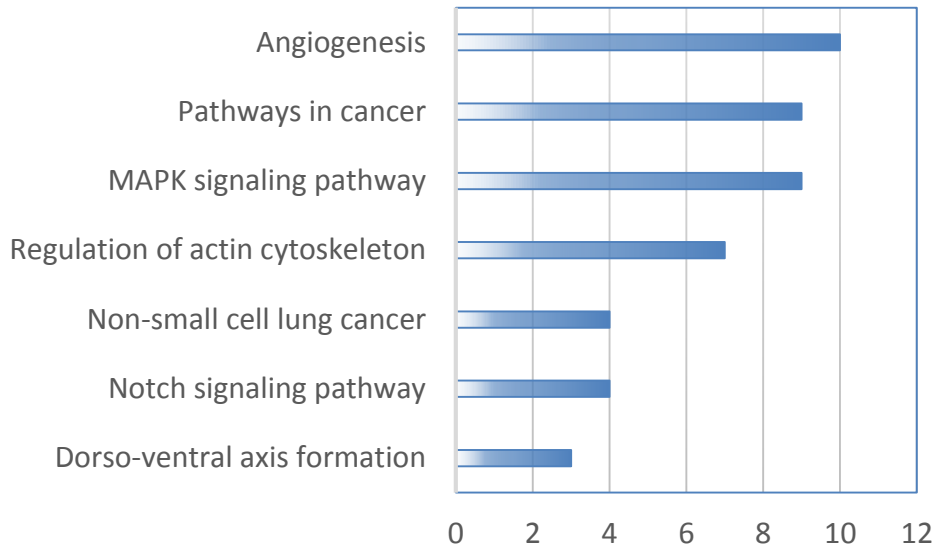
B.

426 Down-regulated genes
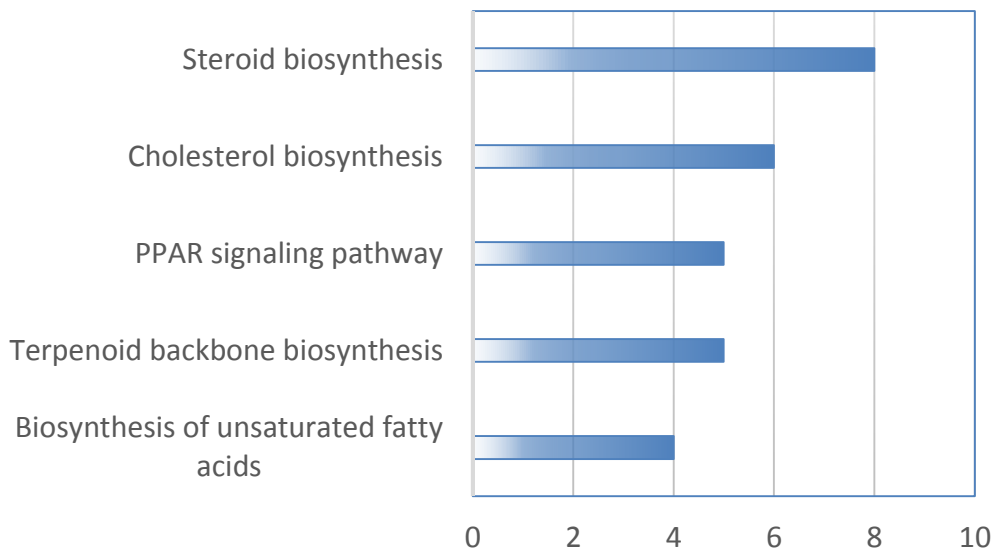
Fig.V.8. Linoleic acid alters the cholesterol homeostasis in B16 cells during hypopigmentation. Pathway analysis of the transcripts up-regulated and down-regulated during LA mediated hypo-pigmentation was performed using DAVID (http://david.abcc.ncifcrf.gov/). The percentage, *P*-value, and ontology, or pathway terms for each class are indicated**.** We found distinct categories of genes involved in several pathways to be enriched in upregulated and downregulated cluster.

A.
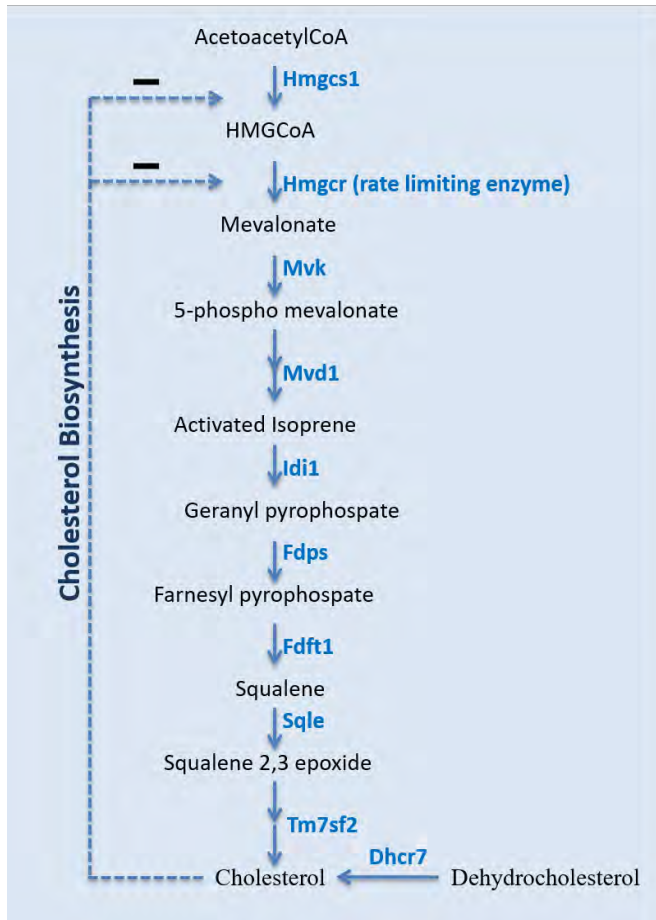
B.
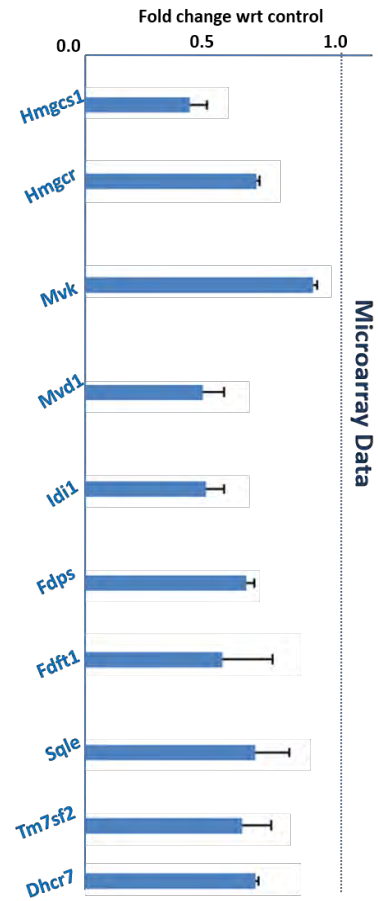
Fig.V.9. The cholesterol biosynthetic genes were found to be downregulated during linoleic acid-induced hypopigmentation in B16 cells. (A) The intracellular cholesterol level is regulated by a feedback mechanism that is operated both at transcriptional and post-transcriptional levels. Cholesterol biosynthesis involves majorly five steps. First the mevalonate is formed from acetyl CoA with the help of two enzymes, HMGCS1 and HMGCR (rate-limiting enzyme). Isoprenoid is formed from mevalonate and further 6 isoprenoid units condense to form squalene. Next through cyclization, squalene give rise to parent steroid lanosterol. Cholesterol is formed from lanosterol. The level of cholesterol are tightly controlled by feedback mechanism by regulating HMGCS1 and HMGCR. **(B)** The expression of genes involved in the process of cholesterol biosynthesis were found to down-regulated during linoleic acid-mediated hypopigmentation. Graph shows the fold change values for cholesterol biosynthetic genes obtained from single color microarray data.

Fig.V.10. The genes involved in the process of lipid synthesis was found to be downregulated during LA-mediated hypo-pigmentation. (A) Schematic shows the regulation of lipid synthesis in nonhepatic cells. The sterol regulatory element binding protein (SREBPs) TF are membrane-bound and when cleaved enters the nucleus to activates genes involved in synthesis and uptake of cholesterol and fatty acid. They bind to the SRE in the promoter region of HMGCoAR gene. SREBPs are escorted by SCAP (SRREP cleavage-activating protein) from ER to Golgi (site of Golgi). Insig1 are involved in regulating the cholesterol biosynthesis by binding to SCAP. It as a result SCAP/SREBP complex stay longer in the ER and thus SCAPs are prohibited from carrying the activated SREB to Golgi. **(B)** Table shows the expression of genes involved in cholesterol biosynthesis. The expression values (log2) are derived from LA microarray data.

A.
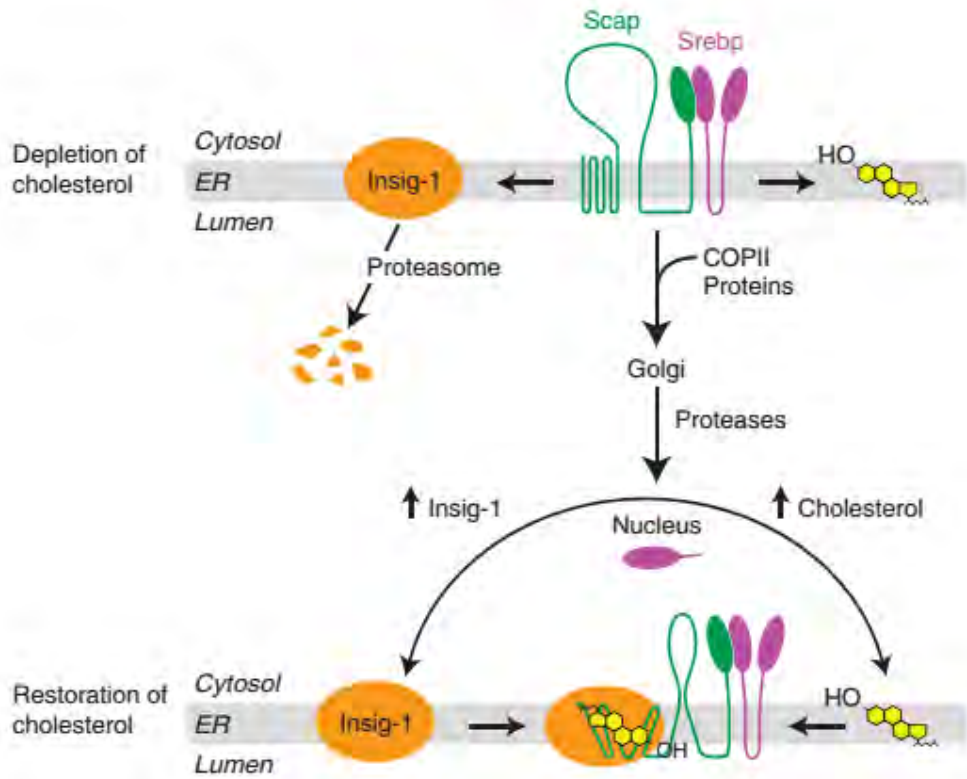
B.

Gene Name	Fold_48h LA 1	Fold_48h LA 2
Insig1	-2.44	-2.36
Srebf1	-0.17	-0.65
Srebf2	-0.48	-0.62
Scap	0.18	0.02

Gene Name	Fold_SiMi 1	Fold_SiMi 2
Insig1	-1.39	-1.52
Insig2	-1.09	-0.78
Srebf1	-0.73	-0.91
Srebf2	-0.79	-1.05
Scap	-0.62	-0.47

Fig.V.11. The expression analysis of genes involved in melanin and cholesterol synthesis genes during LA mediated hypopigmentation B16 cells. (A) Network representation of cholesterol biosynthetic genes from STRING database version 10.0 using evidence type selected for analysis were experimentally determined (Pink lines), co-expression (Black lines), and protein homology(blue lines). **(B)** The microarray validation of cholesterol biosynthetic genes from the samples were B16 cells first induced first with forskolin for 24 and then further treatment was done with LA or EtOH as a control for 48h. The expression of *Hmgcs1*, *Hmgcr*, *Tm7sf2*, *Dhcr7* and *Nsdhl* gene expression was found to be down-regulated during LA mediated hypopigmentation. **(C)** B16 cells were first induced with forskolin for 24h, and then further treatment was done with LA or EtOH as a control for 48h. Real-time qPCR assessed the analysis of melanogenic genes such as Tyr, Tyrp1, Dct and Mitf transcript level at 48h of LA treatment The bar graph plotted shows the expression values in fold change normalized with respect to EtOH. Data are displayed as mean ± S.E. of biological duplicate measurements (*, $p < 0.05$; **, $p < 0.01$; Student's *t*-test).

A.

B.

C.

EtOH   Linoleic acid

48h
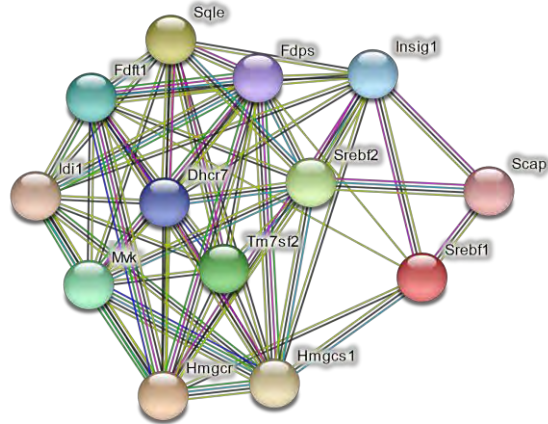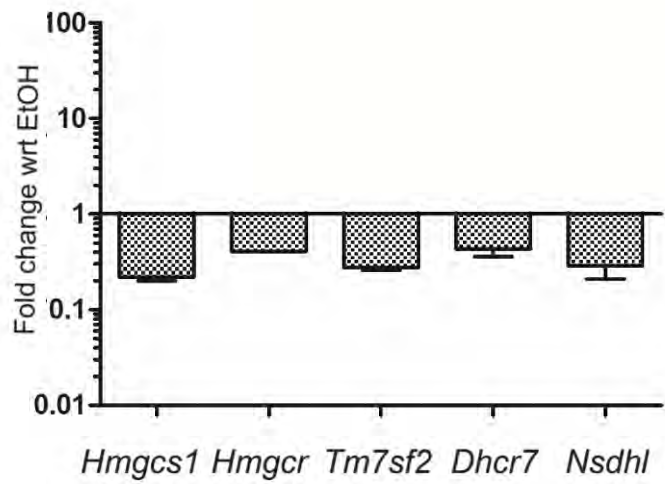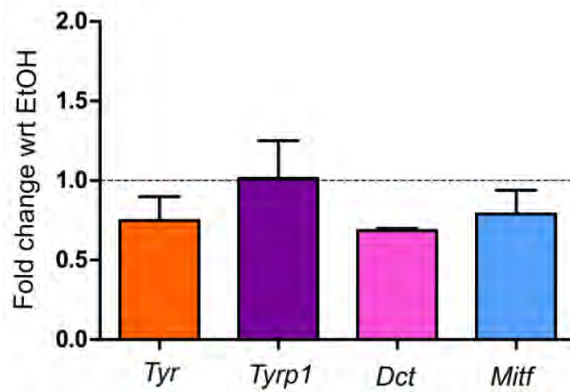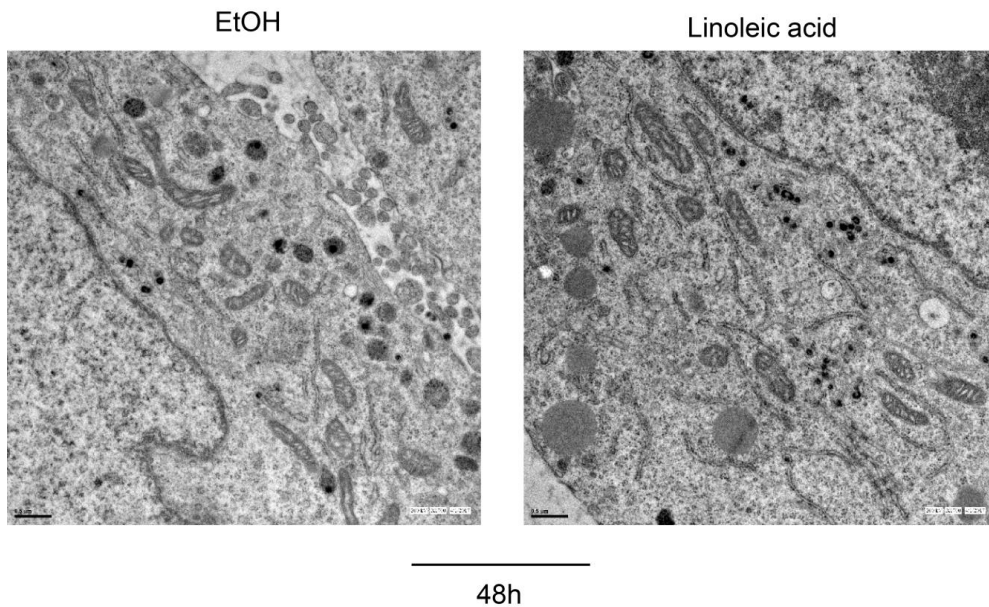
Fig. V.12. Linoleic acid inhibits the formation of melanosome in mouse B16 cells. B16 cells seeded at the density of 0.25x10⁶ cells /T-75 cultured flask and incubated for 24h in the conventional incubator. After overnight adherence cells were treated with LA or EtOH as a control for 48h. After 48h post-treatment cells were harvested, fixed and embedded. Ultrathin sections were cut, stained and imaged in a transmission electron microscope at a magnification of 1700x. The scale bar indicates 1.0μm
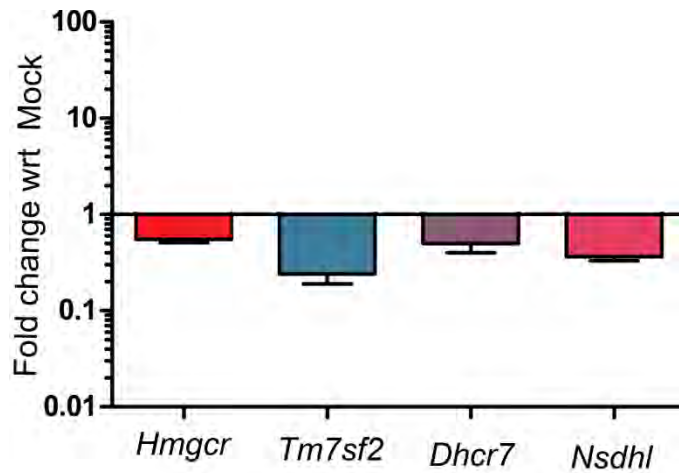
Fig.V.13. The expression of cholesterol biosynthetic genes was found to be downregulated upon *Mitf* silencing. Real-time qPCR assessed the analysis of cholesterol biosynthesis transcript level in B16 cells at 48h of *Mitf* knockdown. The bar graph plotted shows the expression values in fold change normalized with respect to Mock. The expression of *Hmgcr*, *Tm7sf2*, *Dhcr7* and *Nsdhl* gene expression was found to be down-regulated during Mitf knockdown. Data are displayed as mean ± S.E. of biological duplicate measurements. (*, $p < 0.05$; **, $p < 0.01$; Student's *t*-test).
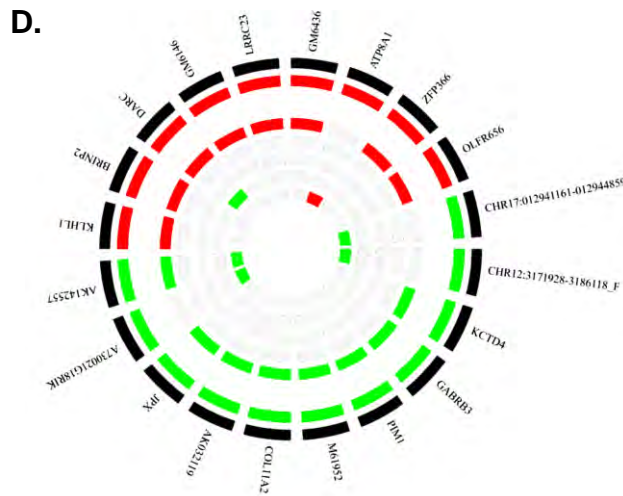
Fig.V.14. **Skin-centric analysis of kojic acid microarray data using eSKIN software (A computational platform for skin research). (A)** KA data was overlaid in eSKIN software to know the nature of the compound and pathway enriched. For analysis 1.5 fold was used. The total of 123 genes from 48h time point was matched with the data available in eSKIN. **(B)** The graph shows the proportion of upregulated, downregulated and unaffected genes across the experimental conditions. **(C)** The skin-associated pathway enrichment analysis was done. Cytoskeletal modification was enriched in KA-induced hypopigmentation. **(D)** The nature of the compound was predicted using eSKIN skin predict. Interestingly we found a close correlation (correlation coefficient:1) between KA data with the signatures already present in eSKIN for hypo-pigmentation. In the circos plot signature present in KA data are shown at the periphery of the circle, and sub tracks show their expression in different cell lines. (Hypo-pigmentation-MC-2,MC-1,MC-3,MC-5,MC-4)

A.

User Input Data Details	
Filename	KA_48_1.5.csv
# genes in the data	123
# genes matching to Skin-Base	7
# experimental conditions	2

Analysis parameters	
Upregulated cutoff	0.585
Downregulated cutoff	-0.585
# genes in organism's genome	25000
Genes considered for analysis	All Genes

B.
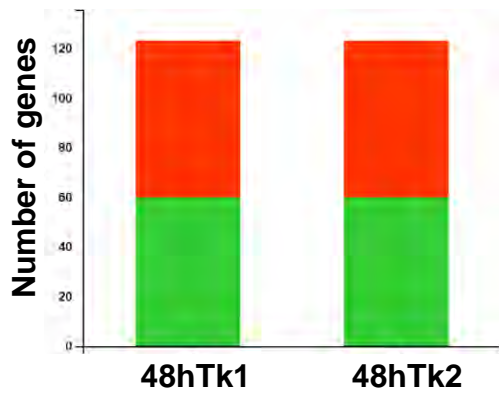
C.
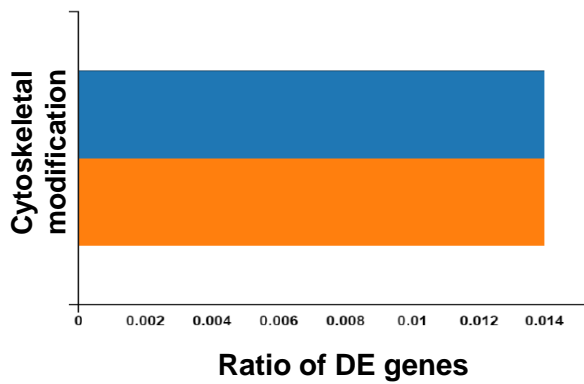
D.
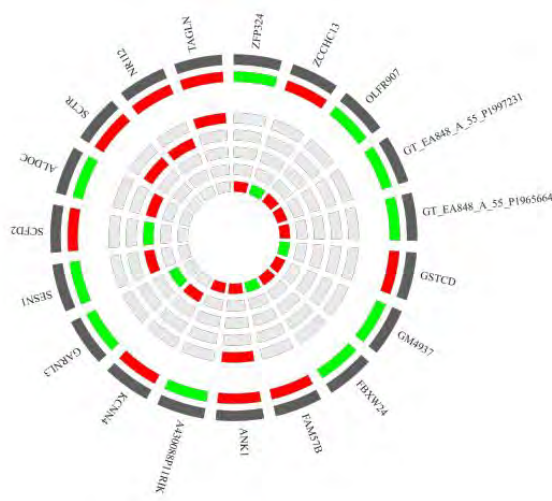
Phenotype	Correlation Coefficient	Distance
Hypopigmentation-MC-2	1.000	0
Hypopigmentation-MC-1	-0.810	6.325
Hypopigmentation-MC-3	-1.000	3.464
Hypopigmentation-MC-5	NA	0
Hypopigmentation-MC-4	NA	0

Fig.V.15. Skin-centric analysis of linoleic acid microarray data using eSKIN software (A computational platform for skin research). (A) LA data was overlaid in eSKIN software to know the nature of the compound and pathway enriched. For analysis 1.5 fold cut off was applied. The total of 977 genes matched with the data available in eSKIN. **(B)** The graph shows the proportion of upregulated, downregulated and unaffected genes across the experimental conditions. **(C)** The skin-associated pathway enrichment analysis was done. We found 5 out of 35 associated skin pathways to be enriched during LA-induced hypopigmentation. **(D)** The nature of the compound was predicted using eSKIN skin predict. Interestingly we found close correlation (correlation coefficient:1) between LA data with the signatures already present in eSKIN for hypo-pigmentation. In the circos plot signature present in LA data are shown at the periphery of the circle and subtracks show their expression in different cell lines. (Hypo-pigmentation-MC-2,MC-1,MC-3,MC-5,MC-4)

A.

User Input Data Details	
Filename	LA_48_1.5.csv
# genes in the data	977
# genes matching to Skin-Base	50
# experimental conditions	2

Analysis parameters	
Upregulated cutoff	0.585
Downregulated cutoff	-0.585
# genes in organism's genome	25000
Genes considered for analysis	All Genes

B.
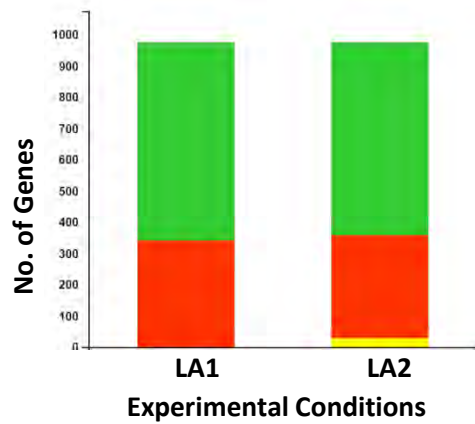
C.
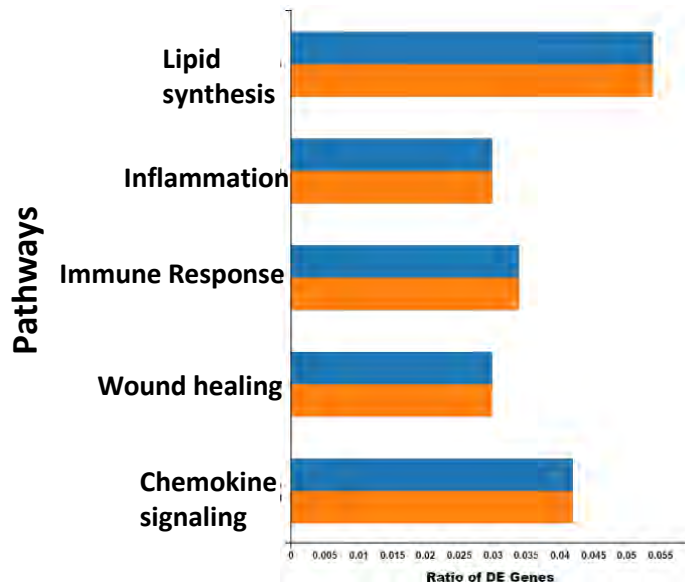
Fig. V.7. kojic acid treatment leads to inhibition of melanosome maturation in B16 cells. (A) B16 cells seeded at the density of 0.25x10^6 cells /T-75 cultured flask and incubated for 24h in the conventional incubator. After overnight adherence cells were treated with 2.5mM KA or DMEM as a control for 48h. After 48h post-treatment cells were harvested, fixed and embedded. Ultrathin sections were cut, stained and imaged in a transmission electron microscope at a magnification of 1700x. The scale bar indicates 1.0µm. **(B)** The bar graph shows the distribution of melanosome at different stages (I, II, III and IV) in KA and DMEM samples. These stages are categorized based on melanin content. The melanosome was counted, and percentage of melanosome were plotted for each stage. Data are displayed as mean ± S.E. of three cells from each condition (*, $p < 0.05$; **, $p < 0.01$; Student's t-test).

A.

DMEM

Kojic acid

B.

No. of melanosmes (%)

Stage I
Stage II
Stage III
Stage IV
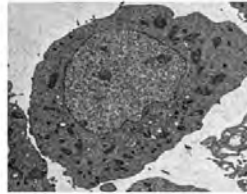
DMEM   Kojic acid
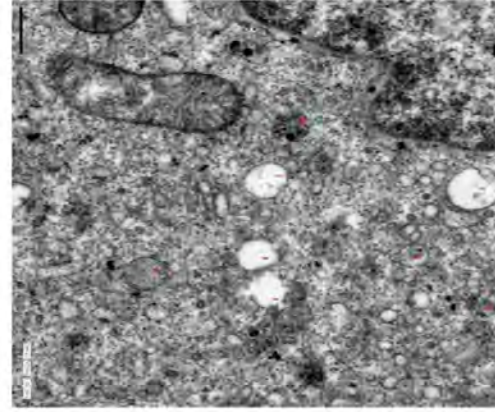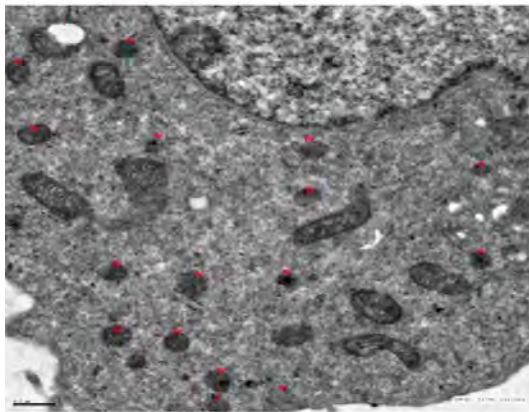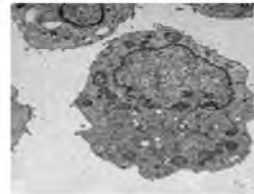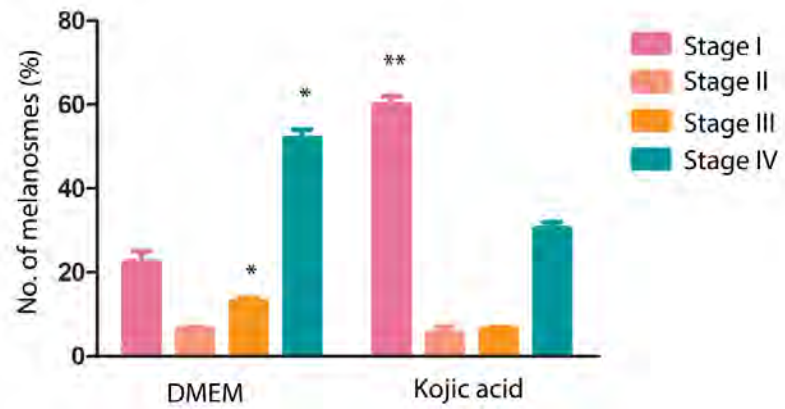
PUBLICATIONS

❑ Natarajan, V.T., Ganju, P., Singh, A., Vijayan, V., Kirty, K., Yadav, S., Puntambekar, S., Bajaj, S., Dani, P.P., Kar, H.K*., et al.* (2014). IFN-gamma signaling maintains skin pigmentation homeostasis through regulation of melanosome maturation. Proc Natl Acad Sci U S A *111*, 2301-2306.

❑ Kirty, K., Yadav, S., Shukla, M., Natarajan, V.T., Gadgil, C., Gokhale, R., Natarajan, K., (2018). Transcriptional Regulatory Networks Involved in Melanogenesis Uncovered by Chemo-genomic Profiling. (In preparation)

❑ Yadav, S., Kirty, K., Natarajan, K., (2018). Multifaceted Regulation of melanogenesis in B16-F10 cells by iron homeostasis. (In preparation)

IFN-γ signaling maintains skin pigmentation homeostasis through regulation of melanosome maturation

Vivek T. Natarajan[a,1], Parul Ganju[b,1], Archana Singh[a,b], Vinaya Vijayan[c], Kritika Kirty[d], Shalini Yadav[d], Shraddha Puntambekar[c,e], Sonali Bajaj[f], Prachi P. Dani[b], Hemanta K. Kar[f], Chetan J. Gadgil[a,c,e], Krishnamurthy Natarajan[d], Rajni Rani[b], and Rajesh S. Gokhale[a,b,g,2]

[a]Council for Scientific and Industrial Research - Institute of Genomics and Integrative Biology, Delhi 110007, India; [b]National Institute of Immunology, New Delhi 110067, India; [c]Chemical Engineering Division, Council for Scientific and Industrial Research - National Chemical Laboratory, Pune, Maharashtra 411008, India; [d]School of Life Sciences, Jawaharlal Nehru University, New Delhi 110067, India; [e]Academy of Scientific and Innovative Research, New Delhi 110001, India; [f]Department of Dermatology, Post Graduate Institute of Medical Education and Research, Dr. Ram Manohar Lohia Hospital, New Delhi 110001, India; and [g]Jawaharlal Nehru Centre for Advanced Scientific Research, Bangalore, Karnataka 560064, India

Cellular homeostasis is an outcome of complex interacting processes with nonlinear feedbacks that can span distinct spatial and temporal dimensions. Skin tanning is one such dynamic response that maintains genome integrity of epidermal cells. Although pathways underlying hyperpigmentation cascade are recognized, negative feedback regulatory loops that can dampen the activated melanogenesis process are not completely understood. In this study, we delineate a regulatory role of IFN-γ in skin pigmentation biology. We show that IFN-γ signaling impedes maturation of the key organelle melanosome by concerted regulation of several pigmentation genes. Withdrawal of IFN-γ signal spontaneously restores normal cellular programming. This effect in melanocytes is mediated by IFN regulatory factor-1 and is not dependent on the central regulator microphthalmia-associated transcription factor. Chronic IFN-γ signaling shows a clear hypopigmentation phenotype in both mouse and human skin. Interestingly, IFN-γ KO mice display a delayed recovery response to restore basal state of epidermal pigmentation after UV-induced tanning. Together, our studies delineate a new spatiotemporal role of the IFN-γ signaling network in skin pigmentation homeostasis, which could have implications in various cutaneous depigmentary and malignant disorders.

interferon | melanin | gene regulation | detanning

In response to external stimuli, biological systems exhibit a variety of complex behaviors attributed to interplay between signaling, metabolic, and regulatory pathways that function over a broad range of timescales. Coordinated functionality of these events is critical in maintaining physiological homeostasis (1). Epidermal pigmentation represents one such central mechanism operative in the body's largest organ, skin, that protects the genome from external damage (2, 3). Pigmentation is an outcome of the interplay between two epidermal cell types: melanocytes and keratinocytes. Several paracrine and autocrine factors are known to regulate this intricate process (4). Although immune cells recruited to the skin protect this organ from various infections, it is not clear whether these cells could also influence skin pigmentation (5).

Melanocytes produce melanin sequestered within a lysosome-related organelle (LRO) called melanosome. The process of pigmentation involves concerted biogenesis, maturation, and transfer of melanosomes to keratinocytes (6, 7). During the irreversible melanosome maturation process, several proteins support formation of core melanosome assembly, and the organelle is progressively filled with melanin polymer. Pmel17/gp100 is among the early structural proteins recruited to the melanosome. Tyrosinase (Tyr), dopachrome tautomerase (Dct), and Tyr-related protein-1 (Tyrp1) are the core enzymes involved in melanin synthesis (8, 9). Microphthalmia-associated transcription factor

(MITF) is suggested to be the master regulator that governs melanocyte development, melanogenesis, and survival (10). The MITF promoter is further regulated by other transcription factors through an array of intrinsic regulators derived from fibroblasts, as well as endocrine, neural, and inflammatory factors (11, 12). The dynamic regulatory aspects of pigmentation have been difficult to establish in physiological models because of the inherent intricacies of dissecting complex interactions along with the fragility of this complex trait (13). To identify regulatory networks underlying melanogenesis, we designed a pigmentation oscillator that can reveal simple negative feedback loops.

Based on mechanistic, physiological, and pathophysiological studies, we show that IFN-γ signaling plays an important role in fine tuning the melanosome maturation process. This effect is mediated through the classical IFN-γ pathway by IFN regulatory factor-1 (IRF1). Interestingly, withdrawal of IFN-γ rapidly restores cellular programming, indicating a crucial role for this inflammatory cytokine in melanocyte biology.

Significance

Skin tanning is a protective response of epidermal cells involving increased melanin formation. Overexposure to sun can cause sunburn and even skin cancer, and such conditions are partly attributable to the accumulation of toxic side products of melanin and its intermediates. In this study, we reveal the importance of key immune cytokine IFN-γ in pigmentation biology by studying cultured human melanocyte cells as well as mice and human disease models. We show that IFN-γ signaling regulates enzymes involved in melanin biosynthesis through a transcription factor IFN regulatory factor-1. Our study identifies a new mechanism of skin pigmentation homeostasis and proposes that strength and durability of local skin immune response may be decisive factors to delineate outcome between skin tanning and cancer.

Results

Design of a Pigmentation–Depigmentation Oscillator. Several studies highlight the essential requirement of negative feedback loops in sustaining rhythmic oscillations (14). Mathematical analysis of periodic information derived from such oscillators provides a robust unbiased approach to delineate regulatory cascades underlying biological processes. We decided to exploit the known unstable melanotic behavior of B16 cells to develop an oscillatory model of pigmentation and depigmentation (15). Passaging of pigmented B16 cells obtained from the tumor grown in C57BL/6 mice results in progressive loss of visible pigmentation in vitro [passage 1 (P1) to P4] (Fig. S1A); s.c. injection of depigmented P4 cells in mice generated dark-colored tumors. By using a stable tumor cell line expressing GFP (TNV2), we confirmed the P4 origin of the tumor cells in vivo (Fig. S1B), thus showing that depigmented cells (P4) possess capability to repigment under the favorable conditions. While exploring several conditions, we identified that low-density (LD) plating (10^2 cells/cm^2) results in reproducible pigmentation in the absence of any extraneous factor (Fig. S2A). Visual pigmentation could be observed over several days during the time course study, and the process of pigmentation could be reversed by replating these cells at higher cell density (10^4 cells/cm^2) in fresh medium. Cellular phenotype could also be confirmed by quantitative melanin estimation (Fig. S2B). One complete cycle of pigmentation and depigmentation could be completed in 20 days, and we confirmed this oscillatory process for several cycles (Fig. 1A).

Periodogram Analysis Reveals Dominant IFN-γ Signature. To identify regulatory features underlying the oscillations, we performed transcriptional analysis over two consecutive pigmentation–depigmentation cycles. The comparison between two microarray datasets showed good correlation ($R^2 = 0.84$). Many genes associated with melanin synthesis and melanosome maturation showed periodic changes (Fig. S3). The plot between normalized gene expression changes and time for all regulated genes showed a complex pattern (Fig. 1B, *Left*). Pigmentation genes showed similar slope with peak at day 8; however, the downward trend exhibited differential decay rates (Fig. 1C, *Left*). Fourier transform (FT) analyses of the high-throughput data provided a means to identify periodicity in gene regulation. Periodogram analysis sorted out gene profiles with a 20-d period (dominant frequency = 1/20 d^{-1}) (Fig. 1B, *Right*). For every profile, we checked the contribution of the frequency = 1/20 d^{-1} component by evaluating the ratio of the FT coefficient corresponding to this frequency to the sum of all FT coefficients. The enriched genes consist of a set of profiles where this ratio is greater than 70%.

Of all trajectories that were inversely associated with pigmentation, surprisingly, 40% of the down-regulated genes were associated with IFN-γ signaling (Fig. 1C, *Right* and Table S1). This observation prompted us to speculate that IFN-γ could possibly be one of the negative factors responsible for mediating depigmentation in the B16 oscillator model. Earlier studies had indicated a hypopigmentating effect for IFN-γ. Analyses of culture supernatant as well cellular mRNA did not detect IFN-γ during the entire pigmentation–depigmentation cycle (*SI Text*). However, the addition of a physiologically relevant low dose of IFN-γ (100 U/mL) to both B16 cells and primary human melanocytes suppressed pigmentation. Whereas depigmentation was complete in the B16 model, substantial hypopigmentation could be reproducibly achieved in foreskin-derived primary melanocyte cells from diverse individuals within 4–5 d (Fig. 1D and Fig. S4).
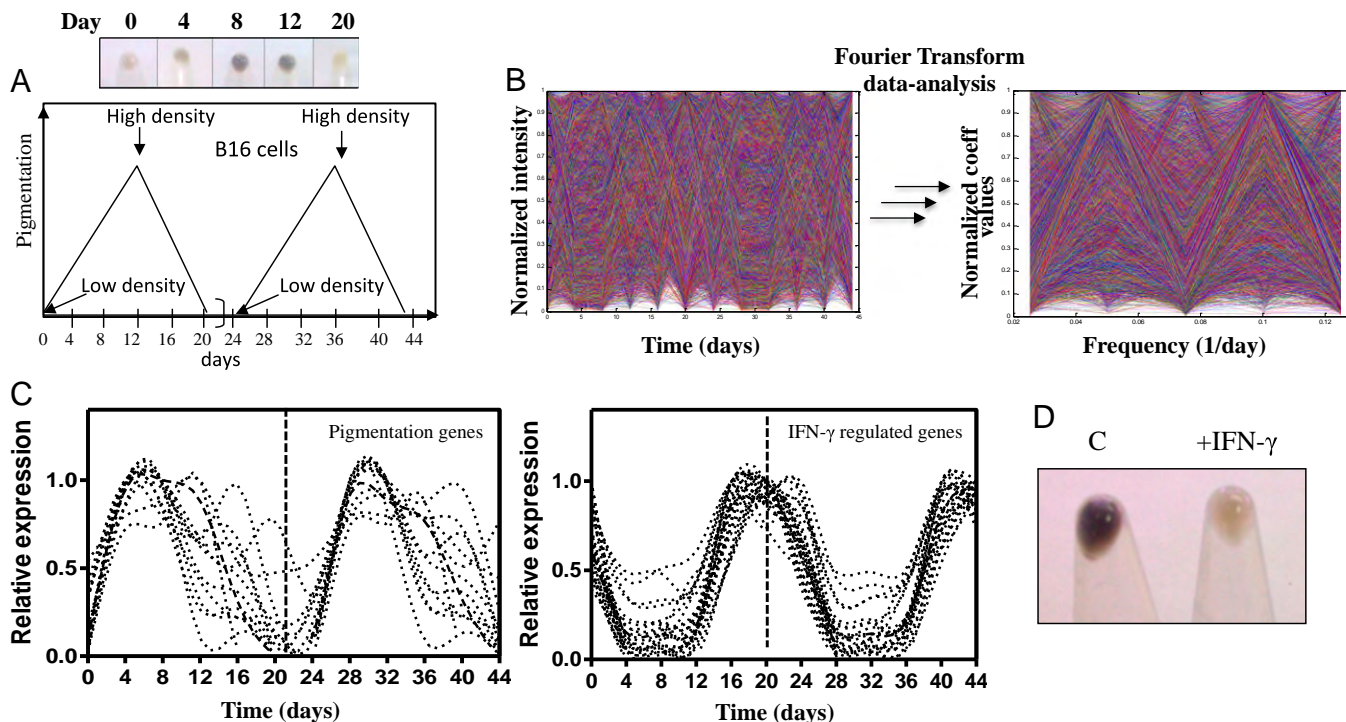
Fig. 1. Analysis of the pigmentation oscillator reveals a dominant IFN-γ signature in depigmented cells. (*A*) Schematic representation of the in vitro biological oscillator showing two cycles of pigmentation and depigmentation of cultured cells at different densities (arrows indicate the time of plating). (*Upper*) Cell pellets of B16 cells on different days for cycle 1. (*B*, *Left*) Time-dependent changes in the relative expression of all genes in the oscillator model. (*B*, *Right*) Normalized coefficient value obtained by FT analysis of all genes as a function of their respective frequencies. (*C*, *Left*) Relative expression level of known pigmentation genes through two cycles of pigmentation and depigmentation. (*C*, *Right*) Relative expression level of known IFN-γ–regulated genes identified by FT analysis across the two cycles. (*D*) Cell pellets of control (C) and IFN-γ–treated B16 cells at day 12.

Fig. 2. IFN-γ signaling mediates hypopigmentation of primary human melanocytes by arresting melanosome maturation. (*A*, *Upper*) Cell pellets of control and IFN-γ–treated primary human epidermal melanocytes after 7 d of treatment. (*A*, *Lower*) Fold change in gene expression levels of IFN-γ–treated melanocyte cultures expressed as mean fold change ± SEM across three independent cultures. (*B*) Western blot analysis of DCT, TYR, and MITF proteins after IFN-γ treatment as a function of time. C, control. (*C*) TEM images of (*Left*) control and (*Right*) IFN-γ–treated melanocytes. (*D*) Corresponding confocal images of melanocytes treated with IFN-γ stained with HMB45 (green). (Scale bar: *C*, 2 μm; *D*, 10 μm.)

IFN-γ Causes Cellular Hypopigmentation by Arresting Melanosome Maturation. Because IFN-γ is known to have pleiotropic effect on various cell types (16), we decided to perform global transcriptional analysis to delineate the mechanism behind the hypopigmenting effect of IFN-γ on cultured primary human melanocytes. Microarray data analysis showed classical IFN-γ signatures with up-regulation of *MHC* genes and *PSMB8, PSMB9* immunoproteasome subunits. Both the IFN-γ receptor subunits (*IFN-γRI* and *IFN-γRII*) also showed substantial up-regulation. Of the pigmentation genes, *DCT* showed a drastic decrease of around 80%. Similar observations were also reported during the course of another study (17, 18). *TYRP1* and *TYR* were decreased to a lesser extent across different primary cultures treated with IFN-γ (Fig. 2*A*). Time course of Western blot analysis revealed a temporal decrease in the levels of TYR and DCT proteins after IFN-γ treatment (Fig. 2*B*). Interestingly, whereas the effect of IFN-γ on melanogenic proteins was evident as early as day 1 of treatment, the

visible phenotypic changes were slow and occurred over a period of 4–5 d.

Rapid decrease in the level of key melanosomal proteins is expected to have an impact on overall maturation of melanosomes. Microarray analysis of the oscillatory model indeed showed a downward trend for the genes involved in melanosome biogenesis and maturation (Fig. S3). Ultrastructural studies with transmission electron microscopy (TEM) confirmed drastic decrease in the number of darkly pigmented stage III and IV melanosomes in IFN-γ–treated cells (Fig. 2*C*). These cells instead accumulated electron-lucent LROs characteristic of early stage I and II melanosomes. Confocal microscopy with melanosome-specific HMB45 antibody showed comparable numbers of melanosomal structures in control and IFN-γ–treated cells (Fig. 2*D*). Cellular investigations, thus, suggest that IFN-γ treatment arrests melanosomes early in the process of maturation by decreasing flux of proteins being trafficked to early melanosomes.

Fig. 3. IFN-γ signaling mediates reversible hypopigmentation of melanocytes independent of MITF. (*A*) Experimental setup for studying reversibility of IFN-γ effect on melanocytes. Cell pellet of primary human melanocytes treated with IFN-γ for 7 d; the cells were allowed to recover for 5 d (day 12) by the removal of IFN-γ. Western blot analysis of DCT, TYR, and MITF proteins of untreated and IFN-γ–treated cells (day 7) and day 12 untreated and recovered cells. C, control; I, IFN. (*B*) Cell pellets of melanocytes. The levels of proteins by Western blot analysis and Tyr activity determined by an in-gel L-dopa assay of cells treated with 600 nM α-MSH and 100 μM isobutyl methyl xanthine (IBMX) for 5 d in the presence and absence of IFN-γ are shown. (*C*) *Dct* promoter (3.7 kb) activity in the presence of 600 nM α-MSH and 100 U/mL IFN-γ (alone or combined) as measured by dual luciferase assay. RLU, relative light units. (*D*) Promoter activity of a 3.7-kb WT *Dct* promoter and M-Box–deleted construct in the presence of α-MSH and IFN-γ. ***$P < 0.001$; ns, not significant.

Hypopigmentation Mediated by IFN-γ Is Reversible and Independent of MITF. To examine whether IFN-γ–mediated hypopigmentation of melanocytes could be reversed, treated cells were replated in fresh medium (Fig. 3A, scheme). Removal of IFN-γ reinitiated the pigmentation process and distinct recovery, as evident from the cell pellets and levels of the melanogenesis proteins, was observed (Fig. 3A). Concomitant with repigmentation, an increased number of mature melanosomes could be visualized by TEM (Fig. S5). These observations reveal that IFN-γ–induced changes in melanogenesis are completely reversible and that normal cellular programming is reinstated on withdrawal of this cytokine. The IFN-γ concentration used (100 units/mL) showed no apparent changes in cell number and viability. Examination of different phases of the cell cycle by FACS analysis also showed no significant differences (Fig. S6A).

Western blot studies showed that MITF protein levels did not change significantly during the hypopigmentation–repigmentation cycle (Figs. 2B and 3A). These data were surprising, since almost all known melanogenesis regulatory pathways converge to MITF. We investigated whether the known downstream MITF target genes were expressed on treatment of melanocytes with IFN-γ (19). More than 80% of the known genes showed expression in the transcriptome data, indicating that MITF is present in the functional form (Fig. S6B). Addition of known MITF-activating factors, such as α-melanocyte stimulating hormone (α-MSH) and isobutyl methyl xanthine (IBMX), to melanocytes could not prevail over IFN-γ–induced hypopigmentation (including reduction in TYR and DCT levels) (Fig. 3B). Because DCT is one of the important biosynthetic proteins in melanin synthesis and showed robust transcriptional regulation by IFN-γ, additional studies were carried out with *Dct* gene to understand the mechanism of MITF-independent hypopigmentation effect.

We cloned 3.7 kb of mouse *Dct* promoter upstream of firefly luciferase reporter and transfected it with Renilla luciferase plasmid on day 3 in the B16 LD model cells (20). The ratio of firefly to Renilla luciferase units measured on day 5 provided an estimate of *Dct* promoter activity. Competition assay between α-MSH and IFN-γ showed clear suppression of *Dct* promoter activity (Fig. 3C). Importantly, deletion of the MITF binding site (M-Box) in *Dct* promoter construct still showed IFN-γ–mediated repression, whereas M-Box deletion, as expected, led to reduction in α-MSH–stimulated *Dct* expression (Fig. 3D), indicating the noninvolvement of MITF in the repression of *Dct* expression. Together, our studies establish an MITF-independent mechanism for IFN-γ in melanocyte hypopigmentation.

IRF1-Mediated Transcriptional Regulation. IFN-γ mediates its effect through canonical and noncanonical signaling routes (21). Microarray analysis showed elevation of transcriptional signatures for the canonical pathway (*IFNGR-I, IFNGR-II, JAK-1,* and *STAT-1*). This activation could also be seen by the increased phosphorylation status of STAT-1 protein (Fig. S7A). siRNA-mediated silencing of *JAK-1* and *STAT-1* rescued the suppression of *DCT* expression by IFN-γ in primary human melanocytes (Fig. 4A and Fig. S7B). The IRF family of transcription factors is among the key downstream effector molecules of IFN-γ signaling (22). Microarray data revealed significant up-regulation of *IRF1, IRF3, IRF7,* and *IRF9* in melanocytes (Fig. S7C). We used siRNA-mediated silencing to investigate the requirement of relevant pathway. Of the four factors, *IRF1* suppression could rescue *DCT* expression in IFN-γ–treated cells, indicating the significance of this signaling arm in mediating hypopigmentation (Fig. 4A and Fig. S7B). Overexpression of Irf1 during the LD phase of B16 cells (day 3) replicated transcriptional regulation observed on IFN-γ treatment, including the suppression of *Dct* (Fig. 4B). We then probed whether Irf1 could directly bind the *Dct* promoter. The avidin-immobilized 3.7-kb biotinylated promoter could specifically pull down Irf1 (Fig. 4C). *Dct* promoter activity

could be repressed by overexpression of Irf1 in a dose-dependent manner (Fig. 4D). To identify the Irf1-responsive sites in *Dct* promoter, we performed systematic deletions to generate 2.1-kb, 1.8-kb, 1.6-kb, and 900-bp *Dct* reporter cassettes. Bioinformatic analysis using the PROMO transcription factor binding site predicted the presence of 13 putative Irf1 binding sites in the 3.7-kb fragment (23) (Fig. S8A). Although Irf1 binding activity could be observed for 2.1-, 1.8-, and 1.6-kb fragments in luciferase assays, the smaller 900-bp fragment showed no binding to Irf1 (Fig. 4E and Fig. S8B). Our data show that Irf1 is the crucial factor through which IFN-γ mediates its hypopigmentation effects.

Relevance of IFN-γ on Physiological and Pathological Hypopigmentation. Earlier studies on skin pigmentation dynamics had indicated a complex outcome of ultraviolet B radiation (UVB) on skin (24). Multiple cytokines secreted by infiltrating immune cells complicate the dissection of individual contributions. The physiological role of IFN-γ in altering the dynamic changes was examined in the mouse model by comparing C57BL/6 IFN-γ null (*IFNG*$^{-/-}$) mice with the corresponding littermate controls (*IFNG*$^{+/+}$). Careful observation of ear and tail regions, where epidermal melanocytes are present, showed small but significant differences (Fig. 5A). Quantitative differences could be established by mexameter across several experiments. Assessment of Dct and Tyr protein levels from the epidermal lysate revealed higher levels of Dct in IFN-γ KO animals, whereas no change was observed for Tyr levels (Fig. 5B). The difference in the two strains could be clearly noted by irradiating these mice with UVB, a stimuli that has been shown to enhance localized IFN-γ secretion by recruiting immune cells to skin (5). Although the WT mice regained basal pigmentation levels by day 11 post-UVB exposure, KO mice showed a hyperpigmentation phenotype (Fig. 5C). The sustained tanning response in the absence of IFN-γ, together with our in vitro studies, suggests a crucial role of this cytokine in dampening UVB-activated melanogenic cascade. Because UV radiation induces powerful changes to the immune landscape, the involvement of other factors cannot be ruled out. However, such modulations are likely to intersect with the IFN-γ signaling network.

In humans, tuberculoid leprosy patients are known to have a dominant Th1 response, whereas the lepromatous form shows a Th2 cytokine predominance (25). Interestingly, tuberculoid leprosy patients are also known to possess hypopigmented patches on their skin. Our analysis of skin samples from leprosy patients showed a strong IFN-γ signature in the visibly hypopigmented lesions compared with matched unaffected skin (Fig. 5D). No apparent pigmentation changes were seen in patients in whom IFN-γ signatures were not observed. However, other clinical features, such as loss of sensation, were reported in these patients. Skin sections from the hypopigmented lesions were positive for melanocytes as determined by S100 immunostaining (Fig. S9A). TEM studies showed reduced numbers of pigmented type III and IV melanosomes within melanocytes of hypopigmented lesions (Fig. S9 B and C). Our studies, thus, suggest that increased levels of IFN-γ may be a determinant of skin hypopigmentation in certain pathological conditions.

Discussion

Skin, with its own immune system and ability to induce pigmentation, provides an efficient barrier against external stressors. The hyperpigmentation response is crucial for maintaining genome integrity of epidermal cells (26). Secreted cytokines, such as IFN-γ, IL-1, and IL-4, provide protection from biological insults and are critical for tissue remodeling. In this study, we provide strong evidence for the physiological relevance of IFN-γ in skin pigmentation homeostasis. We show that IFN-γ signaling mediates its hypopigmenting effect through the transcription factor IRF1, which in turn, controls melanosome maturation in melanocytes. The MITF-independent mechanism
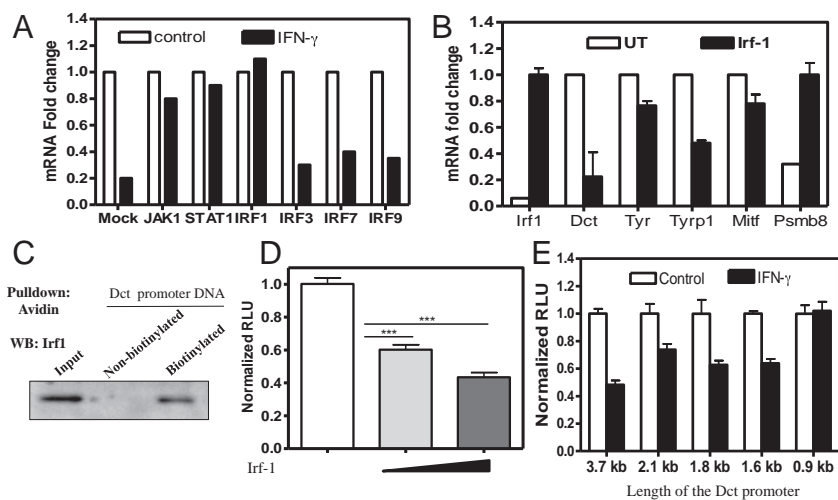
Fig. 4. Mechanism of Irf1-mediated down-regulation of *Dct*. (*A*) Levels of *DCT* mRNA as measured by real-time PCR in mock vs. *JAK-1, STAT-1, IRF1, IRF3, IRF7,* and *IRF9* siRNA-transfected melanocytes in the absence or presence of IFN-γ. (*B*) mRNA levels of transcripts in cells transfected with Irf1 expression construct compared with mock-transfected B16 cells. UT, untransfected. (*C*) Binding of Irf1 to biotinylated *Dct* promoter in avidin pull down from IFN-γ–treated B16 cell lysates was detected by Western blot (WB). (*D*) *Dct* promoter activity in the absence and presence of varying concentrations of Irf1 expression plasmid (*Dct*-luciferase: Irf1 plasmid DNA, 1:0, 1:0.5, and 1:1). Bars represent mean ± SD across replicates. ***$P < 0.001$. (*E*) Dual luciferase reporter assay carried out with several deletion constructs of Dct promoter in the presence and absence of IFN-γ. Bars represent mean ± SD across replicates.

of IRF1 regulation of melanin biosynthetic genes, thus, adds another dimension to the study of melanogenesis.

Although several factors are known to dynamically alter pigmentation of human skin, precise mechanisms that maintain basal state have been difficult to elucidate. We, therefore, developed a cell autonomous cyclical oscillator model of pigmentation and depigmentation that is known to sustain its oscillations through a feedback loop to identify negative regulatory pathways involved in melanogenesis. Unbiased genome-wide transcriptional profiling of this pigmentation oscillator revealed a dominant IFN-γ signature inversely correlated with pigmentation. Although addition of IFN-γ to depigmented B16 melanoma cells prevents cells from pigmentation in the LD state, cultured primary melanocytes show distinct hypopigmentation in 4–5 d of IFN-γ treatment. The density-dependent oscillator model does not function in primary melanocytes, because cell–cell contact is important for culturing these cells. Moreover, proliferation and melanogenesis are tightly coupled in primary cells through MITF (27). Effect of IFN-γ on melanogenic genes and proteins is, however, evident as early as day 1 of the treatment. The delay observed in hypopigmentation of melanocytes is because of the presence of preformed mature melanosomes, which get diluted on melanocyte proliferation and/

or secreted out of the cell. Although IFN-γ signatures were identified in the LD pigmentation oscillator model, at present, it is unclear which cognate ligand is involved in mediating density-dependent IFN-γ signaling. Similar instances of activated signaling without identification of factors have been noted in several earlier studies (28, 29).

IFN-γ is a common secreted cytokine in the skin; therefore, we wanted to explore whether the hypopigmentation mechanism is also operative in the physiological milieu. Interestingly, IFN-γ–overexpressing transgenic mice developed to study eczema have been reported to have a complete penetrance of hypopigmentation phenotype (30). Our studies with IFN-γ KO mice likewise show consistent differences in epidermal pigmentation. Furthermore, we show a clear association of increased IFN-γ signaling to a decreased number of stage III and IV melanosomes in the lesional skin of leprosy patients. Although other immune factors can also perturb skin pigmentation, the identification of a specific IRF1-mediated regulation of pigmentation genes provides confidence that IFN-γ must have a significant role in controlling melanosome maturation and thus, skin pigmentation. We show that chronic overexpression of IFN-γ in both mouse and human skin can result in hypopigmentation phenotype. On UV exposure, a clear delay in
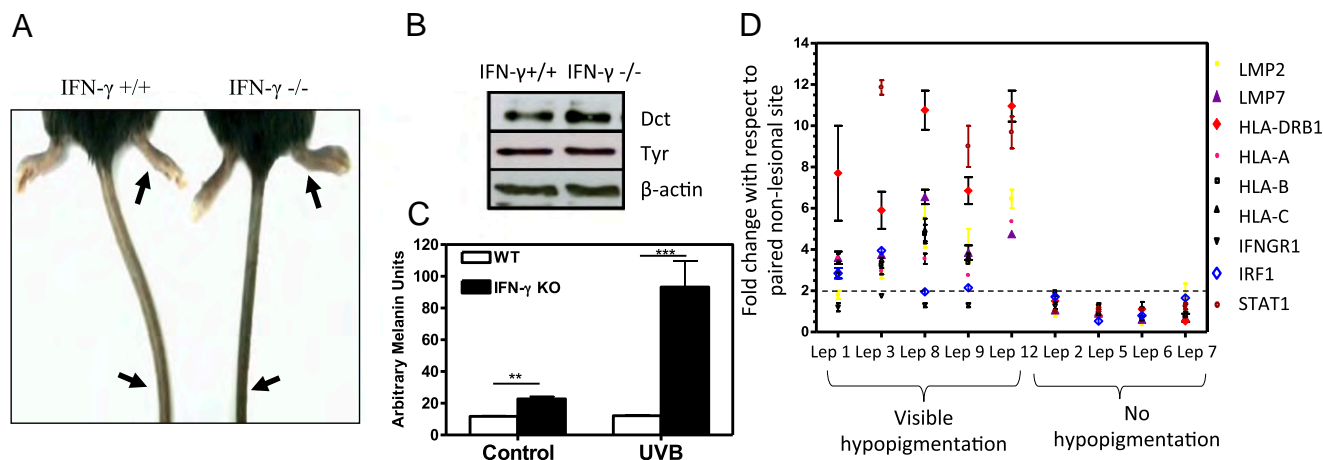
Fig. 5. Physiological and pathophysiological roles of IFN-γ in skin pigmentation. (*A*) Images of IFNG$^{+/+}$ and IFNG$^{-/-}$ mice in C57BL/6 background at 6 wk. Arrows indicate pigmentation at the sites where epidermal melanocytes are present. (*B*) Western blot analysis of Dct and Tyr proteins from the tail epidermis in IFNG$^{+/+}$ and IFNG$^{-/-}$ mice. (*C*) Image analysis for quantitating levels of pigmentation. Bar graphs indicate average ± SEM across 22 measurements across the two ear lobes. **$P < 0.005$; ***$P < 0.001$. (*D*) Comparative real-time PCR analysis for a panel of known IFN-γ–modulated genes in nonlesional vs. lesional epidermis of patients with different manifestations of leprosy (Lep). Dashed line represents a cutoff of twofold considered as significant for up-regulation.

regaining the basal pigmentation of skin can be observed for the IFN-γ KO mice. Recent studies have, indeed, shown that UV radiation of skin elicits a delayed recruitment of IFN-γ–secreting immune cells to the epidermis (5). Together, our studies support the conjecture that the strength, durability, and temporal response of IFN-γ response could be crucial factors for maintaining epidermal pigmentation homeostasis, and this mechanism may have important implications in the detanning of human skin.

Two of the crucial mediators of skin pigmentation, α-MSH and TGF-β, are known to be involved in the protective tanning response and maintenance of melanocytes in an immature state, respectively (27, 31). While α-MSH is secreted by adjacent keratinocytes in response to UV and TGF-β by follicular bulge area cells, the source of IFN-γ could be the immune cells recruited during inflammation or UV exposure. We, thus, propose an αβγ-cytokine regulatory model of melanogenesis, where all three cytokines act in a concerted manner to modulate melanocyte biology. It is likely that all these factors function in an interlinked manner to bring about the spatiotemporal regulation of human skin color. Future studies would dissect detailed pathways associated with IFN-γ–mediated hypopigmentation cross-talk in delicately balancing skin pigmentation and its implications in disease pathophysiology.

Methods

Culture of B16 Cells and Pigmentation Model Setup. B16 cells were maintained at subconfluence with 5% (vol/vol) CO_2 levels in DMEM supplemented with 10% FCS (Invitrogen). Clonal population was isolated by limited dilution, and B16 TNV1 (referred to as B16) was derived. The pigmentation oscillator was set up by plating ~100 cells/cm^2, and cells were harvested at days 4, 8, and 12. For depigmentation, cells were replated at 10,000 cells/cm^2 on day 12 and harvested after 4 and 8 d to complete the 20-d cycle. The second cycle was initiated from the depigmented cells obtained after a gap of 4 d to allow for all changes to stabilize.

Calculation of Correlation Coefficient for the Microarray Analysis. The time profiles for the two cycles were treated as replicate measurements and a linear least squares fit, and the regression coefficient (R^2) for that fit was calculated. Genes with very low expression (average expression score <100) were omitted from this analysis. Reported R^2 value (0.84) is, thus, based on the profiles for 10,937 genes.

Identification of Genes Associated with the Pigmentation–Depigmentation Cycle. Analyses of periodic data (32, 33) and time course microarray data (34) have been used to distinguish truly periodic genes from genes that show oscillatory behavior because of random effects. Identification of genes with frequency of 1/20 d^{-1} was performed using the Matlab function *fft* (an implementation of the fast FT). Genes for which the contribution corresponding to the frequency of 1/20 day^{-1} is more than 70% of the total contribution from all frequencies were selected. For every series of expression values at n time points for every gene i, the discrete FT values y_{ij} = fft (x_{i1}, x_{i2}, …, x_{in}) were calculated at various frequencies, including one $j = j'$ corresponding to a frequency of 1/20 d^{-1}. The criterion used for classifying a particular gene as correlated with the pigmentation–depigmentation cycle was $y_{ij}/\text{sum}_j(y_{ij}) > 0.7$.

Clinical Material. Human ethical review committee approved this study, and it is in agreement with Declaration of Helsinki principles. Skin punch biopsies (2.5 mm) from involved and normal regions from patients with hypopigmentation were obtained after informed consent. RNA isolation and downstream processing were performed as indicated earlier (35).

1. Blanpain C, Fuchs E (2009) Epidermal homeostasis: A balancing act of stem cells in the skin. *Nat Rev Mol Cell Biol* 10(3):207–217.
2. Miyamura Y, et al. (2007) Regulation of human skin pigmentation and responses to ultraviolet radiation. *Pigment Cell Res* 20(1):2–13.
3. Tadokoro T, et al. (2003) UV-induced DNA damage and melanin content in human skin differing in racial/ethnic origin. *FASEB J* 17(9):1177–1179.
4. Yamaguchi Y, Hearing VJ (2009) Physiological factors that regulate skin pigmentation. *Biofactors* 35(2):193–199.
5. Zaidi MR, et al. (2011) Interferon-γ links ultraviolet radiation to melanomagenesis in mice. *Nature* 469(7331):548–553.
6. Ando H, et al. (2012) Melanosomes are transferred from melanocytes to keratinocytes through the processes of packaging, release, uptake, and dispersion. *J Invest Dermatol* 132(4):1222–1229.
7. Raposo G, Marks MS (2007) Melanosomes—dark organelles enlighten endosomal membrane transport. *Nat Rev Mol Cell Biol* 8(10):786–797.
8. Lin JY, Fisher DE (2007) Melanocyte biology and skin pigmentation. *Nature* 445(7130):843–850.
9. Hearing VJ (2005) Biogenesis of pigment granules: A sensitive way to regulate melanocyte function. *J Dermatol Sci* 37(1):3–14.
10. Levy C, Fisher DE (2011) Dual roles of lineage restricted transcription factors: The case of MITF in melanocytes. *Transcription* 2(1):19–22.
11. Hou L, Pavan WJ (2008) Transcriptional and signaling regulation in neural crest stem cell-derived melanocyte development: Do all roads lead to Mitf? *Cell Res* 18(12):1163–1176.
12. Liu JJ, Fisher DE (2010) Lighting a path to pigmentation: Mechanisms of MITF induction by UV. *Pigment Cell Melanoma Res* 23(6):741–745.
13. Bennett DC, Lamoreux ML (2003) The color loci of mice—a genetic century. *Pigment Cell Res* 16(4):333–344.
14. Novák B, Tyson JJ (2008) Design principles of biochemical oscillators. *Nat Rev Mol Cell Biol* 9(12):981–991.
15. Bennett DC (1989) Mechanisms of differentiation in melanoma cells and melanocytes. *Environ Health Perspect* 80:49–59.
16. van Boxel-Dezaire AH, Stark GR (2007) Cell type-specific signaling in response to interferon-gamma. *Curr Top Microbiol Immunol* 316:119–154.
17. Choi H, et al. (2013) IL-4 inhibits the melanogenesis of normal human melanocytes through the JAK2-STAT6 signaling pathway. *J Invest Dermatol* 133(2):528–536.
18. Le Poole IC, et al. (2002) Interferon-gamma reduces melanosomal antigen expression and recognition of melanoma cells by cytotoxic T cells. *Am J Pathol* 160(2):521–528.
19. Hoek KS, et al. (2008) Novel MITF targets identified using a two-step DNA microarray strategy. *Pigment Cell Melanoma Res* 21(6):665–676.
20. Lang D, et al. (2005) Pax3 functions at a nodal point in melanocyte stem cell differentiation. *Nature* 433(7028):884–887.
21. Gough DJ, Levy DE, Johnstone RW, Clarke CJ (2008) IFNgamma signaling-does it mean JAK-STAT? *Cytokine Growth Factor Rev* 19(5–6):383–394.
22. Enesa K, et al. (2012) Pellino1 is required for interferon production by viral double-stranded RNA. *J Biol Chem* 287(41):34825–34835.
23. Messeguer X, et al. (2002) PROMO: Detection of known transcription regulatory elements using species-tailored searches. *Bioinformatics* 18(2):333–334.
24. Aoki H, Moro O (2005) Upregulation of the IFN-gamma-stimulated genes in the development of delayed pigmented spots on the dorsal skin of F1 mice of HR-1 x HR/De. *J Invest Dermatol* 124(5):1053–1061.
25. Modlin RL (1994) Th1-Th2 paradigm: Insights from leprosy. *J Invest Dermatol* 102(6):828–832.
26. Cui R, et al. (2007) Central role of p53 in the suntan response and pathologic hyperpigmentation. *Cell* 128(5):853–864.
27. Nishimura EK, et al. (2010) Key roles for transforming growth factor beta in melanocyte stem cell maintenance. *Cell Stem Cell* 6(2):130–140.
28. Subramaniam S, et al. (2013) Distinct transcriptional networks in quiescent myoblasts: A role for Wnt signaling in reversible vs. irreversible arrest. *PLoS One* 8(6):e65097.
29. Gao B (2012) Wnt regulation of planar cell polarity (PCP). *Curr Top Dev Biol* 101:263–295.
30. Carroll JM, Crompton T, Seery JP, Watt FM (1997) Transgenic mice expressing IFN-gamma in the epidermis have eczema, hair hypopigmentation, and hair loss. *J Invest Dermatol* 108(4):412–422.
31. Abdel-Malek Z, et al. (2000) The melanocortin-1 receptor is a key regulator of human cutaneous pigmentation. *Pigment Cell Res* 13(Suppl 8):156–162.
32. Wichert S, Fokianos K, Strimmer K (2004) Identifying periodically expressed transcripts in microarray time series data. *Bioinformatics* 20(1):5–20.
33. de Lichtenberg U, et al. (2005) Comparison of computational methods for the identification of cell cycle-regulated genes. *Bioinformatics* 21(7):1164–1171.
34. Vijayan V, Deshpande P, Gadgil C, Gadgil M (2013) Comparison of methods for identifying periodically varying genes. *Int J Bioinform Res Appl* 9(1):53–70.
35. Natarajan VT, et al. (2010) Transcriptional upregulation of Nrf2-dependent phase II detoxification genes in the involved epidermis of vitiligo vulgaris. *J Invest Dermatol* 130(12):2781–2789.

Supporting Information

Natarajan et al. 10.1073/pnas.1304988111

SI Methods

RNA Isolation and Microarray. Total RNA was isolated from B16 cells or whole epidermal cells from punch biopsies after separation of dermis using Dispase II as indicated earlier (1).Whole-genome microarray was carried out using Illumina WG-6 array, and preliminary data normalization and analysis carried out using Beadstudio software using manufacturer's instructions.

Western Blot Analysis, Immunochemical Method, and Microscopy. Rabbit α-hTRP2 antibody [against dopachrome tautomerase (DCT); 1:1,000; Abcam], mouse α–h-tyrosinase (1:500; Dako), rabbit α–h-pSTAT1(Y701) (1:1,000; Cell Signaling Technology), mouse α–h-microphthalmia-associated transcription factor (α-hMITF; C5 clone; gift from David E. Fisher, Massachusetts General Hospital, Boston), and HRP α-tubulin (1:2,000; Cell Signaling Technology) were used for Western blot analysis. For tracking melanosomes, melanocytes were grown in LabTek chamber coverglass, fixed, permeabilized, stained with HMB45 followed by secondary Alexa fluor 488, and counterstained with DAPI. The cells were imaged and analyzed with a Ziess LSM 510 Meta confocal microscope. For transmission EM studies, ultrathin sections (80 nm) were cut on an RMC Ultramicrotome, placed on copper grids, stained with uranyl acetate and lead citrate, and examined on a JEM 2100F transmission electron microscope.

Constructs and Transfections. The Dct 3,745-bp promoter (−3,300 to +445 bp from Dct transcription start site) was amplified by PCR and cloned upstream of a luciferase cassette in SacI/XhoI sites of pGL4.23 (Promega). Deletions in the construct were made by site-directed mutagenesis (Stratagene) according to the manufacturer's protocol. Mouse IFN regulatory factor-1 (Irf1)/pcDNA construct was a gift from Nicole Clarke (The University of Nottingham, Nottingham, UK). Transfections were set up at day 3 of low-density cycle with a 6:1 ratio of Cellfectin (Invitrogen) to DNA. Renilla luciferase driven by CMV promoter was cotransfected for normalizations. Posttransfection, low-density media were replaced, and treatments were done; 48 h posttransfection, the cells were lysed with passive lysis buffer (Promega), and luciferase assays were performed according to the manufacturer's protocol (Dual-Luciferase Reporter Assay System; Promega).

siRNA Transfection. Human foreskin-derived melanocytes were plated in antibiotic-free M254 media with supplements at a density of 2×10^5 cells per well of a six-well plate. Transfection was carried out with Cellfectin reagent (Invitrogen) as per the manufacture's protocol. The siRNA concentration used was 100 nM for all siRNAs. Briefly, the cells were incubated with siRNA–cellfectin complexes for 6 h followed by trypsinization of the cells and replating in 24-well plates; 4 h after replating, IFN-γ was added at a concentration of 100 U/mL in the required wells, and 48 h after IFN-γ addition, the cells were harvested for RNA isolation.

Cell Cycle Analysis by Propidium Iodide Staining. Primary human cells were treated with 100 U/mL IFN-γ for 5 d, and the cells were trypsinized and washed one time in 5–10 mL 1× PBS. The cells were resuspended in 1 mL paraformaldehyde fixation solution and incubated on ice for 1 h. Paraformaldehyde was washed using 5 mL 1× PBS, and the cell pellet was resuspended in 0.5 mL 1× PBS; 4.5 mL ice cold 70% ethanol were added dropwise over 30 s to 1 min, and the cells were incubated at 4 °C overnight. The cells were then resuspended in 0.5 mL Propidium Iodide (5 mg/mL) staining solution, incubated for 30 min at 37 °C, and analyzed by flow cytometry. The cells were gated based on the DNA content, and the percentages of cells in each stage of the cell cycle were analyzed based on the nuclear content.

Bead Assay for Detection of Protein Bound to Biotinylated *Dct* Promoter. Biotinylated 3.7-kb Dct promoter was immobilized with avidin-agarose beads (Sigma) followed by incubation with IFN-γ–treated B16 cells for 4 h at 4 °C on a rocker. The supernatant was discarded, and the DNA-bead–bound proteins were washed three times with buffer (10 mM Hepes, 10 mM KCl, 0.1 M EDTA, 0.1 M EGTA, 1× protease inhibitor mixture). The bound proteins were eluted by heating the samples with SDS sample dye at 100 °C for 5 min and loaded onto SDS/PAGE gel followed by Western blot analysis with mouse IRF1 antibody (M-20; Santa Cruz). Nonbiotinylated 3.7-kb Dct promoter was used as control in this assay.

Quantitation of Pigmentaion by Image Analysis. Images of IFNG$^{+/+}$ and IFNG$^{-/-}$ mice were captured using the Nikon camera under similar lighting conditions. For quantifications, 22 measurements were made for each mouse across each earlobe, and mean gray values were calculated (ImageJ).

SI Text

Detection of IFN-γ in the Oscillator Model.

i) Measurement of IFN-γ by ELISA in culture supernatants over the course of pigmentation and depigmentation was performed. As low as 0.01 U/mL recombinant mouse IFN-γ could be detected. There were no detectable levels of IFN-γ in the culture supernatants throughout the cycle.

ii) Real-time PCR detection of IFN-γ transcripts was carried out. IFN-γ mRNA could be detected from splenocyte cells that served as positive control. However, IFN-γ transcripts could not be detected at all phases of the oscillator.

iii) Addition of blocking antibody to IFN-γ during the course of depigmentation did not alter the depigmentation kinetics or the downstream gene expression changes.

Based on all these observations, we conclude that B16 cells do not actively secrete IFN-γ, and the activation of IFN-γ signaling is most likely to occur independent of the known cognate ligand. Several studies in the literature have reported such ligand-independent signaling activation (2, 3).

Future studies should examine this pathway in the laboratory. The key finding based on transcriptome signatures that resulted in identification of IFN-γ as an important mediator of melanogenesis holds true, and the significance of this finding is supported by experiments in multiple model systems. Other than B16 cells, we have performed these studies in primary melanocytes obtained from different subjects. The density-dependent model does not function in primary melanocytes, because cell–cell contact is important for culturing these cells. Moreover, proliferation and melanogenesis are tightly coupled in primary cells through MITF (4).

1. Natarajan VT, et al. (2010) Transcriptional upregulation of Nrf2-dependent phase II detoxification genes in the involved epidermis of vitiligo vulgaris. *J Invest Dermatol* 130(12):2781–2789.
2. Costa-Pereira AP, et al. (2002) Mutational switch of an IL-6 response to an interferon-gamma-like response. *Proc Natl Acad Sci USA* 99(12):8043–8047.
3. Gao B (2012) Wnt regulation of planar cell polarity (PCP). *Curr Top Dev Biol* 101: 263–295.
4. Nishimura EK, et al. (2010) Key roles for transforming growth factor beta in melanocyte stem cell maintenance. *Cell Stem Cell* 6(2):130–140.

Setting up B16 *in vivo* model for pigmentation
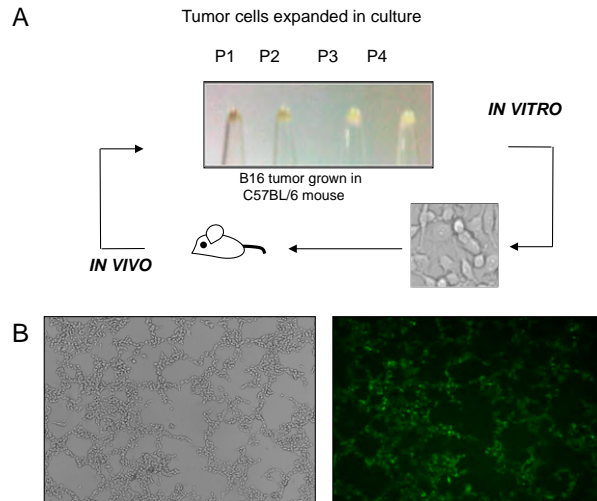
Fig. S1. Setting up the B16 in vivo model for pigmentation. (*A*) B16 cells were grown as tumor in C57BL/6 mice. The tumor was dispersed and grown in vitro as an adherent culture. Cells were harvested, and pellets from days 4 [passage 1 (P1)], 8 (P2), 12 (P3), and 16 (P4) were imaged. Cells progressively depigmented and were completely devoid of melanin by P4. When these cells were injected back into the animal and grown as tumor, the cells regained pigmentation. (*B*) B16 melanoma cells obtained from a tumor using a B16 clone stably expressing GFP (TNV2). (*Left*) Phase contrast. (*Right*) GFP.

Setting up B16 *in vitro* model for pigmentation
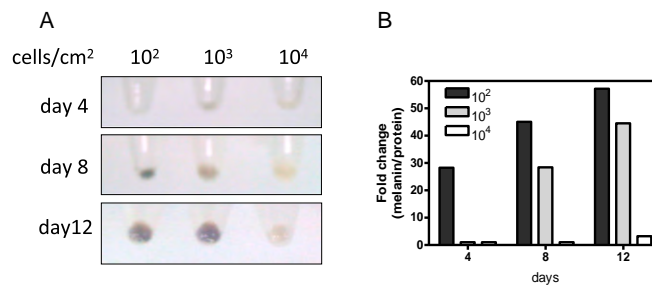
Fig. S2. Setting up the B16 in vitro model for pigmentation. (*A*) B16 cells were plated at the indicated cell density for 4, 8, and 12 d. Cells were harvested, and pellets were imaged. (*B*) Melanin and protein estimations were carried out from the cells, and the ratio of the two is indicated.

Heat map of pigmentation genes regulated in the pigmentation oscillator
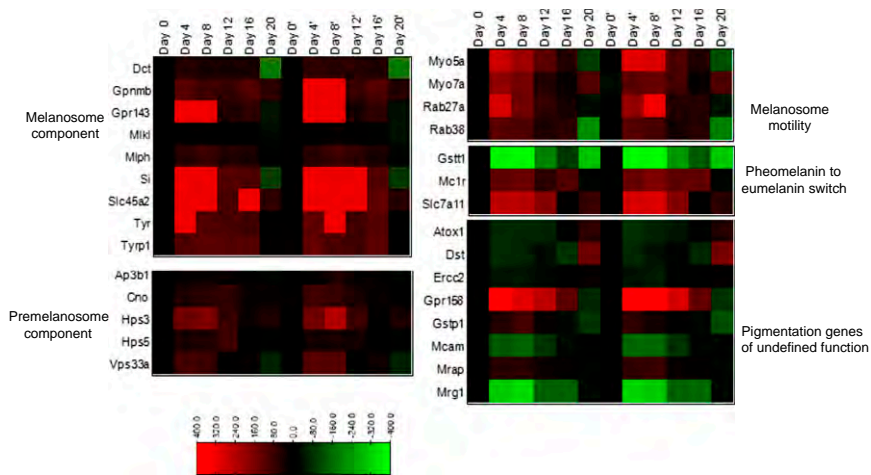
Fig. S3. Heat map of pigmentation genes regulated in the pigmentation oscillator. Genes involved in various melanosome-related processes, such as melanosomal component, premelanosomal component, melanosomal motility, and pheomelanin to eumelanin switch, were chosen, and the relative expression level of these genes in the two cycles with respect to day 0 is represented as a heat map.

Primary human melanocytes are hypopigmented with human IFN-γ treatment
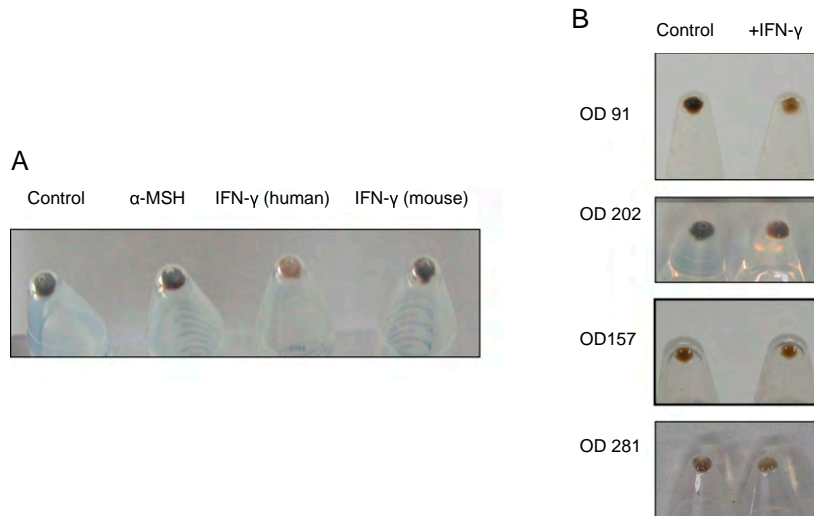
Fig. S4. Primary human melanocytes are hypopigmented with human IFN-γ treatment. (*A*) Primary human melanocytes were treated with 600 nM α-melanocyte stimulating hormone (α-MSH; known propigmenting agent), human IFN-γ (100 U/mL), or mouse IFN-γ (100 U/mL) for 7 d, after which time the cell pellets were observed. Only human IFN-γ caused visible hypopigmentation. (*B*) Four independent primary melanocyte cultures obtained from neonatal foreskin show visible hypopigmentation with IFN-γ treatment.

Electron micrographs of control, IFN-γ treated and recovered primary human melanocytes

Fig. S5. Electron micrographs of control (C) and IFN-γ–treated (+I) and recovered (−I) primary human melanocytes. Electron micrographs of primary human melanocytes were either left untreated [C (d7)] or treated with human IFN-γ [100 U/mL; +I(d7)] for 7 d, after which time IFN-γ was withdrawn from the cultures and grown until day 12. C(d12) and −I(d12) represent electron micrographs of control and IFN-γ–recovered cells, respectively. As is clear from the pictures, after withdrawal of IFN-γ, −I(d12) looks similar to control [C(d12)], thus showing the recovery.

Molecular and cellular changes in response to IFN-γ

Fig. S6. Molecular and cellular changes in response to IFN-γ. (*A*) Cell cycle analysis of primary human melanocytes treated with IFN-γ for 7 d was carried out using flow cytometry. The percentage of cells in different phases of the cell cycle is represented as a bar chart. (*B*) Expression level of known MITF target genes expressed as log (fold change after IFN-γ treatment) from microarray analysis of IFN-γ–treated melanocytes.

Deciphering pathway for IFN-γ mediated DCT regulation
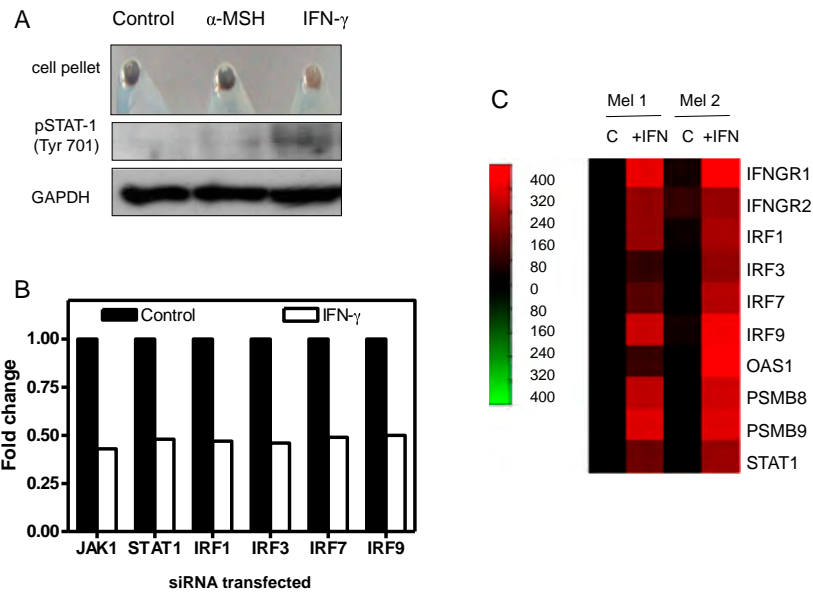
Fig. S7. Deciphering the pathway for IFN-γ–mediated DCT regulation. (*A*) Primary human melanocyte cultures were treated with α-MSH (600 nM) and IFN-γ (100 U/mL), and Western blot analysis was performed with α-pSTAT-1 antibody. GAPDH was used as an equal loading control. (*B*) Primary human melanocytes were transfected with 100 nM concentration of indicated siRNA, and the mRNA levels for the respective genes were quantitated 48 h posttransfection by using real-time PCR. Fold change in the mRNA levels was calculated with respect to the scrambled siRNA–transfected melanocytes. (*C*) Heat map of genes regulated by IFN-γ in two independent melanocyte cultures (Mel 1 and Mel 2). C, Control.

Dct promoter constructs used in the study
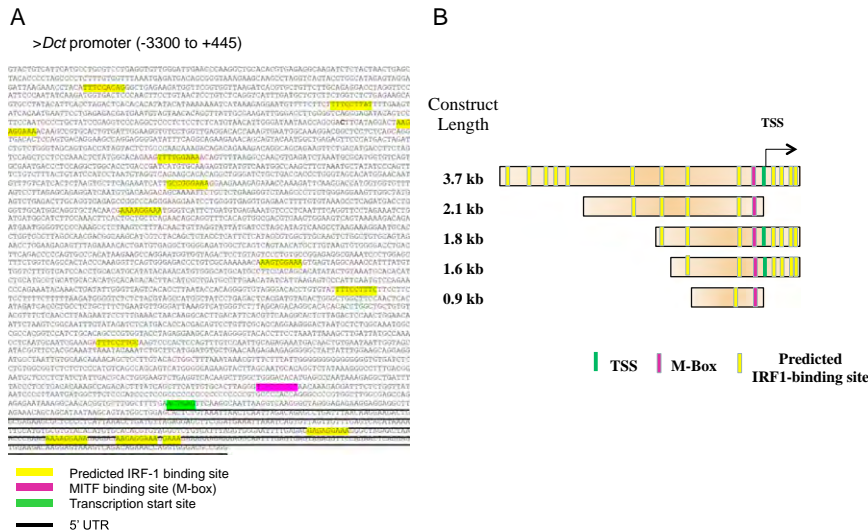
Fig. S8. *Dct* promoter constructs used in the study. (*A*) The full-length 3.7-kb *Dct* promoter with the predicted Irf1 binding sites is highlighted in yellow. (*B*) *Dct* promoter constructs used in our study. M-Box, MITF binding site; TSS, transcription start site.

Analysis of non-lesional and lesional skin from Leprosy

A

Non-lesional skin   **Lesional leprosy skin**

B

Non-lesional   Lesional

C

Quantification of Stage III/IV
Melanosomes in Leprosy
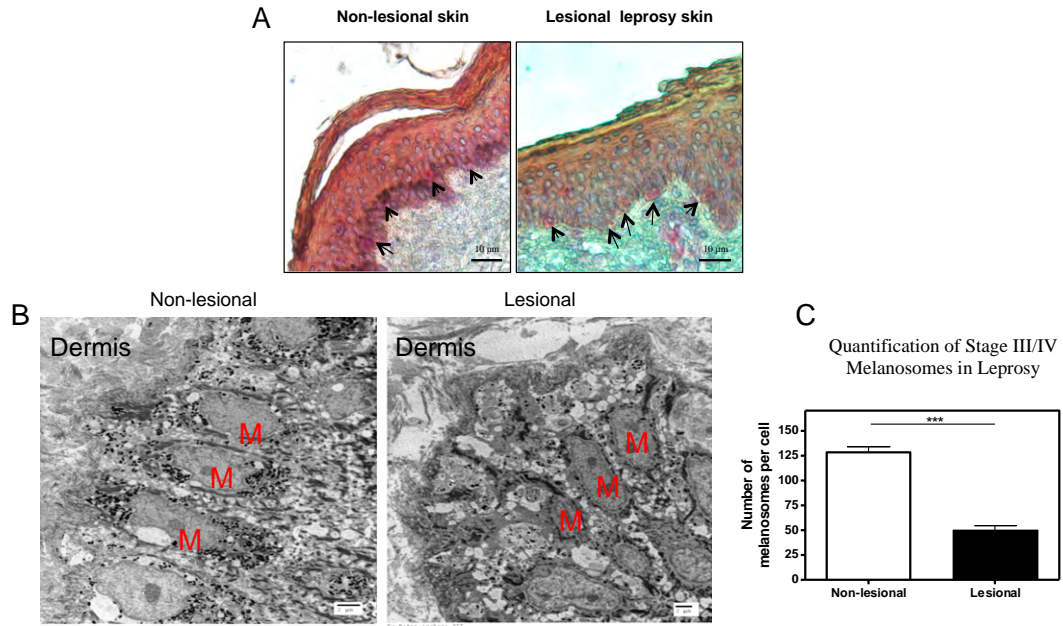
Fig. S9. Analysis of nonlesional and lesional skin from leprosy. (*A*) Immunohistochemical analysis of melanocyte-specific S100 staining in paired nonlesional and lesional leprosy skin. (*B*) Electron micrographs of nonlesional and lesional skin from a leprosy patient showing presence of melanocytes at the epidermal–dermal junction (M). (*C*) Quantitation of stage III and IV melanosomes in 10 melanocytes each from the nonlesional and lesional skin of three leprosy patients. Paired *t* test indicated that the means are significantly different with a *P* value less than 0.001. ***P* value < 0.001.

Table S1. List of enriched genes from periodogram analysis of pigmentation oscillator

Serial no.	Fracmaxamp	Illumina identification	Gene name
1	0.949600	ILMN_195590	
2	0.929992	ILMN_209839	Solute carrier family 44, member 2
3	0.909949	ILMN_209574	Cold shock domain containing e1, rna binding
4	0.883781	ILMN_212867	
5	0.871957	ILMN_193770	
6	0.862152	ILMN_211146	
7	0.851477	ILMN_251332	cdna sequence bc006779
8	0.845110	ILMN_211043	cbp/p300-interacting transactivator with glu/asp-rich C-terminal domain 1
9	0.832459	ILMN_226483	Bone γ-carboxyglutamate protein 2
10	0.828761	ILMN_218405	Expressed sequence ai451617
11	0.827349	ILMN_218425	Adenylate cyclase 2
12*	0.825594	ILMN_196778	IFN-induced transmembrane protein 1
13	0.821260	ILMN_209702	Glycine receptor, β-subunit
14	0.821191	ILMN_186983	
15*	0.818360	ILMN_185224	Dexh (Asp-Glu-X-His) box polypeptide 58
16*	0.818252	ILMN_185344	Proteasome (prosome, macropain) subunit, β-type 8
17	0.816414	ILMN_217565	Predicted gene 6907; predicted gene 6904; predicted gene 4902
18	0.815229	ILMN_225841	Solute carrier family 7, member 11
19	0.812510	ILMN_194594	
20*	0.811365	ILMN_214979	IFN-induced protein with tetratricopeptide repeats 3
21*	0.809468	ILMN_214321	Dexh (Asp-Glu-X-His) box polypeptide 58
22*	0.805007	ILMN_196777	IFN-induced transmembrane protein 3
23	0.804268	ILMN_218436	DNA damage-inducible transcript 4-like
24	0.803234	ILMN_211852	Purinergic receptor p2x, ligand-gated ion channel 4
25	0.801671	ILMN_218343	
26	0.797409	ILMN_193070	
27	0.795983	ILMN_214590	GST, pi 2; GST, pi 1
28	0.795591	ILMN_219340	Glutamate-cysteine ligase, modifier subunit
29	0.792238	ILMN_220932	
30*	0.790793	ILMN_196750	Histocompatibility 2, t-region locus 23
31*	0.785869	ILMN_210061	Phospholipase c, γ2
32*	0.783091	ILMN_253583	Chemokine (C-X-C motif) ligand 10 (IFN-γ–induced protein CRG-2)
33	0.782865	ILMN_213914	Angiopoietin 2
34	0.782641	ILMN_220401	
35	0.780631	ILMN_201755	
36	0.780488	ILMN_196409	
37*	0.779627	ILMN_257425	Dexh (Asp-Glu-X-His) box polypeptide 58
38	0.775060	ILMN_215955	G2 s phase-expressed protein 1
39	0.773665	ILMN_256110	Adenosine deaminase, rna-specific
40*	0.769889	ILMN_209202	IFN-γ–induced GTPase
41*	0.769203	ILMN_186258	Ubiquitin-specific peptidase 18
42	0.769026	ILMN_187187	Tripartite motif-containing 56
43	0.768357	ILMN_222570	Riken cdna 2310016c08 gene
44*	0.767755	ILMN_216138	Myxovirus (influenza virus) resistance 2
45*	0.765728	ILMN_196752	Histocompatibility 2, q-region locus 5
46	0.765117	ILMN_238157	Death inducer-obliterator 1
47	0.765001	ILMN_216376	Integral membrane protein 2b
48*	0.763112	ILMN_223999	Chemokine (c-x-c motif) ligand 10
49	0.762391	ILMN_211080	Thymocyte nuclear protein 1
50	0.762041	ILMN_213913	Atp synthase, h+ transporting, mitochondrial f0 complex, subunit s
51*	0.760474	ILMN_237558	Ww domain containing e3 ubiquitin protein ligase 1
52	0.758913	ILMN_215880	Proline-rich polypeptide 6
53	0.755828	ILMN_213057	MAPK kinase kinase kinase 1
54*	0.755805	ILMN_218776	Guanylate binding protein 6
55*	0.755243	ILMN_215351	ATPase, h+ transporting, lysosomal v0 subunit a1
56*	0.754930	ILMN_212179	2′-5′ oligoadenylate synthetase 1g
57	0.754898	ILMN_237580	High-mobility group box transcription factor 1
58	0.754254	ILMN_223985	
59*	0.753283	ILMN_211229	IRF7
60*	0.752297	ILMN_219577	Sequestosome 1
61	0.751231	ILMN_223944	Family with sequence similarity 70, member A
62	0.750676	ILMN_202718	Similar to unknown (protein for IMAGE: 4910858); predicted gene 4076
63*	0.748676	ILMN_212338	IFN-induced protein 35

Table S1. Cont.

Serial no.	Fracmaxamp	Illumina identification	Gene name
64	0.747622	ILMN_213017	Caveolin, caveolae protein 1
65	0.746548	ILMN_215799	
66*	0.746115	ILMN_217537	Inhibitor of DNA binding 2
67	0.745492	ILMN_214397	Coiled-coil domain containing 84
68*	0.743316	ILMN_214605	Radical s-adenosyl methionine domain containing 2
69	0.742414	ILMN_212540	Lysophosphatidylcholine acyltransferase 2
70	0.742413	ILMN_212110	Apolipoprotein L 9b; apolipoprotein L 9a
71	0.741198	ILMN_230539	Transient receptor potential cation channel, subfamily m, member 1
72	0.740058	ILMN_220818	Phosphoglycolate phosphatise
73	0.739570	ILMN_188510	
74	0.737070	ILMN_217201	Ectodermal-neural cortex 1
75	0.736869	ILMN_222986	Synaptophysin-like protein
76	0.735042	ILMN_210108	Heat-responsive protein 12
77	0.734609	ILMN_217932	Acyl-coa dehydrogenase, long-chain
78*	0.734464	ILMN_219674	Lipocalin 2
79*	0.733974	ILMN_223721	Guanine nucleotide binding protein (g protein), $\gamma7$ subunit
80	0.733795	ILMN_189853	Similar to tripartite motif protein TRIM34-α; tripartite motif-containing
81	0.732014	ILMN_213064	
82	0.731980	ILMN_213156	Rap guanine nucleotide exchange factor (gef) 4
83	0.731704	ILMN_203309	Riken cdna 1200016e24 gene
84	0.729582	ILMN_209247	Eukaryotic translation initiation factor 4e member 2
85*	0.729061	ILMN_209850	IRF1
86	0.728772	ILMN_192852	Ankyrin repeat and FYVE domain containing 1
87	0.728001	ILMN_218499	
88	0.725636	ILMN_220043	Proteolipid protein (myelin) 1
89	0.725446	ILMN_241583	Aldehyde dehydrogenase 4 family, member a1
90	0.725223	ILMN_221196	
91	0.724528	ILMN_203650	Unc-5 homolog c (*Caenorhabditis elegans*)
92	0.723849	ILMN_191462	
93	0.721978	ILMN_210363	
94	0.721533	ILMN_185693	
95	0.720974	ILMN_234373	Riken cdna 1810048j11 gene
96*	0.720583	ILMN_209781	2′-5′ oligoadenylate synthetase-like 2
97	0.720318	ILMN_221506	Bernardinelli-seip congenital lipodystrophy 2 homolog (human)
98	0.719436	ILMN_220771	Testis-expressed gene 2
99	0.719395	ILMN_196495	
100	0.718500	ILMN_186712	Unc-84 homolog a (*C. elegans*)
101*	0.718117	ILMN_193206	Ubiquitin-conjugating enzyme e2n
102	0.717922	ILMN_211574	Importin 13
103	0.717859	ILMN_202582	Stt3, subunit of the oligosaccharyltransferase complex
104	0.717748	ILMN_224259	Formin homology 2 domain containing 1
105	0.715915	ILMN_194391	Transformation-related protein 53-inducible nuclear protein 1
106	0.715812	ILMN_188004	
107*	0.715777	ILMN_192153	TNF receptor-associated factor 2
108	0.715619	ILMN_192099	
109	0.713326	ILMN_216296	Hemicentin 2
110	0.713066	ILMN_190871	Hexokinase 1
111	0.713043	ILMN_220667	Stt3, subunit of the oligosaccharyltransferase complex
112	0.712526	ILMN_210607	Guanine nucleotide binding protein (g protein), β-polypeptide 1-like
113*	0.711394	ILMN_210436	Guanylate nucleotide binding protein 2
114	0.710531	ILMN_208910	Family with sequence similarity 122, member B
115	0.709855	ILMN_215138	Budding uninhibited by benzimidazoles 3 homolog (*Saccharomyces cerevisiae*)
116	0.709693	ILMN_197368	
117	0.709485	ILMN_220503	Plasminogen activator, tissue
118	0.709362	ILMN_215301	Signal transducer and activator of transcription 2
119	0.709157	ILMN_194133	Tetratricopeptide repeat domain 7b
120	0.708279	ILMN_210695	Cdp-diacylglycerol-inositol 3-phosphatidyltransferase
121	0.707780	ILMN_211037	Oligophrenin 1
122	0.705834	ILMN_202025	Poly (ADP ribose) polymerase family, member 14
123	0.705386	ILMN_212511	Eukaryotic translation elongation factor 1 $\beta2$
124	0.704807	ILMN_190833	Inositol 1,4,5-triphosphate receptor interacting protein-like 1
125	0.704760	ILMN_220963	Formin-like 2

Table S1. Cont.

Serial no.	Fracmaxamp	Illumina identification	Gene name
126	0.704545	ILMN_229747	Basic leucine zipper transcription factor, ATF-like 3
127*	0.704483	ILMN_185655	Dual-specificity tyrosine-(Y)-phosphorylation–regulated kinase 3
128	0.704205	ILMN_184842	Mitochondrial ribosomal protein s10
129	0.703600	ILMN_187349	
130	0.702238	ILMN_233734	Carbonic anyhydrase 12
131	0.702040	ILMN_191331	
132*	0.701812	ILMN_221143	Hla-b–associated transcript 5
133	0.701722	ILMN_210247	ρ-GTPase activating protein 12
134	0.701543	ILMN_193808	
135	0.701461	ILMN_213966	Solute carrier family 44, member 3
136	0.701399	ILMN_217326	Coatomer protein complex subunit-α
137	0.701355	ILMN_189204	
138	0.701050	ILMN_224086	Rwd domain containing 2
139	0.700743	ILMN_211093	Nuclear factor of activated T cells 5
140	0.700695	ILMN_239612	Poly (ADP ribose) polymerase family, member 14
141	0.700107	ILMN_224541	Synaptotagmin-like 2

*Genes regulated by IFN-γ.

Turnitin Originality Report

Thesis Final   by Shalini Yadav

From Thesis (Shalini)

- Processed on 20-Jul-2018 23:18 IST
- ID: 983948305
- Word Count: 26379

Similarity Index
10%
Similarity by Source

Internet Sources:
        5%
Publications:
        9%
Student Papers:
        N/A

---

sources:

---

1 1% match (publications)

Hsiao, Jennifer J., and David E. Fisher. "The roles of microphthalmia-associated transcription factor and pigmentation in melanoma", Archives of Biochemistry and Biophysics, 2014.

---

2 < 1% match (publications)

Susanna K. Fistarol. "Disorders of Pigmentation", Journal der Deutschen Dermatologischen Gesellschaft, 09/2009

---

3 < 1% match (publications)

"Neuroscience in the 21st Century", Springer Nature, 2016

---

4 < 1% match (publications)

Maria Carmela Bonaccorsi di Patti, Antimo Cutone, Fabio Polticelli, Luigi Rosa et al. "The ferroportin-ceruloplasmin system and the mammalian iron homeostasis machine: regulatory pathways and the role of lactoferrin", BioMetals, 2018

---

5 < 1% match (Internet from 07-Sep-2017)

http://www.biorxiv.org/content/biorxiv/suppl/2017/08/28/112201.DC3/112201-39.txt

---

6 < 1% match (publications)

Mulaka Maruthi, Dipti Singh, Segireddy Rameswara Reddy, Babu S. Mastan, Satish Mishra, Kota Arun Kumar. " Modulation of host cell SUMOylation facilitates efficient development of and ", Cellular Microbiology, 2017

---

7 < 1% match (publications)

H. Y. Park. "Cellular mechanisms regulating human melanogenesis", Cellular and Molecular Life Sciences CMLS, 01/21/2009